INVESTIGATION OF SOLAR ASSISTED HEAT PUMP SYSTEM INTEGRATED WITH HIGH-RISE RESIDENTIAL BUILDINGS

YU FU, BEng, MSc

Thesis submitted to the University of Nottingham

for the degree of Doctor of Philosophy

SEPTEMBER 2014

ABSTRACT

The wide uses of solar energy technology (solar thermal collector, photovoltaic and heat pump systems) have been known for centuries. These technologies are intended to supply domestic hot water and electricity. However, these technologies still face some barriers along with fast development. In this regards, the hybrid energy system combines two or more alternative technologies to help to increase the total efficiency of the system. Solar assisted heat pump systems (SAHP) and photovoltaic/thermal collector heat pump systems (PV/T-HP) are hybrid systems that convert solar radiation to thermal energy and electricity, respectively. Furthermore, they absorb heat first, and then release heat in the condenser for domestic heating and cooling.

The research initially investigates the thermal performance of novel solar collector panels. The experimental results indicate an average daily efficiency ranging from 0.75 to 0.96 with an average of 0.83. Compared with other types of solar collectors, the average daily efficiency of novel solar thermal collectors is the highest.

The research work further focuses on the integrated system which combines solar collector and air source heat pump (ASHP). The individual components, configurations and layout of the system are illustrated. Theoretical analysis is conducted to investigate thermodynamic cycle and heat transfer contained in the hybrid system. Laboratory tests are used to gauge the thermal performance of the novel SAHP. A comparison is made between the modelling and testing results, and the reasons for error formation are analysed.

The research then considers the specially designed PV/T collector that employs the refrigerant R134a for cooling of PV modules and utilizes the glass vacuum tubes for reducing the heat loss to the ambient air. The PV/T collector consists of 6 glass vacuum tube-PV module-aluminium sheet-copper tube (GPAC) sandwiches which are connected in series. The theoretical analysis and experimental tests all give the satisfactory results of up to 2.9% improvement of electrical efficiency compared with those without cooling.

The research finally focuses on the integrated heat pump system where the PV/T collector acts as evaporator. Based on the energy balance of the four main components of the heat pump system, a mathematical model of the heat pump system is presented. When the instantaneous ambient temperature and solar radiation are provided, results are obtained for the spatial distributions of refrigerant conditions, which include temperature, pressure, vapour quality and enthalpy. Detailed experimental studies are carried out in a laboratory. Three testing modes are proposed to investigate the effect of solar radiation, condenser water flow rate and condenser water supply temperature on energy performance. The testing results show that an average coefficient of performance (COP) reached 3.8,4.3 and 4.0 under the three testing modes with variable radiation, condenser water supply water temperature and water flow rate, respectively. However, this could be much higher for a large capacity heat pump system using large PV panels on building roofs. The COP increases with the increasing solar radiation, but decreases as the condenser water supply temperature and water flow rate increases.

PUBLISHED PAPERS AS A RESULT OF THE PHD PROJECT

Y. Fu, B Mempouo, J Zhu, S. B. Riffat (2010), Basic Analysis of High Performance Air Source Heat Pump Using PCM Storage Tank and No Frost Evaporator, accepted to be published in the proceeding and presented at the SET2010-9th International Conference on Sustainable Energy Technologies, Shanghai, China.

H.Chen, S. B. Riffat, **Y. Fu** (2011), Experimental study on a hybrid photovoltaic/heat pump system, accepted to be published in the proceeding and presented at the Applied Thermal Engineering 31 (2011) 4132-4138.

Yu Fu, Feiying Fu, Xinbin Wang (2013), Assessment of solar thermal technology utilized in China, Applied Mechanics and Materials, Volumes 368-370, 1338.

Xinbin Wang, Jiaping Liu, **Yu Fu** (2013), The Strategies if Passive Energy-Efficiency Design in Low Energy Building, Applied Mechanics and Materials, Volumes 368-370, 1218.

Feiying Fu, **Yu Fu** (2013). Assessment of photovoltaic technologies integrated in building sectors in China, Applied Mechanics and Materials, Volumes 368-370, 1318.

Yu Fu, Kai Chen, Feiying Fu, Xinbin Wang (2014). Architecture design of building integrated solar collector. Advanced Material Research.

ACKNOWLEDGEMENT

During my study at the University of Nottingham in the School of the Built Environment, I received a lot of support and help from many people, who I would like to thank.

I would like to express my gratitude and appreciation to my supervisor, Professor S.B.Riffat, who introduced the heat pump to me and guided me in the right way from the very beginning. His effort, encouragement, and guidance were generous throughout. He created an excellent research environment from which I benefit.

I wish to thank Dr. Jie Zhu, as my second supervisor, for his unlimited support throughout the progress of my research work, and also for his technical instructions and advice during the whole period of the research.

I also wish to thank Mr. David Oliver for the technical skill and patient support he has given me. I would also like to thank the other technical staff members, particularly Mr. Dave Taylor, Mr. Bob Clark for their technical assistance over whole period of experimental work.

I am also grateful to my colleagues and working partners, especially Hongbing Chen and Blaise Mempouo for their continued support.

Finally, I wish to express my sincere thanks to all my family for their great encouragement and support to achieve my goal.

LIST OF CONTENTS

ABSTRACT I

PUBLISHED PAPERS AS A RESULT OF THE PHD PROJECT III

ACKNOWLEDGEMENT IV

LIST OF CONTENTS V

LIST OF FIGURES VIII

LIST OF TABLES XVIII

CHAPTER 1 INTRODUCTION 1

1.1 Statement of Problem 1

1.2 Objective and Scope of Project 3

1.2.1 Scopes 4

1.3 Novelty and Timeliness of Project 5

1.4 Methodology Approach 6

1.5 Structure of Thesis 6

CHAPTER 2 LITERATURE REVIEW 9

2.1 Introduction 9

2.2 Solar Thermal Collector 9

2.2.1 Flat Plate Collector 10

2.2.2 Thermal Analysis of Collectors 13

2.2.3 Solar Collector Applications 15

2.2.4 Architecture Design of Building Integrated Solar Collector 16

2.3 Photovoltaic 25

2.3.1 Types of PV 25

2.3.2 PV Performance 27

2.3.3 Factors Affecting Conversion Efficiency 28

2.3.4 Photovoltaic/Thermal 29

2.4 Heat Pump and Solar Assisted Heat Pump 31

2.4.1 Heat Pump 31
2.4.2 Performance of ASHP 34
2.4.3 Solar Assisted Heat Pump System 34
CHAPTER 3 INVESTIGATION OF NOVEL SOLAR COLLECTORS . 53
3.1 Investigation of Photovoltaic/Thermal Collectors 53
3.1.1 PV/T Collector Panel Description 54
3.1.2 Mathematical Model and Simulation of PV/T Collector 57
3.1.3 Experimental Study of PV/T Collector 63
3.1.4 Performances of PV/T Collector 65
3.2 Investigation of Solar Thermal Collector 76
3.2.1 Solar Thermal Collector Description 76
3.2.2 Experimental Study of Solar Thermal Collector 79
3.2.3 Performance of Novel Solar Thermal Collector 79
3.3 Conclusion 82
CHAPTER 4 NUMERICAL AND EXPERIMENTAL ANALYSIS ON PHOTOVOLTAIC/THERMAL HEAT PUMP 84
4.1 Photovoltaic/ Thermal Heat Pump Description 84
4.2 Mathematical Model and Simulation of PV/T-HP 87
4.2.1 Compressor Mode 87
4.2.2 Expansion Valve Model 90
4.2.3 Water Cooled Condenser Model 91
4.2.4 Evaporator Model 95
4.2.5 Refrigerant Charge 95
4.2.6 Numerical Procedure 97
4.3 Experimental Study of PV/T-HP 98
4.3.1 Layout of the Testing Rig 98
4.3.2 Performance Assessment 99
4.3.3 Test Methodology 99

4.4 Performances of Photovoltaic/Thermal Heat Pump 100
4.4.1 Parameters Affect the Performance of PV/T-HP 100
4.4.2 Performance of PV/T-HP 107
4.5 Discussion 109
CHAPTER 5 NUMERICAL AND EXPERIMENTAL ANALYSIS ON SOLAR ASSISTED HEAT PUMP 110
5.1 Solar Assisted Heat Pump Description 110
5.1.1 Summer Condition 114
5.1.2 Winter Condition 114
5.2 Mathematical Model and Simulation of ASHP 116
5.3 Experimental Work 116
5.3.1 Layout of the Testing Rig 116
5.3.2 Performance Assessment 117
5.3.3 Test Methodology 118
5.4 Performance of Novel Solar Assisted Heat Pump System 120
5.4.1 Performance of SAHP under Summer Condition 120
5.4.2 Performance of SAHP under Winter Condition 134
5.4.3 Performance of SAHP under Extreme Cold Condition 149
5.4.4 Performance of SAHP under Transitional Season 151
5.5 Conclusion 156
CHAPTER 6 CONCLUSION AND FURTHER WORK 158
6.1 Conclusion 158
6.2 Further Works 160
REFERENCE 162
APPENDIX 188

LIST OF FIGURES

Figure 1. 1 Thesis structure 7

Figure 2. 1 Expanded view of a flat plate solar collector 11

Figure 2.2 Selected proposed and commercial design of solar air heaters 12

Figure 2.3 Selected proposed and commercial designs of solar liquid collectors 13

Figure 2.4 Collector efficiencies of various liquid collectors 14

Figure 2.5 Direct and indirect solar water heating systems 15

Figure 2.6 Passive and active solar water heating systems 16

Figure 2.7 Application of roof integrated solar collector in building sectors 18

Figure 2.8 Pictures of Solar collectors on the roof 18

Figure 2.9 Yearly distribution of solar radiation on vertical collector in Graz 19

Figure 2.10 Application of south wall integrated solar collector in building sectors 19

Figure 2.11 Application of parapet integrated solar collector in building sectors 20

Figure 2.12 Application of roof integrated unglazed solar collector system 20

Figure 2.13 Application of roof integrated unglazed solar collector system in swimming pool..... 21

Figure 2.14 Flat plate solar collector integrate into a rainwater gutter . 23

Figure 2.15 Thermal solar structure of the novel solar thermal collector 23

Figure 2.16 Application of solar modules integrated with balcony 24

Figure 2.17 Application of solar wall integration in Canada 24

Figure 2.18 Application of solar cladding integration 25

Figure 2.19 The chart of typical I-V measurement system 27

Figure 2.20 Current-voltage characteristics of PV modules at 25^{o}C and 60^{o}C under 830W/m^{2}..... 28

Figure 2. 21 Energy Consumption in UK, 2002 31

Figure 2. 22 Electricity powered heat pump system 32

Figure 2. 23 Diagrams of an ideal vapour compression refrigerant cycle 33

Figure 2. 24 Comparison distribution of DX-SAHP system application area from literatures review..... 36

Figure 2. 25 Illustration of operation in meeting demand for a particular day time period..... 37

Figure 2. 26 Schematic diagram of SAHP for drying, air conditioning and water heating..... 37

Figure 2. 27 Schematic diagram of SAHP for drying and water heating 38

Figure 2. 28 Schematic diagram of DX-SAHP, (a) heating (b) cooling 39

Figure 2. 29 Cycles of the two-functional air conditioning..... 39

Figure 2. 30 Cycles of the three-functional air conditioning 40

Figure 2. 31 Possible time variation of refrigeration cycle for an ASHP42

Figure 2. 32 Schematic diagram of a solar boosted 44

Figure 2. 33 DX-SAHP- combine with two different types of solar collectors acting as evaporator..... 45

Figure 2. 34 Radiative type of flat plate solar collector 45

Figure 2. 35 Collector surface design of an SAHP 46

Figure 2. 36 Schematic diagram of integral type SAHP..... 48

Figure 2. 37 Schematic diagram of heat pipe enhanced SAHP..... 48

Figure 2. 38 Schematic diagram of ZNEH 49

Figure 2. 39 Cross sectional of sheet and tube PV/T evaporator 50

Figure 2. 40 Cross sectional and dimension of modified PV/T evaporator 51

Figure 2. 41 Structure of PV/T evaporator..... 51

Figure 2. 42 Parallel refrigerant tubes on the back of modified PV/T evaporator 52

Figure 3. 1Layout of PV/T collector panel..... 55

Figure 3. 2 Cross-sectional view of a glass vacuum tube..... 55

Figure 3. 3 The diagram of U-type heat exchanger 56

Figure 3. 4 The thermal network of the internal vacuum glass tube. ... 58

Figure 3. 5 The thermal network of the PV module 59

Figure 3. 6 The thermal networks of the aluminium sheet and copper tube 61

Figure 3. 7 Flow diagram of simulation model 63

Figure 3. 8 The schematic diagram of the electric circuit for power testing..... 64

Figure 3. 9 Variation of solar radiation and ambient temperature whole year 66

Figure 3. 10 The ambient temperature and solar radiation on a typical day 67

Figure 3. 11 Temperatures of the PV cell at different PV/T collector area 68

Figure 3. 12 The heat gain of PV/T-HP at different PV/T collector area 68

Figure 3. 13 The power output at different PV/T collector area 69

Figure 3. 14 The PV efficiency at different PV/T collector area 69

Figure 3. 15 COP of PV/T-HP at different collector area 70

Figure 3. 16 Variation of temperatures at different layers..... 71

Figure 3. 17 Variation of the thermal efficiency and heat gain of the PV/T collector panel 72

Figure 3. 18 Variation of the electrical efficiency, power and electricity output 73

Figure 3. 19 Comparison of electrical efficiency with and without cooling 73

Figure 3. 20 Variation of electrical efficiency and PV power with radiation 74

Figure 3. 21 Variation of electrical efficiency and PV power with condenser water supply temperature 75

Figure 3. 22 Variation of electrical efficiency and PV power with different condenser water flow rate 75

Figure 3. 23 The diagram of a novel solar collector 77

Figure 3. 24 Cross sectional view of vacuum glass tube 77

Figure 3. 25 The diagram of solar collector with U-type heat exchanger 78

Figure 3. 26 The testing results of solar radiation and water temperature 80

Figure 3. 27 Varieties of average daily efficiency with total solar radiation 81

Figure 3. 28 Varieties of average daily efficiency with increased water temperature 81

Figure 3. 29 Varieties of average daily efficiency with (ΔTH) 82

Figure 3. 30 Varieties of Water Temperature with glass tube diameter 82

Figure 4. 1 The schematic diagram of the novel PV/T-HP system 85

Figure 4. 2 Flow chart of the simulation program of compressor 90

Figure 4. 3 Flow chart of the simulation program of novel PV/T-HP 97

Figure 4. 4 Testing point position..... 98

Figure 4. 5 Outlet entropy changed with different solar radiations..... 101

Figure 4. 6 Outlet entropy changed with different ambient temperature 102

Figure 4. 7 Outlet entropy changed with different length of tube 102

Figure 4. 8 Outlet entropy changed with different dry degree of inlet 103

Figure 4. 9 Variation of COP, condenser capacity and compressor power with radiation 105

Figure 4. 10 Variation of COP, condenser capacity and compressor power with condenser water supply temperature 105

Figure 4. 11 Variation of COP, condenser capacity and compressor power with condenser water flow 107

Figure 4. 12 Variation of electrical efficiency and PV power with different condenser water flow rate 107

Figure 4. 13 The power consumption and electrical efficiency of PV/T-HP 108

Figure 4. 14 COP and condenser capacity of the PV/T-HP..... 108

Figure 5. 1 The schematic diagram of the novel SAHP 111

Figure 5. 2 Cross sectional view of solar collector with U-type heat exchanger..... 111

Figure 5. 3 Testing point position..... 117

Figure 5. 4 Evaporating and condensing pressure change with simulating operation 124

Figure 5. 5 Suction and discharge temperature change with simulating operation 124

Figure 5. 6 Water temperature change with simulating operation..... 125

Figure 5. 7 COP change with simulating operation..... 125

Figure 5. 8 Variation of evaporating and condensing pressure as a function of time with increasing water temperatures during experimental operation at nominal load condition 126

Figure 5. 9 Variation of evaporating and condensing pressure as a function of time with increasing water temperatures during experimental operation at minimum load condition 126

Figure 5. 10 Variation of evaporating and condensing pressure as a function of time with increasing water temperatures during experimental operation at maximum load condition 127

Figure 5. 11 Variation of suction and discharge temperature as a function of time with increasing water temperatures during experimental operation at nominal load condition 128

Figure 5. 12 Variation of suction and discharge temperature as a function of time with increasing water temperatures during experimental operation at minimum load condition 128

Figure 5. 13 Variation of suction and discharge temperature as a function of time with increasing water temperatures during experimental operation at maximum load condition 129

Figure 5. 14 Variation of COP at increasing water temperature during experimental operation at nominal load condition 131

Figure 5. 15 Variation of COP at increasing water temperature during experimental operation at minimum load condition 131

Figure 5. 16 Variation of COP at increasing water temperature during experimental operation at maximum load condition 132

Figure 5. 17 Comparison of evaporating and condensing pressure at increasing water temperature on nominal load condition 133

Figure 5. 18 Variation of suction and discharge temperature at increasing water temperature on nominal load condition 133

Figure 5. 19 Comparison of COP on nominal load condition..... 134

Figure 5. 20 Evaporating and condensing pressure change with simulating operation 138

Figure 5. 21 Suction and discharge temperature change with simulating operation 138

Figure 5. 22 Water temperature change with simulating operation ... 139

Figure 5. 23 COP change with simulating operation..... 139

Figure 5. 24 Evaporating and condensing pressure as a function of time for decreasing water temperatures during experimental operation at nominal load condition (ambient 7^{o}C/room 20^{o}C)..... 141

Figure 5. 25 Evaporating and condensing pressure as a function of time for decreasing water temperatures during experimental operation at minimum load condition (ambient 24^{o}C/room 27^{o}C)..... 142

Figure 5. 26 Evaporating and condensing pressure as a function of time for decreasing water temperatures during experimental operation at maximum load condition (ambient 2^{o}C/room 20^{o}C)..... 142

Figure 5. 27 Variation of suction and discharge temperature at increasing water temperature during experimental operation at nominal load condition (ambient 7^{o}C/room 20^{o}C)..... 143

Figure 5. 28 Variation of suction and discharge temperature at increasing water temperature during experimental operation at minimum load condition (ambient 24^{o}C/room 27^{o}C)..... 143

Figure 5. 29 Variation of suction and discharge temperature at increasing water temperature during experimental operation at maximum load condition (ambient 2^{o}C/room 20^{o}C)..... 144

Figure 5. 30 Variation of COP during experimental operation at nominal load condition (ambient 7^{o}C / room 20^{o}C) 146

Figure 5. 31 Variation of COP during experimental operation at minimum load condition (ambient 24^{o}C / room 27^{o}C) 147

Figure 5. 32 Variation of COP during experimental operation at maximum load condition (ambient 2^{o}C / room 20^{o}C)..... 147

Figure 5. 33 Comparison of evaporating and condensing pressure at increasing water temperature on nominal load condition..... 148

Figure 5. 34 Variation of suction and discharge temperature at increasing water temperature on nominal load condition..... 148

Figure 5. 35 Comparison of COP (simulation results and experimental results) for space heating and domestic hot water supply on nominal load condition..... 149

Figure 5. 36 Parameters of guaranteed hot water usage 150

Figure 5. 37 Parameters of do not guarantee hot water usage..... 150

Figure 5. 38 Evaporating and condensing pressure and water temperature change during experimental operation at nominal load condition (ambient 20^{o}C) 153

Figure 5. 39 Evaporating and condensing pressure and water temperature change during experimental operation at minimum load condition (ambient 7^{o}C) 153

Figure 5. 40 Variation of suction and discharge temperature at increasing water temperature during experimental operation at nominal load condition (ambient 20^{o}C) 154

Figure 5. 41 Variation of suction and discharge temperature at increasing water temperature during experimental operation at minimum load condition (ambient 7^{o}C) 154

Figure 5. 42 Variation of COP during experimental operation at nominal load condition (ambient 20^{o}C) 155

Figure 5. 43 Variation of COP during experimental operation at minimum load condition (ambient 7^{o}C) 156

LIST OF TABLES

Table 2. 1 Different collector types thermal efficiency and thermal loss coefficient 14

Table 2. 2 Photovoltaic cell efficiencies 26

Table 3. 1 The characteristics of PV/T collector 56

Table 3. 2 Characteristic dimension of novel solar collector panel 78

Table 4. 1Specification of main equipment in PV/T-HP 86

Table 4. 2 List of testing modes 100

Table 5. 1Characteristic of different kinds of capillary 112

Table 5. 2 Cycle controls of novel SAHP 113

Table 5. 3 Working conditions in summer seasons 120

Table 5. 4 Simulation results under different operating conditions 121

Table 5. 5 Simulation results under different operating conditions 122

Table 5. 6 Comparison of results for space cooling 122

Table 5. 7 Working conditions in winter seasons 134

Table 5. 8 Simulation results under different operating conditions 135

Table 5. 9 Simulation results under different operating conditions 136

Table 5. 10 Comparison of results for space heating 137

Table 5. 11 Working conditions in extreme cold seasons 149

Table 5. 12 Working conditions in transition seasons 151

Chapter 1 Introduction

1.1 Statement of Problem

Along with fast economic development, the world is facing huge pressure on energy supplement, environmental pollution and consequences of climate change. The Renewable Energy Law of the People's Republic of China provided legal guarantee for the purpose of promoting the development and utilization of renewable energy in order to protect the environment and realize a sustainable economic and social developments on January 1, 2006 (Renewable Energy Law, 2006). The statistics show that the building sector (22% of residential and 19% of commercial) accounts for over 40% of the total energy requirements (Motte et al. 2013). It is a key sector to develop renewable energy and strives to make better use of existing energy.

The rapid increase in energy consumption by building sectors is mainly devoted to space heating (26.5%), followed by electrical consumption (20%), space cooling (15.8%) and water heating (13.2%). It is thus very important to take effective ways to minimize the needs of energy use in buildings, especially for heating and cooling, and adopt renewable energy and other technologies to meet the remaining energy needs (Li, Yang & Lam, 2013).

There are various strategies that should be attempted to develop alternative energy sources for major energy demands, such as a greater share of solar energy in residential building loads. However, each system has its own advantages and limitations. In this project, a hybrid energy system combined with two or more alternative technologies will help to increase the total efficiency of the system. Therefore, creating

highly efficient methods for space heating and cooling, domestic hot water supply as well as electricity, present a distinct set of infrastructural challenges to the industry as this is a demanding objective requiring innovation.

All of the world's energy forms as we know are solar in origin. The reduction of greenhouse gases pollution is the main advantage of utilizing solar energy. The wide applications of solar energy are solar thermal technology and photovoltaic (PV) technology.

Solar thermal technologies on the market today are efficient and highly reliable. Most of the systems are intended to supply domestic hot water. However, solar thermal technologies still face some barriers alongside fast development. At first, buyers and building occupants pay much more attention to the comfort, performance and energy cost of the buildings. It means not only domestic hot water supply is needed, but also space heating and cooling. Because solar radiation is relatively low and heat requirements are quite large in winter, using solar thermal technology for space heating is hard to achieve. Secondly, more and more high-rise residential buildings are constructed with the developing urbanization in China. Due to the increasing household numbers, the amount of heat requirement is increasing as well. Then, limited roof space is another key barrier. Therefore, it is necessary to design a novel type of solar collector which could supply domestic hot water as well as space heating and cooling. Meanwhile, it could be integrated with building sectors such as a parapet on the balcony.

Solar energy also can be used to generate electricity by photovoltaic (PV) modules. Unfortunately, photovoltaic modules have low efficiency, which converts solar radiation to electricity with the efficiencies in the range of

5% to 20%, depending on the type of solar cell, radiation level and cell temperature. In addition, many studies were carried out to investigate the effect of PV cell temperature on the electrical efficiency of PV modules and discovered that the electricity generating efficiency of solar cells decreased with the rise in the operating temperature. To harness the available PV technology effectively, the reduction of PV cell temperature is especially necessary.

In the field of thermal energy generation, heat pumps are advantageous due to high performance, low energy costs and environmental benefits. The most popular heat pumps which are used for space heating and domestic hot water supply are ground source heat pumps (GSHP) and ASHP. Traditionally, the COP of GSHP can be more than 3.0. However, the disadvantages of GSHP are the high cost of drilling boreholes and need for land for the installation of ground heat exchanger loops. A typical ASHP has a COP of 2.0 to 3.0 at the beginning of the heating season and then decreases gradually due to freezing of the outdoor heat exchanger. Air source has found renewed favour as an effective heat source although frost can form on the evaporator coils in winter limiting the usage. To address these drawbacks by developing a higher performance of heat pumps, design of a novel type of evaporator should be necessary.

1.2 Objective and Scope of Project

In order to tackle the above problems, a novel solar thermal collector, a novel evaporator for PV/T heat pump system and a novel SAHP are independent proposed. Therefore, the overall objectives and targeted unique outcomes of this research are:

- Aesthetic. Architectural integration is a major factor when employing solar collectors or PVs for domestic usage. Unfortunately, most solar collectors are installed on the roof top using flat or pitched methods, which is a bad integration of being less visible and having minor architectural impact. In this project, it is achieved through development and validation of a novel solar thermal collector which integrates with a parapet placed on a balcony and requires no additional water tank.
- Efficiency. Due to the barriers of ASHP and PV module, in this project, focus on increasing the evaporator temperature and decreasing the PV module temperature. In this project, it is achieved through development and validation of novel photovoltaic/thermal (PV/T) heat pump evaporator, which uses Direct Expansion (DX) vacuum tubes to cool the solar cells.
- Multi-function. Nowadays, solar collectors, and heat pump systems are intended to supply domestic hot water, space heating and cooling, respectively. In this project, it is achieved through development and validation of novel SAHP system, which supplies domestic hot water for one whole year, space heating in winter and cooling in the summer.

1.2.1 Scopes

In order to successfully meet the above targets, the scope of the project is divided into four separate areas:

- Review of past work on solar collectors, PV modules and SAHP technologies.
- Theoretical and experimental investigation of the performances of solar collector and PV/T.

- Theoretical and experimental investigation of the performances of photovoltaic/thermal heat pump (PV/T-HP) and SAHP.
- Validation of the theoretical results findings with experimental results.
- Discussion of the technical and environmental benefits of the novel systems.

1.3 Novelty and Timeliness of Project

This project has the following novelty aspects:

- The use of solar collectors which can be architecturally integrated with high-rise residential building sectors without water tanks.
- The use of PV/T collector/evaporator which can effectively achieve better cooling effect and better electrical performance of PV modules.
- The use of PV/T-HPs which can effectively collect heat at a low temperature (when the atmosphere in winter is about -5^{o}C) with no frost and provide PV/T-HP for satisfying heating requirements.
- The use of traditional ASHP as high efficiency heat transfer device incorporates in the solar collector panel to design multi-functional SAHP which is proposed to operate all year round.

The project is timely in view of the Republic of China government's commitment to reduce CO_2 emissions by 40%~50% by 2020 compared to 2005 (Communities and Local Government, 2009). The novel solar thermal collectors are expected to contribute to wide usage in high-rise residential buildings. In addition, the novel heat pump systems present an excellent opportunity to expand the market for space heating and cooling as well as domestic hot water supply for heat pumps. Finally, the

novel heat pump systems are expected to give rise to significant economic and environmental benefits.

1.4 Methodology Approach

The project work involves the following stages:

Stage 1: Literature Review

A literature review is conducted to collect relevant information on the use of solar thermal and PV/T collector panels as evaporators for heat pump systems and summarises previously published theory that is crucial to understanding this project.

Stage 2: Mathematical Modelling/Thermodynamic Analysis

Mathematical modelling is used to evaluate the performance of the systems in various ways and under different operating conditions including different radiation levels. The sensitivity analysis of the effects of the physical characteristic of the collector/evaporator on the efficiency of the system is also investigated.

Stage 3: Testing Using Small-Scale Rig in the laboratory

Small-scale test rigs are designed and constructed to test the performance of the novel systems. Results are compared with those obtained by mathematical modelling. Systems under various solar radiations are tested in a rig to determine the optimum performances.

1.5 Structure of Thesis

This thesis is composed of six chapters. Figure 1.1 illustrates the link between chapters and the plan of the thesis.

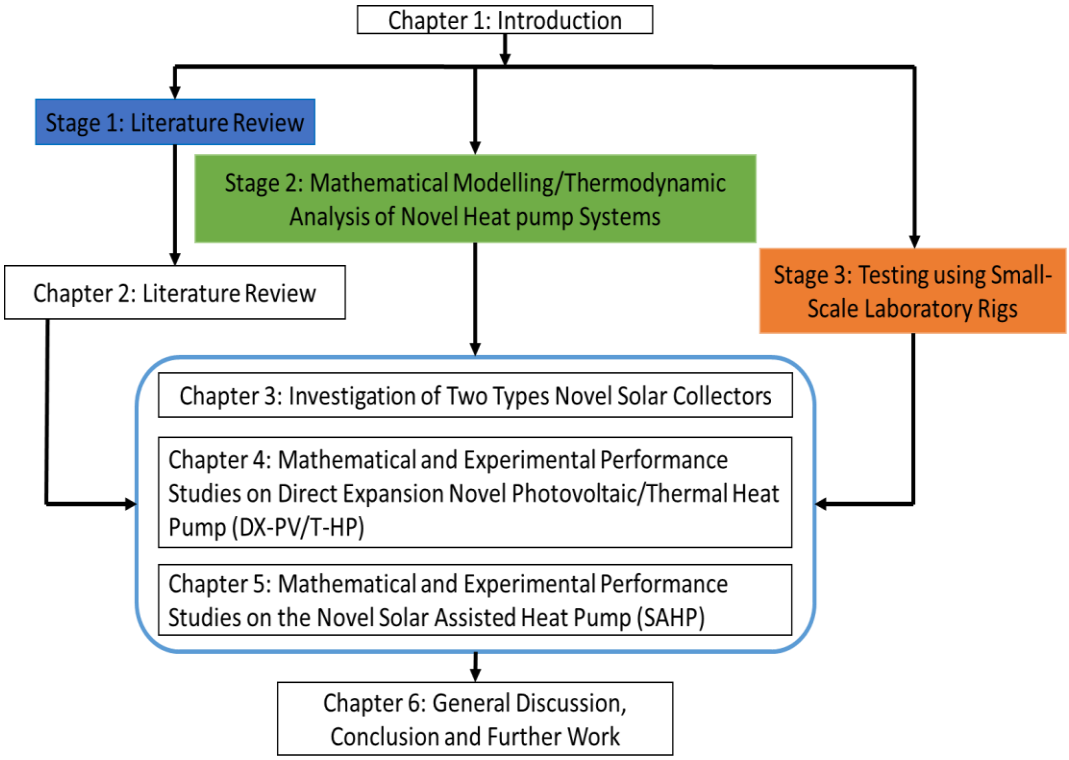

Figure 1. 1 Thesis structure

The six chapters involve the following:

The first chapter covers the introduction of the project driving forces. The project objectives, scopes are detailed. The methods of approach to meet various objectives are also given in this chapter.

The second chapter summarises previously published concept and theory that is crucial to understanding this project. It also provides a brief review of the various studies and the state of art heat pump technologies and solar thermal technologies relevant to this work.

The third chapter describes the design of novel solar thermal collectors and PV/T collectors, and analyses design specifications. It also shows the mathematical model and experimental analysis of these systems. Furthermore, it evaluates the performance of the system in various ways and under different operating conditions.

The fourth chapter presents mathematical models and experimental performance analysis of the DX-PV/T-HP. It also evaluates the performance of the system in various ways and under different operating conditions. The sensitivity analysis of the effects of physical characteristics of the PV/T evaporator on the COP of PV/T-HP is also given.

The fifth chapter presents the experimental set up of a SAHP and analyses design specifications of the main five components which made the loop of refrigerant circuit of the experimental rig. It also presents the mathematical model and experimental analysis of SAHP system. Furthermore, it evaluates the performance of the system in various ways and under different operating conditions. The sensitivity analysis of the effects of the physical characteristic on the COP of SAHP is also given.

The sixth chapter gives a general discussion. The conclusions are based on the theoretical and experimental investigation. It also suggests further works.

Chapter 2 Literature Review

2.1 Introduction

This chapter reviews existing relevant research work and provides an in-depth understanding of the different technologies used. The purpose of the review is to identify key points in each technology that affect their performance in order to achieve the best possible integration between them.

In section 2.2, a survey of the various types of solar thermal collector and applications is presented. An introduction into the use of solar energy is attempted via a description of flat plate collector. It is followed by thermal and thermodynamic analysis of the collectors. Typical applications of the collector are presented in order to show the extent of their applicability.

Work in Section 2.3 begins with the basic principles underlining the PV technology. The performance of photovoltaic modules and the temperature effect on the performance of PVs are presented. In addition, a review of the available literature on PV/T collectors is presented.

Section 2.4 introduces the basic principles of heat pumps. An overview of heat pump structures, operations and limitations are analysed. In addition, different types of heat pump are investigated the performance in accordance with their structure, shape and working fluid.

2.2 Solar Thermal Collector

Solar thermal collector, acts as a special kind of heat exchanger, converts solar radiation energy into useful thermal energy and transfers

to a transport fluid (usually air, water, or oil) flowing through the system. The collected energy can be used either direct to space or water heating equipment, or to a thermal storage tank. Based on the heat temperature requirement, solar thermal collectors can be classified into non-concentrating collectors (less than 100^{o}C) and concentrating collectors (250^{o}C -2500^{o}C). Normally, in order to provide space heating and hot water supplement (less than 100^{o}C), non-concentrating solar collectors are generally employed, which include flat plate collectors and evacuated tube collectors.

2.2.1 Flat Plate Collector

A typical flat plate solar collector is shown in Figure 2.1. It consists of an insulated metal box, transparent cover, absorber plate, and recuperating tubes filled with heat transfer fluids and other auxiliaries (http://www.greenspec.co.uk/solar-collectors.php). According to flat plate collectors, transparent glazing and absorber plate are important components that should be considered when designing novel types of collectors.

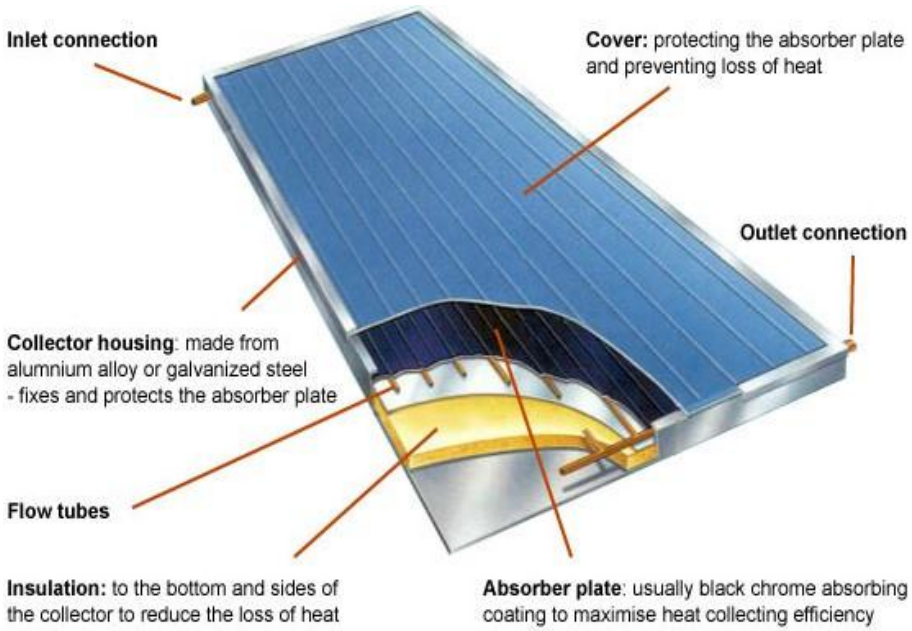

Figure 2. 1 Expanded view of a flat plate solar collector (http://www.greenspec.co.uk/solar-collectors.php)

The transparent cover is used to reduce convection losses from the absorber plate and irradiation losses from the collector, and that should be high transmittance for short wave radiation and low transmittance for long wave radiation. Single or multiple sheets of glass have been widely used. Various prototypes of transparent insulated flat plate collectors have been built and tested in the last decades (Spate, 1999; Scheweiger, 1997).

Colour and surface type should be considered when designing the absorber plate. Commonly, black colour is used in the collector plate to absorb as much of the radiation as possible. In addition, selective surface is particularly important when the temperature of collector surface is much higher than the ambient temperature. Typically, selective surfaces consist of a thin upper layer and a thin lower layer. Thin upper layer is highly absorbent to shortwave radiation but relatively transparent to long wave thermal radiation and thin lower layer is highly reflective and low emitting tor long wave radiation.

A number of absorber plate designs focused on the good thermal bond between tubes and absorber plates without incurring excessive costs for labor or materials. Material most frequently used for absorber plates are copper, aluminium and stainless steel. Some studies suggested the modifications in the design and air movement in solar air collectors, as shown in Figure 2.2. Figure 2.2 (1) shows the counteraction of the low heat transfer coefficient between metal and air. Figure 2.2 (2) and (3) shows use of metal or fabric matrices, or thin corrugated metal sheets as selective surface. In addition, Figure 2.2 (4)-(8) shows the use of finned,

corrugated absorbers and multiple pass air flow configurations to require high level of performance (Yong and Taebeom, 2007).

For fluid heating solar collectors, there are a number of absorber plate designs are shown in Figure 2.3. Referring to Figure 2.3 (1), it shows a bonded sheet design, in which the transfer fluids are integrated with the plate to make good thermal conduct between the metal and fluid. Figure 2.3 (2) and (3) show the fluid in copper tubes is lower and upper the plate surface, respectively. Referring to Figure 2.3 (4), it shows the fluid in extruded rectangular tubes, which allows a larger heat transfer area between tube and plate (Yong and Taebeom, 2007).

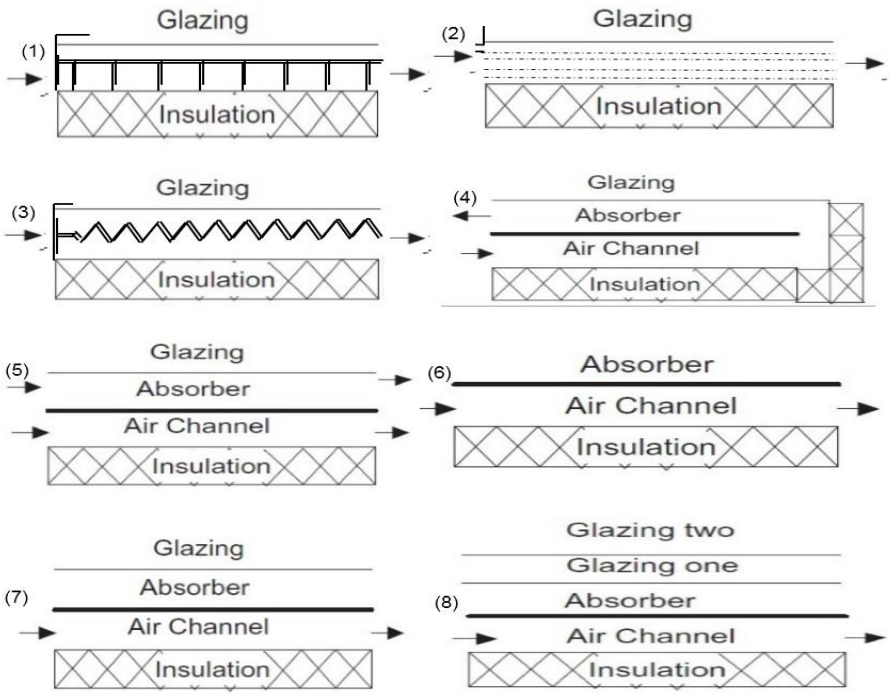

Figure 2.2 Selected proposed and commercial design of solar air heaters (Yong and Taebeom, 2007)

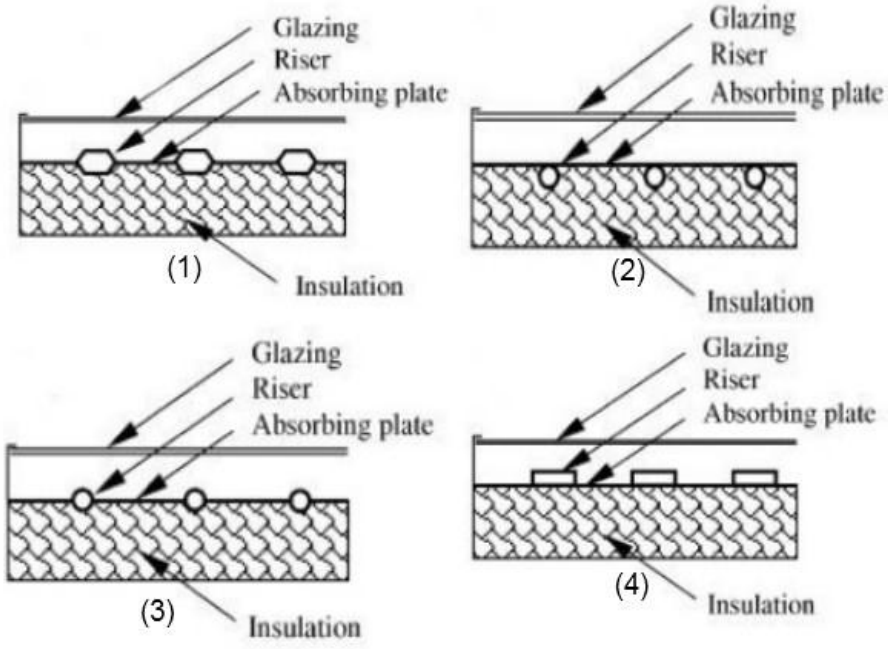

Figure 2.3 Selected proposed and commercial designs of solar liquid collectors (Yong and Taebeom, 2007)

2.2.2 Thermal Analysis of Collectors

The basic parameter to consider for a collector is thermal efficiency. It is defined as the ratio of the useful energy extracted from the fluid passing the collector to the energy incident on the collector aperture. The incident solar flux consists of direct and diffuse solar radiation. The efficiency of solar collector depends on the design of the collector and on the system of which the collector is a part. Table 2.1 summarises the thermal efficiencies and heat loss coefficients of different types of collector (www.solarserver.de).

Table 2.1 Different collector types thermal efficiency and thermal loss coefficient (www.solarserver.de)

Type of collector	Thermal efficiency	Heat loss coefficient ($W/m^2\ ^oC$)	Temperature range (^oC)
Uncovered absorber	0.82~0.90	10~30	Up to 40
Flat plate	0.66~0.83	2.9~5.3	20~80
Evacuated tube	0.62~0.84	0.7~2	50~120
Air collector	0.75~0.90	8~30	20~50

The thermal performance of collector is determined by the variables of incident radiation, ambient temperature, and inlet fluid temperature (ASHERAE Standard 93, 1986). It requires experimental measurements under the steady state or quasi-steady-state conditions. The best way to accomplish this is to identify the expected range of the parameter $\Delta T/G$ for the load and climate on a plot of efficiency η_{th}as a function of the heat loss parameters indicated in Figure 2.4 (Kalogirou, 2004).

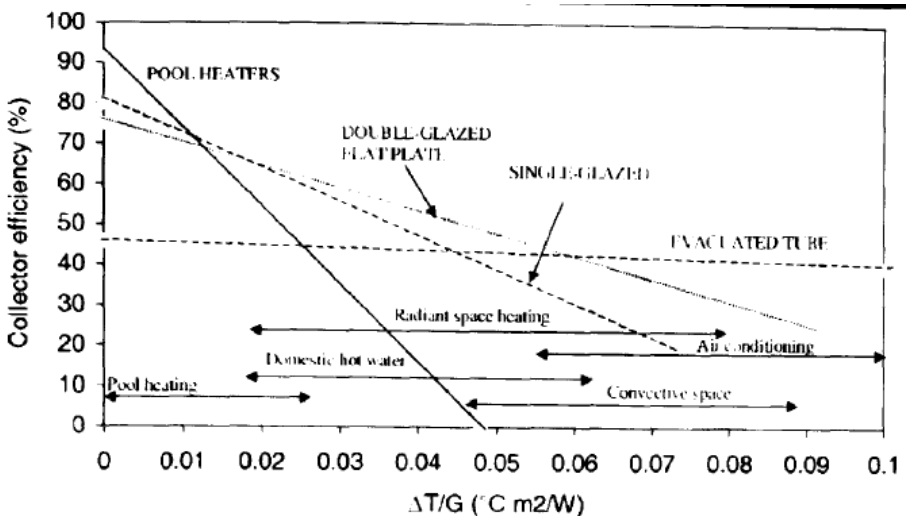

Figure 2.4 Collector efficiencies of various liquid collectors (Kalogirou, 2004)

2.2.3 Solar Collector Applications

Solar collectors have commonly been used in solar water heating systems and solar space heating systems. Solar water heating systems can be either active or passive. The most common is active systems. Active solar water heaters rely on electric pumps and controllers to circulate water through the collectors. There are two types of active solar water heating systems (direct and indirect) shown in Figure 2.5. Direct circulation system uses pumps to circulate pressurized potable water directly through the collectors. The system is appropriate in areas which do not freeze for long periods and do not have hard or acidic water. Indirect circulation system pumps transfer fluids through collector. Heat exchanger transfers the heat from the fluid to the potable water (Southface, 2007)

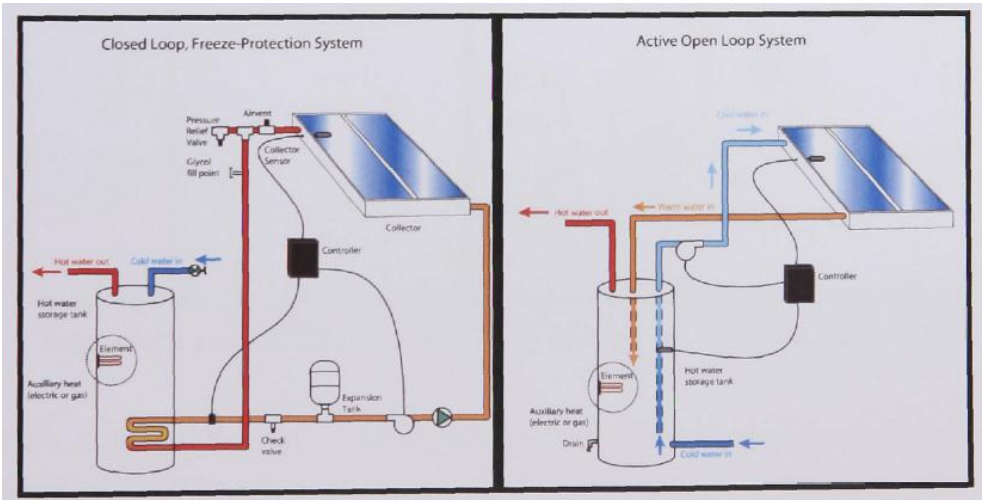

Figure 2.5 Direct and indirect solar water heating systems (Southface, 2007)

Passive solar water heater relies on gravity and tendency for water to naturally circulate as it is heated. Because the system contains no electrical components, passive system is generally more reliable, easier to maintain, and possibly has a longer work life than active system. Two common types of passive system are shown in Figure 2.6. Integral

collector storage system consists of one or more storage tanks placed in an insulated box with a glazed side facing the sun which is suited for areas where temperatures rarely go below freezing. Thermo-syphon system is an economical and reliable choice. It relies on the natural convection of warm water rising to circulate water through the collectors and to the tank (located above the collector). As water in the solar collector heater, it becomes lighter and rises naturally into the tank above. Meanwhile, the cooler water flows down the pipes to the bottom of the collector, enhancing the circulation.

Solar space heating can be either liquid based system or air based systems. Solar liquid collectors are same with solar water heater systems. Air based systems circulate air through the solar collector with fans.

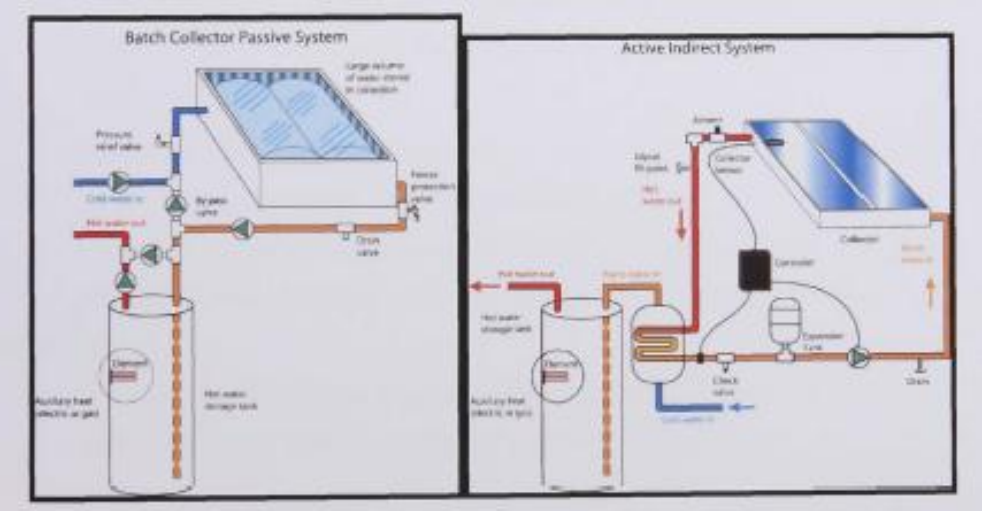

Figure 2.6 Passive and active solar water heating systems (Southface, 2007)

2.2.4 Architecture Design of Building Integrated Solar Collector

At present, most of the building integration of solar thermal systems is mounted on the roof top at a flat or tilted angle. However, Maria and Christian (2007) showed the classic roof integration is considered to be

a failure because the collector is used only for thermal application, and seems as an independent technical element of the building (Figure 2.7). The awful roof with collectors and tanks are shown in Figure 2.8. It presents a low level of architectural quality (Herzog, 1999).

In addition, along with fast development, high-rise residential building construction is growing rapidly in recent years. Due to the increased household numbers, the amount of heat required increases as well. Limited roof space restricts the collector installation. Bergmann (2002) presented that vertical use of collectors and showed the yearly distribution of solar radiation on vertical collector in Figure 2.9. It has better heat production distributed over the year in mid-latitudes although solar radiation gained of collector is less compared with tilt 45^{o} from April to September (Considered the overheating in summer with tilt 45^{o}) (Bergmann, 2002). Furthermore, it greatly increases the installation area because the building facades can be used. Some buildings have installed solar collectors on building facades, such as south facing walls (Figure 2.10) and parapets (Figure 2.11). Although the installation area is increased, the solar collector also seems as an independent technical element of the building and presents the low level of architectural quality. More importantly, the safety issue becomes the biggest problem when typhoons or rainstorms occur.

In order to solve above problems, several researches have focused on solar heating systems integrated with building direction, especially for high-rise building sectors. Great integration of solar thermal collector into buildings should be considered the aesthetics and sustainability aspects, financial, technical and psychological obstacles (Nahar and Garg, 1980).

Figure 2.7 Application of roof integrated solar collector in building sectors (http://image.baidu.com/)

Figure 2.8 Pictures of Solar collectors on the roof (http://image.baidu.com/)

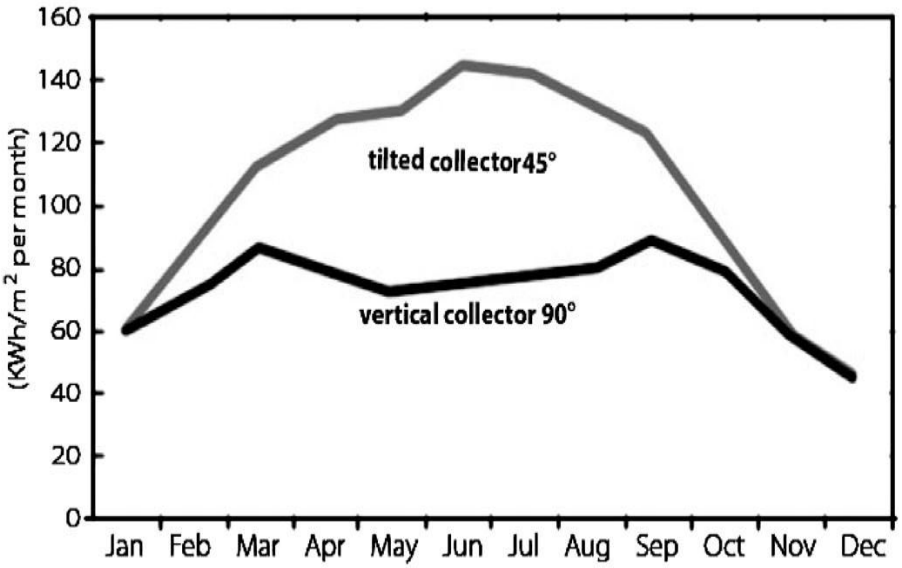

Figure 2.9 Yearly distribution of solar radiation on vertical collector in Graz (Bergmann, 2002)

Figure 2.10 Application of south wall integrated solar collector in building sectors (http://image.baidu.com/)

Figure 2.11 Application of parapet integrated solar collector in building sectors (http://image.baidu.com/)

Figure 2.12 Application of roof integrated unglazed solar collector system (Maria and Christian, 2007)

Maria and Christian (2007) and Maurer et al. (2012) summarised the integration guidelines on integration quality. It includes size and position of collector field, shape and size of the modules, type of jointing, collector material and surface texture and absorber colour.

Maria and Christian (2007) presented that the most appreciated roof integration systems are roof integrated unglazed solar collector systems, shown in Figure 2.12 and Figure 2.13, respectively.

De Beijer (1998) developed a solar collector to replace the ridge tiles on building roofs. There are two tubes in this collector, one is assembled into the other, the inner tube serves as storage tank and the outer is the absorber. The space between the two tubes is a vacuum. Hassan and Beliveau (2007) designed an integrated roof solar collector to replace the roof ridge. Huang et al. (2008) developed the solar collector to replace the shutter. Canaletti et al. (2011) developed a solar collector to replace parapet or sun shading canopy of the building.

Yang et al. (2012) introduced a new type of all ceramic flat plate solar collector made from ordinary ceramic and V-Ti black ceramic. This new type of collector replaces balcony railings and building roofs with the thermal efficiencies 47.1% and 50%, respectively.

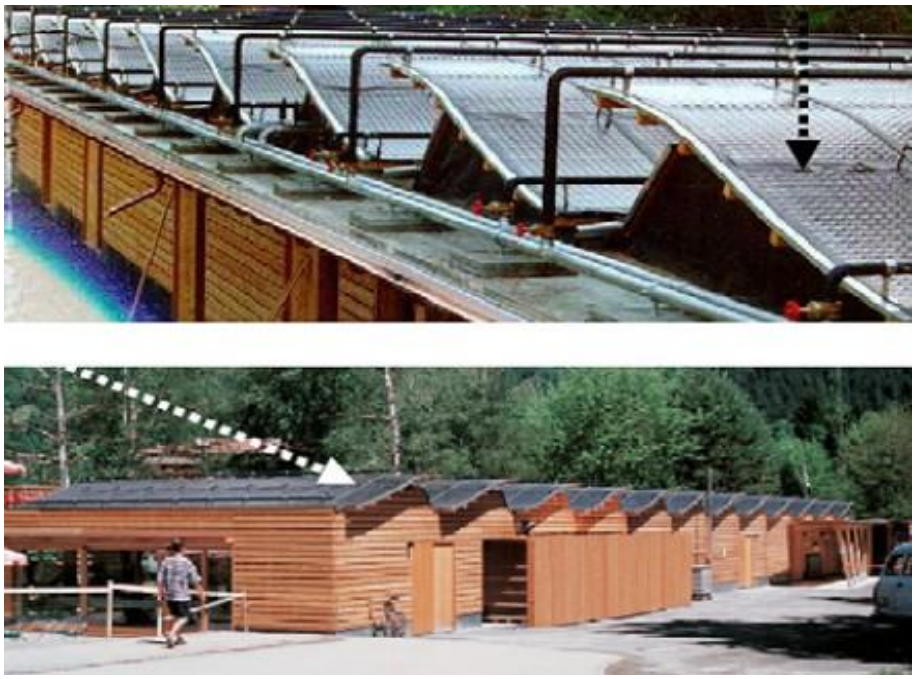

Figure 2.13 Application of roof integrated unglazed solar collector system in swimming pool (Maria and Christian, 2007)

Maurer et al. (2012) investigated transparent façade collectors to replace the balustrade for space heating and cooling. Air is used as the heat transfer medium in the inner tubes. The tubes have openings at both ends to allow for continuous horizontal flow with low pressure drops.

In addition, Motte et al. (2013) presented a new concept of flat plate solar collectors integrated into a rainwater gutter in building sectors, shown in Figure 2.14. Figure 2.15 showed the structure of thermal solar module. The thermal module is composed of glass, an air layer, a highly selective absorber and an insulation layer. Cold fluid from the tank flows through the inferior insulated tubes, then in the upper tubes contact with the absorber to transfer heat.

Maria and Christian (2007) presented that the best rating is balcony integration with the solar modules installed along the whole parapet area of upper stage centre, and are used as parapet external finishing, shown in Figure 2.16. The size and shape of the modules fit the grid and match the rhythm of façade. In addition, the followed ratings are solar wall integration (Figure 2.17) and solar cladding integration (Figure 2.18).

Figure 2.14 Flat plate solar collector integrate into a rainwater gutter (Motte et al., 2013)

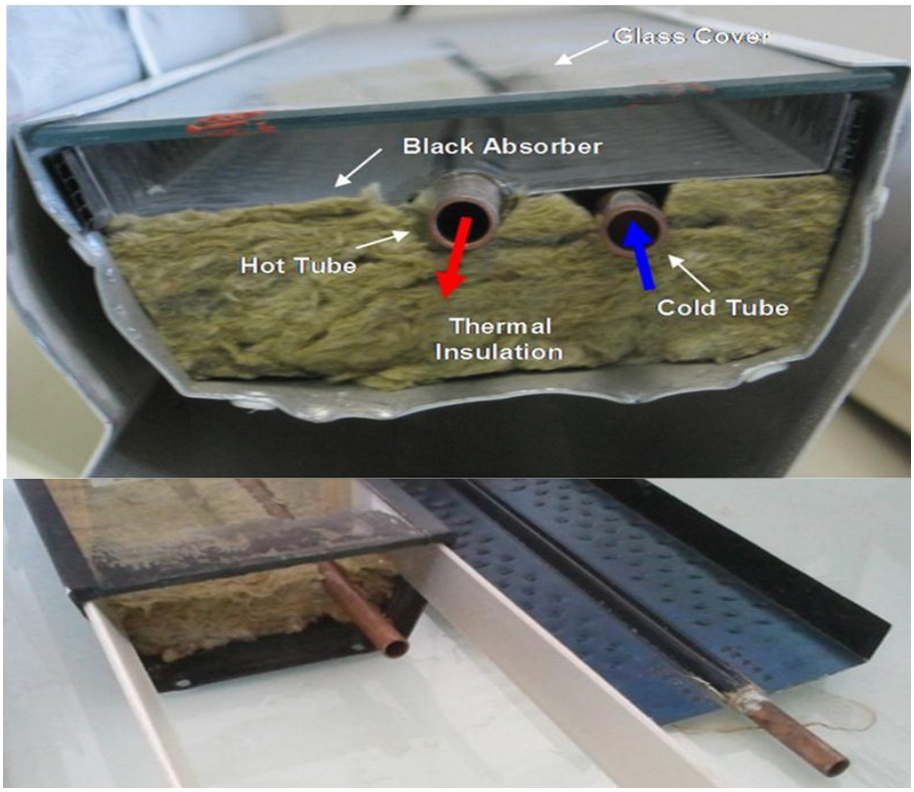

Figure 2.15 Thermal solar structure of the novel solar thermal collector (Motte et al., 2013)

Figure 2.16 Application of solar modules integrated with balcony (Maria and Christian, 2007)

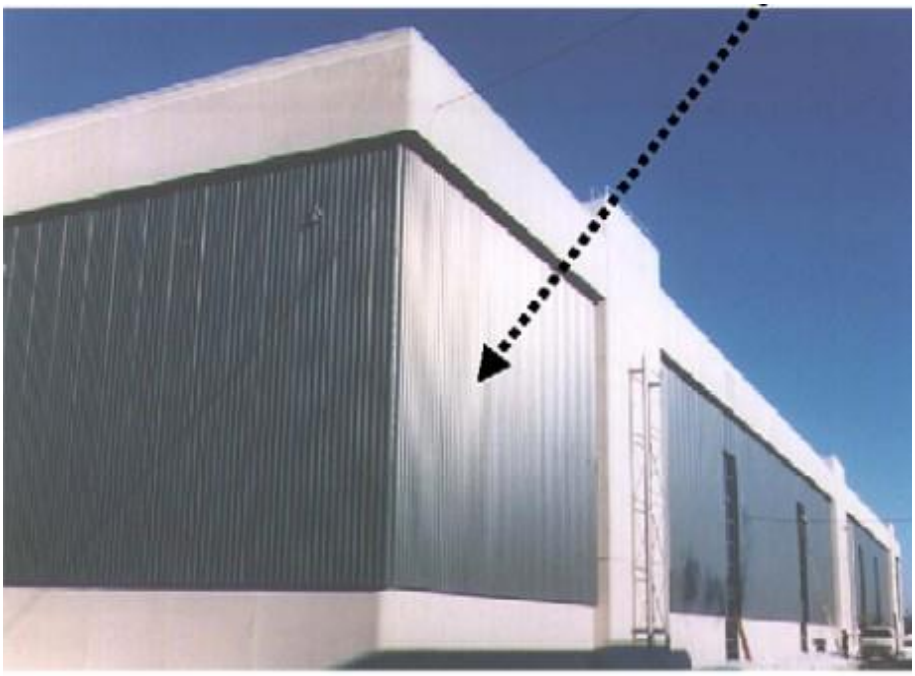

Figure 2.17 Application of solar wall integration in Canada (Maria and Christian, 2007)

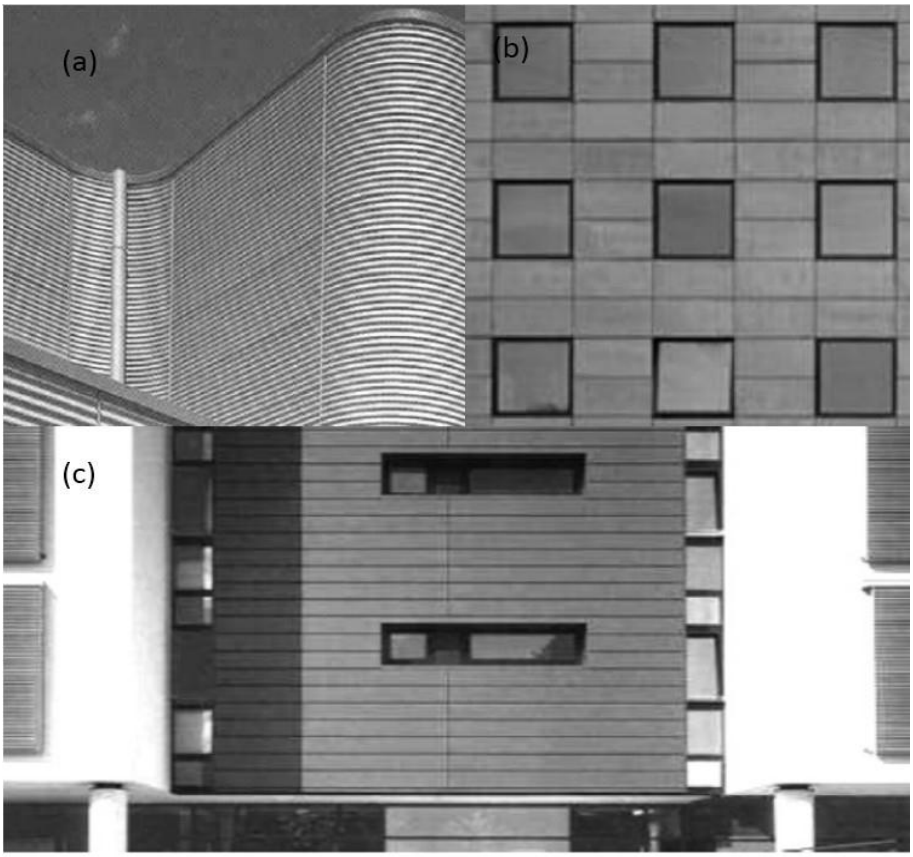

(a) Profiled metal sheets (b) Cassette cladding (c) Tongue and groove panel

Figure 2.18 Application of solar cladding integration (Maria and Christian, 2007)

2.3 Photovoltaic

2.3.1 Types of PV

A typical silicon PV cell is comprised of a thin wafer consisting of an ultra-thin layer of phosphorus-doped (N-type) silicon on top of a thicker layer of boron-doped (P-type) silicon. An electrical field is created near the top surface of the cell where these two materials are in contact, called P-N junction (Florida solar energy centre, 2007). When light energy is applied to a PV cell, and when the sun shines on it, it gives the electrons enough energy to move across the p-n junction. There is an energy variation across the p-n junction called a potential difference or voltage. The existence of this voltage when a PV cell is exposed to light

is called the photovoltaic effect. If a circuit is made, via a cable to the electrical loads, the potential difference drives a current and the electrons can flow through the circuit (Florida solar energy centre, 2007).

There are three basic types of photovoltaic cells, mono-crystalline cells, polycrystalline cells and amorphous cells. In addition, a number of other promising materials such as cadmium telluride (CdTe) and copper indium diselenide (CIS) are now being used for PV modules. Table 2.2 shows the electrical efficiency for different PV cells taken from different manufacturers (Zondag, 2004).

Table 2.2 Photovoltaic cell efficiencies (Zondag, 2004)

Type of cell	Range commercial module efficiency	Producer highest performance modules	Corresponding cell manufacturer
Multicrystalline Si	11~15%	Sharp	Sharp
Monocrystalline Si	10~17%	Suntechnics	Sun Power
HIT cells	16~17%	Sanyo Electric	Sanyo Electric
Ribbon & EFG cells	12~13%	Titan Energy	RWE Schott
a-Si (single junction)	4~6%	Mitsubishi	Mitsubishi Heavy
a-Si (triple junction)	5~7%	Sunset	United Solar
CIS	9~11%	Worth Solar	Worth Solar
CdTe	6~9%	First Solar	First Solar

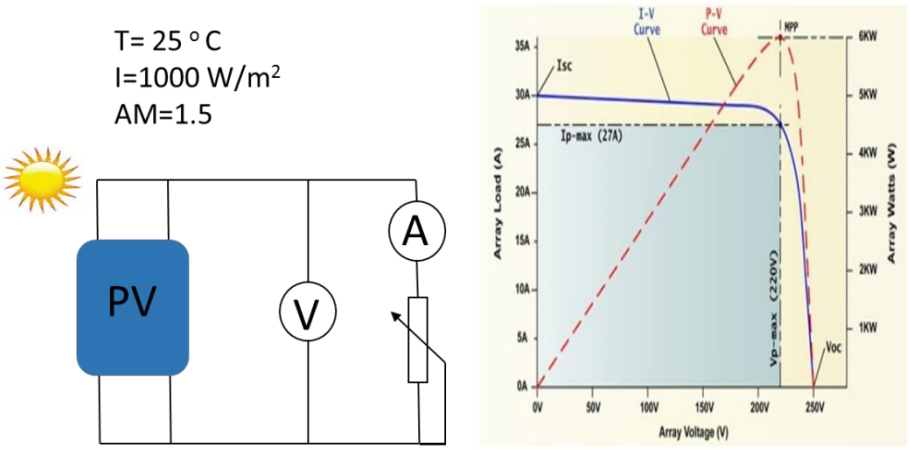

Figure 2.19 The chart of typical I-V measurement system (Ross, 1980)

2.3.2 PV Performance

The performance of PV module is determined by short circuit current, open circuit voltage, maximum output power, fill factor and instantaneous efficiency. In common, short circuit current I_{sc} and open circuit voltage V_{oc}, and the maximum power point (P_{max}) are the three main important parameters presented in I-V curve. The chart of typical I-V measurement system is shown in Figure 2.19 (Ross, 1980).

The fill factor (FF) is indicated how ideal the diode properties are, and calculated by:

$$\mathrm{FF} = \frac{P_{max}}{V_{oc} I_{sc}} \quad \text{(Equation 2. 1)}$$

The PV module performance in terms of SRC is commonly expressed in terms of conversion efficiency. The PV module conversion efficiency η is defined as:

$$\eta = \frac{P_{max}}{E_{in} A} \quad \text{(Equation 2. 2)}$$

Where P_{max} is the measured maximum PV power (W); A is the surface area of solar cell (m^2); E_{in} and is the input solar radiation under SRE (W/m^2).

2.3.3 Factors Affecting Conversion Efficiency

Photovoltaic (PV) technology has been widely used for generating electricity. However, PV modules have low solar to electricity conversion efficiency, less than 20% for commercial PV products. There are many factors that affect the performance of the PV which include the module encapsulating material, thermal dissipation and absorption of material, the maximum power point of module as well as the atmospheric parameter (solar radiation, ambient temperature, and wind speed). However, temperature is a major parameter that has great influence on the behaviours of the electrical efficiency of PV module, shown in Figure 2.20 (Radziemska, 2002).

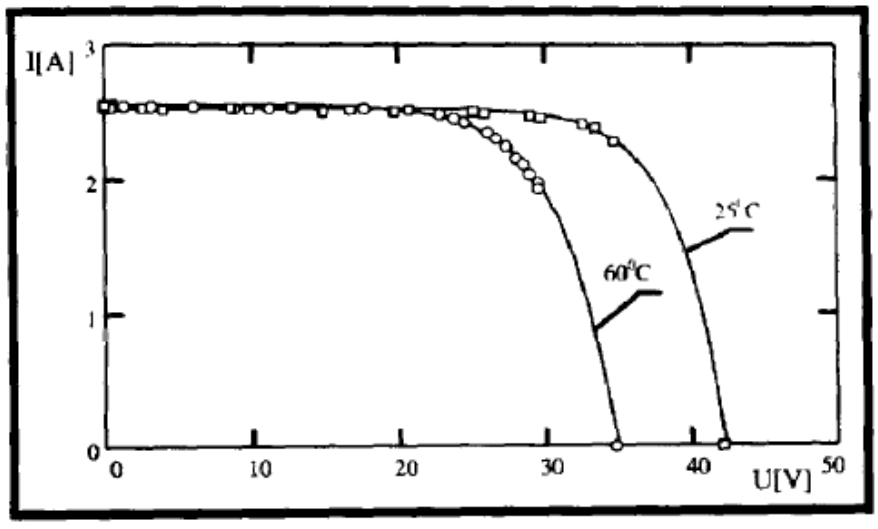

Figure 2.20 Current-voltage characteristics of PV modules at 25°C and 60°C under $830W/m^2$ (Radziemska, 2002)

In common, nominal operating cell temperature (NOCT), which is defined as the mean solar cell junction temperature within an open rack

mounted module in standard reference environment (SRE), indicates the PV module temperature. NOCT is a reference of how the module will work when operating in real conditions. SRE is the standard test conditions of tilt angle at normal incident to the direct solar beam at local solar noon, total solar radiation of 800W/m^2, ambient temperature of 2^{o}C, wind velocity of 1m/s and nil electrical loading.

In order to calculate the module temperature from the NOCT, using the equation that is presented by Ross (1980):

$$\mathrm{T} = T_{air} + (NOCT - 20^o C)\frac{\phi}{800} \quad \text{(Equation 2. 3)}$$

The PV module efficiency depends on the linear relation on solar cell temperature was defined by Sandnes and Rekstad (2002):

$$\eta = \eta_r - \mu(T_c - T_r) \quad \text{(Equation 2. 1)}$$

Where η_r is the efficient when temperature is 25^{o}C ($T_r = 25^o C$).

2.3.4 Photovoltaic/Thermal

Many studies were carried out to investigate the effect of PV cell temperature on the electrical efficiency of PV modules. The results showed that the reduction of PV cell temperature would increase the electrical efficiency (Skoplaki and Palyvos, 2009).

Researchers proposed using air and water as the working fluids to cool PV modules. The heat extracted from the PV modules by air and water was also used for space heating and domestic hot water supplement. Tonui et al. (2007) proposed a suspended thin flat metallic sheet at the middle or fins at the back wall of an air duct as heat transfer augmentations in an air cooled photovoltaic/thermal (PV/T) solar collector to improve its overall performance.

Kumar and Rosen (2011) investigated the performance of a double pass PV/T solar air heater with and without fins. The study showed that the extended fin area reduces the cell temperature considerably from 82^{o}C to 66^{o}C, which leads to a significant improvement on the electrical and thermal efficiencies.

In New Delhi, Dubey et al. (2008) presented a theoretical and experimental investigation on a PV/T solar water heater with different PV module coverage on the absorber. The study indicated that there is a significant increase in the instantaneous efficiency from 33% to 64% due to increase in glazing area.

He et al. (2011) found that the primary energy saving efficiency of a hybrid PV/T solar system under natural circulation of water is about 60~75%, much higher than that of an individual PV plate and a traditional solar collector.

Tiwari et al. (2006) carried out a performance evaluation of hybrid PV/T water/air heating system using four different configurations and found that an overall efficiency of the system for summer and winter conditions is about 65% and 77%, respectively.

Chow et al. (2007) proposed a new design of thermal absorbers with flat box structure. They found that the new type collector has an annual average thermal efficiency of 38.1%.

A new type of PV/T collector with dual heat extraction operation, either with water or with air circulation was developed by Tripanagnostopoulos (2007). Most of the above studies were using air and water for the cooling of PV modules and found water is better than air in terms of PV cooling and energy performance. A few studies proposed the direct

expansion flat plate PV evaporator heat pump system using a refrigerant for cooling PV modules, are shown the detail in next section.

2.4 Heat Pump and Solar Assisted Heat Pump

2.4.1 Heat Pump

The heat pump application is expected to reduce energy consumption and CO_2 emission. IEA Heat Pump Centre (2004) predicted that the electric heat pump requires less fuel than conventional boilers by about 35 to 50%. The Energy White Paper (2003) presented the energy consumption in UK, 2003, as shown in Figure 2.21. It can be seen that 44% of energy consumption can be supplied by heat pumps including hot water (8%), space heating (26%) and process use (10%). In addition, the total reduction of CO_2 emission will attain 5.4% with heat pumps operated in the residential, commercial and industrial sectors (IEA Heat Pump Centre, 2004).

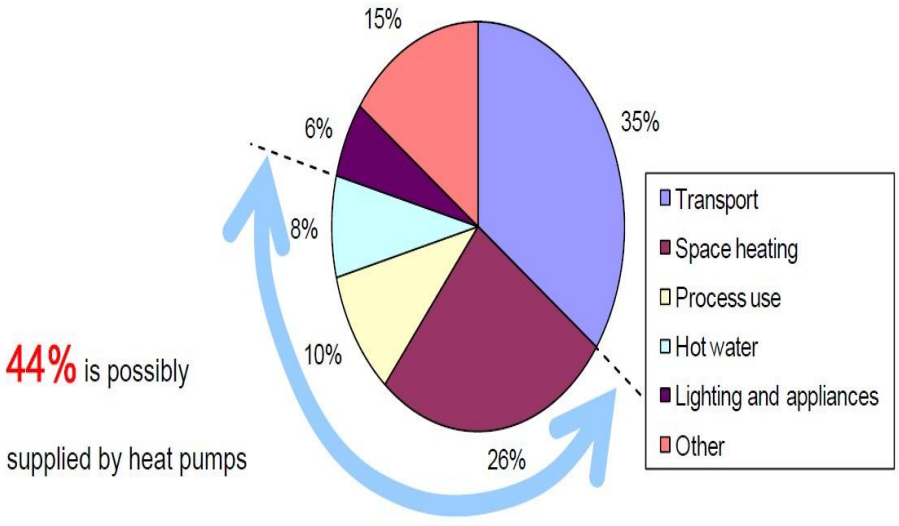

Figure 2. 21 Energy Consumption in UK, 2002 (Energy White Paper, 2003)

Heat pump is a mechanical device. it uses electricity as external power to viable alternative recover heat from different sources to supply

heating energy, cooling energy and both. Because heat pump flexibility provides thermal energy at a required temperature in dependence on the demand all through a year, the device has found applications in a wide variety of areas.

Heat pump system normally consists of four main components: evaporator, compressor, expansion valve and condenser in case of vapour compression type, shown in Figure 2.22. The heat pump system consists of two main loops which are refrigerant loop and loads loop, and are linked by the heat exchanger (condenser) (Herold et al., 1996).

Referring to the refrigerant loop, it is a reverse of the Rankine cycle or the reverse of a Carnot cycle. The cycle of the refrigerant loop requires an electrical energy input (W_{in}) to provide heat from low temperature side (Q_L) to high temperature side (Q_H) as the useful heat (Figure 2.23 (a)). The four processes are illustrated by the Temperature-Entropy (T-s) diagram (Figure 2.23 (b)) and Pressure-Enthalpy (P-h) diagram (Figure 2.23 (c)) in an ideal vapour compression refrigerant cycle (Herold et al., 1996).

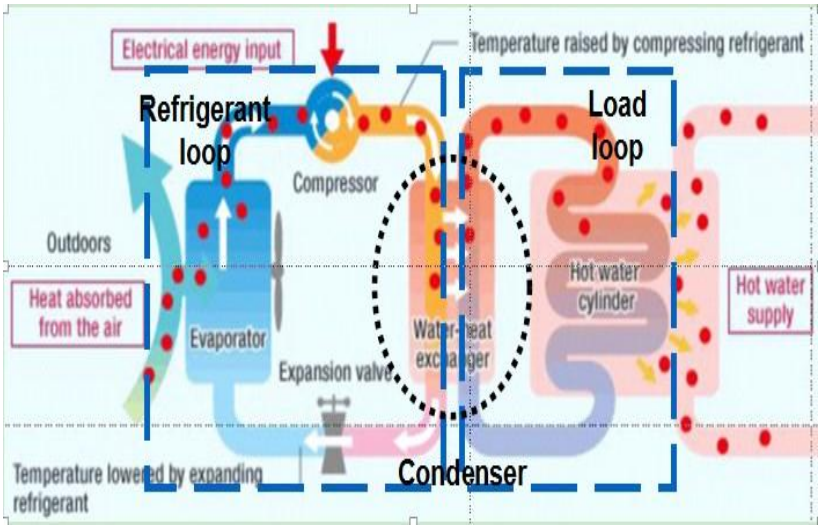

Figure 2. 22 Electricity powered heat pump system (Herold et al., 1996)

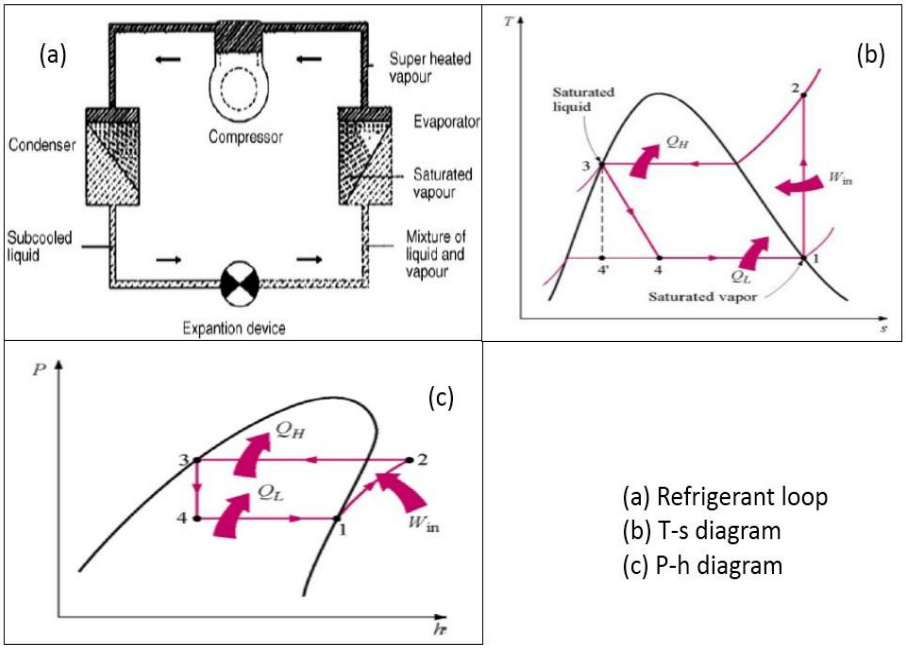

Figure 2. 23 Diagrams of an ideal vapour compression refrigerant cycle (Herold et al., 1996)

In addition, it has the maximum thermal efficiency (COP_{max}) for given temperature limits between evaporator and condenser, shown as (Cantor and Harper, 2011):

$$COP_{max} = \frac{T_H}{T_H - T_L} = \frac{1}{1 - \frac{T_L}{T_H}} \quad \text{(Equation 2. 2)}$$

The COP increases when T_L of evaporator increases. In addition, decreasing the T_H of condenser increases the COP, because heating and cooling are the main objectives of heat pump, decreasing the T_H of condenser is not expected.

The COP of heat pump system depends on many factors, such as the temperature of evaporator, the temperature of delivered useful heat, the working medium used, and the characteristics of components. Among the above mentioned, the temperature of evaporator is the key factor (Pan and Li, 2006).

2.4.2 Performance of ASHP

In general, ASHP is applicable and widely used in building sectors for heating and cooling and could play a significant role in reducing CO_2 emissions because of low cost and simplicity of installation. The most important shortcoming of ASHP is their application in climates where the ambient temperature is low in winter. The capacity of the ASHP decreases sharply when the outdoor temperature deviates greatly from that of mild working conditions. As ambient air temperature (the evaporator fluid inlet temperature) increases, the COP increases, as does the capacity. As the air temperature drops, frost can form on the evaporator coil, which adds heat transfer resistance and blocks airflow. A reverse operation of the heat pump cycle on frequent basis removes the frost (a defrost cycle), but this reduces the capacity and COP of the system. At low ambient temperatures, a heat pump will have inadequate capacity to heat the building, and so a supplemental heat source (often an electric resistance heater) is required.

2.4.3 Solar Assisted Heat Pump System

Since the major drawback of the ASHP is the temperature of evaporator, the frequent defrost of the ASHP evaporator during the operation in cold seasons, a solution is proposed. The hybrid system with a supplementary heat source such as solar energy linked to the evaporator, a configuration has received little attention. In addition, a hybrid energy system combining the use of two or more alternative technologies will help to increase the total efficiency of the system. Therefore, using solar energy as the supplementary source to the heat pump is necessary, which is called solar assisted heat pump system (SAHP).

There are various ways to categorize SAHP. Based on heat transfer fluid, solar assisted heat pump systems can be classified into direct expansion solar assisted heat pump (DX-SAHP) and indirect expansion solar assisted heat pump. The DX-SAHP combines the collector and evaporator into one unit. The refrigerant is directly expanded in the solar collector and undergoes phase change from liquid to vapour by absorbing the solar energy. The advantages of DX-SAHP are higher heat transfer efficiency and lower cost. The indirect SAHP employs a solar collector and a heat pump as separate units. The solar heat collector absorbs the sun radiation by water or air and transfers into heat pump through an intermediate heat exchanger.

Solar assisted heat pump systems also can be classified into solar thermal assisted heat pump (SAHP) and photovoltaic/thermal heat pump system (PV/T-HP). SAHP is the hybrid system that enhances the performance of heat pumps by taking heat from solar energy. PV/T-HP is a hybrid system which integrates of solar collector, PV module, and heat pump together.

2.4.3.1 Application of Solar Assisted Heat Pump System

Although heat pump systems could supply heating and cooling in the same system, Peter and Cornelia (2013) presented that most of the SAHPs are mainly focused on the benefit for all kinds of heating application. The comparison of the application area is shown in Figure 2.24. There are 75% of studies have been attributed to water heating, 19% of studies to space heating and only 1% of studies to space cooling.

Day and Karayiannis (1994) presented Figure 2.25 to show the operation of DX-SAHP in meeting demand for a particular period of time in a day. According to them, the heating and cooling demand could be

met directly when the available energy is highest and the stored energy could be used to assist or provide for small consumption at low solar energy availability.

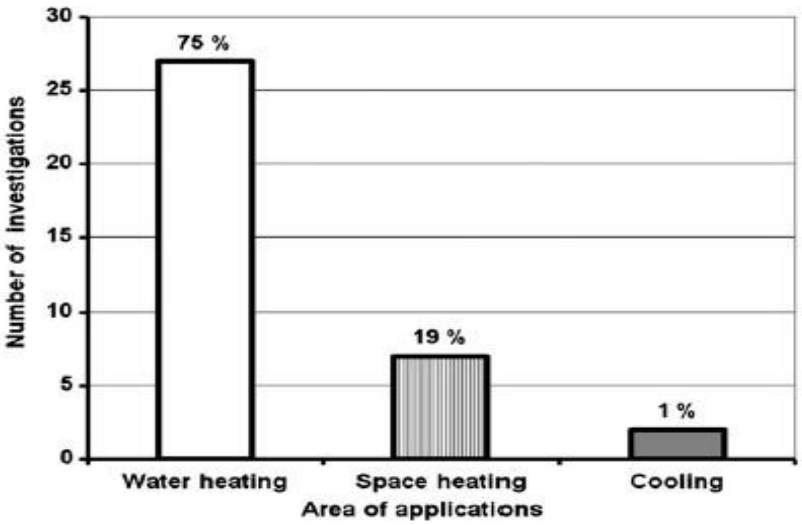

Figure 2. 24 Comparison distribution of DX-SAHP system application area from literatures review (Peter and Cornelia, 2013)

O'Dell et al. (1984) investigated the design method and performance for heating and cooling performance of heat pumps with refrigerant filled solar collectors for heating and cooling applications. The results revealed that the cooling performance of a refrigerant filled collector heat pump is inferior to conventional heat pumps.

Hawlader and Jahangeer (2004) and Hawlader and Jahangeer (2006) investigated SAHP for air conditioning, water heating and drying. The solar collector and evaporator are connected in parallel with individual expansion valves. The air cooled and water cooled condensers are connected in series. The schematic diagrams of SAHP are shown in Figure 2.26 and Figure 2.27, respectively.

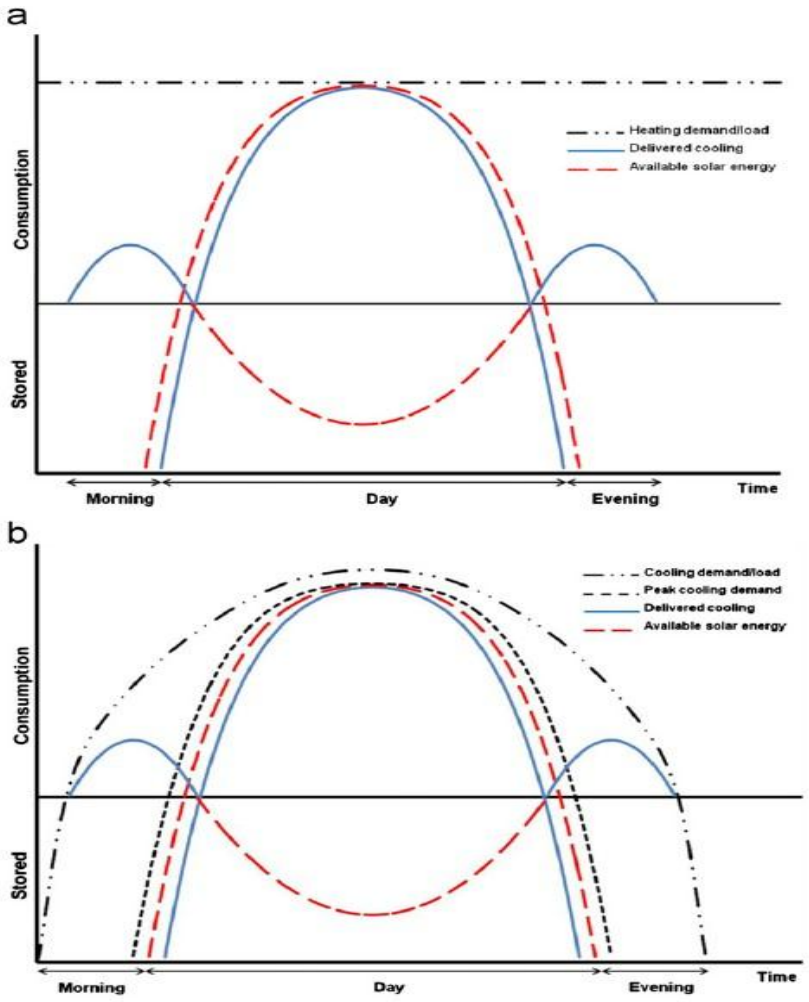

Figure 2. 25 Illustration of operation in meeting demand for a particular day time period (Day and Karayiannis, 1994)

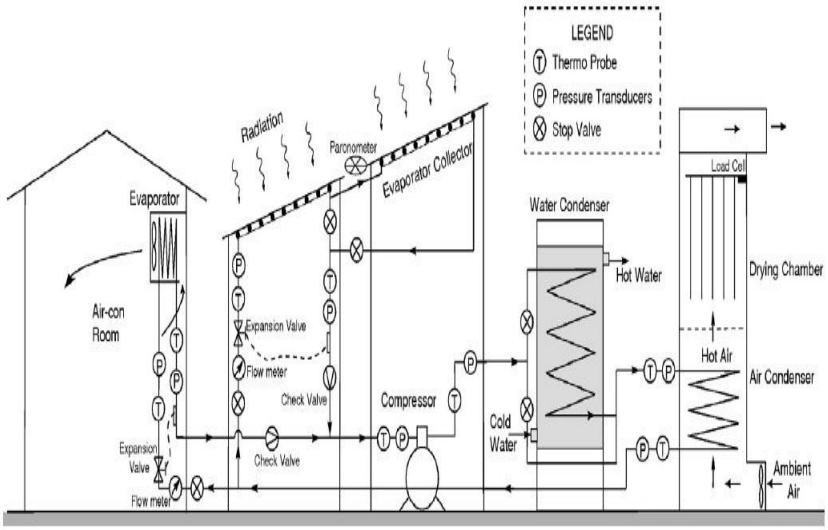

Figure 2. 26 Schematic diagram of SAHP for drying, air conditioning and water heating (Hawlader and Jahangeer, 2004)

Yang et al. (2009) experimentally analysed the characters of the indirect solar multi-function heat pump system. Kuang and Wang (2006) investigated the multi-functional DX-SAHP, shown in Figure 2.28. The obtained COP of heating and cooling is 2.7 and 2.9, respectively. When operates in cooling mode, it stores about 49.5 kW of cold energy with the efficiency of 30%.

Ji et al. (2003) experimentally investigated the multi-functional air conditioning products. The two-functional and three-functional air conditioners are shown in Figure 2.29 and Figure 2.30, respectively. The experimental tests showed that the average COP is 2 when it operates space cooling only, 2.91 when water heating only, 4.02 when both space cooling and water heating.

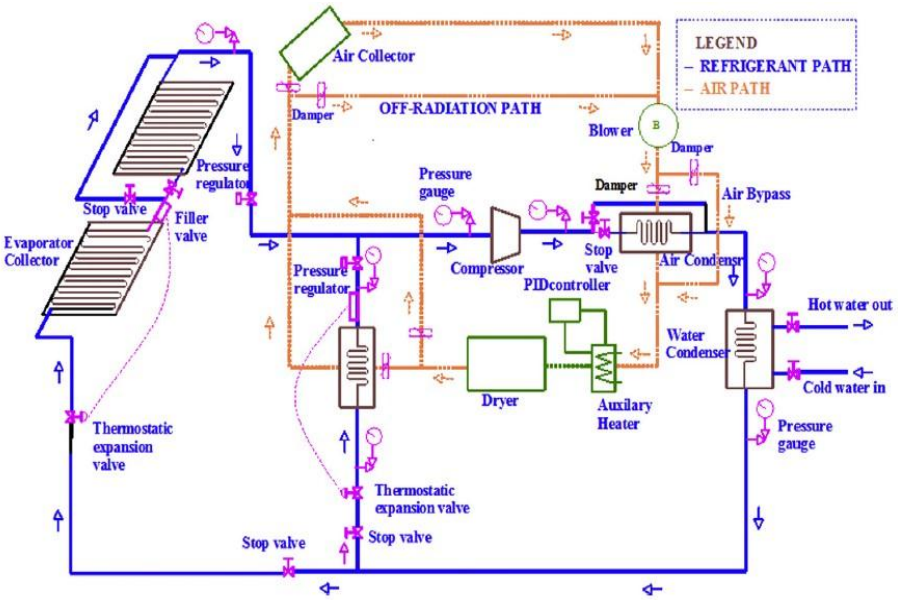

Figure 2. 27 Schematic diagram of SAHP for drying and water heating (Hawlader and Jahangeer, 2006)

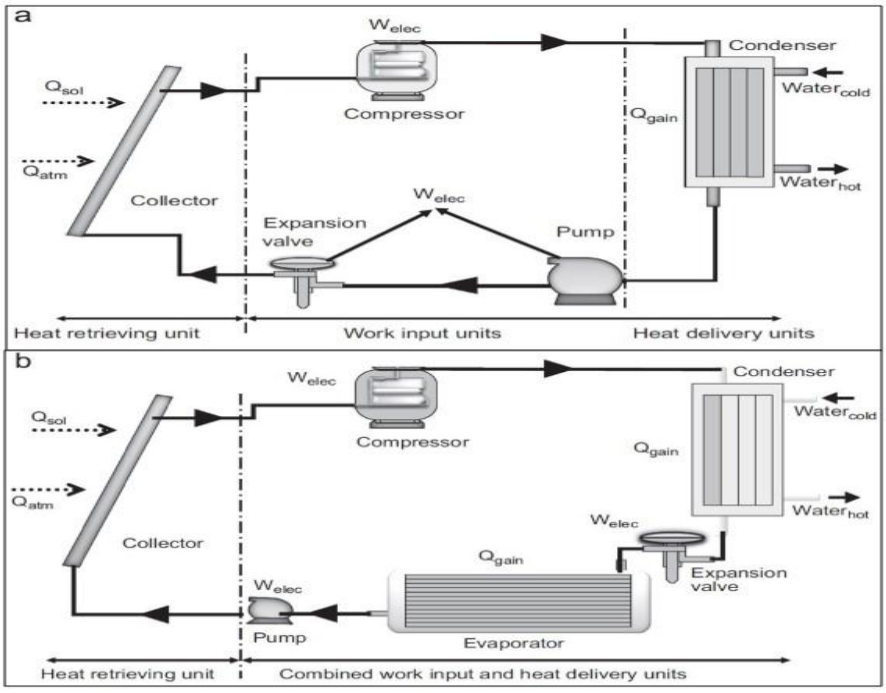

Figure 2. 28 Schematic diagram of DX-SAHP, (a) heating (b) cooling (Kuang and Wang, 2006)

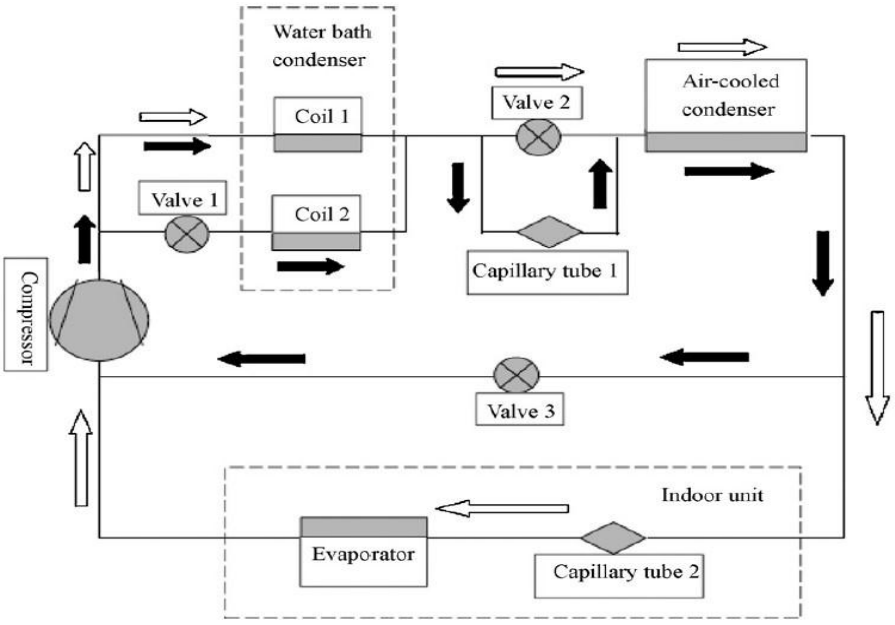

Figure 2. 29 Cycles of the two-functional air conditioning (Ji et al., 2003)

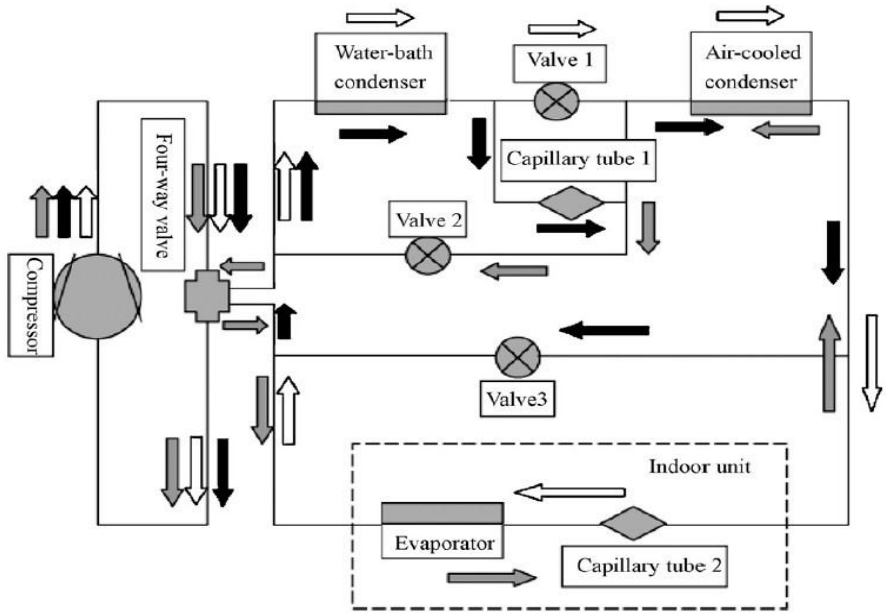

Figure 2. 30 Cycles of the three-functional air conditioning (Ji et al., 2003)

2.4.3.2 Improve COP of Solar Assisted Heat Pump System

Chaturvedi and Abazeri (1987) reported that many parameters affect the performance of solar assisted heat pump systems, which include compressor speed, collector area and slope, storage volume, load temperature, wind speed as well as refrigerant properties. Trilliant et al. (2006) presented the factors which affect the COP include heat exchanger between condenser and evaporator, vapour at the entrance to evaporator, motor efficiency, heat losses, vapour density, ambient temperature, and refrigerant.

Literature review also indicated that the collector-evaporator and the compressor are the common components that are highly influenced by the amount of heat obtained from the heat source (Sporn and Ambrose, 1955). Moreover, the power consumption occurs at the compressor and pumps which the collector-evaporator performance is dependent upon. The influence of the available solar heat on the performance of both the collector evaporator and compressor are highly important (Kuang and

Wang, 2006). Li et al. (2006) also presented the highest exergy loss occurs in the compressor and collector-evaporator based on the exergy analysis for each components.

Compressor speed and efficiency are two main factors in function of raising refrigerant pressure and increasing heating temperature. It is suggested that keeping the compressor at low speed will not only improve COP, it will also prolong the service life span of the compressor (Chaturvedi et al. 1998 & Raisul et al. 2012 & Soldo et al. 2004). The variable frequency compressor is the best choice. Another advantage of achieving higher COP through compressors is the opportunity of reducing the compressor energy consumption. Studies showed that the power consumption of compressor is represented by the empirical functions of the evaporation temperature and water temperature at the condenser (Guoyuan and Xianguo, 2007; Guoyuan and Huixia 2008).

2.4.3.3 Collector/Evaporator

From an engineering point of view, efficiency and reliability should be considered for designing the system. Thus, the design of a collector-evaporator is quite complicated. It is concluded that solar radiation and ambient temperature are the most important parameters that should affect the efficiency of collector and COP of the system. However, their high instability is a concern. Wind velocity and the area of collector have not a great influence on the system performance. Furthermore, fluid mass flow rate and heat losses through designs at the point of conversion should be considered carefully,

Huang and Chyng (2001) showed that a SAHP operates at much more severe condition than a conventional air conditioner, usually at unsteady state, shown in Figure 2.31.

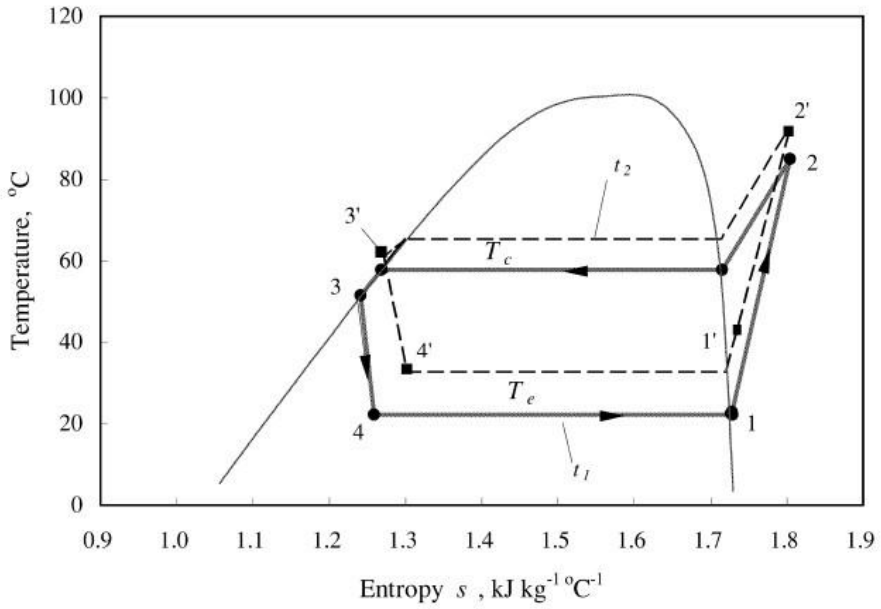

Figure 2. 31 Possible time variation of refrigeration cycle for an ASHP (Huang and Chyng, 2001)

Depending upon the design of the SAHP system, heat may be dissipated to the ambient air from the collector surface if the ambient temperature is lower than the collector temperature. In order to achieve high performance, the evaporating temperature needs to be kept higher than the ambient temperature. Chaturvedi et al. (1980) carried out a theoretical analysis of the SAHP. The results confirmed that the evaporating temperature T_e depends on the solar radiation G and the ambient temperature T_a. Whether a SAHP will operate at $T_e > T_a$, depends on the system match and the weather conditions. Chaturvedi et al. (1980) also presented that a high evaporating temperature will cause a high compressor discharge temperature, which possibly exceeds the allowable temperature limit. Hence, operated at $T_e < T_a$ has an advantage of having lower compressor exhaust temperature and dual heat source from both solar radiation and ambient air. So a proper design of the collector for a specific condition should be important.

Unglazed and glazed flat plate solar collectors are the two major types of collector-evaporator that most employ in SAHP system applications. The use of unglazed and glazed flat plates has been encouraged by its ability to obtain good collector efficiency. Among the two types, it is clear that the unglazed flat plate collector is the most widely used. In the absence of collector covers, heat loss transfer activity is reduced because all available heat absorbed by the plate is transferred to the low temperature flowing fluid. Since solar radiation is the main source by which solar energy is transferred, reducing heat losses through designs at the point of conversion has largely been considered in determining system performance. This main advantage of recovered saving by the collector-evaporator modifications have been cited by many research work for SAHP system applications.

Morrison (1994) investigated the performance of heat pump water heaters with solar boosted evaporators, shown in Figure 2.32. A simulation model in the TRNSYS package was developed for assessing annual performance. He used a packaged heat pump system with a passive evaporator and condenser in the one unit to eliminate parasitic energy consumption of the usual circulating pump and fan coil unit under various weather conditions.

Chaturvedi et al. (1998) developed a variable capacity DX-SAHP for domestic hot water application. The proposed system employs a bare solar collector and variable frequency compressor. This study used the theoretical and experimental analysis, and the collector temperature is maintained $5^{o}C$ -$10^{o}C$ higher than the ambient temperature.

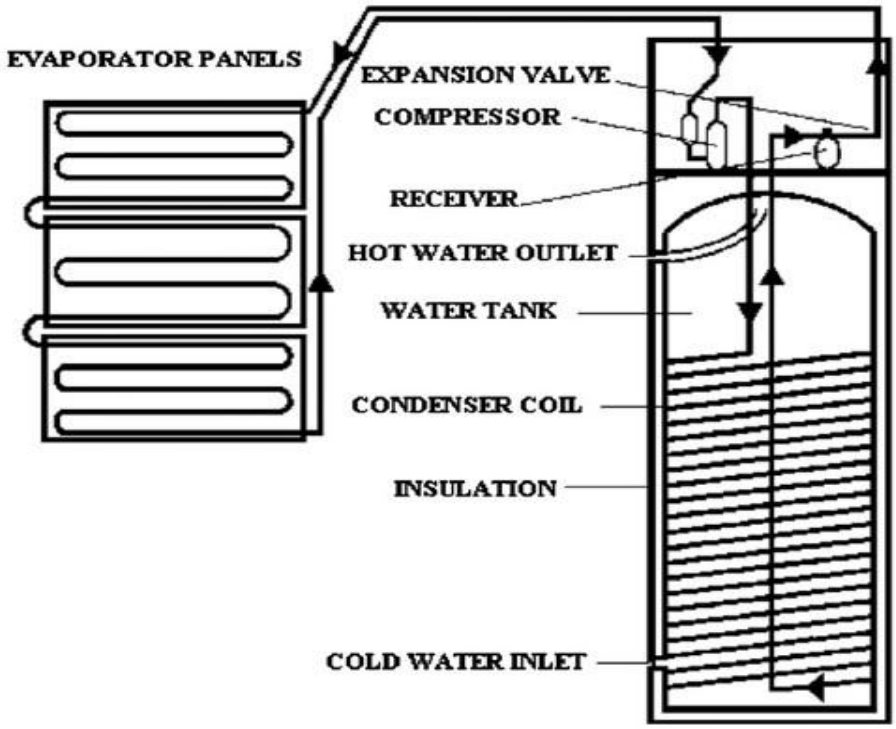

Figure 2. 32 Schematic diagram of a solar boosted (Morrison, 1994)

Ito et al. (1999) designed a SAHP employing an unglazed solar collector as the evaporator, shown in Figure 2.33 and Figure 2.34. During operating period, the evaporating temperature is always higher than the ambient temperature. Electricity consumption of the compressor and COP were defined as functions of evaporation temperature and condenser inlet temperature of the refrigerant. Evaporation temperature was found to be 17^{o}C above the ambient and COP was found to be 5.3, while condenser inlet temperature of the refrigerant was 40^{o}C.

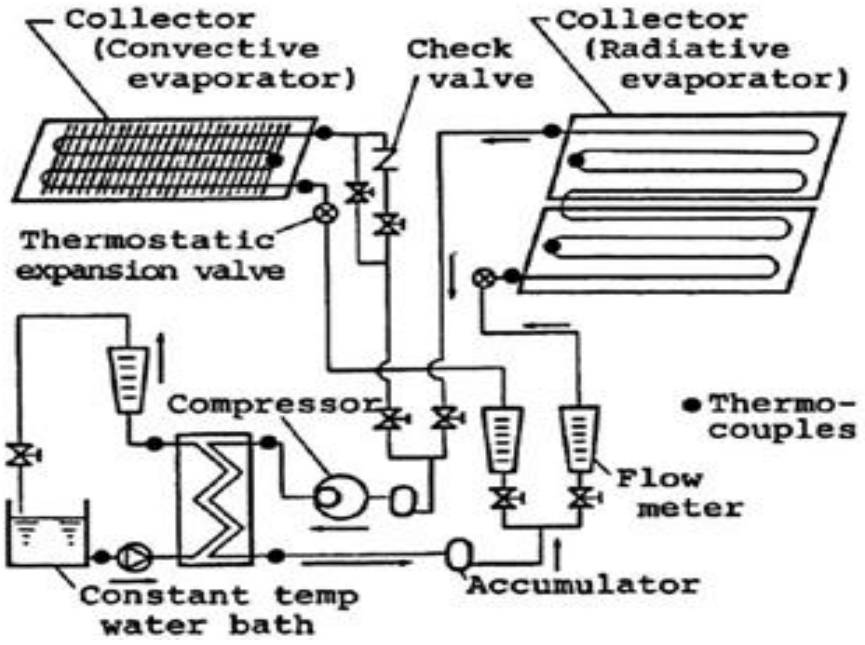

Figure 2. 33 DX-SAHP- combine with two different types of solar collectors acting as evaporator (Ito et al., 1999)

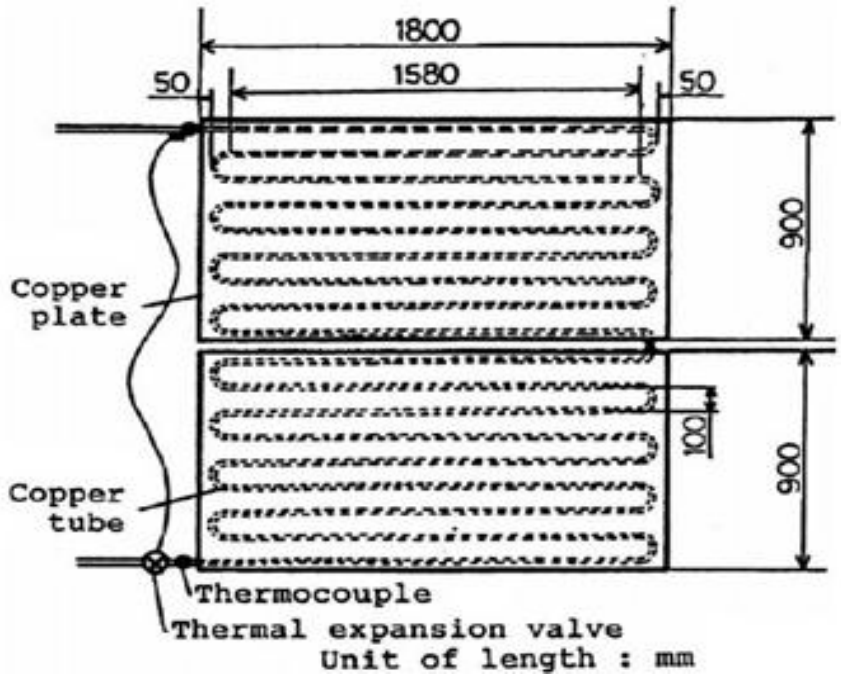

Figure 2. 34 Radiative type of flat plate solar collector (Ito el al., 1999)

Huang and Chyng (2001) presented a 105 litre SAHP using a bare collector (showed in Figure 2.35) and a small R134a reciprocating type compressor with rated input power 250 W. The system operates at

$T_E < T_a$ and with a match condition (near saturated vapour compression cycle and compressor exhaust temperature below 100^{o}C), which is suitable for application in the subtropical area. The COP of the system reaches in the range 2.5 – 3.7 at water temperature between 61^{o}C and 25^{o}C.

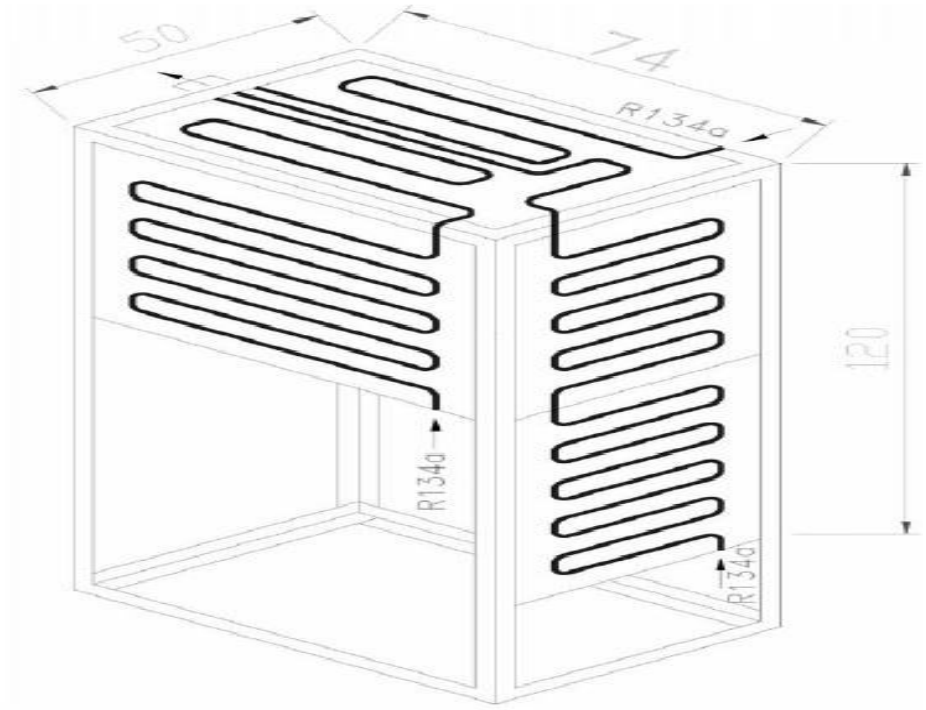

Figure 2. 35 Collector surface design of an SAHP (Huang and Chyng, 2001)

Kong et al. (2011) described a DX-SAHP for domestic hot water during an entire year. The system employs a bare flat plate collector and an electrical rotary type compressor. Based on lumped and distributed parameter approach, the simulation model is developed to predict the thermal performance of the system. The results showed that the effect of wind velocity depends on the relation between temperature of collect plate and ambient air.

2.4.3.4 Other Types of Collector

Many studies were carried out to investigate other tyoes of collectors for SAHPs, such as vacuum tube collectors and finned coil collectors. Krakow and Lin (1983) designed the finned coil collector as the evaporator. The results showed that the output temperature of 2.8^{o}C is above the ambient temperature. Islam et al. (2012) investigated the U-pipe evacuated tube for trans-critical cycle performance on SAHP. The efficiency of collector varies from 50% to 55%.

Saad et al. (2004) presented and analysed a new configuration of a solar assisted heat pump. The system employs a double-tube evaporator. Water is pumped through an inner tube. Refrigerant (R134a) flows in the annular space between the inner and outer tubes. The results showed that the ratio of heat transferred from surrounding air and water to the evaporator double affects the heating evaporator. In addition, the heat delivered by the double effect heating system is significantly higher than other systems. Double-effect heating evaporator collectors energy from various sources when it is installed outdoor: hot water from collector, latent heat released by condenser by condensation on the evaporator, sensible heat gain from atmosphere, and sensible heat gain from rainwater passing over the evaporator.

Chyng et al. (2003) investigated the integral type SAHP, shown in Figure 2.36. The daily total COP ranges from 1.7 to 2.5 depending on seasons and weather conditions year-round. Huang et al. (2005) investigated the heat pipe enhanced SAHP water heater to achieve high energy efficiency. This system uses solar heat pipe collector and heat pump together with dual heat sources, shown in Figure 2.37. The COP of the

novel system is 3.32, which 28.7% of increased conventional heat pump of 2.58.

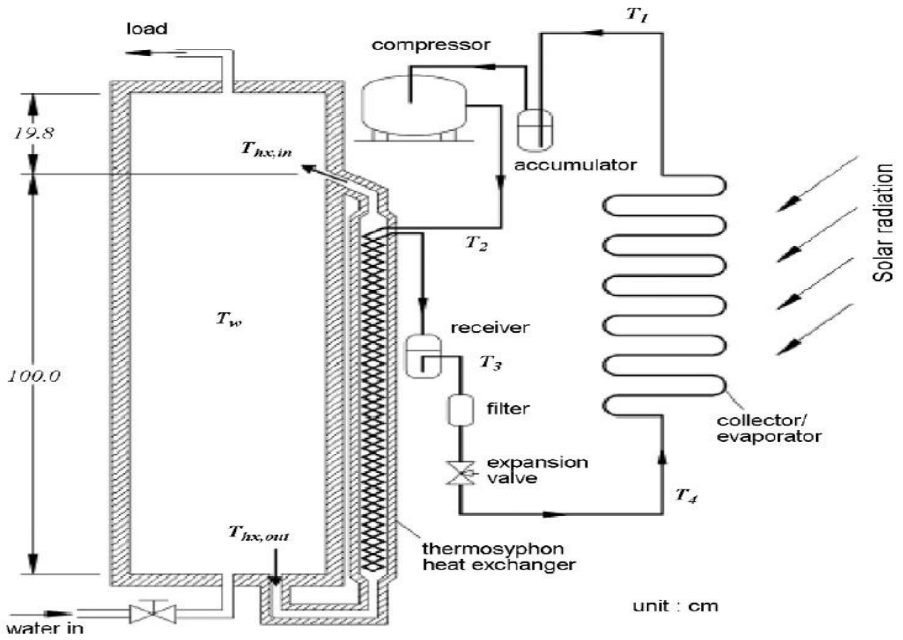

Figure 2. 36 Schematic diagram of integral type SAHP (Chyng et al., 2003)

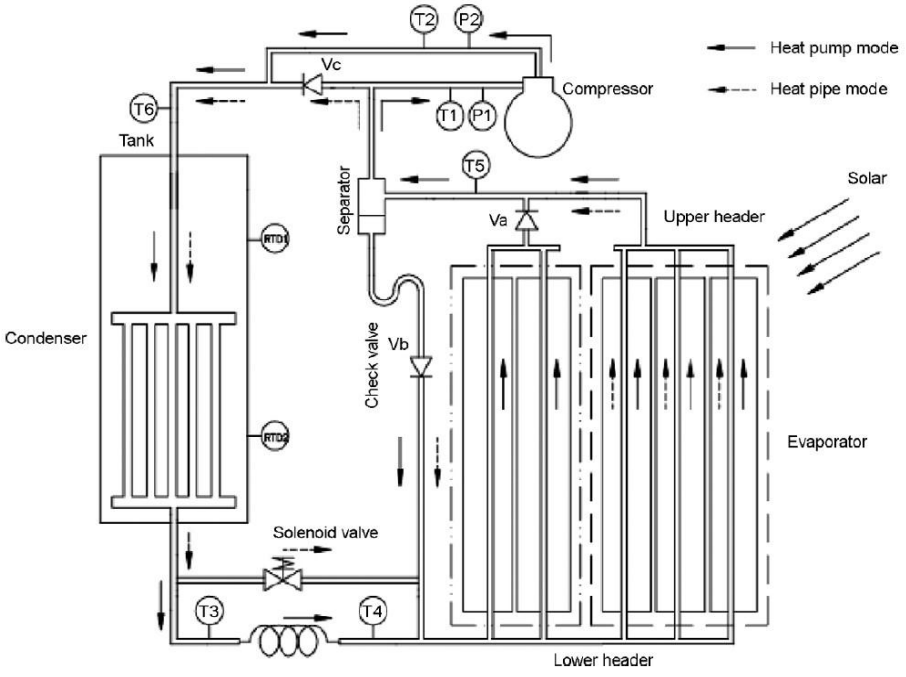

Figure 2. 37 Schematic diagram of heat pipe enhanced SAHP (Huang et al., 2005)

2.4.3.5 PV/T Collector Panel Heat Pump System

PV/T collectors are usually combined with a ground or air source heat pump to adapt building energy needs in heating and cooling demands. Photovoltaic/thermal heat pump system (PV/T-HP) is an effective way, in which low grade heat energy extracted from PV/T collector is upgraded by heat pump system to an appropriate temperature for heating purposes. In addition, the electricity produced by PV panel covers the electrical demands of heat pump. PV/T-HP presents higher total energy conversion efficiency.

Biaou and Bernier (2008) examined zero net energy house (ZNEH) in Montreal and Los Angeles, shown in Figure 2.38. It indicated that heating domestic hot water with thermal solar collectors with an electric backup provided by the PV panel is the best solution for ZNEH.

Gang et al. (2007) investigated the performance of a SAHP combined with photovoltaic modules in a typical climate zones. The results obtained an overall COP of 9.5 because the PV/T-HP presents higher total energy conversion efficiency.

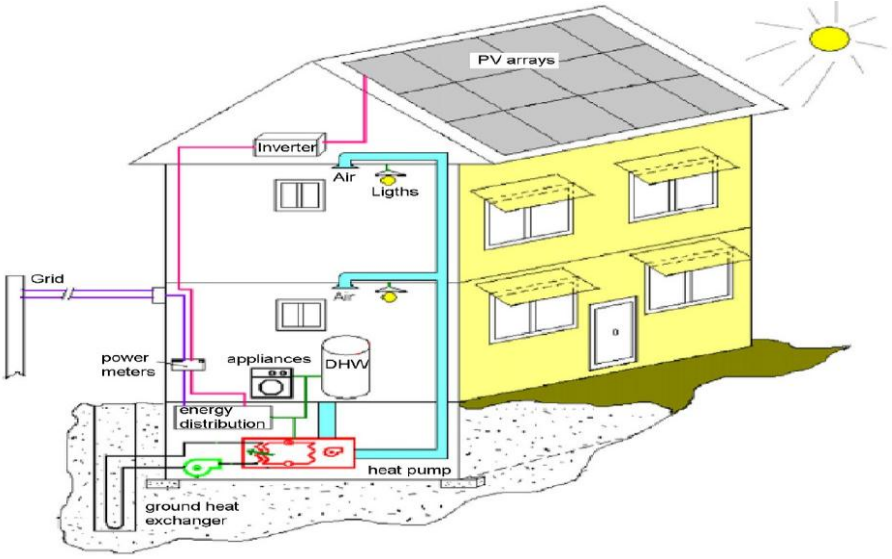

Figure 2. 38 Schematic diagram of ZNEH (Biaou and Bernier, 2008)

A PV/T collector plays an important role in a PV/T-HP system. Fujita et al. (1998) showed the structure of sheet and tube solar thermal collectors with round copper tubes adhered to the back of the absorber copper or aluminium plate in Figure 2.39. Because it is difficult to firmly adhere between the absorber plate and the evaporator tube, large contact heat resistance happens. Fujita et al. (1998) also showed the modified evaporator with aluminium roll bond panels and poly-crystal PV modules bound to surface to make low cost and lightweight. Ito et al. (2005) showed the modified evaporator in order to reduce a large pressure loss for refrigerant flow.

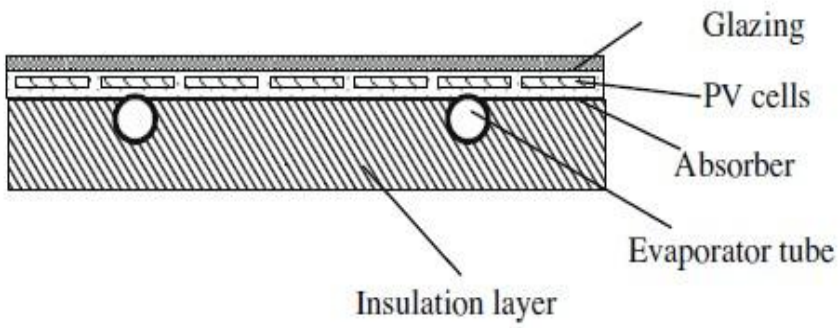

Figure 2. 39 Cross sectional of sheet and tube PV/T evaporator (Fujita et al., 1998)

Ji et al. (2009) developed and numerically studied a new PV/T-HP with a modified collector/evaporator. According to the modified evaporator, portrayed in Figure 2.40, multi-port flat extruded aluminium tubes are directly adhered to the back of absorber by using conductive glue. Refrigerant tubes are arranged in parallel with a spacing of 180 mm, as shown in Figure 2.41. The results showed that the novel system achieves a higher COP for water heating under a typical weather condition in summer.

Ji et al. (2009) showed the structure of PV/T evaporator module in Figure 2.42. A specially designed PV/T evaporator, which is laminated with PV cells on the front surface of the thermal absorber. The results showed that the PV efficiency is up to 12%, which is higher than the performance on the other types of PV/T systems.

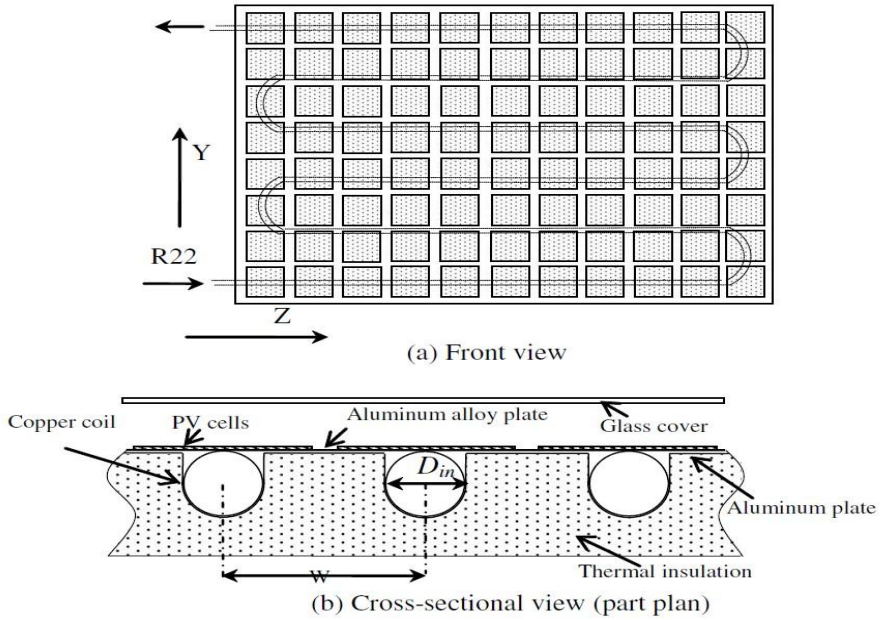

Figure 2. 40 Cross sectional and dimension of modified PV/T evaporator (Ji et al., 2009)

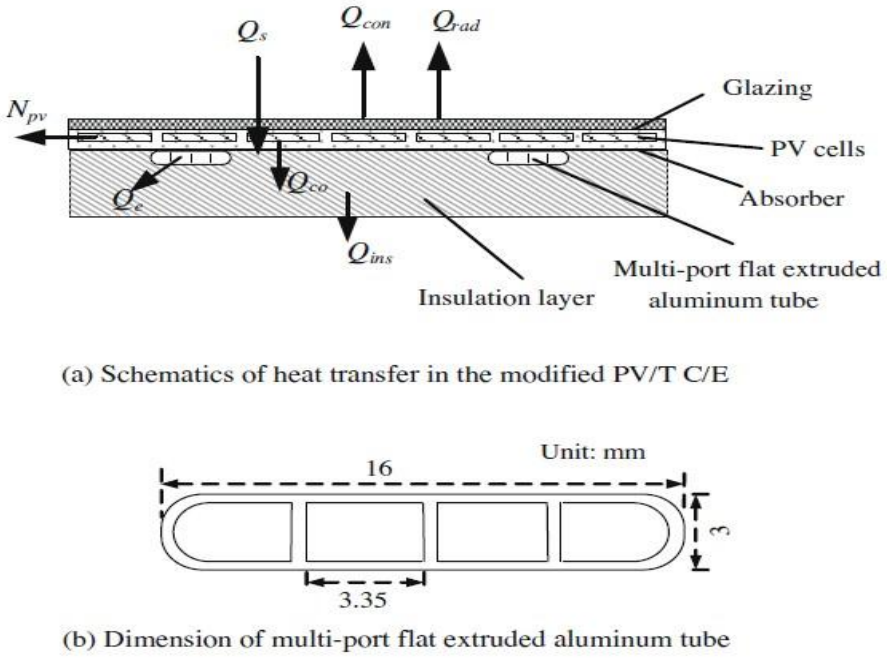

Figure 2. 41 Structure of PV/T evaporator (Xu et al., 2009)

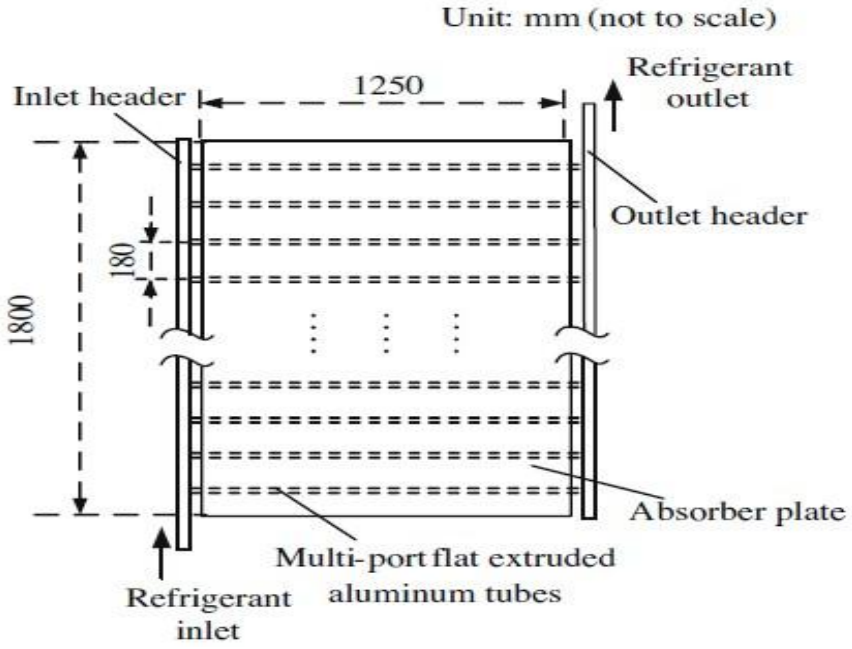

Figure 2. 42 Parallel refrigerant tubes on the back of modified PV/T evaporator (Ji et al., 2009)

Chapter 3 Investigation of Novel Solar Collectors

In this chapter, novel PV/T collector and novel solar thermal collector are presented. Firstly, a specially designed PV/T collector is adopted in the novel system to acquire simultaneously thermal energy and electricity from solar radiation. A dynamic model of the PV/T collector based on the distributed parameter approach is presented. Secondly, a specially designed solar thermal collector is presented and the experimental investigations are detailed.

3.1 Investigation of Photovoltaic/Thermal Collectors

The idea of improving the electrical efficiency, by reducing the photovoltaic collector temperature, as well as taking advantage of the thermal energy produced, constitutes the basic idea in the development of hybrid PV/T collectors. Different working fluids such as air and water have been used for the cooling of PV modules, but the improvement in energy performance has been found to be small.

This section is firstly trying to cool down the PV by incorporating a heat extraction device being a U type copper tube adhered in a copper sheet with refrigerant R134a as a heat transfer medium. The simulation is carried out using TRNSYS before the experiments in order to evaluate how useful it can be as a design tool. The system is experimentally tested in order to evaluate the electrical and thermal efficiency. The results from this section will help to compare the performance of the system and perform as a prophase work that is going to be used in the Chapter 4.

3.1.1 PV/T Collector Panel Description

Figure 3.1 shows a view of the PV/T collector. It consists of 6 glass vacuum tube-PV module-aluminium sheet-U type copper tube (GPAC) sandwiches connected in series. PV cells are made of amorphous silicon. Figure 3.2 shows a cross sectional view of a GPAC sandwich. The aluminium sheet (1 mm) adhered on the back of the PV module (3 mm thick) with thermal glue for good thermal conductance and the PV cells are made of amorphous silicon. The U-type heat exchanger (copper tube of 8 mm diameter, shown in Figure 3.3) is tightly wrapped with the aluminium sheet at two side ends along the copper tube under precise pressure control to provide a good contact between the aluminium sheet and the copper tube. This enables a good heat transfer from the aluminium sheet to the refrigerant. The copper tube pitch is 40 mm. The GPAC sandwich is insulated with a transparent glass vacuum tube (58 mm internal diameter). The total aperture area and PV cell area are 0.42m^2 and 0.383m^2, respectively. The list of the dimension parameters of PV/T evaporator panel are shown in Table 3.1.

The PV/T collector panel acting as evaporator is coupled with a heat pump system. The refrigerant R134a is employed in the PV/T-HP. The small portion of the absorbed solar energy is converted to electricity. The rest of the energy is converted to waste heat, extracted by the refrigerant at the back surface of the PV panel. After the Rankine refrigerant cycle operation, the heat is released later at the condenser. With the low evaporating temperature, it was expected to achieve better cooling effect and better electrical performance of the PV modules.

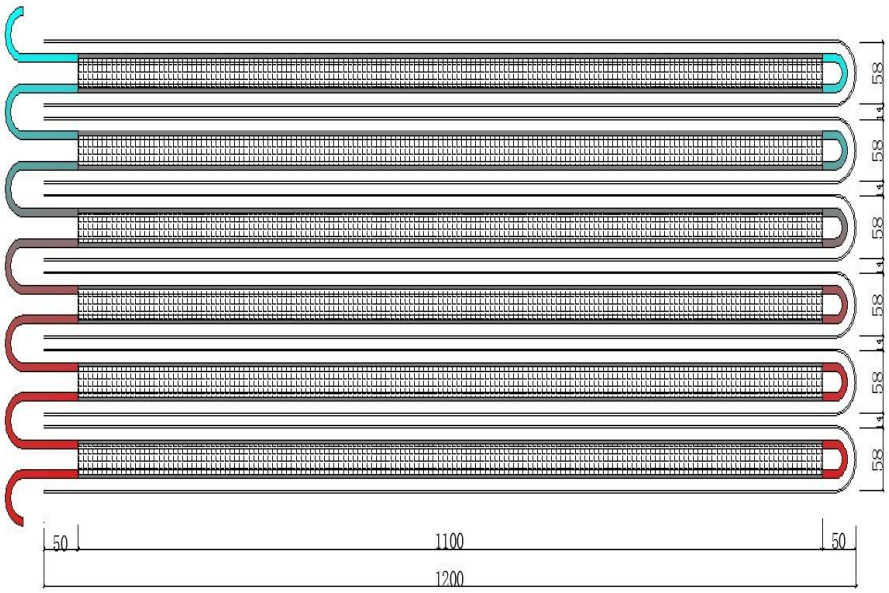

Figure 3. 1Layout of PV/T collector panel

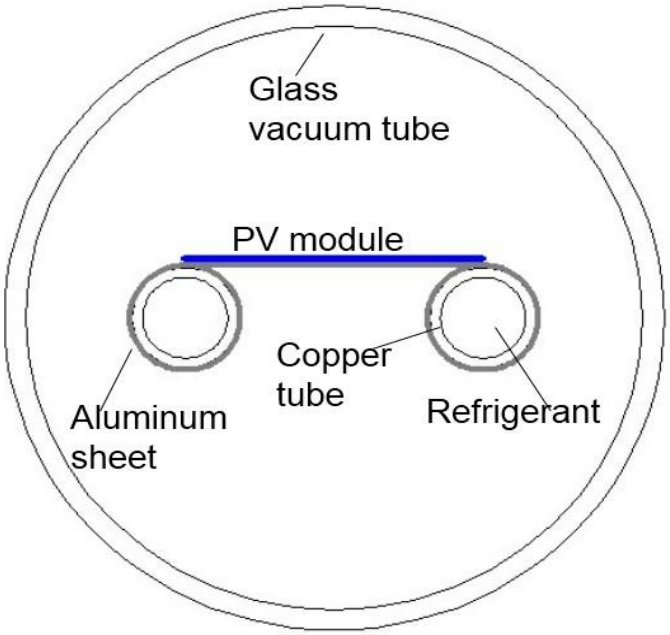

Figure 3. 2 Cross-sectional view of a glass vacuum tube

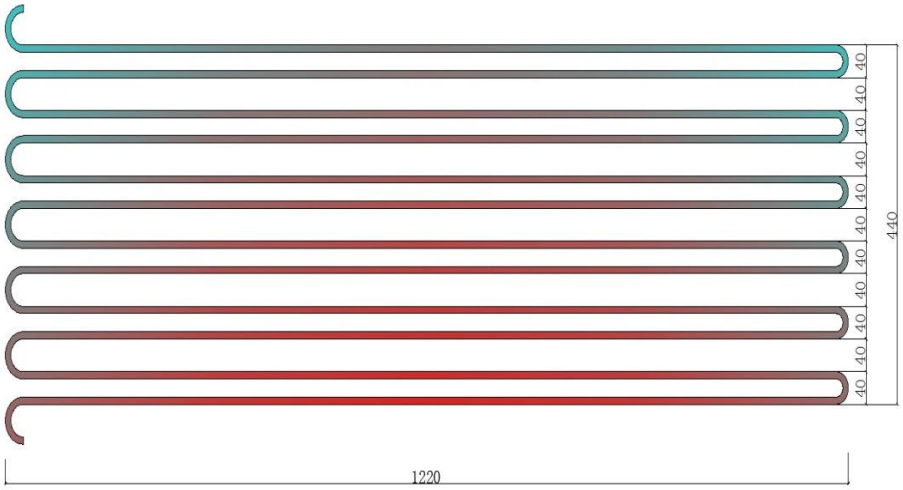

Figure 3. 3 The diagram of U-type heat exchanger

Table 3. 1 The characteristics of PV/T collector

Component	Parameter	(mm)
Solar collector panel	Length	1300
	Width	480
Vacuum glass tube	Diameter	56
	Length	1200
PV module	Length	1100
	Width	40
	Thickness	2
Aluminium sheet	Length	1100
	Width	55
	Thickness	1
Copper tube	External diameter	10
	Internal diameter	8
	Length	1220*6
	Tube pitch	40

3.1.2 Mathematical Model and Simulation of PV/T Collector

The assumptions used in this model are shown as follows:

- The refrigerant flow inside the collector copper tube is one dimension and homogeneous. The liquid and vapour refrigerant have the same average transport velocity.
- The liquid and vapour phase are in saturated thermal equilibrium and the pressure of the liquid and vapour at the same cross section are equal.
- The pressure drop of the PV/T system is neglected.
- For the purpose of the preliminary results, the view factor of the vacuum tube is neglected.

3.1.2.1 Glass Vacuum Tube Model

Figure 3.4 shows the thermal network of the internal vacuum glass tube, and the heat balance at the glass vacuum tube is given by:

$$0 = \beta_g G\left(A_g/2\right) + q_{r,P-g}A_P + q_{r,al-g}A_{al} - q_{r,g-sky}\left(A_g/2\right) - q_{v,g-a}A_g \quad \text{(Equation 3. 1)}$$

Where β_g is the absorptance of glass vacuum tube; G is the solar radiation (W/m^2); A_g is the outer surface area of the glass vacuum tube, m^2; A_P and A_{al} are respectively the area of the PV module and the aluminium sheet, m^2.

The heat radiation from the PV module to glass vacuum tube (W/m^2) is given by:

$$q_{r,P-g} = \varepsilon_P \sigma (T_P^4 - T_g^4) \quad \text{(Equation 3. 2)}$$

Where ε_P is the emittance of PV module; σ is the Stefan-Boltzmann constant; T_P and T_g are the temperature (K) of PV module and glass vacuum tube, respectively.

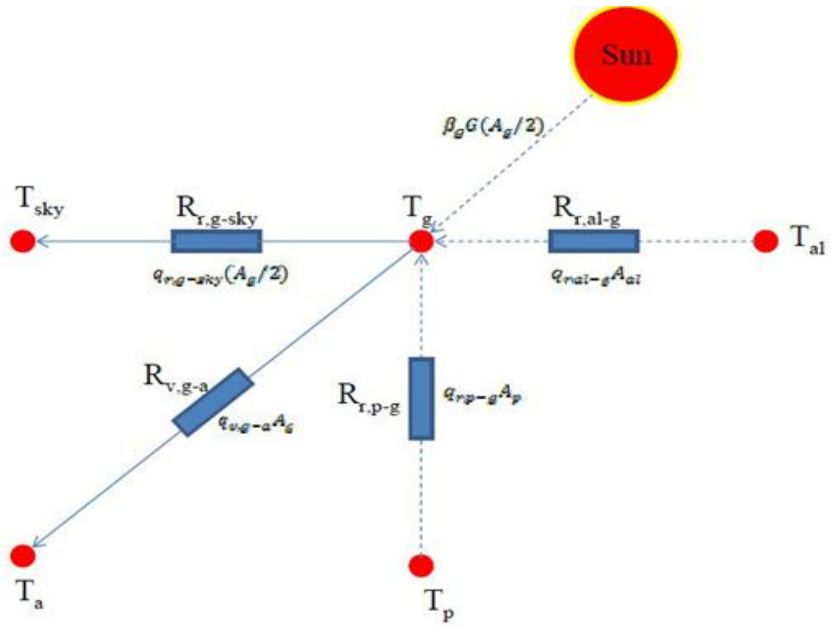

Figure 3. 4 The thermal network of the internal vacuum glass tube.

The heat radiation from the aluminium sheet to glass vacuum tube (W/m^2) is given by:

$$q_{r,al-g} = \varepsilon_{al}\sigma(T_{al}^4 - T_g^4) \quad \text{(Equation 3. 3)}$$

Where ε_{al} is the emittance of aluminium sheet; T_{al} is the temperature (K) of aluminium sheet.

The heat radiation from glass vacuum tube to sky (W/m^2) is given by:

$$q_{r,g-sky} = \varepsilon_g\sigma(T_g^4 - T_{sky}^4) \quad \text{(Equation 3. 4)}$$

Where T_{sky} is the background sky temperature (K) with a function of ambient temperature T_a:

$$T_{sky} = 0.0552T_a^{1.5} \text{ (Equation 3. 5)}$$

The heat convection from glass vacuum tube to ambient air (W/m^2) is given by:

$$q_{v,g-a} = \alpha_{g-a}(T_g - T_a) \quad \text{(Equation 3. 6)}$$

Where α_{g-a} is the convectional heat transfer coefficient between glass vacuum tube and ambient air (W/m^2 K), which is a function of wind velocity.

According to Duffie and Beckman (1991),

$$\alpha_{g-a} = 2.8 + 3.0 v_{wind} \quad \text{(Equation 3. 7)}$$

Where v_{wind} is the wind velocity.

3.1.2.2 PV Module Model

Figure 3.5 shows the thermal network of the PV module, and the heat balance equation at PV module is given by:

$$0 = A_P(\beta\tau)_P G f_P + G(\beta\tau)_{bp}(1 - f_P)A_P - A_P E - A_P q_{d,P-al} - q_{r,P-g} A_P \quad \text{(Equation 3. 8)}$$

Where $(\beta\tau)_P$ and $(\beta\tau)_{bp}$ are the effective absorptance of the solar cells and base plate, respectively.

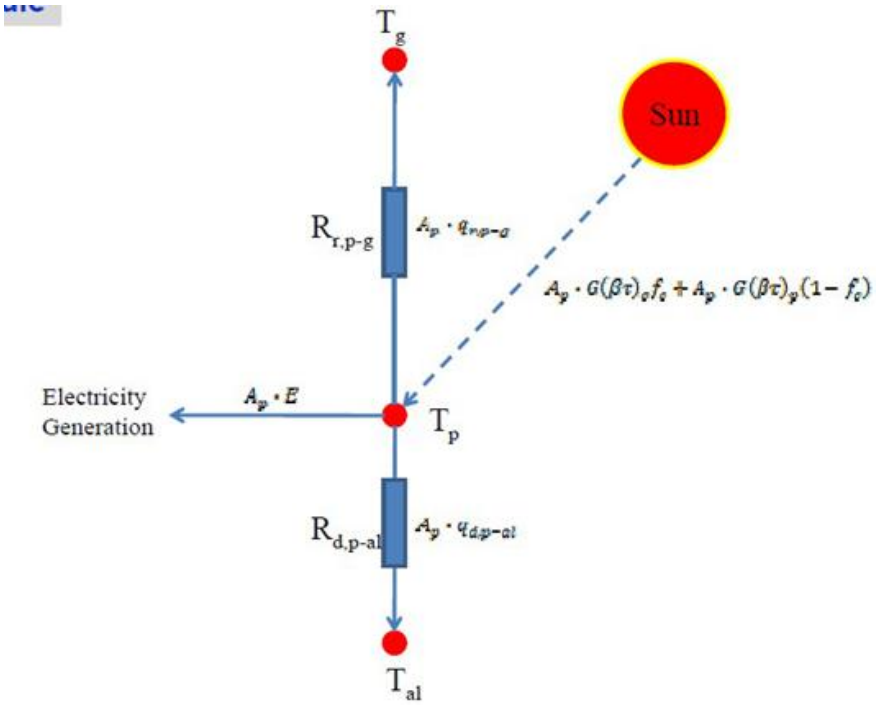

Figure 3. 5 The thermal network of the PV module

According to Duffie and Beckman (1991),

$$(\beta\tau)_P = \frac{\tau_g \tau_P \beta_P}{1-(1-\beta_P)R_g} \quad \text{(Equation 3. 9)}$$

$$(\beta\tau)_{bP} = \frac{\tau_g \tau_P \beta_{bp}}{1-(1-\beta_{bP})R_g} \quad \text{(Equation 3. 10)}$$

Where τ_g is the transmittance of glass vacuum tube considering only absorptance loss and τ_P is the transmittance of PV module considering only reflection loss; β_P and β_{bp} are the absorptance of solar cells and base plate, respectively; R_g is the diffuse reflectance of glass vacuum tube.

The heat conduction from the PV module to the aluminium sheet (W/m^2) is given by:

$$q_{d,P-al} = \frac{(T_P - T_{al})}{\frac{\delta_P}{2\lambda_P} + \frac{\delta_{al}}{2\lambda_{al}}}$$ (Equation 3. 11)

Where δ_P and δ_{al} are the thickness of the PV module and the aluminium sheet, respectively (m); λ_P and λ_{al} are the heat conductivity of the PV module and the aluminium sheet, respectively (W/m K).

The electricity production (W) is given by:

$$\mathrm{E} = \eta_P f_P (\beta\tau)_P G$$ (Equation 3. 12)

Where η_P is the temperature dependent electrical efficiency of solar cell (PV module), and is given by

$$\eta_P = \eta_{rc}[1 - \beta(T_P - T_{rc})]$$ (Equation 3. 13)

Where η_{rc} is the reference electrical efficiency (0.15) at the reference operating temperature T_{rc} (298K); β is the temperature coefficient (0.0045) (ji, et al., 2009); f_P is the ratio of solar cell area to PV module area.

3.1.2.3 Aluminium Sheet Model

Figure 3.6 (a) shows the thermal network of aluminium sheet modules. The heat balance equation at aluminium sheet module is given by:

$$0 = q_{d,bP-al} A_P - q_{d,al-co} A_{al-co} - q_{r,al-g} A_{al}$$ (Equation 3. 14)

Where A_{bp} and A_{al} are the areas of solar cell base plate and aluminium sheet (m^2);

A_{al-co} is the contact area between aluminium sheet and copper tube (m^2), which is given by:

$$A_{al-co} = 2(\frac{3}{4} \times \pi d_{e,co} L_{bp}) \quad \text{(Equation 3. 15)}$$

Where $d_{e,co}$ is the external diameter of the copper tube (m); L_{bp} is the length of solar cell base plate (m).

The heat conduction from aluminium sheet to the copper tube (W/m^2) is given by:

$$q_{al-co} = \frac{(T_{al} - T_{co})}{\frac{\delta_{al}}{2\lambda_{al}} + \frac{\delta_{co}}{2\lambda_{co}}} \quad \text{(Equation 3. 16)}$$

Where T_{co} is the temperature of copper tube (K); δ_{co} is the thickness of copper tube (m); λ_{co} is the thermal conductivity of copper tube (W/m K).

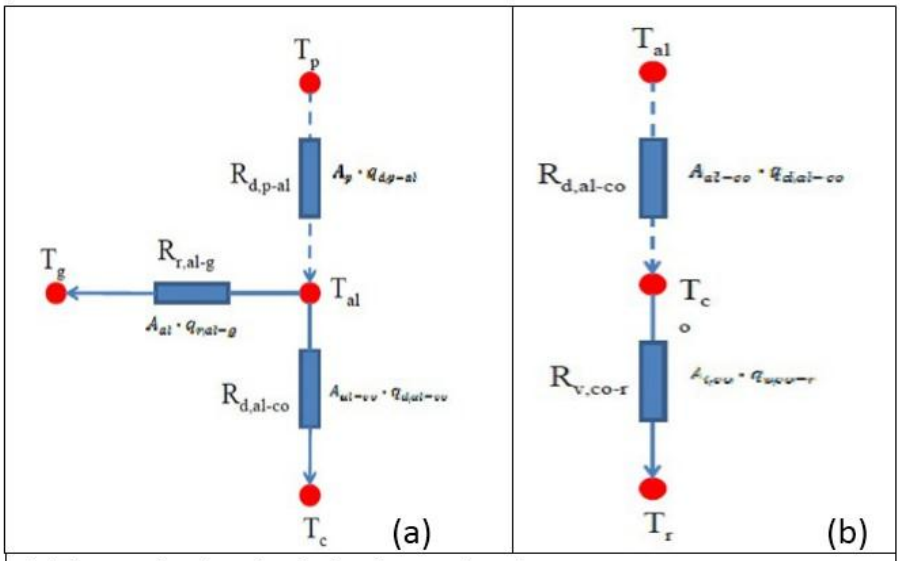

(a)Thermal network of aluminum sheet
(b) Thermal network of copper tube

Figure 3. 6 The thermal networks of the aluminium sheet and copper tube

3.1.2.4 Copper Tube Model

Figure 3.6 (b) shows the thermal network of the copper tube module. The heat balance equation at copper tube module is given by:

$0 = q_{d,al-co}A_{al-co} - q_{v,co-r}A_{i,co}$ (Equation 3. 17)

Where $A_{i,co}$ is the internal surface area of the copper tube (m^2), and is given by:

$A_{i,co} = \pi d_{i,co}L_{co}$ (Equation 3. 18)

Where $d_{i,co}$ is the internal diameter of copper tube (m); L_{co} is the length of copper tube (m).

The heat convection (W/m^2) from copper tube to the refrigerant is given by:

$q_{v,co-r} = \frac{(T_{co}-T_r)}{\frac{1}{\alpha_r}+\frac{\delta_{co}}{2\lambda_{co}}}$ (Equation 3. 19)

Where T_r is the temperature of the refrigerant (K); α_r is the convective heat transfer coefficient between copper tube and refrigerant (W/m·K), which is given by:

For single phase flow:

$\alpha_r = 0.023\frac{Re^{0.8}Pr^{\alpha}\lambda_r}{d_i}$ ($\alpha = 0.3$ for liquid, $\alpha = 0.4$ for vapour)

(Equation 3. 20)

For two phase flow:

$\alpha_r = \alpha_L[(1-x)^{0.8} + \frac{3.8x^{0.76}(1-x)^{0.04}}{Pr^{0.38}}]$ (Equation 3. 21)

Where x is the average dryness fraction of the refrigerant.

$\mathrm{Pr} = \frac{\mu_r Cp_r}{\lambda_r}$ (Equation 3. 22)

$\mathrm{Re} = \frac{\rho_r v_r d_{i,co}}{\mu_r}$ (Equation 3. 23)

3.1.2.5 PV/T Collector Panel

The heat balance equation at the refrigerant is given by:

$A_{i,co}\mathrm{d}q_{v,co-r} - m_r dh_r = 0$ (Connect in series) (Equation 3. 24)

$6A_{i,co}\mathrm{d}q_{v,co-r} - m_r dh_r = 0$ (Connect in parallel) (Equation 3. 25)

Where m_r is the mass flow rate of refrigerant (kg/s); dh_r is the infinitesimal segment of refrigerant enthalpy difference between inlet and outlet of copper tube (J/kg).

3.1.2.6 Numerical Simulation

The simulation model of the PV/T collector is carried out using TRNSYS and then presents the results, shown in Figure 3.7.

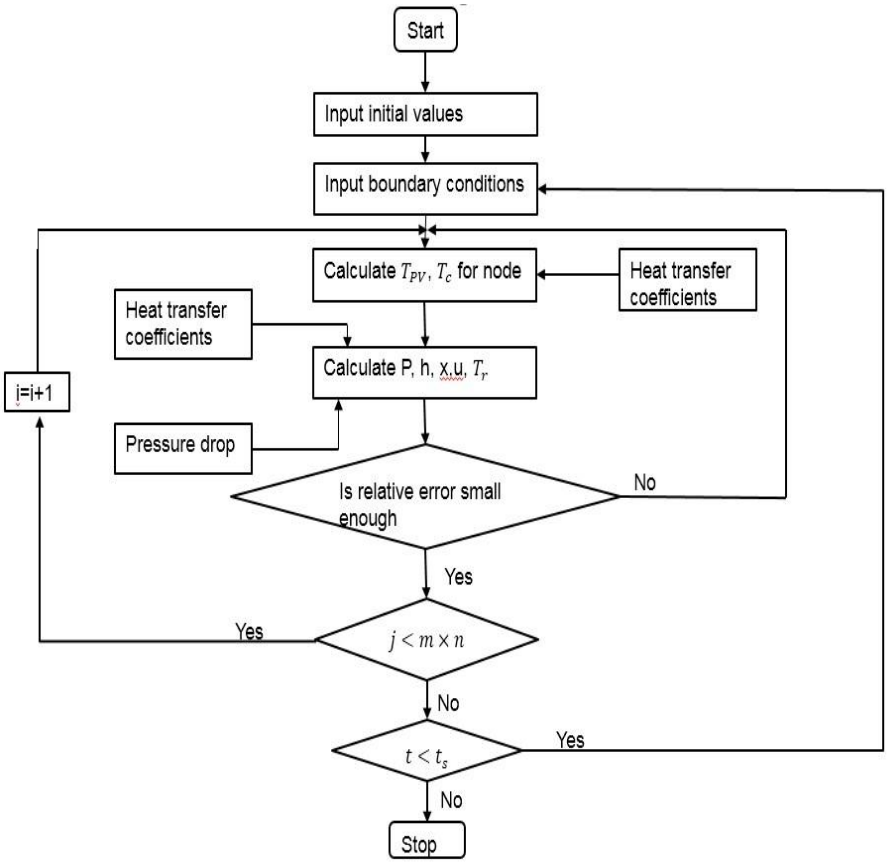

Figure 3. 7 Flow diagram of simulation model

3.1.3 Experimental Study of PV/T Collector

3.1.3.1 Layout of the Testing Rig

The 6 PV modules (made of amorphous silicon) in parallel are connected to an electronic circuit in order to evaluate the electrical parameters. The experimental rig is shown in Figure 3.8. The main components of the electronic circuit are composed of rheostat, current

shunt, resistances and data logger. The rheostat (0~250 Ω) is regulated to measure the power output under different load. The current shunt is used to measure the circuit current. Since the voltage of PV modules is about 10 V, which is out of the voltage range of data logger (2.5 V), two resistances (100 KΩ and 10 KΩ) in series are connected to the rheostat in parallel for the testing of voltage output. The power output is calculated with the tested voltage and current outputs.

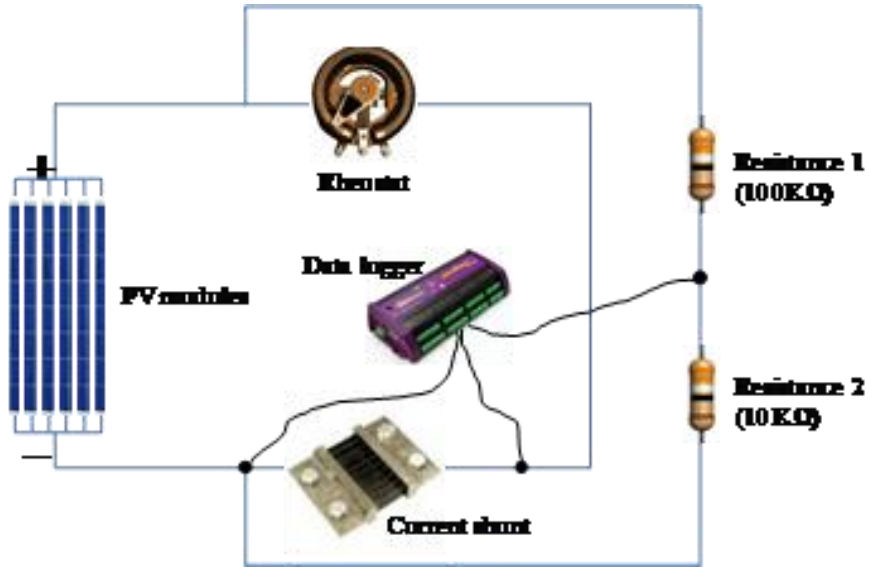

Figure 3. 8 The schematic diagram of the electric circuit for power testing

3.1.3.2 Performance of PV/T Collector

The heat gain of the PV/T collector is measured by means of the amount of heat carried away in the refrigerant passing through it, which is given by:

$$Q = m_r C_r (T_{out} - T_{in}) \quad \text{(Equation 3. 26)}$$

Where m_r is the refrigerant mass flow; C_r is the specific heat of refrigerant; T_{in} and T_{out} are the temperature at the inlet and outlet of the PV/T collector panel, respectively.

The electrical efficiency of the PV modules is given by:

$$\eta_P = \frac{E}{A_P(\beta\tau)_P G}$$ (Equation 3. 27)

Where E is the electricity generation; G is the solar radiation; A_P is the area of PV cells; $(\beta\tau)_P$ is the effective absorptance of PV cells,

$$(\beta\tau)_P = \frac{\tau_a\tau_\rho\beta_P}{1-(1-\beta_P)R_g}$$ (Equation 3. 28)

Where τ_a is the transmittance of glass vacuum tube considering only absorptance loss and τ_ρ is the transmittance of glass vacuum tube considering only reflection loss; β_P is the absorptance of PV cells; R_g is the diffuse reflectance of glass vacuum tube.

The thermal efficiency of the PV modules is expressed as:

$$\eta_t = \frac{Q-W_{in}}{A_P(\beta\tau)_P G}$$ (Equation 3. 29)

3.1.4 Performances of PV/T Collector

3.1.4.1 Solar Radiation and Ambient Temperature

The climatic data is obtained from the British Atmospheric Data Centre, and includes monthly average horizontal solar radiation and ambient temperature. In addition, the horizontal solar radiation is converted to that on a tilted surface with an angle of 30^o for calculation. Figure 3.9 shows the ambient temperature and monthly average solar radiation on tilt surface with an angle of 30^o. According to the Figure that the monthly average solar radiation is low from October (187.5 W/m^2) to March (241.8 W/m^2). The lowest month is December, with only 65 W/m^2 of the solar radiation. From April to August, the solar radiation fluctuates slightly between 300 W/m^2 and 330 W/m^2. The annual average solar radiation is 223 W/m^2 in the south facing. From this we can see that the ambient temperature is low from November (6.8^{o}C) to April (7.1^{o}C). The lowest temperature is 3.7^{o}C in January. From May to September, the

ambient temperature is up to 10^{o}C. From June to September, ambient temperature fluctuates slightly between 13.5^{o}C and 16.8^{o}C. The annual average ambient temperature is 9. 4^{o}C.

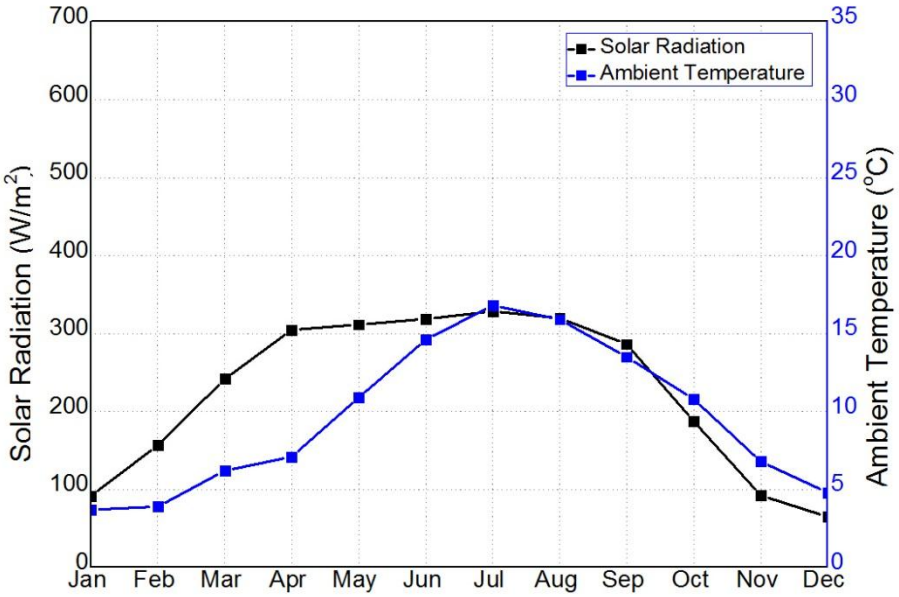

Figure 3. 9 Variation of solar radiation and ambient temperature whole year

Figure 3.10 shows the ambient temperature and solar radiation on tilted surface with an angle of 30^{o} on a typical day in Nottingham. The climatic data are obtained from the British Atmospheric Data Centre. The solar radiation is low from 6:00 (92.4 W/m^2) to 8:00 (297.5 W/m^2), and 16:00 (287.6 W/m^2) to 18:00 (83.8 W/m^2). From 8:00 to 16:00, the solar radiation fluctuates between 297.5 W/m^2 and 628.7 W/m^2. The average solar radiation is 461.68 W/m^2 in the south facing. The ambient temperature is low from 6:00 (11.2^{o}C) to 16:00 (18.2^{o}C). The annual average ambient temperature is 15.8^{o}C.

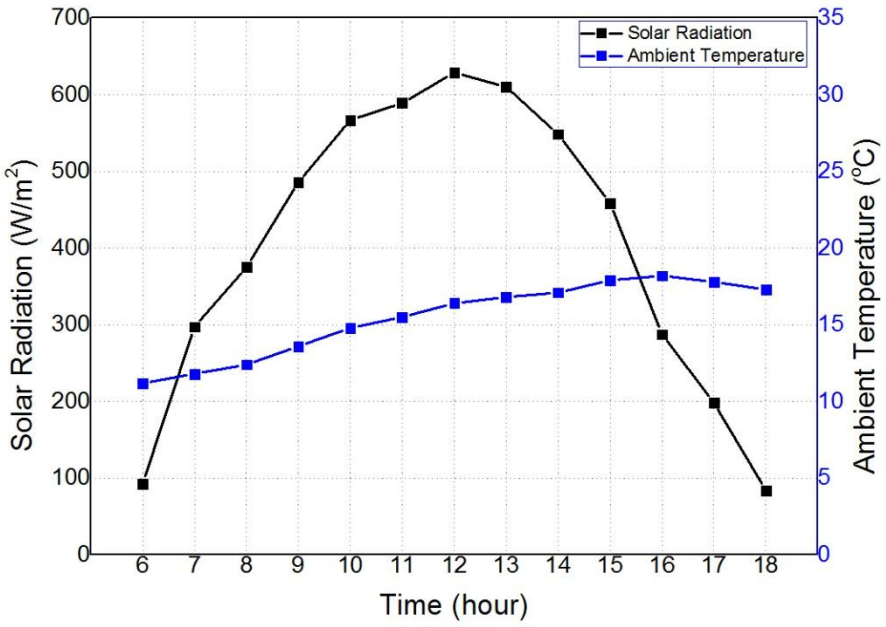

Figure 3. 10 The ambient temperature and solar radiation on a typical day

3.1.4.2 Area Affect the Performance of PV/T Collector

In order to investigate the performance of PV/T collector panels, the effects of PV/T collector area are investigated. Figure 3.11 shows the temperature of the PV cell at different PV/T collector areas. Based on this, we know the temperature increases with the increasing PV/T collector area. The temperatures increase in the morning and reach the peak value at 12:00 noon, then gradually decrease. The trend is same as solar radiation.

Figure 3.12 shows the heat gain of PV/T-HP at different PV/T collector areas. From the Figure, we can see that the heat gain increases with the increasing PV/T collector area, and with the same trend of solar radiation. That is because solar radiation has the great effect on the heat gain of the system. The heat gain increases with the increasing solar radiation, and vice versa.

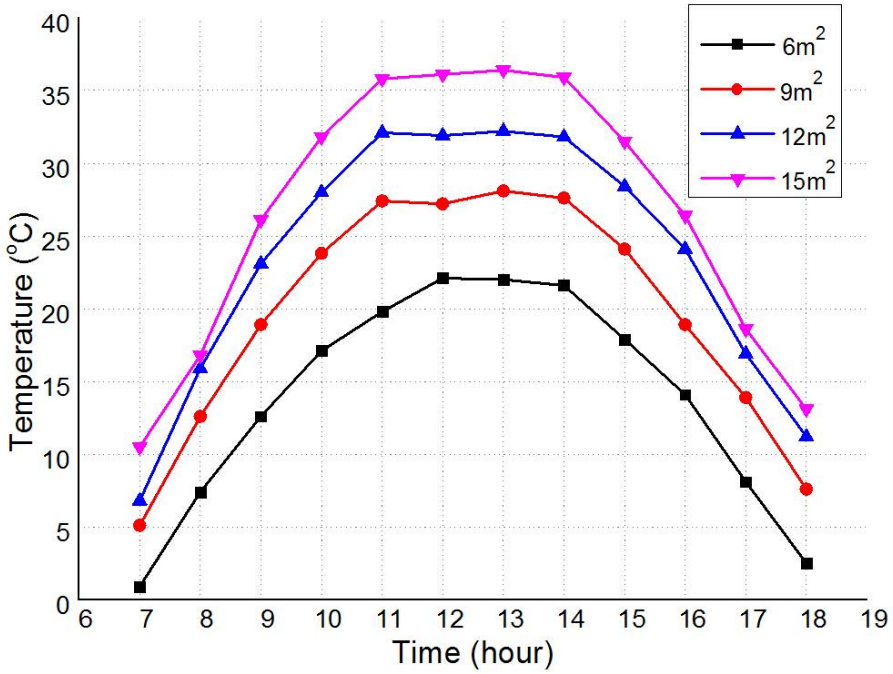

Figure 3. 11 Temperatures of the PV cell at different PV/T collector area

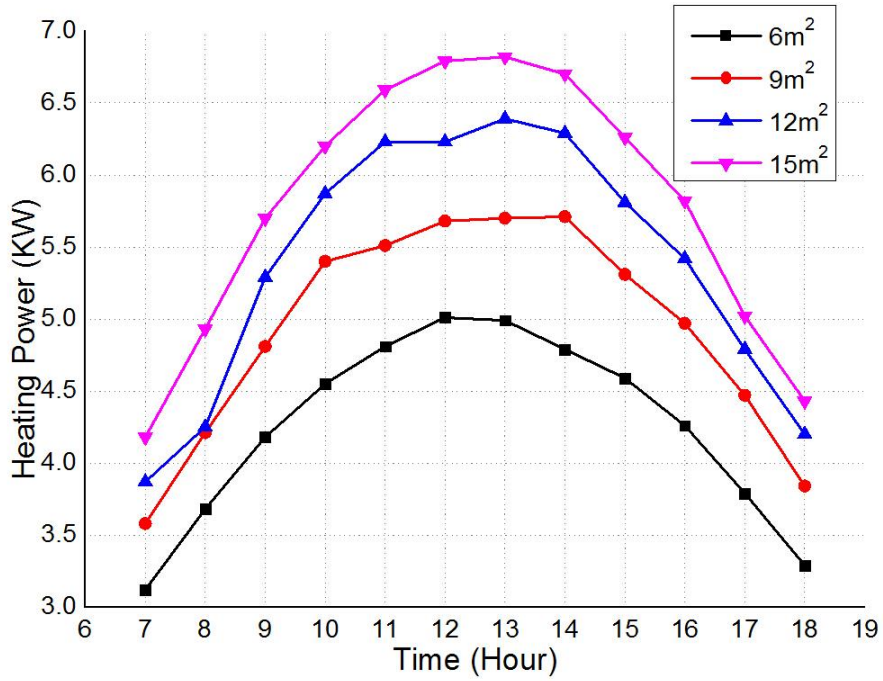

Figure 3. 12 The heat gain of PV/T-HP at different PV/T collector area

Figure 3.13 and Figure 3.14 show the electrical output and PV efficiency at different PV/T collector areas. Based on the two Figures, we can see that the electricity output has the same trend with solar radiation, and the electricity efficiency has an opposite trend. However, the electricity has an opposite trend. With the increasing PV/T collector area, the electrical

power increases and the electrical efficiency decreases, respectively. That is because the increasing area of PV/T collector leads to the increase of collector temperature and PV module temperature, which reduces the electrical efficiency of PV modules.

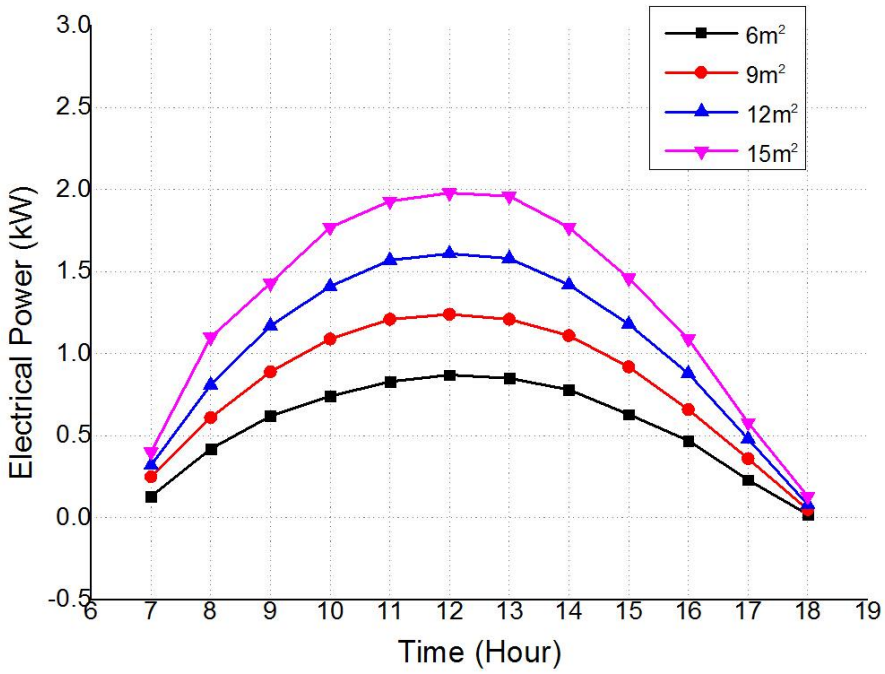

Figure 3. 13 The power output at different PV/T collector area

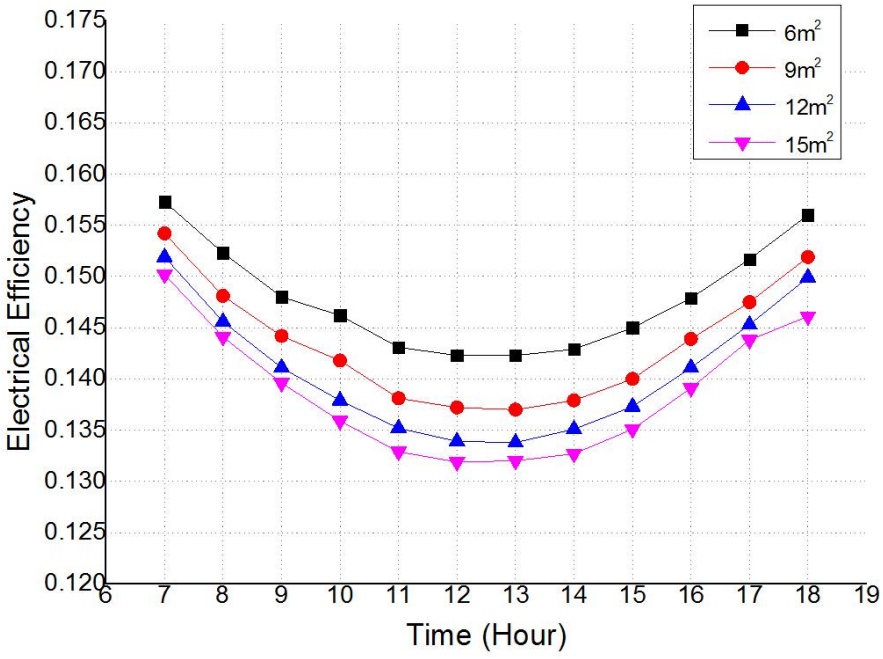

Figure 3. 14 The PV efficiency at different PV/T collector area

Figure 3.15 shows the COP of PV/T-HP at different PV/T collector areas. In the Figure, the COP increases with the increasing area of PV/T collector. This is because the increasing area of the PV/T collector leads to the increase of collector temperature and PV module temperature, which increases the thermal output of the system. Although the increased temperature of PV module will lead the decrease of electrical efficiency, the heat transfer between the PV module and refrigerant also increases. Then the COP of the whole system increases.

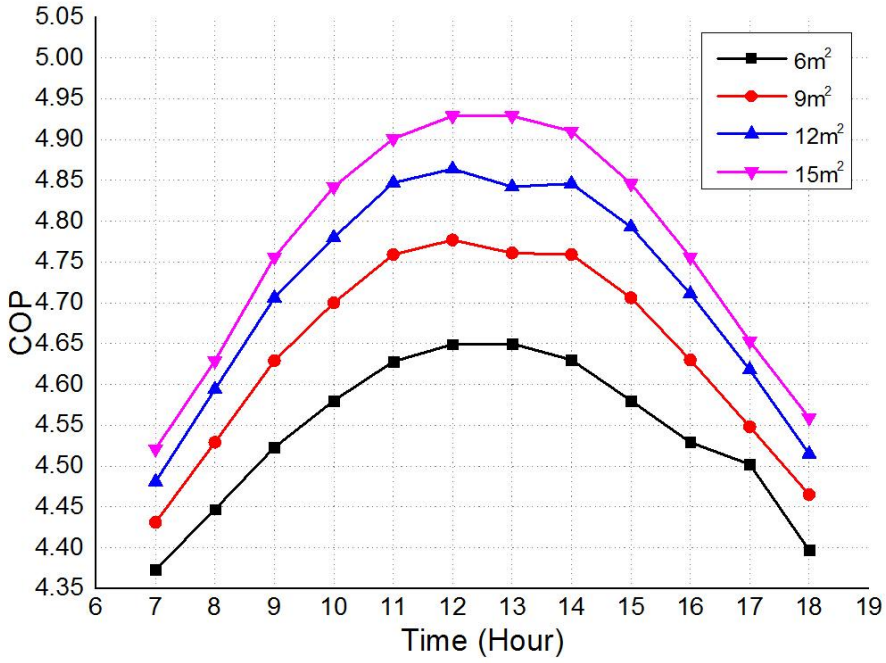

Figure 3. 15 COP of PV/T-HP at different collector area

3.1.4.3 Electrical Performance of PV/T Module

Figure 3.16 shows the variation temperature at different layers of glass tube, PV base plate, refrigerant and the ambient temperature. Based on this, we know that the ambient temperature increases from 12.2^{o}C at 8:00 to 17.2^{o}C at 14:00, and then drops gradually afterwards. The temperature curves of PV module and refrigerant have the same trend as that of ambient temperature, rising up to the maximums in 15:00 and going down. The temperature of PV module rises from 12.1^{o}C to 32.7^{o}C,

which is much lower than that of PV modules without cooling. The temperature difference ranging from 15°C to 24°C between PV module and refrigerant provides the motivation for heat extraction. The glass tube temperature is very close to the ambient due to the vacuum insulation and the heat loss from glass tube to the ambient. In addition, at about 18:00, ambient temperature, glass tube temperature, and PV module temperature are nearly the same.

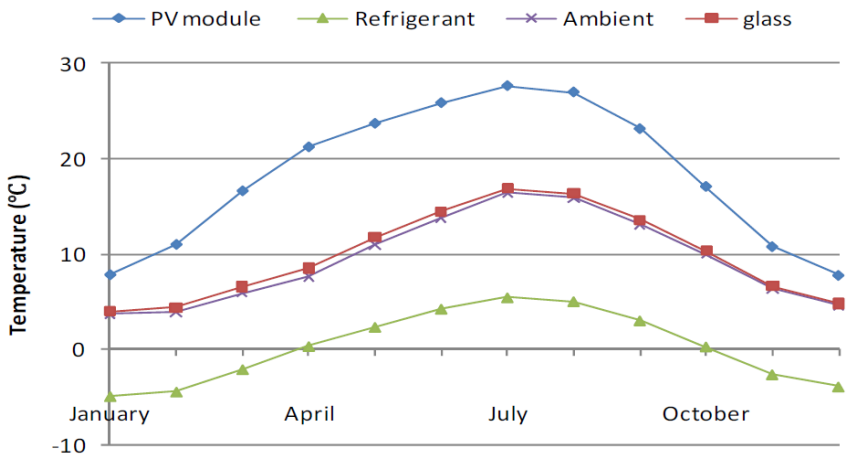

Figure 3. 16 Variation of temperatures at different layers

Figure 3.17 shows the variation of the heat gain and thermal efficiency of the PV/T collector panel. The heat gain generally increases from 308 W to 510 W and changes with solar radiation. The thermal efficiency varies from 0.72 to 0.83 with an average value of 0.752, which is much higher than the typical thermal efficiency of conventional flat plate PV/T collector panels ranging from 0.4 to 0.5. That is because the vacuum glass tube reduces the heat loss to the ambient.

Figure 3.18 shows the variation of the electrical efficiency, power and electrical output of the PV/T collector. The electricity efficiency has an opposite trend with the solar radiation and ambient temperature. It varies from 0.148 to 0.163 with an average value of 0.155. The electricity output ranges from 22W to 110W vary with the solar radiation.

Before the construction of the testing rig, the electrical performance of PV modules without cooling is tested for investigation on the performance improvement made by refrigerant cooling. Figure 3.19 shows the variation of electrical efficiency for the PV modules with and without cooling under different radiation. It can be seen that the electrical efficiency with refrigerant cooling is higher than that without cooling. In addition, electrical efficiency improvement is made by refrigerant cooling increased with the increasing radiation. At the radiation 200W/m^2, the electrical efficiency is 0.21% without cooling and 0.5% with refrigerant cooling, respectively, make 0.29% improved. At the radiation of 800 W/m^2, the electrical efficiency is 2.7% without cooling and 4.6% with refrigerant cooling, respectively, make 1.9% improved.

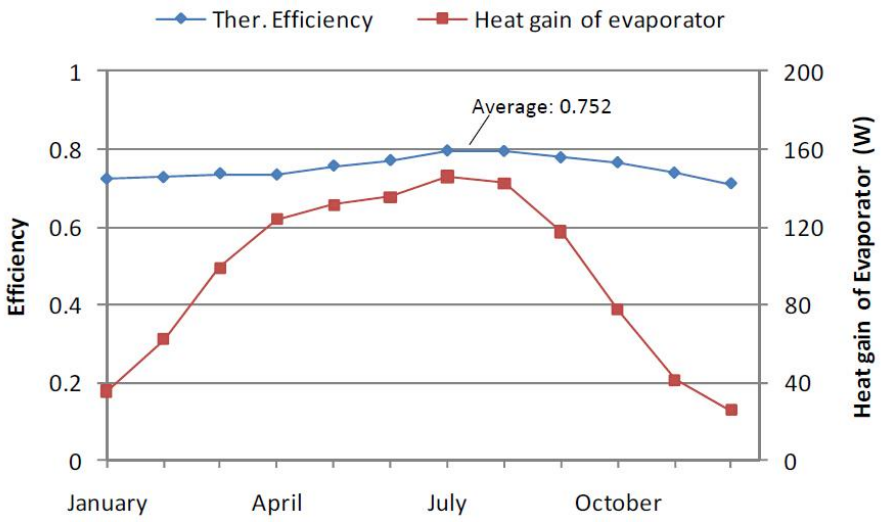

Figure 3. 17 Variation of the thermal efficiency and heat gain of the PV/T collector panel

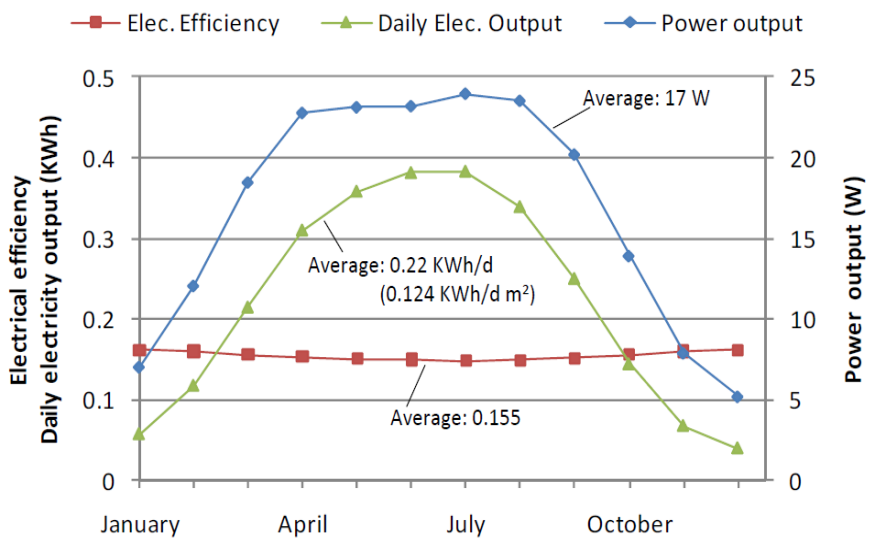

Figure 3. 18 Variation of the electrical efficiency, power and electricity output

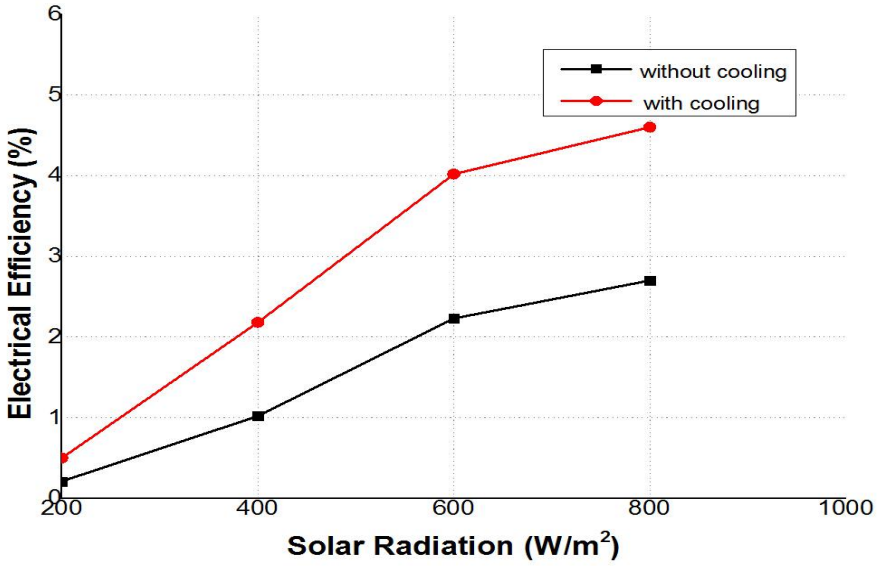

Figure 3. 19 Comparison of electrical efficiency with and without cooling

Figure 3.20 shows the variation of electrical efficiency and PV power output under different radiation. The Figure indicates the electrical efficiency and PV power output increases with the increasing radiation. At the radiation 200W/m^2, the electrical efficiency and PV power are 0.5% and 0.2W, respectively. As the radiation increases to 800W/m^2, the electrical efficiency and PV power are 4.6% and 6.1W, respectively.

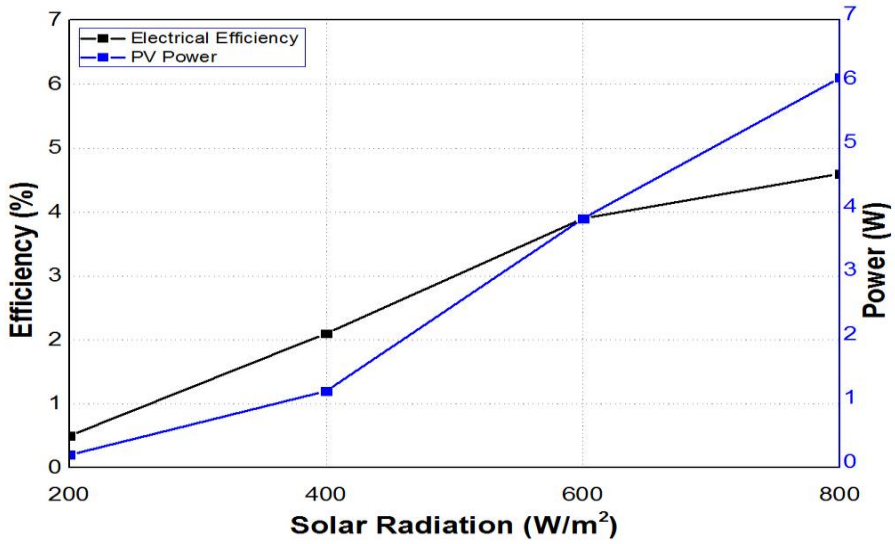

Figure 3. 20 Variation of electrical efficiency and PV power with radiation

Figure 3.21 shows the variation of electrical efficiency and PV power output under different condenser water supply temperature. Based on this, we know that the radiation varies within 600±30 W/m^2 during the testing mode B. The electrical efficiency and PV power output are mainly affected by the radiation instead of the condenser water supply temperature. The minimum radiation 573.6 W/m^2 at the condenser water supply temperature of 30^{o}C leads to the minimum electrical efficiency of 4.77% and the minimum PV power output of 4.5 W, while the maximum radiation 625.6 W/m^2 at the condenser water supply temperature of 45^{o}C leads to the maximum electrical efficiency of 4.86% and the maximum PV power output of 5.0 W.

Figure 3.22 shows the variation of electrical efficiency and PV power output under different condenser water flow rate. The radiation varies within 590-630 W/m^2 during the testing mode C. It has an important impact on the electrical efficiency and PV power output instead of the condenser water flow rate. The minimum radiation 598.1W/m^2 at the condenser water flow rate 2L/min leads the minimum electrical efficiency of 4.2% and the minimum PV power output of 4.1 W, while the maximum

radiation 622.8W/m^2 at the condenser water supply temperature of 5L/min leads to the maximum electrical efficiency of 4.8% and the maximum PV power output of 4.6W.

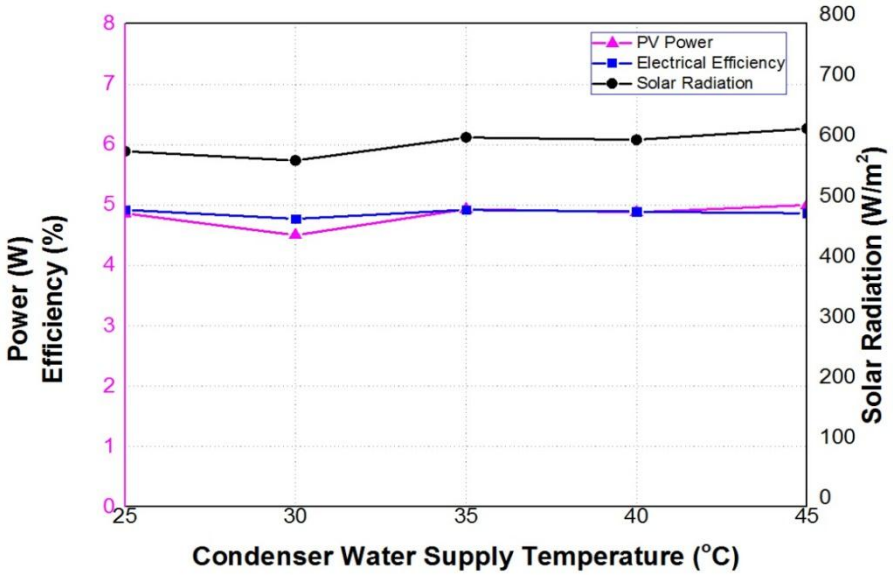

Figure 3. 21 Variation of electrical efficiency and PV power with condenser water supply temperature

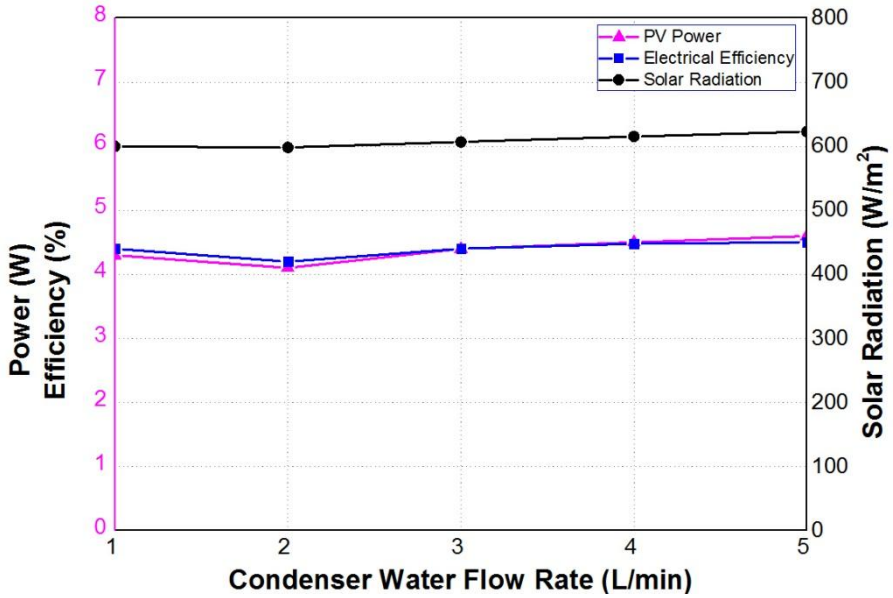

Figure 3. 22 Variation of electrical efficiency and PV power with different condenser water flow rate

3.2 Investigation of Solar Thermal Collector

Typically solar collectors are considered merely technical elements and installed on the roof top where the visible impact is less prominent. The idea of better integrating of solar thermal collector panels in building is developed by the linear design approach.

In order to achieve the results from technical and aesthetic point of view, the novel solar collector presents a high building integration without any visual impact. The model is experimentally tested in order to evaluate the thermal efficiency. The results from this section will work as a prophase work that is going to be used in the Chapter 5.

3.2.1 Solar Thermal Collector Description

The novel solar collector is made from 6 glass tube (diameter 150mm) - casing tubes made by stainless steel withstands pressure with solar selective absorbing coat (diameter 130mm) - copper tubes (GCC) connected in series, shown in Figure 3.23. The casing tubes are made of stainless steel and covered with selective absorbing coating to effectively inhibit the vacuum tube conduction, convection and radiation heat loss. In order to effectively inhibit the conduction, convection and radiation loss, keeps the vacuum between glass tubes and casing tubes. Figure 3.24 shows a cross sectional view of the vacuum glass tube. The characteristic dimensions of solar collector panel are shown in Table 3.2. In addition, it has a particularly large capacity for storage water in the glass tubes due to the large diameter of glass tubes, 80 litres in 6 glass tubes, therefore no additional water tank is needed, which means the novel solar collector is not only convert solar radiation into heat, but also act as the water storage.

The novel solar thermal collector is combined with ASHP together. The novel U-type heat exchanger inserts into the glass vacuum tubes and employs refrigerant R134a as the heat transfer fluid instead of water, shown in Figure 3.25. In this novel hybrid SAHP, it provides heat by air and solar combined.

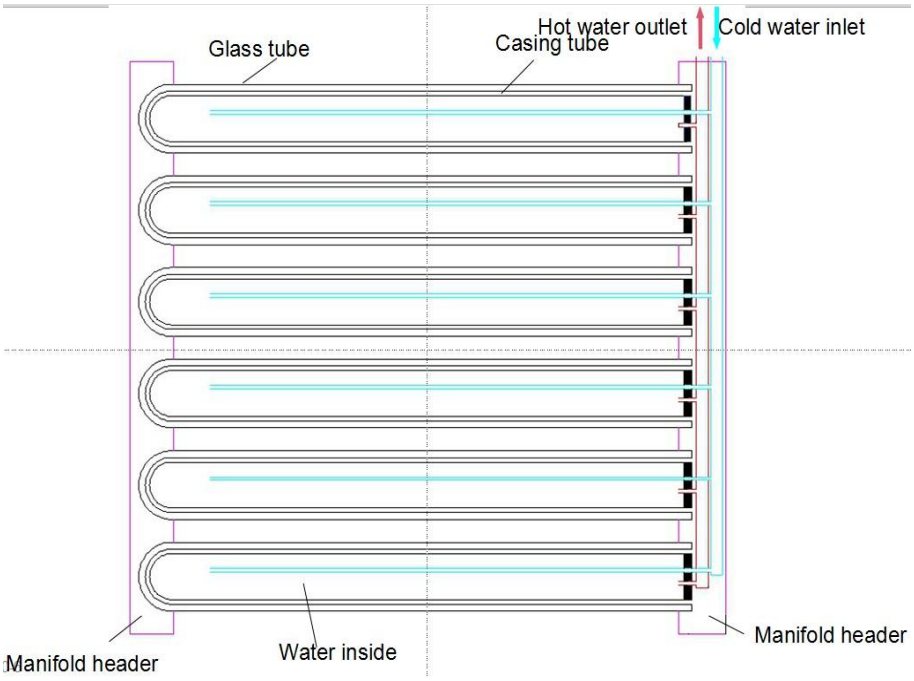

Figure 3. 23 The diagram of a novel solar collector

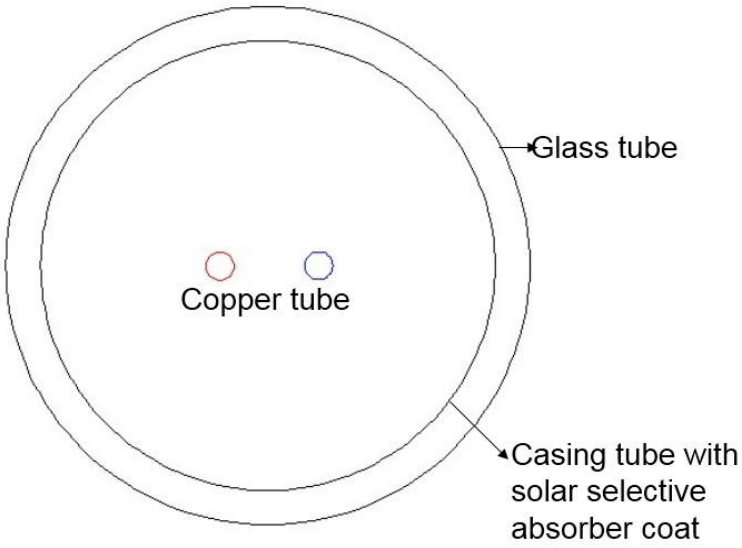

Figure 3. 24 Cross sectional view of vacuum glass tube

Table 3. 2 Characteristic dimension of novel solar collector panel

Component	Parameter	Dimension (mm)
Solar collector panel	Length	1400
	Width	1250
Manifold header	Length	1250
	Width	200
Copper tube in manifold	Diameter	28
Glass tube	External Diameter	150
	Length	1150
Casing tube	Diameter	130
	Length	1200
Copper tube in glass tube	External diameter	10
	Internal diameter	8

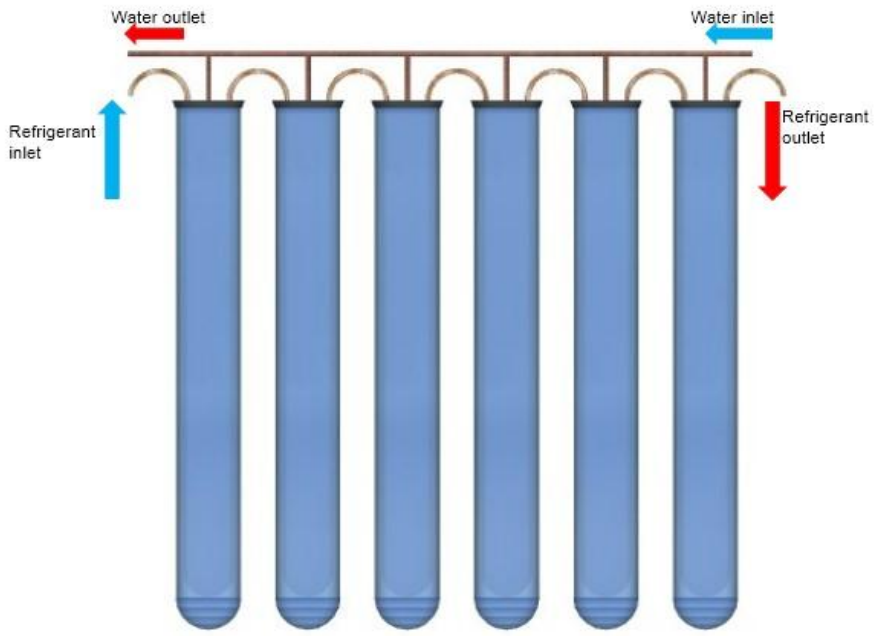

Figure 3. 25 The diagram of solar collector with U-type heat exchanger

3.2.2 Experimental Study of Solar Thermal Collector

The novel solar collector converts solar radiation into heat and acts as water storage. In order to ensure the accuracy of test results, K-type thermocouples are installed at the inlet and outlet of the collector. Fully filled with water in all glass vacuum tubes of solar collectors are tested the initial water temperature. The mean temperature of inlet and outlet of collector is the initial water temperature. Make sure the difference temperature between inlet and outlet is less than 0.2^{o}C within 5 minutes. Terminal temperatures of water in solar collector are tested by the pump circulate water in water heater according to connect the inlet and outlet pipe. The mean temperature of inlet and outlet of water heater is the terminal water temperature. Make sure the difference temperature between inlet and outlet is less than 0.2^{o}C within 5 minutes.

3.2.3 Performance of Novel Solar Thermal Collector

The experimental test of water temperature in glass tubes (130mm) with solar radiation on about 800 W/m^2 is shown in Figure 3.26. From this, we can see that the water temperature increases from 31^{o}C to 54^{o}C when solar radiation varies between 804 W/m^2 and 850 W/m^2 in a 160-minute time span.

The results of average daily efficiency with total radiation and the increased water temperature are plotted in Figure 3.27 and Figure 3.28. The average daily efficiency varies between 0.75 and 0.96 with an average of 0.83, which is higher than the traditional collectors. However, the average daily efficiency is not presented the same trend with the total radiation and the increased water temperature as expected.

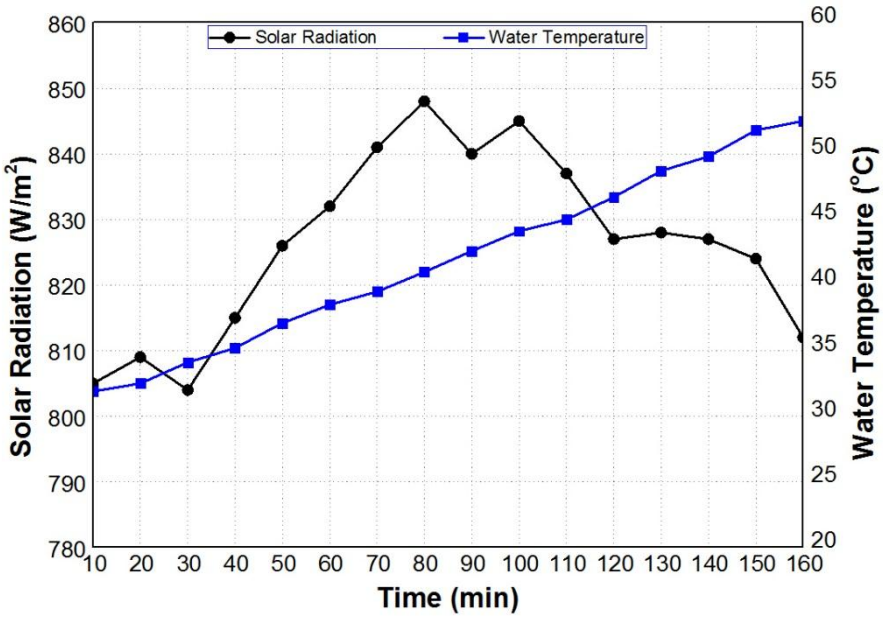

Figure 3. 26 The testing results of solar radiation and water temperature

Because the amount of water is quite large in glass tubes, the average daily efficiency with temperature enthalpy $(\Delta T/H)$ should be considered (Figure 3.29). The results showed that the average daily efficiency presents the same trend with temperature enthalpy.

In order to get the expected increased water temperature, different diameters of glass tubes are tested. The results in Figure 3.30 show that the increased water temperature increases with the reducing diameter of glass tubes. The glass tube with diameter 50 mm presents the highest increased water temperature of 40.5^{o}C, and the glass tube with diameter 210 mm presents the lowest increased water temperature of 14.4^{o}C. The water temperature of the novel solar thermal collector increases with the reducing the diameter of glass tubes.

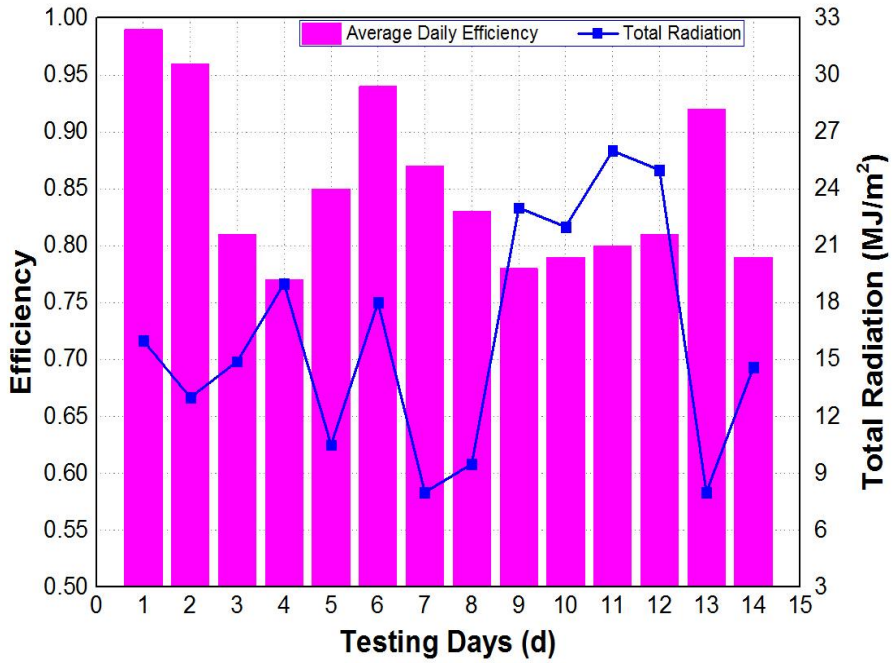

Figure 3. 27 Varieties of average daily efficiency with total solar radiation

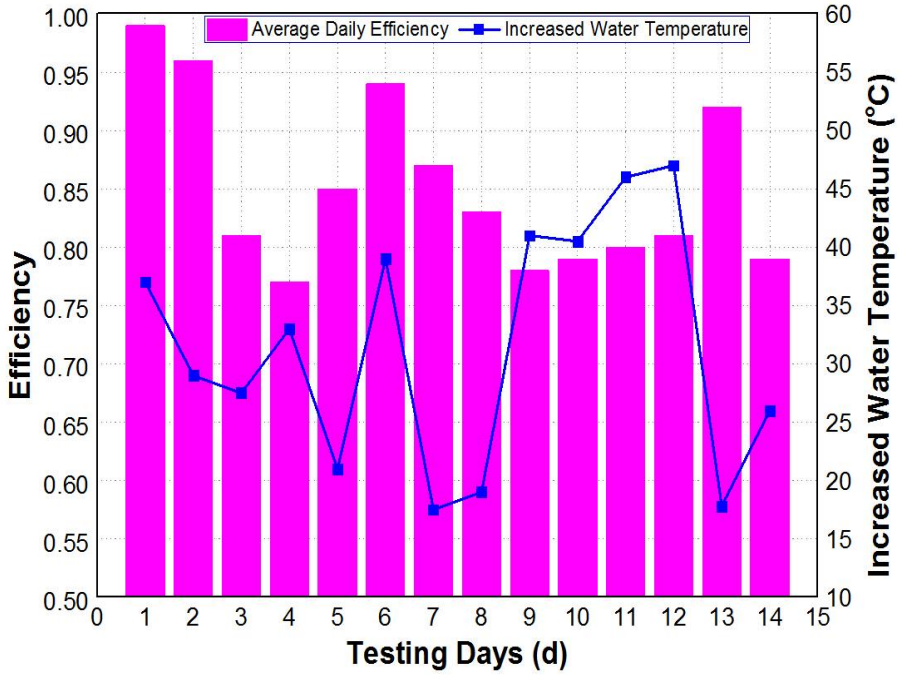

Figure 3. 28 Varieties of average daily efficiency with increased water temperature

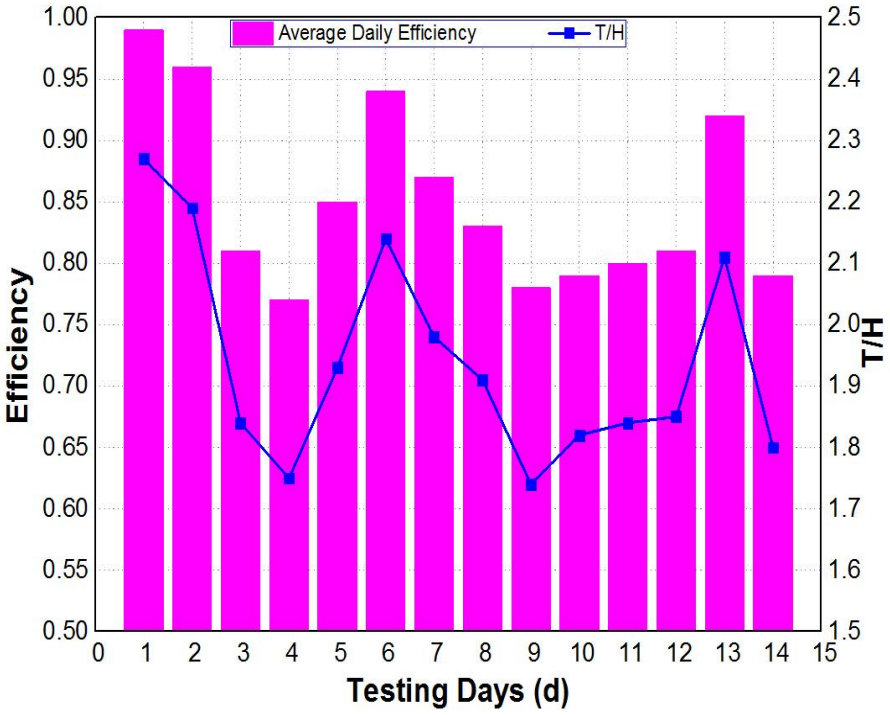

Figure 3. 29 Varieties of average daily efficiency with $(^{\Delta T}/_{H})$

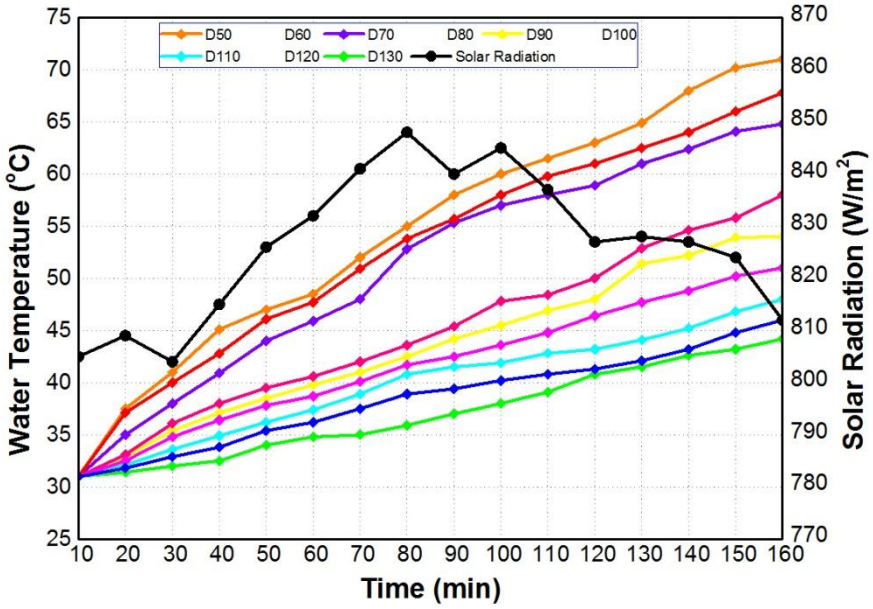

Figure 3. 30 Varieties of Water Temperature with glass tube diameter

3.3 Conclusion

Concerning the investigation results above, it can be concluded that:

- The electrical efficiency of PV/T collector using R134a as heat

transfer fluid is improved by up to 1.9%, compared with that without cooling.

- The novel solar thermal collector has average daily efficiency ranging from 0.75 to 0.96 with an average of 0.83. Compared with other types of solar collector, the average daily efficiency of novel solar thermal collector is the highest.

Chapter 4 Numerical and Experimental Analysis on Photovoltaic/ Thermal Heat Pump

In this chapter, a novel photovoltaic/ thermal heat pump system (PV/T-HP) is investigated. In this novel system, the PV/T collector panel (GPAC sandwich), acting as the evaporator is coupled with a heat pump system to provide a stable capacity for space heating and domestic hot water as well as electricity for compressor and pump usages. The working principles and the basic cycles are presented. In addition, a dynamic model of the novel PV/T-HP based on the distributed parameter approach is presented. All components in the circuit are assumed, including compressor, evaporator, condenser and capillary under the operating conditions with different solar radiations and different ambient temperatures. The test rig is constructed and tested for the determination of the steady state thermal efficiency and the electrical efficiency at a laboratory in Nottingham University, UK. Additionally, comparison between the simulation results and the experimental measurements is presented and showed that the model is able to give satisfactory prediction.

4.1 Photovoltaic/ Thermal Heat Pump Description

The schematic diagram of the novel PV/T-HP is shown in Figure 4.1. It is made up of four main components: glass vacuum tube type PV/T collector panel acting as evaporator, compressor, water-cooled condenser and thermostatic expansion valve. Receiver and filter are installed at the location between condenser and expansion valve. Since the testing is carried out in a laboratory, the PV/T collector is limited to a small size, and thus the heat capacity of PV panel is low. A small

capacity DANFOSS household compressor is employed to match the PV panel. The refrigerant R134a is used for the heat pump system. The principals' characteristics of each component of the system are summarised in Table 4.1. The PV/T evaporator-GPAC sandwich is the key part of the system, the detail descriptions are shown in Chapter 3.

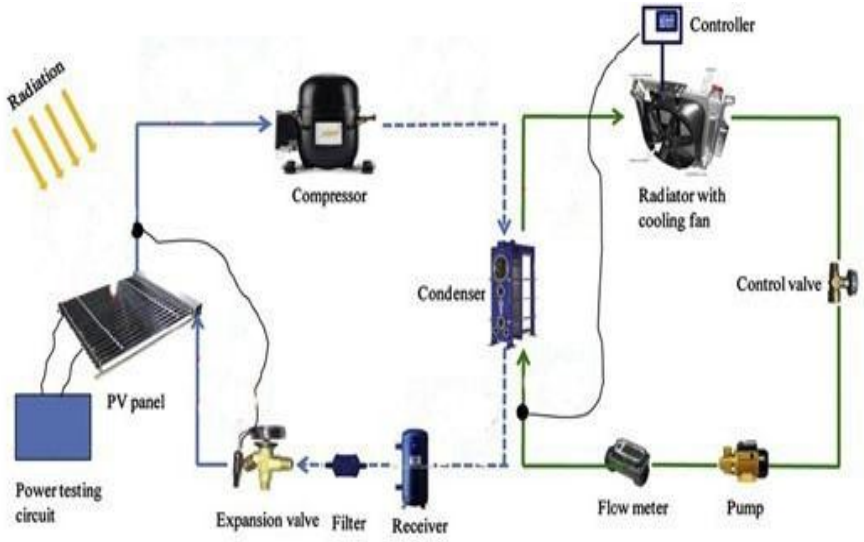

Figure 4. 1 The schematic diagram of the novel PV/T-HP system

When the heat pump system is in operation, the refrigerant mixture (liquid and gas) with low temperature enters the PV/T collector panel. It extracts the solar heat to evaporator and becomes the superheated refrigerant gas entering the compressor where the refrigerant pressure and temperature are lifted up. After that, the refrigerant gas enters the water-cooled condenser, it releases heat energy to water and condenses to liquid during the process. Finally, the refrigerant liquid with high pressure enters the expansion valve where the pressure drops sharply, and then enters the PV/T collector panel as a mixture and continues another cycle operation.

The water is supplied to the condenser by the pump. It absorbs heat from the refrigerant gas. Then, it enters the radiator and releases heat to the ambient. The water supplement temperature to the condenser is

automatically controlled by the controller for the cooling fan. When the supplement temperature is higher than the setting point (T+0.2^{o}C), the cooling fan starts to run and the temperature decreases. The cooling fan is switched off when the temperature is lower than the setting point (T-0.2^{o}C).

Table 4. 1Specification of main equipment in PV/T-HP

<table>
<tr><th>Component</th><th>Type</th><th colspan="2">Comments</th></tr>
<tr><td rowspan="4">Evaporator</td><td rowspan="4">Serpentine tubes in black flat plate heat exchanger with vacuum glass tubes</td><td colspan="2">Aluminium sheet effective absorptivity: 0.90</td></tr>
<tr><td colspan="2">Aluminium sheet effective emissivity: 0.90</td></tr>
<tr><td colspan="2">Tubes spacing: 40mm</td></tr>
<tr><td colspan="2">Thermal conductivity (aluminium): 235 W/m ^{o}C</td></tr>
<tr><td rowspan="3">Compressor (Danfoss Compressor)</td><td rowspan="3">Hermetic constant speed compressor, TL 3F</td><td colspan="2">For refrigerant R134a</td></tr>
<tr><td colspan="2">Displacement: 15.28cm^3</td></tr>
<tr><td colspan="2">Rated input power: 107 W</td></tr>
<tr><td rowspan="2">Condenser</td><td rowspan="2">Contraflow Flat Plate L-line type heat exchanger</td><td colspan="2">SWER: B8×10H/1P</td></tr>
<tr><td colspan="2">Made of stainless steel with a transfer area of 172 cm^2</td></tr>
<tr><td rowspan="5">Thermostatic Expansion Valve</td><td rowspan="5">Thermostatic Expansion Valve (TXV), type TEN 2, variable orifice with external equalizer</td><td rowspan="4">Angle way valve body</td><td>Inlet size: 3/8 inch</td></tr>
<tr><td>Outlet size: 1/2 inch</td></tr>
<tr><td>Capillary tube length: 1.5 m</td></tr>
<tr><td>Maximum working pressure: 34.0 bar</td></tr>
<tr><td>TE 2, flare/flare, versions with external equalization</td><td>Equalization connection size: 1/4 inch/ 6 mm</td></tr>
</table>

4.2 Mathematical Model and Simulation of PV/T-HP

A dynamic model of the novel PV/T-HP based on the distributed parameter approach is presented and used subsequently for evaluating the performance. It was assumed that the system is operated at a quasi-state condition within every time step in numerical simulation.

4.2.1 Compressor Mode

Compressor is the core component of the heat pump. In this system, hermetic constant speed compressor is employed. Keep the structure dimensions of the compressor as constant, establishes the mathematical model to calculate outlet of the compressor which includes mass flow rate of the refrigerant, power, cooling capacity and exhaust temperature.

Assumptions used in simulation are shown:

- Refrigerant at the compressor is a quasi-steady single stage condition;
- Neglecting the pressure drop in the discharge line.

4.2.1.1 Mass Flow Rate of Refrigerant

The mass flow rate of refrigerant (kg/s) is given by:

$$m_r = \lambda \frac{V_{th}}{v_{suc}} \quad \text{(Equation 4. 1)}$$

Where λ is the volumetric coefficient; V_{th} is the theoretical displacement volume of the compressor, $V_{th} = 3.13cm^3$; v_{suc} is the specific volume of the refrigerant at the inlet of the compressor.

For piston type of compressor:

$$V_{th} = \mathrm{i}\frac{\pi D^2}{240} S \cdot n \quad \text{（Equation 4. 2）}$$

Where D is the diameter of piston; S is the length of compressor; n is the compressor speed; and i is the number of cylinder.

The transmission coefficient is calculated by:

$$\lambda = \lambda_V \lambda_P \lambda_T \lambda_D \quad \text{（Equation 4. 3）}$$

Where λ_V is the volumetric coefficient,

$$\lambda_V = 1 - \alpha \left[\left(\frac{P_c + \Delta P_c}{P_e} \right)^{\frac{1}{m}} - 1 \right] \quad \text{（Equation 4. 4）}$$

Where P_c is the condensing pressure (Pa); P_e is the evaporating pressure (Pa), $P_e = (0.10 \sim 0.15) P_c$; α is the relative clearance volume (normally 0.02 ~ 0.06); and m is the changeable swelling index (normally 0.95 ~ 1.05).

λ_P is the pressure coefficient, which is given by:

$$\lambda_P = 1 - \frac{1+\alpha}{\lambda_V} \frac{\Delta P_c}{P_e} \quad \text{(Equation 4. 5)}$$

$$\Delta P_e = (0.05 \sim 0.07) P_e$$

λ_r is the temperature coefficient, which is given by:

$$\lambda_T = \frac{T_e}{T_c} \quad \text{(Equation 4. 6)}$$

Where T_e is the evaporating temperature (K); and T_c is the condensing temperature (K). The leakage coefficient λ_D is equal to volume coefficient.

4.2.1.2 Power Consumption of Compressor

As mentioned earlier, since the compression of the refrigerant vapour is assumed to be a polytrophic process, the compressor power N_e is given as follow:

$$N_e = \frac{m_{com}(h_{dis} - h_{suc})}{\eta_i \eta_m} \quad \text{（Equation 4. 7）}$$

Where h_{suc} is the enthalpy of the suction of the refrigerant (J/kg); and h_{dis} is the enthalpy of the isentropic discharge (J/kg).

η_i is the efficiency of the compressor, and given by

$$\eta_i = \frac{T_e}{T_c} + bT_e \quad \text{（Equation 4. 8）}$$

In there, $\mathrm{b} = 0.0025$.

And η_m is the mechanical efficiency of the compressor (normally 0.85~0.90).

The compressor input power P_{el} is given by

$$P_{el} = \frac{N_e}{\eta_{mo}} \quad \text{（Equation 4. 9）}$$

Where η_{mo} is the motor efficiency of the compressor (normally 0.8), which is the value changed with the load rate.

4.2.1.3 Discharge Temperature

The compressor discharge temperature T_{dis} is based on the compression process equation:

$$T_{dis} = T_{suc}(\frac{P_{dis}}{P_{suc}})^{\frac{1-\kappa}{\kappa}} \quad \text{(Equation 4. 10)}$$

Where T_{dis} and T_{suc} are the compressor discharge temperature (K) and suction temperature (K), respectively; P_{dis} and $P_{suc}$are the discharge pressure (Pa) and suction pressure (Pa), respectively; κ is the polytrophic exponent, 1.05-1.18.

4.2.1.4 Numerical Procedure

Based on the above detailed analysis of compressor, a simulated model is developed to estimate thermal performance of compressor. The thermodynamic properties of the refrigerant R 134a are available in the

form of computer sub-routines. The flow chart of the simulation program is shown in Figure 4.2.

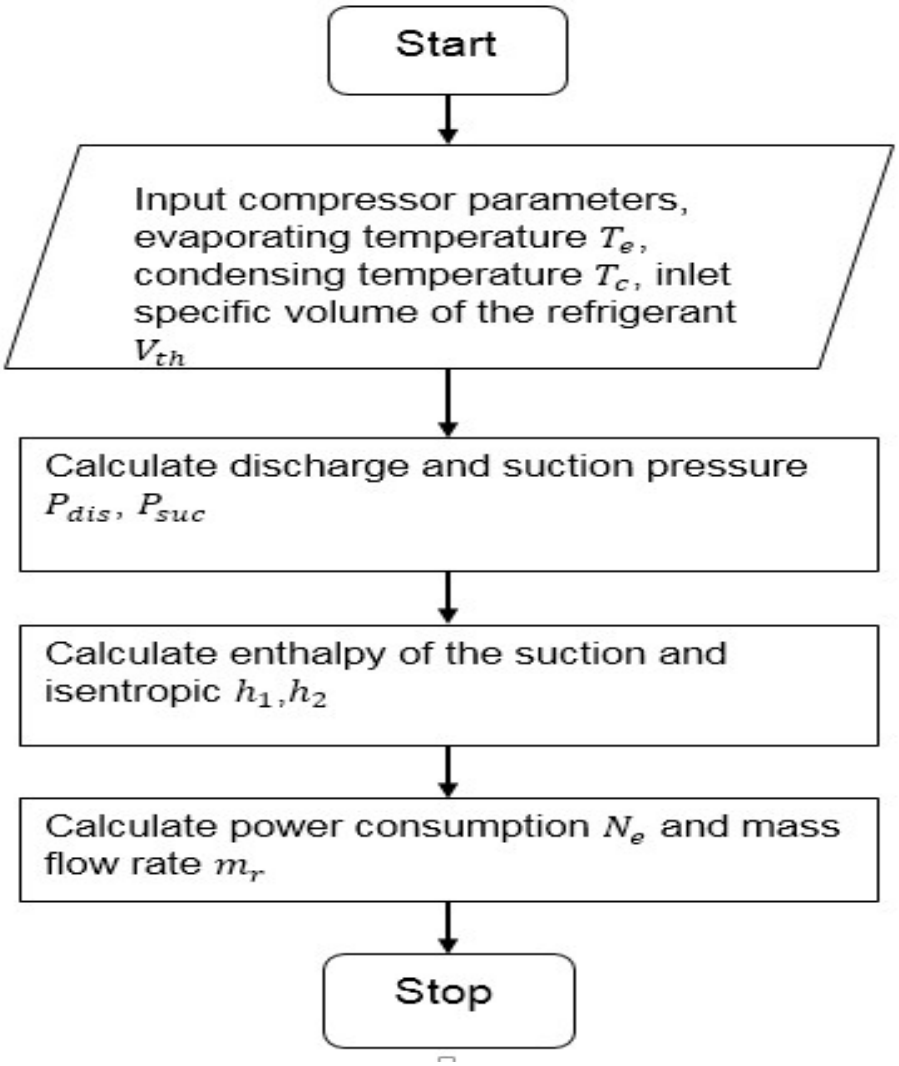

Figure 4. 2 Flow chart of the simulation program of compressor

4.2.2 Expansion Valve Model

The throttling process is regarded as the isenthalpic one. The mass flow rate is given by:

$$m_r = K_{ex}\sqrt{2\rho_{in}(P_c - P_e)} \quad \text{(Equation 4. 11)}$$

Where, K_{ex} is a proportionality constant and is changed as required to maintain the superheat in the evaporator.

The thermostatic expansion valve is modelled as an orifice through which the liquid is expanded from condensing to evaporating pressures. The mass flow rate through it can be correlated according to Bernoulli equation,

$$m_r = C_d A\sqrt{2\rho_{in}(P_c - P_e)} \quad \text{(Equation 4. 12)}$$

Where, ρ_{in} is the density of the refrigerant (liquid) at the inlet of the valve (kg/m^3); A is the minimum flow area across the orifice; C_d is the flow coefficient, which depends upon the degree of opening of the valve; The maximum value of C_d is reached when the valve is fully open. C_d is evaluated through the empirical equation by D.D. Wile (1935):

$$C_d = 0.02\sqrt{\rho_{in}} + 0.63\nu_{out} \quad \text{(Equation 4. 13)}$$

Where ν_{out} is the specific volume of outlet of refrigerant.

For an isenthalpic process in the expansion device, the following equation is obtained:

$$h_3 = h_4 \quad \text{(Equation 4. 14)}$$

Where h_3 and h_4 are the specific enthalpies of the refrigerant at the inlet and outlet of the valve.

4.2.3 Water Cooled Condenser Model

The overall heat transfer coefficient in the condenser κ is equal to the ratio between the heat flow rate Q_c, and the nominal heat transfer area F_c and the logarithmic mean temperature difference ΔT_m

$$\kappa = Q_c/(F_c\Delta T_m) \quad \text{(Equation 4. 15)}$$

The nominal heat transfer area of the condenser is:

$$F_c = N \cdot A \quad \text{(Equation 4. 16)}$$

That is equal to the nominal projected area $\mathrm{A} = \mathrm{L} \times \mathrm{W}$ of the single plate multiplied by the number N of the effective elements in the heat transfer. The use of the projected area instead of the actual area allows comparing different plate patterns on an equal volume basis, shown in Shah and Focke (1988). Moreover, due to the brazing material deposition, the actual heat transfer area of a BPHE is different from that of the plates and generally unknown. Therefore, the surface extension of the plate is included directly in the heat transfer coefficient.

The logarithmic mean temperature difference is equal to:

$$\Delta T_m = (T_{wo} - T_{wi})/\ln[(T_c - T_{wi})/(T_c - T_{wo})] \quad \text{(Equation 4. 17)}$$

Where T_{sat} is the average saturation temperature of the refrigerant derived from the average pressure measured on refrigerant side; T_{wi} and T_{wo} are the water temperatures at the inlet and outlet of the condenser. The logarithmic mean temperature difference is computed with reference to the average saturation temperature on the refrigerant side without taking into account any sub-cooling or super heating as is usual in the condenser design procedure (Bell and Mueller, 1984). In fact, when temperature of the heat transfer surface is below the saturation temperature, the super-heated vapour condenses directly with a heat transfer coefficient near to that of saturated vapour condensation and there is no de-super-heating area at the inlet of the condenser working only with gas single- phase heat transfer coefficient. Similarly the condensate film along the whole heat transfer surface is sub-cooled and there is no sub-cooling area at the outlet of the condenser working only with liquid single-phase heat transfer coefficient. Therefore, it is possible to use the saturation temperature as the temperature driving force and consider an average condensation heat transfer coefficient along the whole heat transfer surface.

The heat flow rate is derived from a thermal balance on the water side of the condenser:

$$Q_c = m_w C_{pw} \Delta T_w \quad \text{(Equation 4. 18)}$$

Where m_w is the water flow rate, C_{pw} is the water specific heat capacity and ΔT_w is the absolute value of the temperature variation on the water side of the condenser.

The calibration correlation for water side heat transfer coefficient obtains results:

$$h_w = 0.277(\lambda_w / d_h) Re_w^{0.766} Pr_w^{0.333} \quad \text{(Equation 4. 19)}$$

Where, $5 < Pr_w < 10,200 < Re_w < 1200$.

Webb (1998) proposed the following model to calculate the local heat transfer coefficient during forced convection condensation of super-heated vapour:

$$h_{sup} = h_{sat} + F[h_{fc} + {C_{pg} q_{lat}}/{\Delta h_{LG}}] \quad \text{(Equation 4. 20)}$$

Where h_{sat} is the local heat transfer coefficient for forced convection condensation of saturated vapour; h_{fc} is the local single-phase heat transfer coefficient between the super-heated vapour and the condensate interface; C_{pg} is the specific heat capacity of the super-heated vapour; Δh_{LG} is the latent heat of condensation; q_{lat} is the local heat flux due only to phase change and F is a factor equal to the ratio between the local degree of super-heat and the driving temperature difference:

$$\mathrm{F} = (T_{sup} - T_{sat})/(T_{sup} - T_{wall}) \quad \text{(Equation 4. 21)}$$

The F-factor approaches zero as the super-heat is depleted. The group $C_{pv} q_{lat} / \Delta h_{LG}$ is a correction term which accounts for the effect of mass transfer on sensible heat transfer between super-heated vapour and

condensate interface. The super-heated vapour condensation heat transfer coefficient h_{sup} is referred to the temperature difference between average saturation temperature T_{sat} and average wall temperature T_{wall}.

$$T_{wall} = \frac{(T_{wall1}+T_{wall2})}{2} \quad \text{(Equation 4. 22)}$$

$$T_{wall1} = \frac{\lambda_c h_w T_{wa}+\lambda_c h_{sat} T_c+\delta_c h_w h_{sat} T_c}{\lambda_c h_{sat}+\delta_c h_w h_{lat}+\lambda_c h_w} \quad \text{(Equation 4. 23)}$$

$$T_{wall2} = \frac{T_{wa}+\lambda_c T_{wall1}+\delta_c h_w}{\lambda_c+\delta_c h_w} \quad \text{(Equation 4. 24)}$$

$$T_{wa} = 0.4T_{wc} + 0.6T_{wi} \quad \text{(Equation 4. 25)}$$

Where λ_c is the heat transfer coefficient assuming the heat exchanger plates; δ_c is the depth of heat exchanger plate.

$$h_{sat} = \phi h_{AKERS} \quad \text{(Equation 4. 26)}$$

$$h_{AKERS} = 5.03(\lambda_L/d_h) Re_q^{1/3} Pr_L^{1/3} \quad \text{(Equation 4. 27)}$$

$$Re_q = \mathrm{G}[(1-\mathrm{x}) + x(PL/PG)^{1/2}]\, d_h/\mu_L \quad \text{(Equation 4. 28)}$$

$$\mathrm{G} = \frac{m_r}{n_{ch} W b} \quad \text{(Equation 4. 29)}$$

Where λ_L is thermal conductivity assuming vapour refrigerant; x is the dryness fraction.

$$Pr_L = \mu_L Cp_L/\lambda_L \quad (\mathrm{Re} < 50000) \text{ (Equation 4. 30)}$$

$$h_{fc} = 0.2267(\lambda_G/d_h) Re_G^{0.631} Pr_G^{1/3} \quad (50 < Re_G < 15000)$$
(Equation 4. 31)

The overall heat transfer coefficient is expressed as:

$$\frac{1}{K} = \frac{1}{h_w} + \frac{\delta}{\lambda_c} + \frac{1}{h_{sup}} \quad \text{(Equation 4. 32)}$$

4.2.4 Evaporator Model

The mathematical model of PV/T evaporator is the same utilized in the Chapter 3 and detailed in the section 3.1.3.

4.2.5 Refrigerant Charge

The amounts of refrigerant charge are closely related to the operation of the refrigerant cycle and the performance of the system. Excessive or small refrigerant will cause the system performance degradation. In order to achieve the high performance, a moderate amount of refrigerant should be necessary. Therefore, after making sure the other parameters of system, the amount of refrigerant needed in the system should be calculated accuracy.

When the PV/T-HP system operates, most of the refrigerant works in the evaporator and condenser, only a small percentage of refrigerant works in the compressor and the connecting pipes. The refrigerant charge is calculated according to the component configurations and the refrigerant states in each component.

4.2.5.1 Compressor

$$m_{com} = \bar{\rho} V_{com} \quad \text{(Equation 4. 33)}$$

Where $\bar{\rho}$ is the average refrigerant density.

4.2.5.2 Condenser

The void fraction can be calculated with the Zivi equation (1964):

$$\alpha_i = \frac{1}{1+\left(\frac{1}{x}-1\right)s\frac{\rho_g}{\rho_f}} \quad \text{(Equation 4. 34)}$$

$$\mathrm{s} = \left(\frac{\rho_f}{\rho_g}\right)^{\frac{1}{3}} \quad \text{(Equation 4. 35)}$$

For the two phase zone in the condenser:

$$m_1 = \left[\alpha_i \rho_g + (1-\alpha_i)\rho_f\right] \mathrm{A} L_{TP} \quad \text{(Equation 4. 36)}$$

For the superheated zone and sub-cooled zone in the condenser:

$$m_2 = \rho \mathrm{A} L_{SP} \quad \text{(Equation 4. 37)}$$

The refrigerant charge for the condenser is:

$$m_{com} = m_1 + m_2 \quad \text{(Equation 4. 38)}$$

Where m_1 and m_2 are the refrigerant charge for the two phase zone and single phase zone, respectively. x is the quality of the two phase zone. A is the area of the tube. L_{TP} and L_{SP} are the tube length of the two phase zone and single phase zone, respectively.

4.2.5.3 Expansion Valve

The throttling process is regarded as the isenthalpic one. The mass flow rate is given by

$$m_r = K_{er}\sqrt{\rho_{in}(\rho_c - \rho_e)} \quad \text{(Equation 4. 39)}$$

Where, K_{er} is a proportional constant and is changed as required to maintain the superheat in the evaporator.

The thermostatic expansion valve is modelled as an orifice through which the liquid is expanded from condensing to evaporating pressures. The mass flow rate through it can be correlated according to Bernoulli equation,

$$m_r = C_d A\sqrt{2\rho_{in}(\rho_c - \rho_e)} \quad \text{(Equation 4. 40)}$$

Where, ρ_{in} is the density of the refrigerant (liquid) at the inlet of the valve (kg/m^3), A is the minimum flow area across the orifice. C_d is the flow coefficient, which depends upon the degree of opening of the valve. The maximum value of C_d is reached when the valve is fully open. C_d is evaluated through the empirical equation by D.D. Wile (1935):

$C_d = 0.02\sqrt{\rho_{in}} + 0.63 v_{out}$ (Equation 4. 41)

Where v_{out} is the specific volume of outlet of refrigerant.

For an isenthalpic process in the expansion device, the following equation is obtained:

$h_3 = h_4$ (Equation 4. 42)

Where h_3 and h_4 are the specific enthalpies of the refrigerant at the inlet and outlet of the valve.

4.2.5.4 PV/T Collector Panel

The heat balance equation at the refrigerant of PV/T evaporator is given in Chapter 3 and detailed in Section 3.1.3.

4.2.6 Numerical Procedure

The simulation of the whole system is carried out using TRNSYS (Figure 4.3).

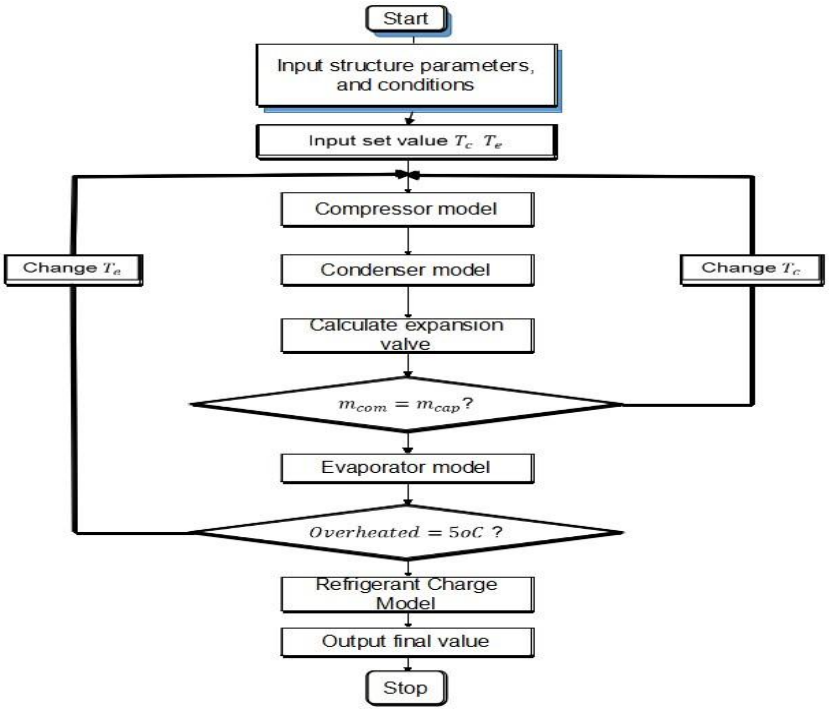

Figure 4. 3 Flow chart of the simulation program of novel PV/T-HP

4.3 Experimental Study of PV/T-HP

The experimental model is constructed and tested at a laboratory for the determination of the steady state performance of PV/T-HP.

4.3.1 Layout of the Testing Rig

In order to evaluate the system efficiency and the heat gain at the condenser, a Data-Taker is used to record solar radiation, temperatures and pressures at the key points in the circuit. There are 13 temperature testing points, 2 are provided for the inlet and outlet of each of the PV/T collector panel, 2 are provided for the inlet and outlet of the compressor, 2 are provided for the inlet and outlet of the water side of condenser, and 6 are provided for the inside of the PV/T collector panel. In addition, 4 pressure transducers are provided for the inlet and outlet of the compressor and expansion valve. The positions of these testing points are shown in Figure 4.4. In addition the water mass flow rates and compressor power consumption are also recorded. All the measuring equipment is detailed description in Appendix. Then these data are analysed using Microsoft Excel. The experiment performances obtained are also compared with the simulation results and the COP.

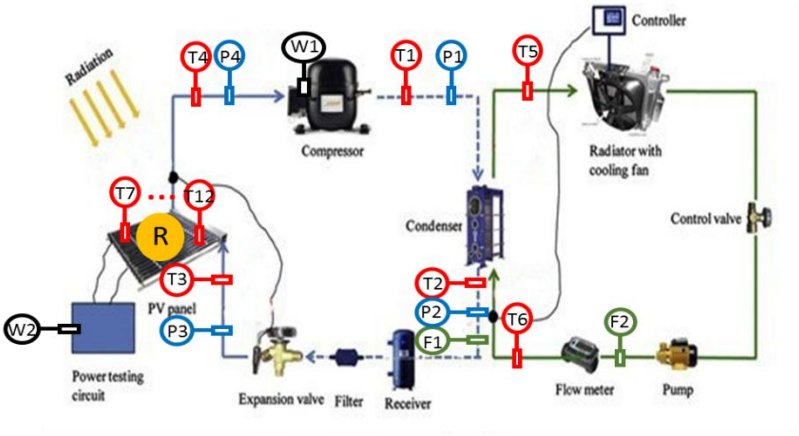

T1-T12: Thermocouples; P1-P4: Pressure sensors;
F1-F2: Flow meters; W1-W2: Watt meters

Figure 4. 4 Testing point position.

4.3.2 Performance Assessment

The heat gain of PV/T-HP is measured by means of the amount of heat carried away in the water passing through it, which is given by:

$$Q_{out} = m_w C_p (T_{out} - T_{in}) \quad \text{(Equation 4. 43)}$$

Where m_w is the water mass flow; C_p is the specific heat of water; T_{in} and T_{out} are the water temperature at the inlet and outlet of the condenser, respectively.

The thermal efficiency of the PV modules is expressed as:

$$\eta_t = \frac{Q_{out} - W_{in}}{A_P (\beta\tau)_P G} \quad \text{(Equation 4. 44)}$$

The energy performance of the heat pump system is assessed by the COP, which is given by:

$$\mathrm{COP} = \frac{Q_{out}}{W_{in}} \quad \text{(Equation 4. 45)}$$

Where W_{in} is the compressor power input.

4.3.3 Test Methodology

The solar radiation is simulated by a radiation simulating panel, which is made up of 12 well-distributed tungsten halogen floodlights with 500W power each (detailed in Appendix). The radiation can be adjusted to any requested value by a control box. The condenser water flow is regulated by a control valve. The condenser water supplement temperature is controlled by a control panel with manual setting.

This section includes the results taken under three different sets of experiments. In the first series of experiments, the rig is tested with different solar radiation. The purpose evaluates how the solar radiation affects the performance of the system. In the second set of the experiment, the rig is tested with different condenser water flow rates.

The purpose evaluates how the flow rate affects the performance of the system. Finally, the third set of the experiment, the rig is tested with varying the condenser water supplement temperature in order to evaluate the thermal and electrical efficiency under different operating temperatures. Three testing modes are listed in Table 4.2.

Table 4. 2 List of testing modes

Mode	Radiation (W/m^2)	Ambient temperature (^oC)	Condenser water flow (L/min)	Condenser water supply temperature (^oC)
A	200±10	21.7±2	2	35
	400±10			
	600±10			
	800±10			
B	600±30	22.5±2	2	25, 30, 35, 40, 45
C	590-630	23±1.3	1, 2, 3, 4, 5	35

4.4 Performances of Photovoltaic/Thermal Heat Pump

4.4.1 Parameters Affect the Performance of PV/T-HP

4.4.1.1 Simulated of Change with Outlet Entropy of Evaporator

In order to investigate the performance of PV/T-HP, the effect of PV/T collector area, ambient temperature, solar radiation, length of tubes and the dry degree of inlet are investigated by simulating of the change with outlet entropy of evaporator.

Figure 4.5 shows the outlet entropy of evaporator changed with different solar radiations at the ambient temperature of -5^{o}C, 0^{o}C and 5^{o}C. The outlet entropy is greatly increased as solar radiation increased, no

matter whether it operates at the ambient temperature of -5°C, 0°C or 5°C. When the solar radiation increases, the outlet entropy increases greatly at beginning, then the increasing rate lowers. The reason is as the temperatures of aluminium sheet and refrigerant increased, there is much more heat transfer to ambient air.

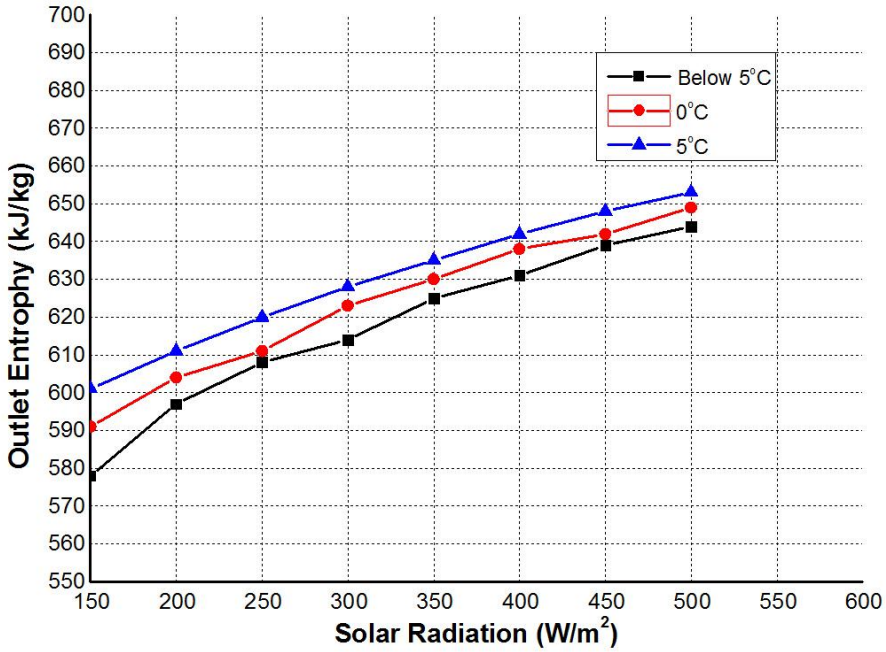

Figure 4. 5 Outlet entropy changed with different solar radiations

Figure 4.6 shows the outlet entropy of evaporator changed with different ambient temperature at solar radiations of 300 W/m^2, 400 W/m^2 and 500 W/m^2. The outlet entropy is increased as the ambient temperature increases, no matter whether it operates at 300 W/m^2, 400 W/m^2 or 500 W/m^2 of solar radiations.

Figure 4.7 shows the outlet entropy of evaporator changed with the length of the tube at solar radiation of 300 W/m^2. It can be seen that the outlet entropy increases when the tube length is increasing. However, the trend of increasing will be smaller and smaller. That is because the heat transfer increases with the increasing length of the tube.

Figure 4.8 shows the outlet entropy of evaporator changed with the inlet dry degree of refrigerant at different solar radiation of 300 W/m^2, 400 W/m^2 and 500 W/m^2. With the increasing of inlet dry degree, outlet entropy has greater increased at beginning, the increasing trend slows. This is because the increase of inlet dry degree leads to a longer length of super-heated zone, and thus, a higher refrigerant temperature and higher heat transfer rate.

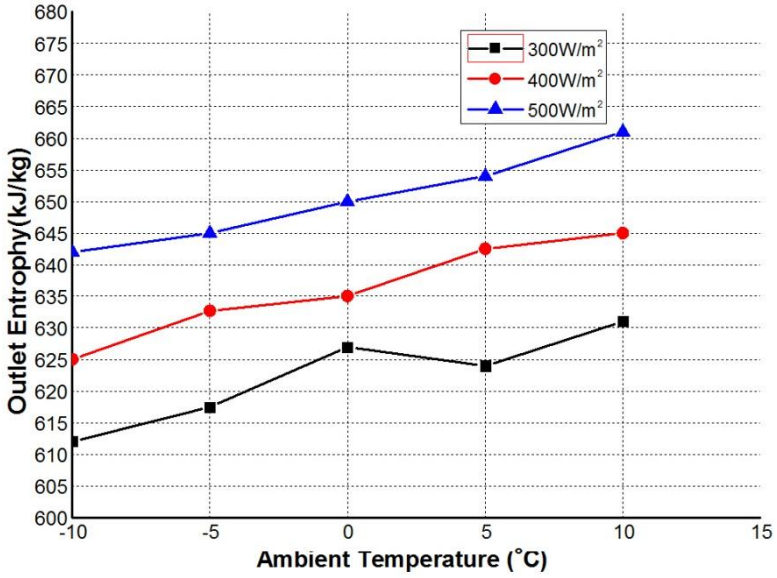

Figure 4. 6 Outlet entropy changed with different ambient temperature

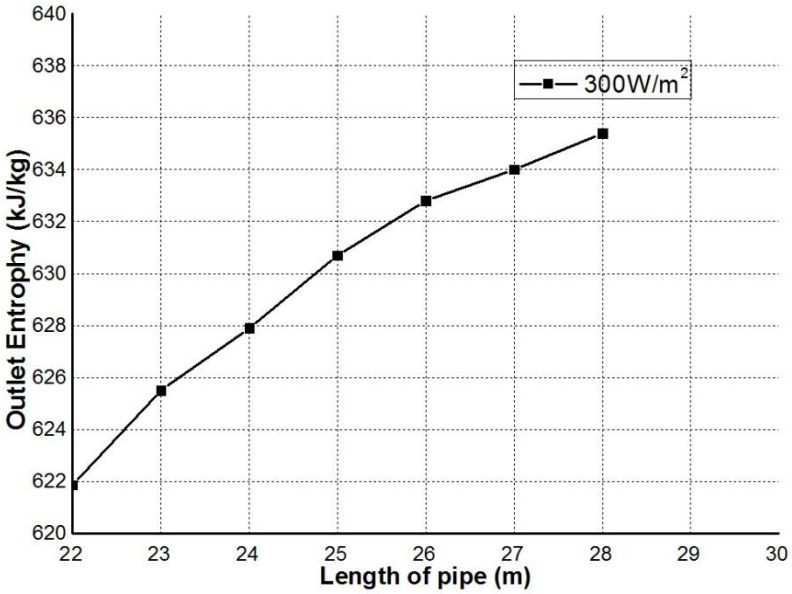

Figure 4. 7 Outlet entropy changed with different length of tube

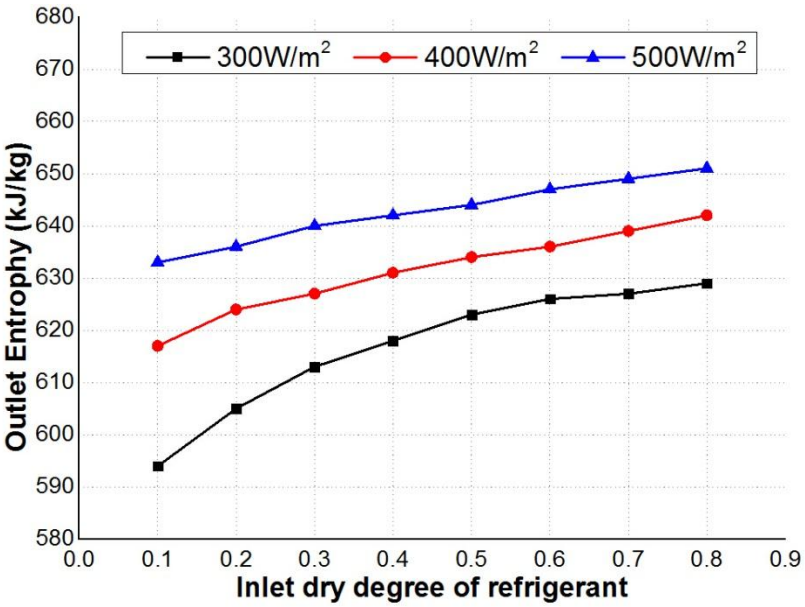

Figure 4. 8 Outlet entropy changed with different dry degree of inlet

4.4.1.2 Experimental Results

The testing on the effect of solar radiation on energy performance of the hybrid heat pump system is carried out under the testing mode A. During the testing, the ambient temperature, condenser water flow rate and condenser water supply temperature are kept constant. Figure 4.9 shows the variation of COP, condenser heat capacity and compressor power input under different radiation. From this we can see that the COP and condenser heat capacity increases with the increasing radiation. At the radiation of 200W/m^2, the COP is 2.9 and the condenser heat capacity is 345 W. As the radiation increases to 800 W/m^2, the COP and condenser heat capacity rise to 4.6 and 582 W, respectively. The COP is not as high as expected due to the low capacity compressor. In addition, the results show that the compressor power decreases slightly from 126.8 W to 120.9 W with the increasing radiation from 200 W/m^2 to 800 W/m^2. This is because the increasing radiation leads to the increase of evaporating temperature and pressure, which reduces the compression ratio, and thus reduces the compressor power input.

The testing on the effect of condenser water supply temperature on energy performance of the hybrid heat pump system is carried out under the testing mode B. During the testing, the radiation, ambient temperature and condenser water flow rate are kept constant. Figure 4.10 shows the variation of COP, condenser capacity and compressor power input under different condenser water supply temperature. It can be seen that the COP and condenser heat capacity decreases with the increasing condenser water supplement temperature. At the condenser water supply temperature of 25^{o}C, the COP and condenser heat capacity are 5.2 and 586 W, respectively. As the condenser water supplement temperature increases to 45^{o}C, the COP and condenser heat capacity drops to 3.2 and 495 W, respectively. It can also be found that the compressor power input rises from 111.8 W to 153.9 W when the condenser water supply temperature increases from 25^{o}C to 45^{o}C. This is because the increase of condenser water supply temperature leads to a higher condensing pressure, and thus, a higher compression ratio and higher compressor power input. When the condenser water supplement temperature increases, the temperature difference between the refrigerant and water at the condenser decreased. Therefore, the condenser heat capacity drops. Meanwhile, the compressor power input increases, so the COP drops more sharply than the condenser heat capacity.

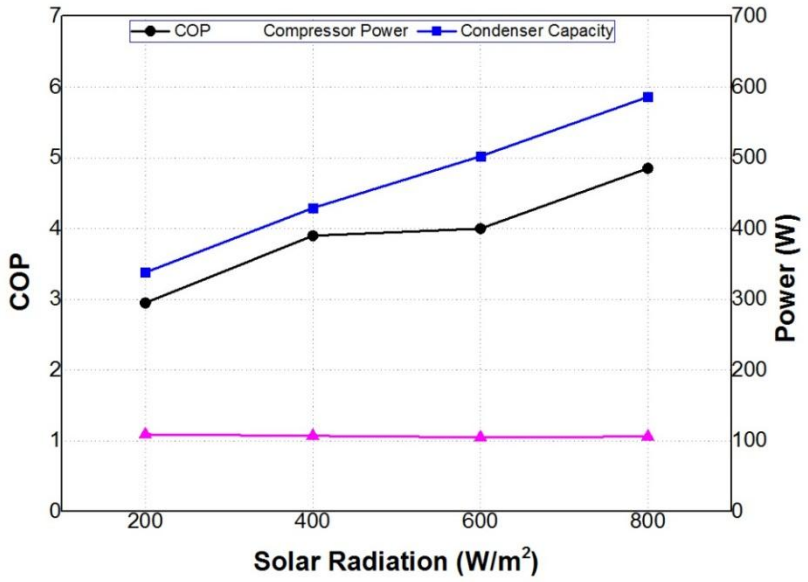

Figure 4. 9 Variation of COP, condenser capacity and compressor power with radiation

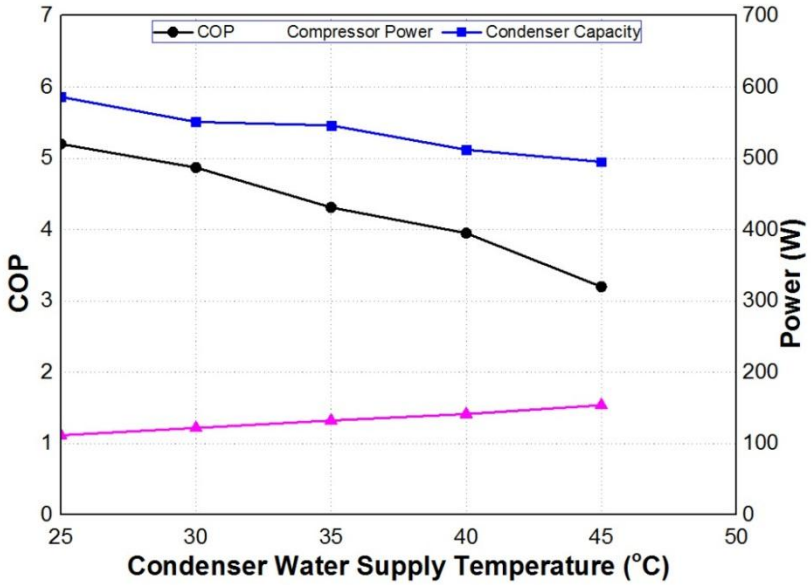

Figure 4. 10 Variation of COP, condenser capacity and compressor power with condenser water supply temperature

The testing on the effect of condenser water flow on energy performance of the hybrid heat pump system is conducted under the testing mode C. During the testing, the radiation, ambient temperature and condenser water supply temperature are kept constant. From Figure 4.11, it can be seen that the COP and condenser heat capacity drops sharply as the

condenser water flow increases from 1 L/min to 2 L/min, and then the drop trends to be smooth as the condenser water flow continues to increase from 2 L/min to 5 L/min. At the condenser water flow of 1 L/min, the COP and condenser heat capacity are 6.7 and 916 W, respectively. As the condenser water flow increases to 5 L/min, the COP and condenser heat capacity drop to 2.8 and 352 W, respectively. It can also be found that the compressor power input decreases slightly from 137.4 W to 125 W with the increasing condenser water flow.

Figure 4.12 shows the variation of electrical efficiency and PV power output under different condenser water flow rate. It can be seen that the radiation varies within 590-630 W/m^2 during the testing mode C. It has an important impact on the electrical efficiency and PV power output instead of the condenser water flow rate. The minimum radiation 598.1W/m^2 at the condenser water flow rate 2L/min leads to the minimum electrical efficiency of 4.2% and the minimum PV power output of 4.1 W, while the maximum radiation 622.8W/m^2 at the condenser water supplement temperature of 5L/min leads to the maximum electrical efficiency of 4.8% and the maximum PV power output of 4.6W.

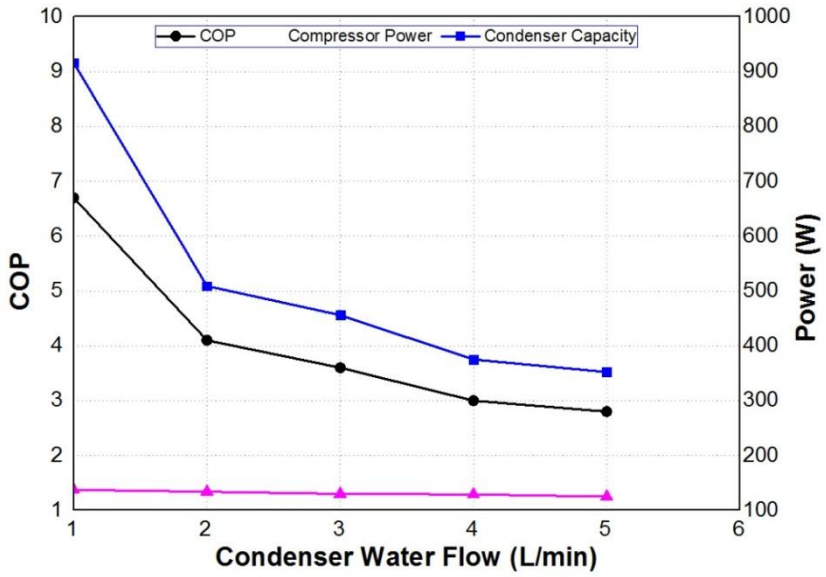

Figure 4. 11 Variation of COP, condenser capacity and compressor power with condenser water flow

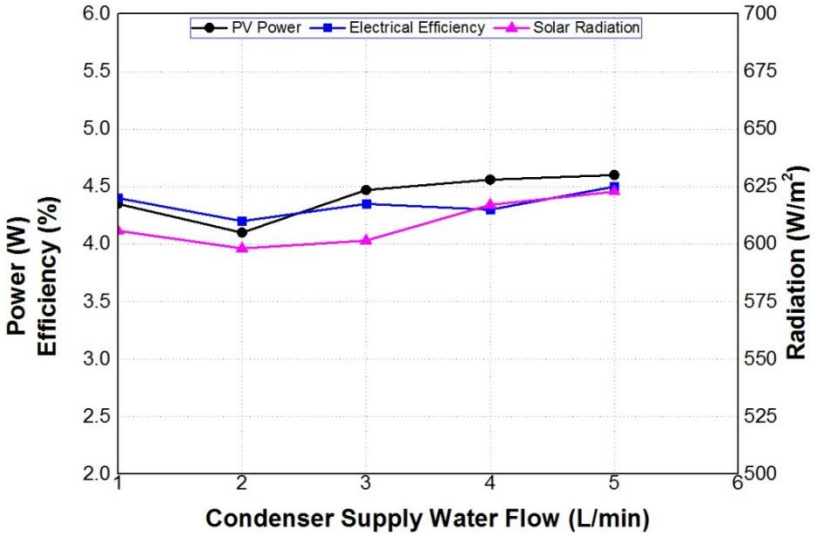

Figure 4. 12 Variation of electrical efficiency and PV power with different condenser water flow rate

4.4.2 Performance of PV/T-HP

Figure 4.13 shows the power consumption of PV/T-HP and the PV electrical output power. It can be seen that the PV output power increases rapidly in the morning until the peak value at 12:00 noon, then gradually decreases. PV output electricity is over the system power

consumption before 15:00, which means the system is able to operate the PV/T-HP by itself from 7:00 to 15:00.

Figure 4.14 shows the variation of COP and condenser capacity of the PV/T-HP system. It can be seen that the COP varies from 4.90 to 6.22 with an average value of 5.42. The condenser capacity varies from 273 W to 435 W would provide the heat source for space heating and domestic hot water.

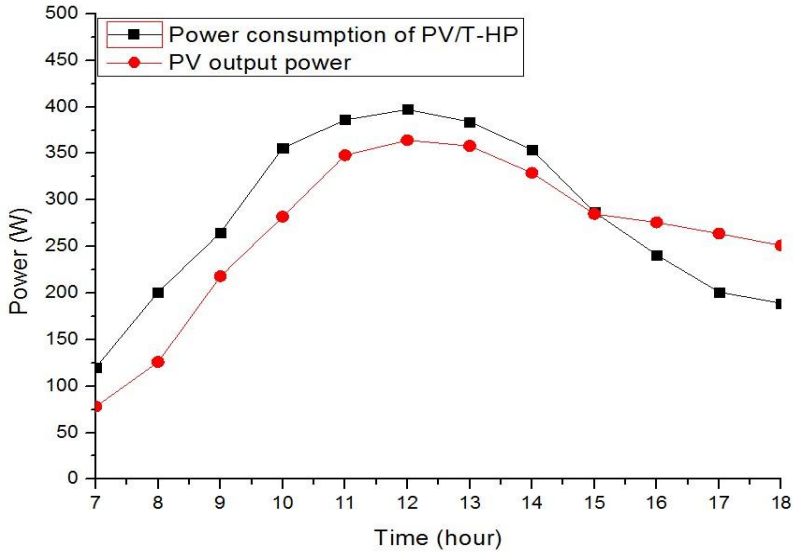

Figure 4. 13 The power consumption and electrical efficiency of PV/T-HP

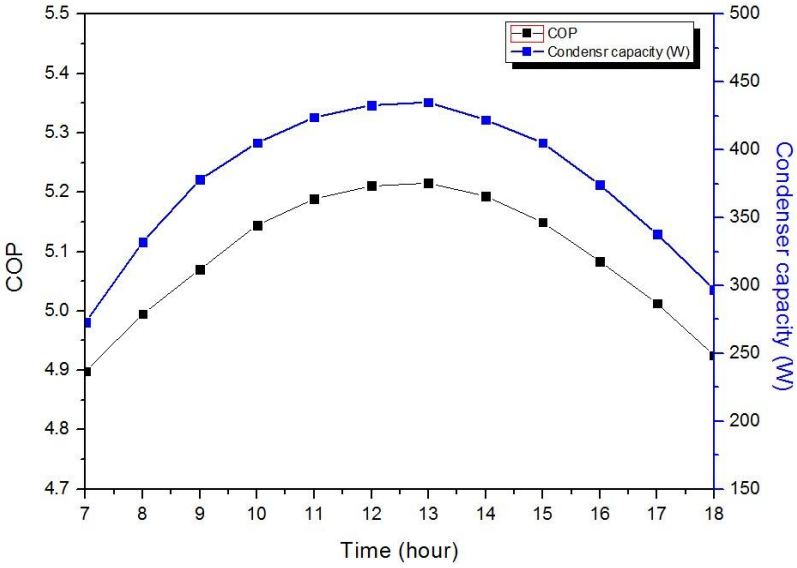

Figure 4. 14 COP and condenser capacity of the PV/T-HP

4.5 Discussion

This chapter presents numerical and experimental study on the energy performance of PV/T-HP. It can be concluded that:

- The COP of the heat pump system increases with increasing radiation. The COP varies from 2.9 to 4.6, responding to the radiation from 200 W/m^2 to 800 W/m^2, at the constant condenser water supply rate of 2 L/min and water supply temperature of 35^{o}C. The COP is not as high as expected due to the low capacity compressor, selected to match the small size and low capacity of PV panel limited indoors.

- The COP of the heat pump system decreases with the increasing condenser water supplement temperature. The COP drops from 5.2 to 3.2, responding to the condenser supplement temperature from 25^{o}C to 45^{o}C, at the radiation of 600 W/m^2 and condenser water flow rate of 2 L/min. The condenser water supply temperature has little effect on the PV power output and electrical efficiency.

- The COP of the heat pump system decreases with the increasing condenser water flow rate. The COP drops from 6.7 to 2.8, responding to the condenser water flow rate from 1 L/min to 5 L/min, at the radiation of 600 W/m^2 and condenser water supply temperature of 35^{o}C. The condenser water flow rate has little effect on the PV power output and electrical efficiency.

Chapter 5 Numerical and Experimental Analysis on Solar Assisted Heat Pump

In this chapter, a novel SAHP is investigated. The SAHP combines a novel solar thermal collector (presented in Chapter 3) with an ASHP together. In this novel system, solar thermal energy can be used on one hand directly to charge the water storage and on the other hand as heat source for the evaporator of the heat pump. The working principles and the basic cycles are presented. Then, different combinations of solar energy and heat pump system are considered through dynamic system simulation and experimental investigation.

5.1 Solar Assisted Heat Pump Description

The schematic diagram of the novel SAHP is shown in Figure 5.1. It consists of novel solar thermal collector and traditional ASHP. The ASHP system is made up of components: compressor, outdoor shell and tube heat exchanger, indoor shell and tube heat exchanger, filter drier, coiled adiabatic capillary, liquid tube and some accessories. The U-type copper tube, named U-type heat exchanger in this thesis, is connected in series and inserted into the glass tubes to contact solar collector with ASHP. The internal and external heat exchangers are connected with U-type heat exchanger in parallel and automatically controlled by the one-way valve and electro-magnetic valve. The cross sectional view of novel U-type heat exchanger within solar collector panel is shown in Figure 5.2. The refrigerant R22 is provided by Huachuang Company in China and employed in the ASHP.

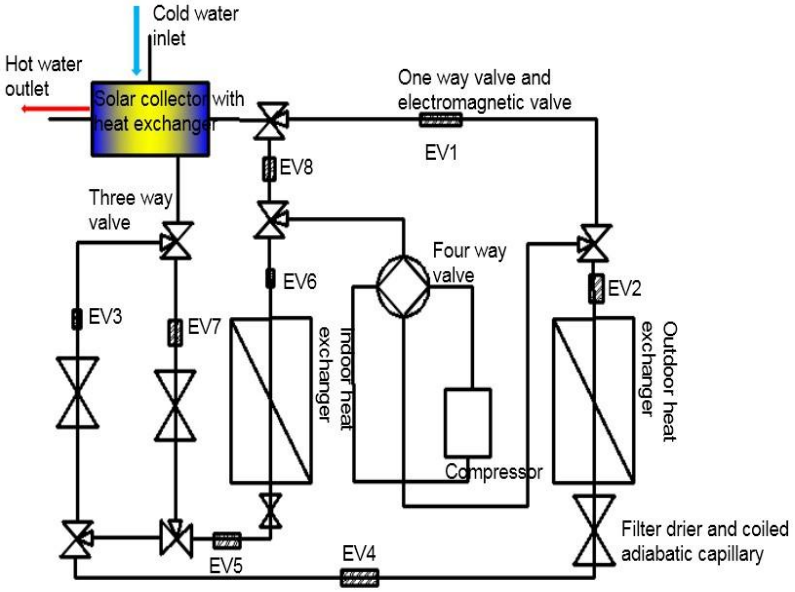

Figure 5. 1 The schematic diagram of the novel SAHP

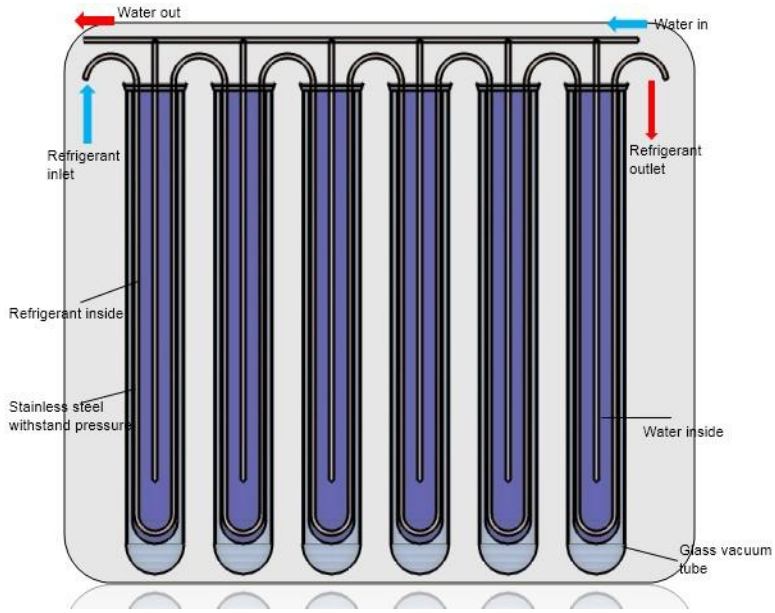

Figure 5. 2 Cross sectional view of solar collector with U-type heat exchanger

In the refrigerant cycle, the reciprocating compressor (SL232CV, Haili) is used in this project, which compresses the refrigerant gas and sends it on its way to the condenser. The compressor of this experimental has a rated capacity of about 1.1 kW. Theoretical suction capacity is $1.32 \times 10^{-3}\ m^3/s$. Voltage is 220/240 V (50 Hz). There are four kinds of capillary used in this novel system, presented in Table 5.1.

Table 5. 1Characteristics of different kinds of capillary

No.	Electronic Valve	Internal Diameter	Length	Quantity
1	3	1.8 mm	1.5 m	1
2	4	1.4 mm	1.1 m	3
3	5	1.4 mm	1.2 m	2
4	7	2.0 mm	1.6 m	1

Interior shell and tube heat exchanger is formed by the continuous integral shells that are made of aluminium and copper tubing arranged in an equilateral triangle. The dimension of cooper tube is $\emptyset 10 \times 0.5$ mm. The tube pitch and row pitch are 20 mm and 17.32 mm, respectively. There are two rows of tubes along with the flow direction, 14 rows in height direction. The aluminium sheet is 0.1 mm in depth, the baffle spacing is 1.6 mm, and thermal conductivity is 204 W/ (m·K). The dimension of area is 875 mm×285 mm×35 mm.

External shell and tube heat exchanger is formed by the continuous integral shells that are made of aluminium and copper tube arranged in an equilateral triangle. The dimension of cooper tube is $\emptyset 10 \times 0.5$ mm. The tube pitch and row pitch are 25 mm and 21.65 mm, respectively. There are three rows of tubes along with the flow direction, 15 rows in height direction. The aluminium sheet is 0.15 mm in depth, the baffle spacing is 1.8 mm, and thermal conductivity is 204 W/ (m·K). The dimension of area is 420 mm×375 mm×150 mm.

According to the source of heat that is supplied the evaporator of heat pump, dual sources of heat are provided by air and solar. In this novel system, on one hand, solar thermal energy can be used directly to charge the water storage that parallel operation of solar thermal collector

and heat pump. On the other hand, solar thermal energy can be used as the heat source for the heat pump. There are four operation modes when operating, which include air source heat pump, solar source heat pump, and solar-air source heat pump as well as solar-water source heat pump systems. In addition, based on operation modes, there are nine cycles when operating in an entire year. Nine cycles are shown in detail. The cycle controls of novel SAHP are shown in Table 5.2.

Table 5. 2 Cycle controls of novel SAHP (√ -Turn on, X-Turn off, FV-Four way valve, HWV-Heat water valve)

	Summer Operation (^oC)			Winter Operation (^oC)					
	Cycle 1	Cycle 2	Cycle 3	Cycle 4	Cycle 5	Cycle 6	Cycle 7	Cycle 8	Cycle 9
	T_1<45	T_1>45 T_2<40	T_2>40	T_2>5	T_2<5 T_1>15	T_3<8 T_1>15	T_3<8 T_1<15	T_2<10 T_1>15	T_1<45
1	√	X	√	X	X	X	X	X	X
2	X	√	X	X	X	√	√	X	X
3	X	X	X	X	√	X	X	√	X
4	X	X	X	√	X	X	X	X	√
5	√	√	√	X	X	X	X	X	X
6	X	X	X	√	√	X	X	√	X
7	X	X	X	X	X	√	X	X	X
8	X	X	X	X	X	X	X	X	√
9	√	√	√	X	X	√	√	X	X
	X	X	√	X	X	X	X	X	X

5.1.1 Summer Condition

Cycle 1—Air Source Heat Pump System for Space Cooling and Domestic Hot Water Supplement

When solar radiation is weak in summer, the water temperature in solar collector is not high enough for domestic hot water supplement, cycle 1 is operated. This cycle is an ASHP without any solar thermal system. The ASHP provides heat to the solar collector acting as water storage for domestic hot water supplement by internal heat exchanger. When water temperature in solar thermal collector reaches to 45^{o}C, this cycle is stopped to avoid excessive heat splitting vacuum glass tubes.

Cycle 2—Air Source Heat Pump and Solar Collector Run Separate

Solar thermal collector and ASHP run separately during summer sunny days. ASHP operates as the cooling mode that extracts heat from indoor and transfers it to the ambient through the external heat exchanger. Simultaneously, the solar thermal collector extracts solar radiation to supply domestic hot water.

Cycle 3—Water Source Heat Pump for Space Cooling

During extremely hot in summer, open the water valve and control the water flow rate. The system then employs the U-type heat exchanger as evaporator. Refrigerant enters the U-type heat exchanger to extract heat from water of controlled flow rate for space cooling.

5.1.2 Winter Condition

Cycle 4—Air Source Heat Pump and Solar Collector Run Separately

Solar thermal collector and ASHP operate separately during normal days in winter. ASHP operates as the heating mode that extracts heat

from ambient and transfers to indoor through the indoor heat exchanger. Simultaneously, solar thermal collector extracts solar radiation to supply domestic hot water.

Cycle 5—Solar-Water source Heat Pump for Space Heating

During the cold days in winter, the solar loop is divided into a solar side and a water storage loop, whereby the heat transfer between them takes place. In order to increase the evaporation temperature, refrigerant enters the U-type heat exchanger to extract heat from hot water for space heating. When water temperature drops below 15^{o}C, it stops in order to avoid cracking the vacuum glass tubes.

Cycle 6—Solar-Water Source Heat Pump for Defrost

During extremely cold days, frost forms on the external heat exchanger. The system is operated the reverse mode. The solar energy is used to load the solar collector on the one hand, and to preheat the external heat exchanger. This cycle stops to avoid cracking the vacuum glass tubes of solar collector when the water temperature below 1^{o}C.

Cycle 7—Air Source Heat Pump for Defrost

When ambient temperature is low, frost forms on the external heat exchanger. Meanwhile, water temperature in solar collector is low. In order to operate the system steadily, the reverse mode operates. The system extracts heat from indoor air to defrost the outdoor heat exchanger.

Cycle 8—Solar-Water Source Heat Pump for Space Heating

When ambient temperature is extremely low, heat is extracted heat from hot water in the collector for space heating, which does not guarantee hot water usage.

Cycle 9—Air Source Heat Pump for Hot Water Supply and Space Heating

When ambient temperature is extremely cold, water in solar collector is used to defrost the outdoor heat exchanger until the system operates steadily. Then, heat is extracted from ambient air by outdoor heat exchanger for domestic hot water supplement and space heating.

5.2 Mathematical Model and Simulation of ASHP

A dynamic model of the PV/T-HP based on the distributed parameter approach is presented. It is assumed that the system is operated at a quasi-state condition within every time step in numerical simulation. The mathematical model used in this simulation is shown in Appendix I.

5.3 Experimental Work

The experimental rig is constructed and laboratory tested for the determination of the steady state performance of SAHP.

5.3.1 Layout of the Testing Rig

In order to evaluate the COP of the novel system and the heat gain at the condenser, a Data-Taker is used to record solar radiation, temperatures and pressures at the key points in the circuit. There are 13 temperature testing points, 4 are provided for the inlet and outlet of each of the U-type heat exchangers, 2 are provided for the inlet and outlet of the compressor, 3 are provided for the inlet, outlet and middle of the indoor heat exchangers, and 4 are provided for the inlet, outlet, middle and the tube of the outdoor heat exchangers. In addition, 4 pressure transducers are provided for the inlet and outlet of the compressor and capillary tube. The positions of these testing points are shown in Figure

5.3. In addition, the water and air mass flow rates and compressor power consumption are also recorded. All the measuring equipment is detailed in Appendix IV. Then those data is analysed using Microsoft Excel. The experiment measurements obtained are compared with simulation results.

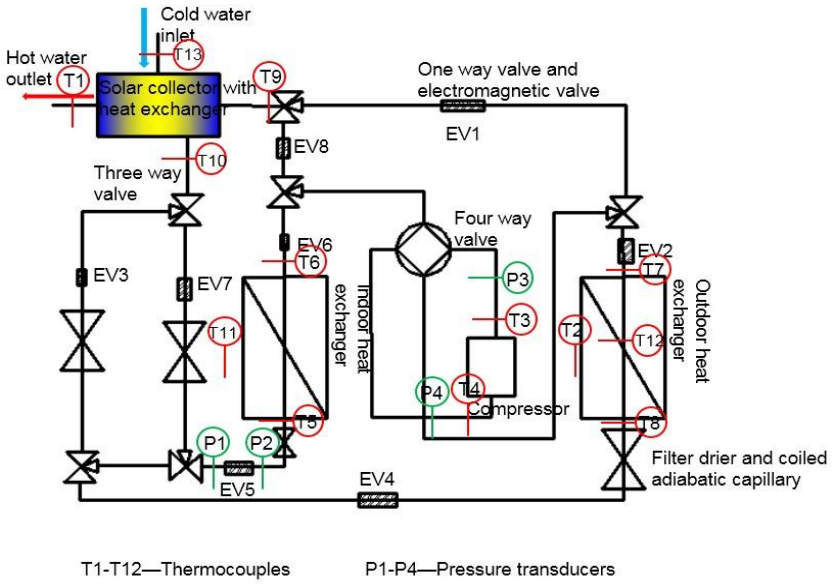

Figure 5. 3 Testing point position

5.3.2 Performance Assessment

The heat gain of the U-type heat exchanger in the solar collector is measured by means of the amount of heat carried away in the water passing through it, which is given by:

$$Q_{cw} = m_w C_{pw}(T_{out} - T_{in}) \quad \text{(Equation 5. 1)}$$

Where m_w is the mass flow rate of water, T_{in} and T_{out} are the temperature of water at the outlet and inlet of the U-type heat exchanger, and C_{pw} is the specific heat coefficient of water.

The heat gain of the heat exchanger in the heat pump is measured by means of the amount of heat carried away in the air passing through it, which is given by:

$Q_{ca} = m_a C_{pa}(T_{out} - T_{in})$ (Equation 5. 2)

Where m_a is the mass flow rate of air, T_{in} and T_{out} are the temperature of the air at the exit and the inlet of the heat exchanger, respectively, and C_{pa} is the specific heat coefficient of the air.

The energy performance of the heat pump system is assessed by the COP, which is given by:

$\mathrm{COP} = Q_{out}/W_{in}$ (Equation 5. 3)

Where W_{in} is the power of compressor.

5.3.3 Test Methodology

5.3.3.1 Indoor Heat Exchanger

The indoor heat exchanger is placed in artificial environment simulation room 1 to adjust the inlet and outlet temperatures of indoor heat exchanger. The wind velocity of inlet keeps a constant air flow by a constant speed fan. The inlet and outlet air temperatures of indoor heat exchanger are measured by platinum resistance thermometers (PRT), and wind velocity of inlet is measured by hot bulb anemometer.

Temperature difference method is used to test the water heating and cooling capacities in the novel heat pump system under summer and winter seasons. The outlet water temperatures in the solar thermal collector are measured by the T-type thermocouple probe. The inlet water temperatures in the solar thermal collector are adjusted by three-way valves.

For the inlet wind velocity of indoor heat exchanger, it divides the rectangular surface into 12 rectangular areas, tests each area by hot bulb anemometer, and takes the average value as the experiment data. For the outlet temperature of indoor heat exchanger, it divides the outlet

through the longitudinal direction into 8 areas, tests each area by T-type thermocouples, and takes the average value as the experiment data.

5.3.3.2 Outdoor Heat Exchanger

The outdoor heat exchanger is placed in artificial environment simulation room 2 for adjusting the inlet and outlet temperatures of indoor heat exchanger. The temperature around the copper tube is measured by T-type thermocouples. In order to prevent the accuracy of measurement, the welded tip PTFE is fixed on the outside of the unit. The pressure transducer is used to test the pressures on suction and discharge of compressor as well as the inlet and outlet of capillary. In addition, a digital power meter is used to measure the power consumption of the compressor every five minutes.

5.3.3.3 Solar Thermal Collector System

The solar thermal collector system is placed in artificial environment simulation room 2. Simulated lights are used in the laboratory to supply solar radiation. A solar pyrometer is placed at the middle of the collector plate to measure the instantaneous simulated solar radiations. 6 K-type thermocouples are adhered on the collector plate uniformly in order to test the temperature of the collector. In addition, the inlet and outlet temperature and pressure are also tested by T-type thermocouple Probes and pressure transducers, respectively. Mass flow rate of water is measured using flow meter.

All data is measured and controlled by a personal computer via data logger software.

5.4 Performance of Novel Solar Assisted Heat Pump System

5.4.1 Performance of SAHP under Summer Condition

In order to analysis the cooling performance of system, the working conditions in summer seasons are shown in Table 5.3.

Table 5. 3 Working conditions in summer seasons

Condition	Ambient temperature	Room temperature
Minimum Load Condition	21^{o}C	21^{o}C
Nominal Load Condition	35^{o}C	27^{o}C
Maximum Load Condition	43^{o}C	32^{o}C

5.4.1.1 Air Source Heat Pump for Space Cooling

When the system operates for space cooling, the simulation and experimental results operated under different working conditions are shown in Table 5.4 and Table 5.5, respectively. In addition, Table 5.6 shows the parameters comparison of simulation and experimental results for space cooling during nominal load conditions.

In Table 5.4, the simulation results show that the COP and cooling capacity decreases with the increasing cooling load. At the minimum load condition, the COP is 3.31 and the condenser cooling capacity is 3051 W. At the nominal working condition, the COP is 2.94 and the condenser cooling capacity is 3864 W. At the maximum load condition, the COP is 2.71 and the condenser cooling capacity is 3575 W. The increasing system load leads to the increase of suction and discharger temperature, evaporation and condensation temperature, and the power consumption of compressor, which reduces the cooling capacity, and thus reduces the COP.

Table 5. 4 Simulation results under different operating conditions

	Minimum load condition	Nominal working condition	Maximum load condition
Suction temperature (^{o}C)	18.62	20.95	24.36
Discharge temperature (^{o}C)	76.65	78.12	84.12
Evaporating pressure (k Pa)	248.2	612.3	684.3
Condensing pressure (k Pa)	964.1	1924.6	2141.3
Cooling capacity (W)	3051	3864	3575
Power (W)	951.3	1331.2	1394.5
COP	3.31	2.94	2.71

The experimental results from Table 5.5 indicate that the COP and cooling capacity decreases with the increasing cooling load. At the minimum load condition, the COP is 3.02 and the condenser cooling capacity is 2841.2 W. At nominal working condition, the COP is 2.56 and the condenser cooling capacity is 3501.2 W. At the maximum load condition, the COP is 2.14 and the condenser cooling capacity is 3341.2 W. The increasing system load leads to the increase of suction and discharger temperature, evaporation and condensation temperature, and the power consumption of compressor, which reduces the cooling capacity, and thus reduces the COP.

The parameters comparison of simulation results and experimental results for ASHP for space cooling during nominal load conditions are shown in Table 5.6. Based on this, we can see that the errors of discharge temperature, condensing pressure, cooling capacity, power and COP are relatively small. Only the evaporating pressure and suction temperature have a certain error. This is because the pressure drop is

ignored in the evaporator during the simulation which causes the high numerical value. In addition, small changes of pressure are corresponded to the big substantial changes of temperature.

Table 5. 5 Simulation results under different operating conditions

	Minimum load condition	Nominal working condition	Maximum load condition
Suction temperature (^{o}C)	28.89	30.87	34.82
Discharge temperature (^{o}C)	84.9	86.5	91.97
Evaporating pressure (k Pa)	217.5	507.12	559.8
Condensing pressure (k Pa)	784.5	1806.2	2057.6
Cooling capacity (W)	2841.2	3501.2	3341.2
Power (W)	1004.3	1402.1	1459.6
COP	3.02	2.56	2.14

Table 5. 6 Comparison of simulation results and experimental results for space cooling

	Experimental	Numerical	Relative error (%)
Suction temperature (^{o} C)	30.87	20.95	32.13
Discharge temperature (^{o} C)	86.5	78.12	9.68
Evaporating pressure (k Pa)	507.12	612.3	20.74
Condensing pressure (k Pa)	1806.2	1924.6	6.55
Cooling capacity (W)	3501.2	3864	10.36
Power (W)	1402.1	1331.2	5.05
COP	2.56	2.94	14.84

5.4.1.2 Novel Solar Assisted Heat Pump System for Space Cooling and Domestic Hot Water Supply

5.4.1.2.1 Simulation Results

The simulations of the system that is operated for space cooling and domestic hot water supplement under different working conditions are carried out. Figure 5.4 and Figure 5.5 show the evaporating and condensing pressure as well as suction and discharge temperature, respectively. It can be seen that the increasing cooling load leads to the increase of suction and discharge temperature as well as evaporating and condensing pressure, which accelerates the growth rate of water temperature, and thus increases the final water temperature.

Figure 5.7 shows the variation of COP under different working conditions for space cooling and hot water supplement. It can be seen that the COP increases with the increasing ambient temperature. This is because the increasing ambient temperature leads to the increase of the cooling load, which reduces the condensation temperature and consumption power, and thus increases the cooling capacity. However, the condensation heat is difficult to release along with the increasing water temperature, and thus reduces the COP gradually.

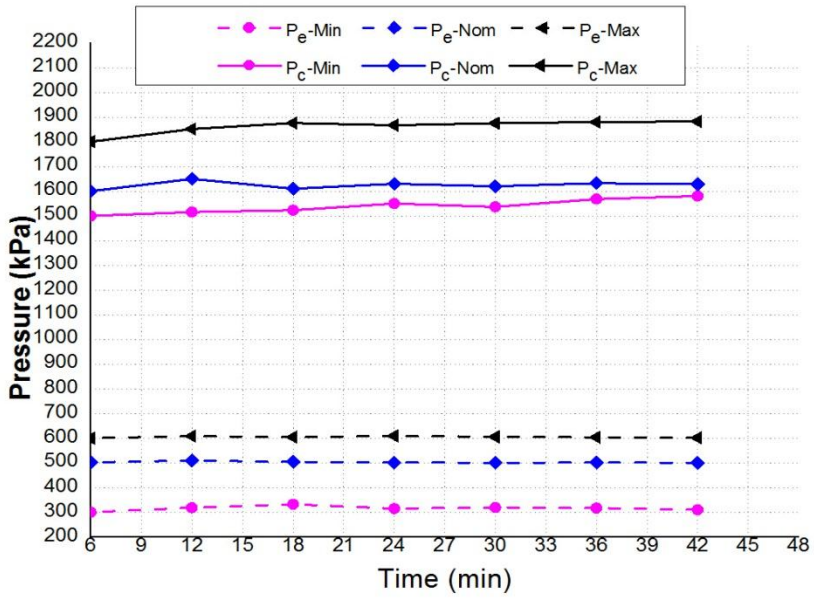

Figure 5. 4 Evaporating and condensing pressure change with simulating operation

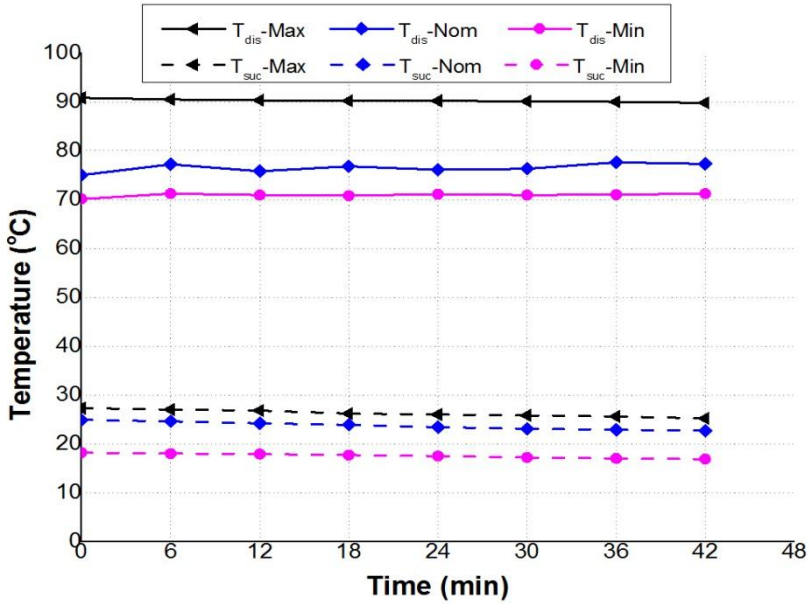

Figure 5. 5 Suction and discharge temperature change with simulating operation

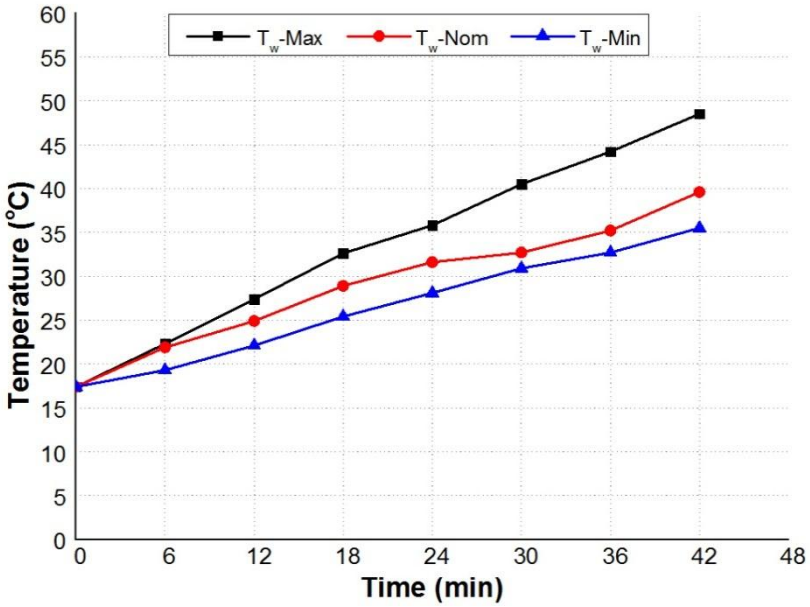

Figure 5. 6 Water temperature change with simulating operation

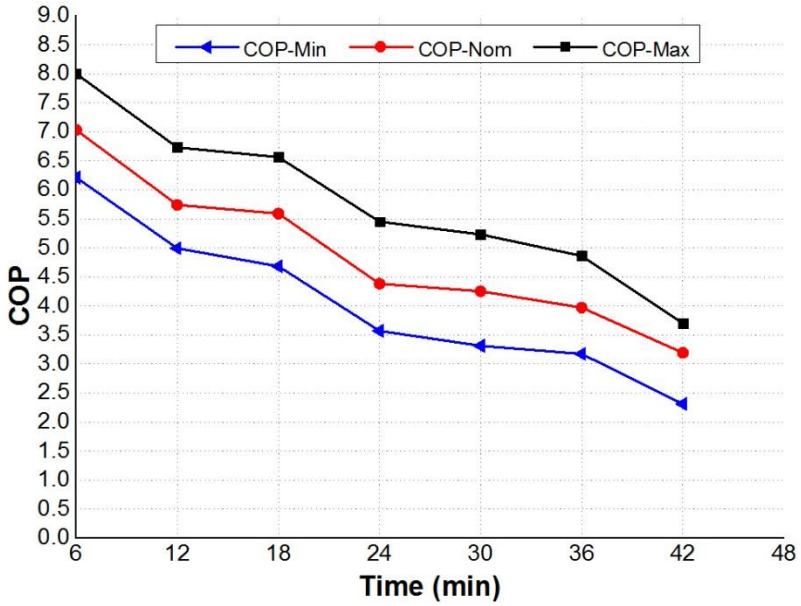

Figure 5. 7 COP change with simulating operation

5.4.1.2.2 Experimental Results

The testing on the influence of increasing water temperature as a function of time on temperature and pressure of the novel heat pump system is carried out. Figure 5.8, Figure 5.9 and Figure 5.10 show the influence of increasing water temperature as a function of time on evaporating and condensing pressure during operation at nominal,

minimum and maximum load conditions, respectively. It can be seen that the evaporating pressure increases with the increasing room temperature. This is because the increasing room temperature leads to the increase of temperature gap between refrigerant and room air, which increases the cooling load.

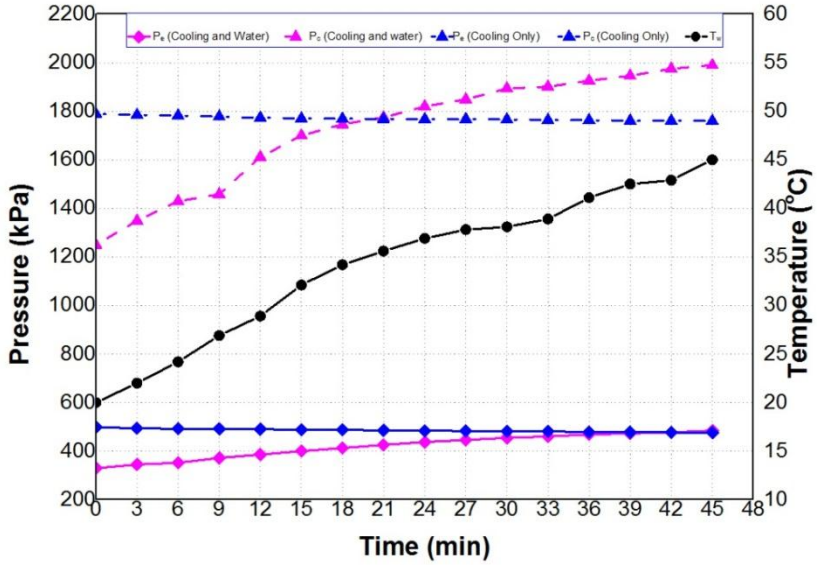

Figure 5. 8 Variation of evaporating and condensing pressure as a function of time with increasing water temperatures during experimental operation at nominal load condition

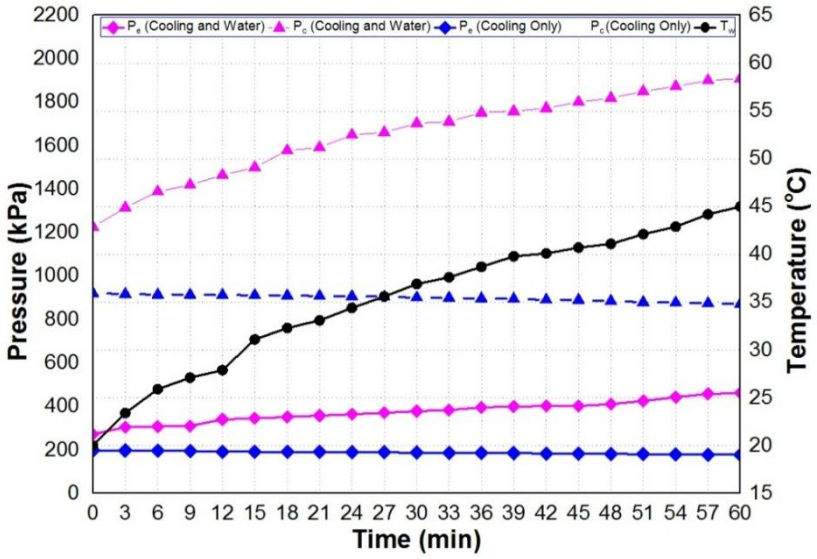

Figure 5. 9 Variation of evaporating and condensing pressure as a function of time with increasing water temperatures during experimental operation at minimum load condition

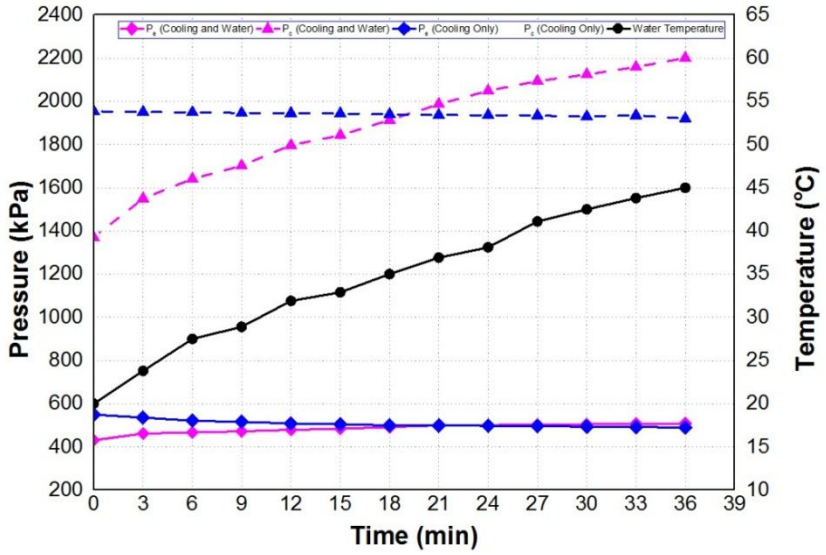

Figure 5. 10 Variation of evaporating and condensing pressure as a function of time with increasing water temperatures during experimental operation at maximum load condition

Figure 5.11, Figure 5.12 and Figure 5.13 show the influence of increasing water temperature as a function of time on suction and discharge temperature during operation at nominal, minimum and maximum load conditions, respectively. It can be attributed to the fact that the length of time becomes shorter on water temperature reaches to 45^{o}C with the increasing room temperature. That is because the increasing room temperature leads to the increase of temperature gap between the refrigerant in internal heat exchanger and ambient air, which increases the heating load, and thus shorts the length of time. However, the rate of temperature rises slowly from 35^{o}C to 45^{o}C. That is because the area of heat exchanger in solar thermal collector is designed at certain value according to the nominal conditions. The heat transfer area is relatively large before the water temperature at 35^{o}C. It means large heat transfer rate causes the temperature rise sharply before water temperature at 35^{o}C. Unfortunately, with the water temperature is increasing from 35^{o} C to 45^{o}C, the reduction of heat

transfer area leads to the decline of heat transfer, which causes the rate of water temperature to rise slightly.

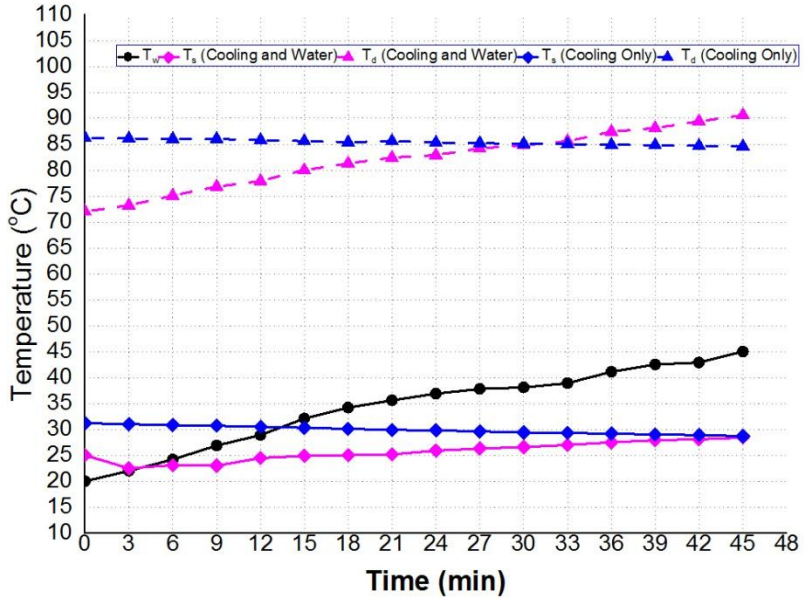

Figure 5. 11 Variation of suction and discharge temperature as a function of time with increasing water temperatures during experimental operation at nominal load condition

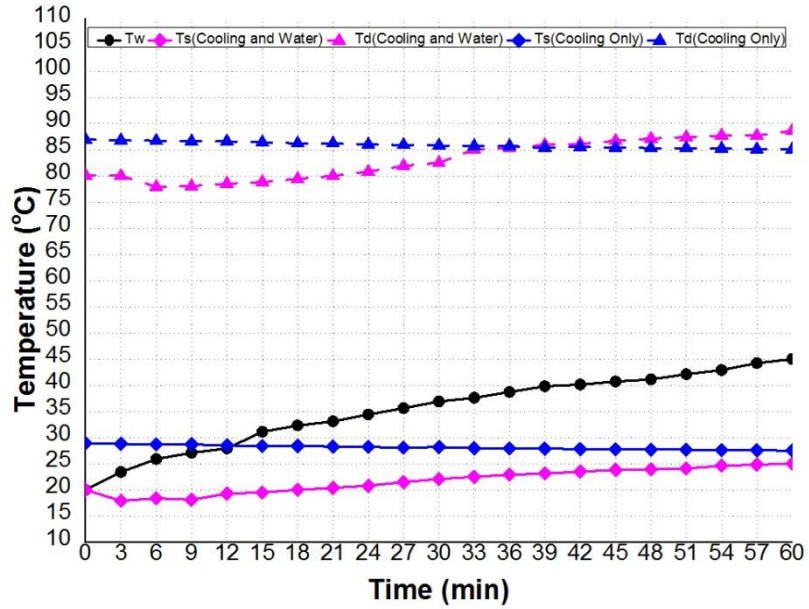

Figure 5. 12 Variation of suction and discharge temperature as a function of time with increasing water temperatures during experimental operation at minimum load condition

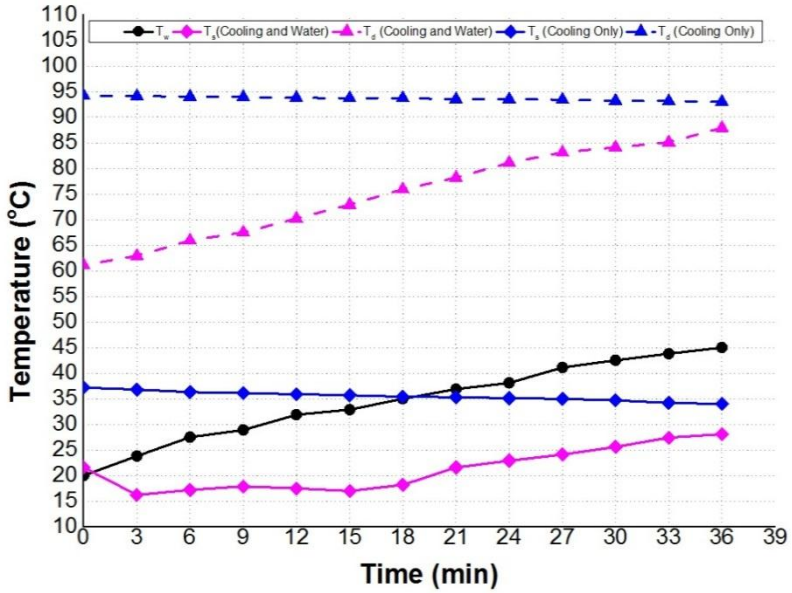

Figure 5. 13 Variation of suction and discharge temperature as a function of time with increasing water temperatures during experimental operation at maximum load condition

The testing on the influence of increasing water temperature as a function of time on COP_{Total} of the system is carried out. Because this novel system is operated for space cooling and domestic hot water supplement, the COP_{Total} of the system should be comprehensive considered the COP_w of hot water supplement and the COP_c of space cooling.

Figure 5.14, Figure 5.15 and Figure 5.16 show the influence of increasing water temperature as a function of time on COP_{Total} during nominal, minimum, and maximum load conditions, respectively. Based on these Figures, we can see that COP_w, COP_c, and COP_{Total} are declined with the increasing water temperature. In addition, COP_w and COP_c have the same relatively stable downward trend, the COP_{Total} decreases rapidly. The COP_{Total} of 6.8, 7.7 and 7.9 is higher than the traditional ASHP of 1.6, 3.3 and 3.5 when the ambient temperature at 21°C, 35°C and 43°C, respectively.

When the system is operated under the nominal conditions, the COP_w and COP_c are lower than the COP of ASHP as the water temperature reaches to 35^{o}C. However, the COP_{Total} is still higher than the COP of ASHP. It reflects a great energy saving of novel SAHP than traditional ASHP for space cooling and domestic hot water supplement in most usage times in summer.

When the system is operated at the minimum load conditions, the COP_w and COP_c are lower than the COP of ASHP, and the COP_{Total} is lower than the COP of ASHP as the water temperature reaches to 35^{o}C. It reflects that the COP of novel SAHP is not as high as expected for space cooling and domestic hot water supply together when operating at the lower ambient temperature. In order to achieve great energy savings, the best way is using traditional ASHP for space cooling and solar thermal collector for hot water supplement separately.

When operating at the maximum load conditions, the COP of ASHP is the lowest due to the ambient temperature is particular high at 43^{o}C. The COP_c is still higher than the COP of ASHP. When the hot water is constantly used and the cold water is continuously injected into the glass tubes, the COP_{Total} will be further improved. It reflects an efficient energy saving of novel SAHP than traditional ASHP for space cooling and domestic hot water supplement in particularly high ambient temperature in summer.

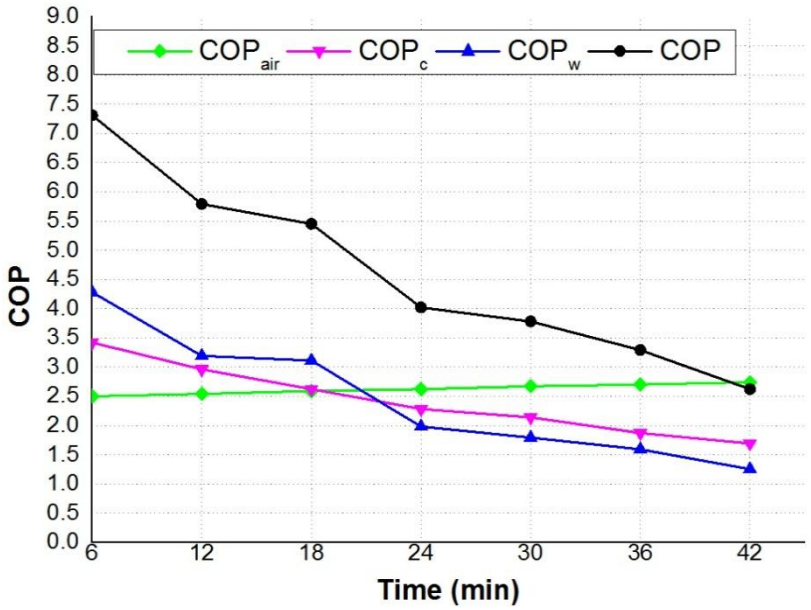

Figure 5. 14 Variation of COP at increasing water temperature during experimental operation at nominal load condition

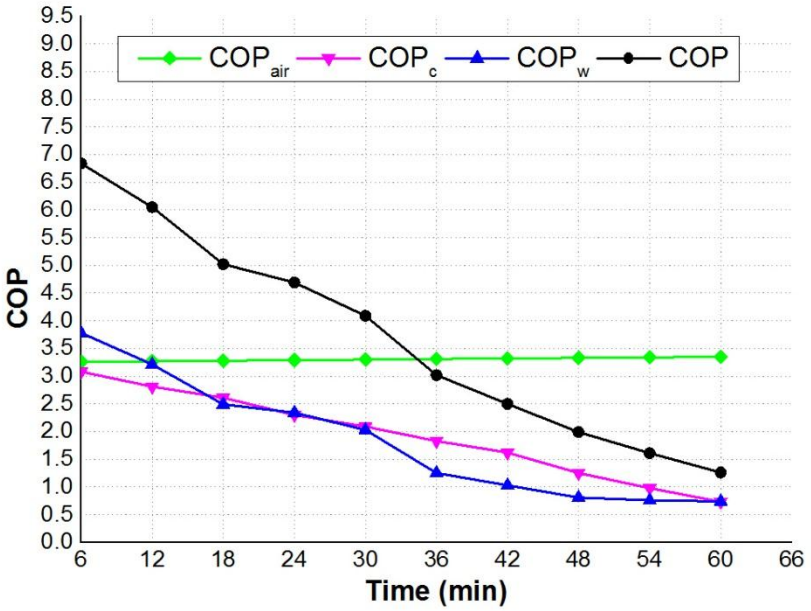

Figure 5. 15 Variation of COP at increasing water temperature during experimental operation at minimum load condition

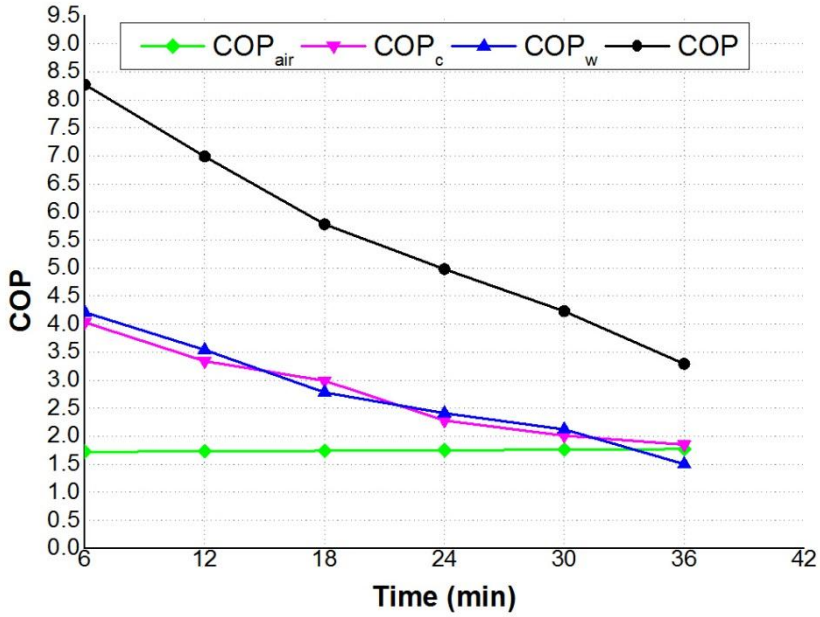

Figure 5. 16 Variation of COP at increasing water temperature during experimental operation at maximum load condition

5.4.1.2.3 Comparison of Simulation and Experimental Results

Figure 5.17, Figure 5.18 and Figure 5.19 show the comparison of evaporating and condensing pressure, suction and discharge temperature, and COP on nominal load conditions, respectively. The errors of parameter are within the allowable range, only the deviations of the predicted and measured the cycle for space cooling and hot water supplement are more than the allowable range. That is because the overall of the numerical analysis is the dynamic model. However, the every iterative calculation is the steady state model.

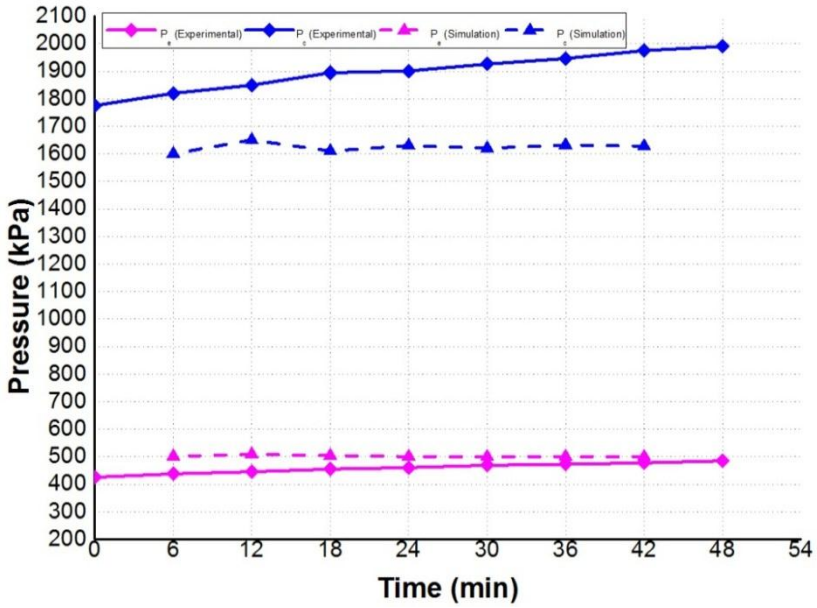

Figure 5. 17 Comparison of evaporating and condensing pressure at increasing water temperature on nominal load condition

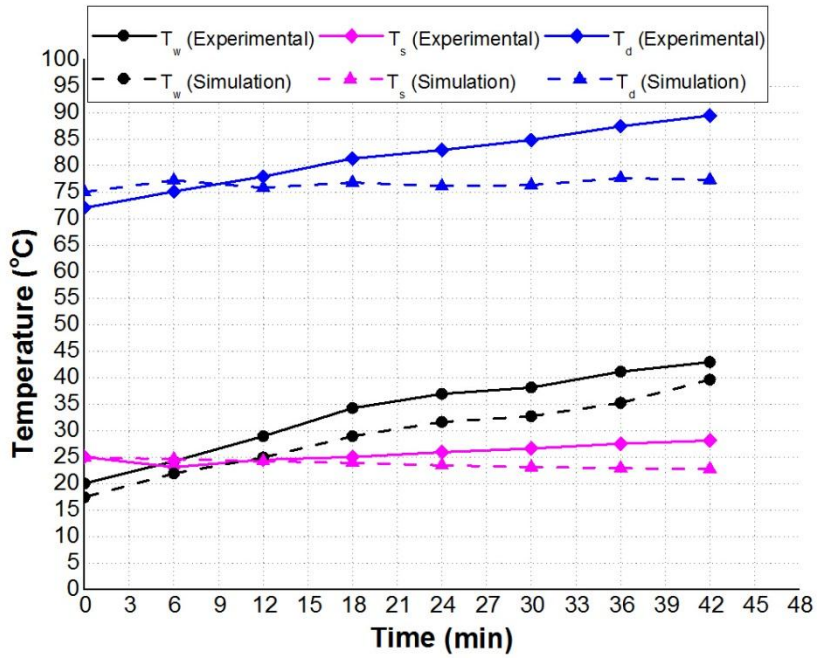

Figure 5. 18 Variation of suction and discharge temperature at increasing water temperature on nominal load condition

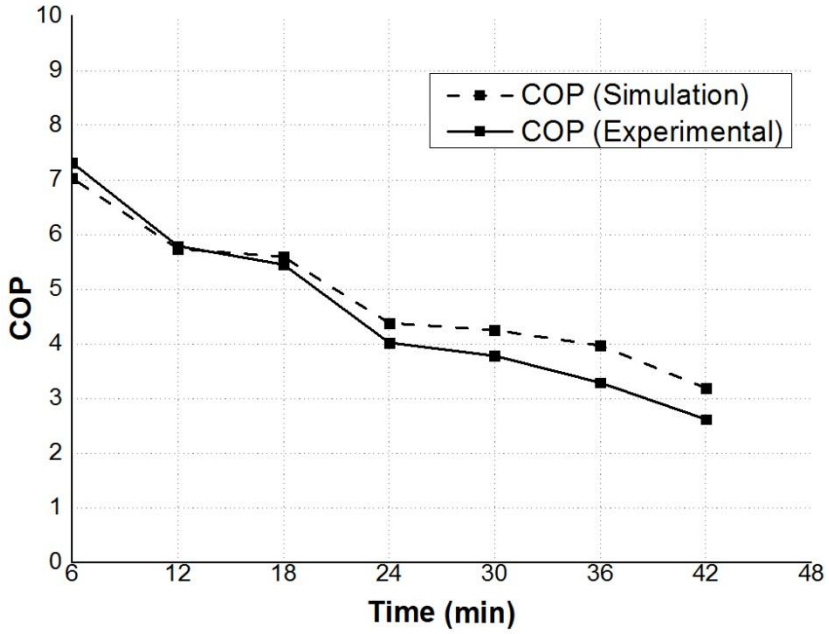

Figure 5. 19 Comparison of COP on nominal load condition

5.4.2 Performance of SAHP under Winter Condition

In order to analysis the heating performance of system, the working conditions in winter seasons are shown in Table 5.7.

Table 5. 7 Working conditions in winter seasons

Condition	Ambient temperature	Room temperature
Minimum Load Condition	24^{o}C	27^{o}C
Nominal Load Condition	7^{o}C	20^{o}C
Maximum Load Condition	2^{o}C	20^{o}C

5.4.2.1 Air Source Heat Pump for Space Heating

When the system operates for space heating, the simulation and experimental results operated under different working conditions are shown in Table 5.8 and Table 5.9, respectively. In addition, Table 5.10 shows the parameters comparison of simulation and experimental results for space heating during nominal load conditions.

In Table 5.8, the simulation results show that the COP and heating capacity decreases with the decreasing heating load At the minimum load condition, the COP is 3.38 and the condenser heating capacity is 3410 W. At the nominal working condition, the COP is 3.12 and the condenser heating capacity is 2981 W. At the maximum load condition, the COP is 2.61 and the condenser cooling capacity is 2547 W. The decreasing system load leads to the decrease of suction and discharger temperature, evaporation and condensation temperature, and the power consumption of compressor, which reduces the heating capacity, and thus reduces the COP.

Table 5. 8 Simulation results under different operating conditions

	Minimum load condition	Nominal working condition	Maximum load condition
Suction temperature (^{o}C)	22.74	8.52	4.10
Discharge temperature (^{o}C)	65.12	50.21	45.19
Evaporating pressure (k Pa)	401.23	413.59	285.97
Condensing pressure (k Pa)	1384.57	951.78	1152.47
Heating capacity (W)	3410	2981	2547
Power (W)	1029.87	985.12	974.12
COP	3.38	3.12	2.61

The experimental results from Table 5.9 indicate that the COP and heating capacity decreases with the decreasing heating load. At the minimum load condition, the COP is 2.98 and the condenser heating capacity is 3864 W. At the nominal working condition, the COP is 2.62 and the condenser heating capacity is 2558.98 W. At the maximum load condition, the COP is 2.01 and the condenser cooling capacity is 2102.3

W. The decreasing system load leads to the decrease of suction and discharger temperature, evaporation and condensation temperature, and the power consumption of compressor, which reduces the heating capacity, and thus reduces the COP.

Table 5. 9 Simulation results under different operating conditions

	Minimum load condition	Nominal working condition	Maximum load condition
Suction temperature (^{o}C)	25.16	10.02	4.68
Discharge temperature (^{o}C)	68.92	61.54	46.2
Evaporating pressure (k Pa)	289.4	311.24	194.6
Condensing pressure (k Pa)	1617.3	1132.1	1321.5
Heating capacity (W)	3864	2558.98	2102.3
Power (W)	1204.3	1020.1	997.3
COP	2.98	2.62	2.01

The parameters comparison of simulation results and experimental results for ASHP for space heating during nominal load conditions are shown in Table 5.10. From these, we can see that the errors of the parameter are relatively small, and only evaporating pressure has a certain error. This is because the pressure drop is ignored in the evaporator during the simulation which causes the high numerical value. In addition, small changes of pressure are corresponded to the big substantial changes of temperature.

Table 5. 10 Comparison of simulation results and experimental results for space heating

	Experimental	Numerical	Relative error (%)
Suction temperature (^{o}C)	10.02	8.52	14.97
Discharge temperature (^{o}C)	61.54	50.21	18.41
Evaporating pressure (k Pa)	311.24	413.59	32.88
Condensing pressure (k Pa)	1132.1	951.78	15.92
Cooling capacity (W)	2558.98	2981	16.49
Power (W)	1020.1	985.12	3.42
COP	2.62	3.12	19.08

5.4.2.2 Novel Solar Assisted Heat Pump for Space Heating and Hot Water Supply

5.4.2.2.1 Simulation Results

The simulations of the system that is operated for space heating by extracting heating from water in solar collector under different working conditions are carried. Figure 5.20 and Figure 5.21 show the evaporating and condenser pressures as well as suction and discharge temperatures, respectively. It can be seen that the increasing load leads to the increase of suction and discharge temperature as well as evaporating and condenser pressure, which accelerates the declined rate of water temperature, and thus decreases the final water temperature.

Figure 5.22 shows the variation of COP under different working conditions for space heating by extracting heating from water in solar collector. It can be seen that the COP increases with the decreasing

room air temperature. This is because the decreasing room air temperature leads to the increasing of the heating load, which increases the evaporation temperature and reduces the consumption power. However, the evaporation heat is difficult to release along with the decreasing water temperature, and thus reduces the COP gradually.

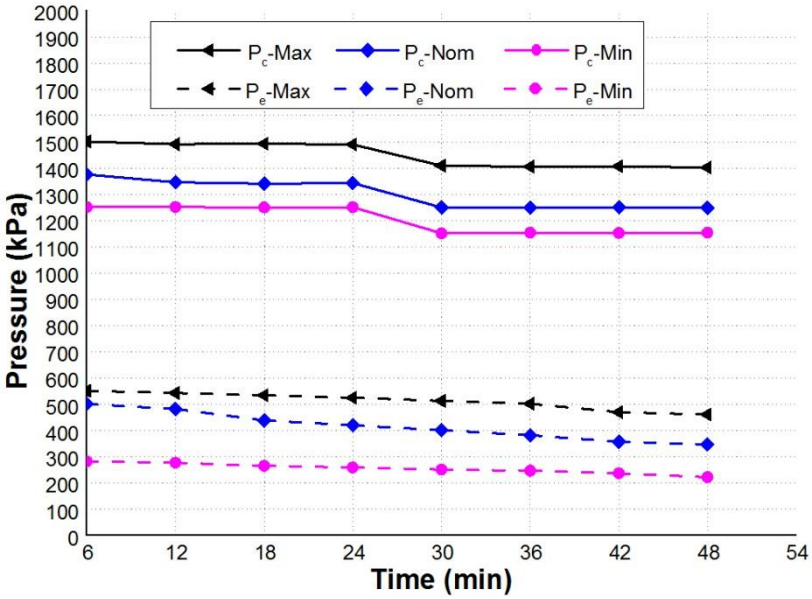

Figure 5. 20 Evaporating and condensing pressure change with simulating operation

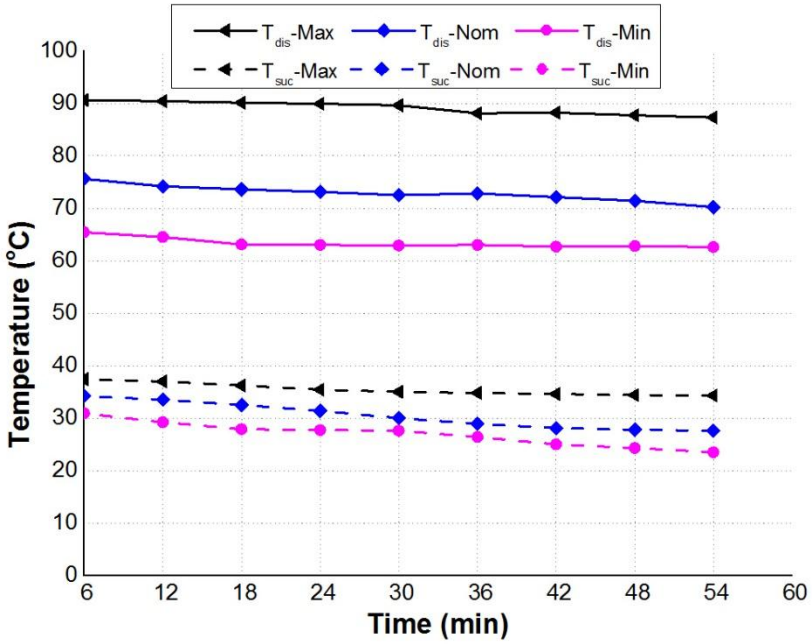

Figure 5. 21 Suction and discharge temperature change with simulating operation

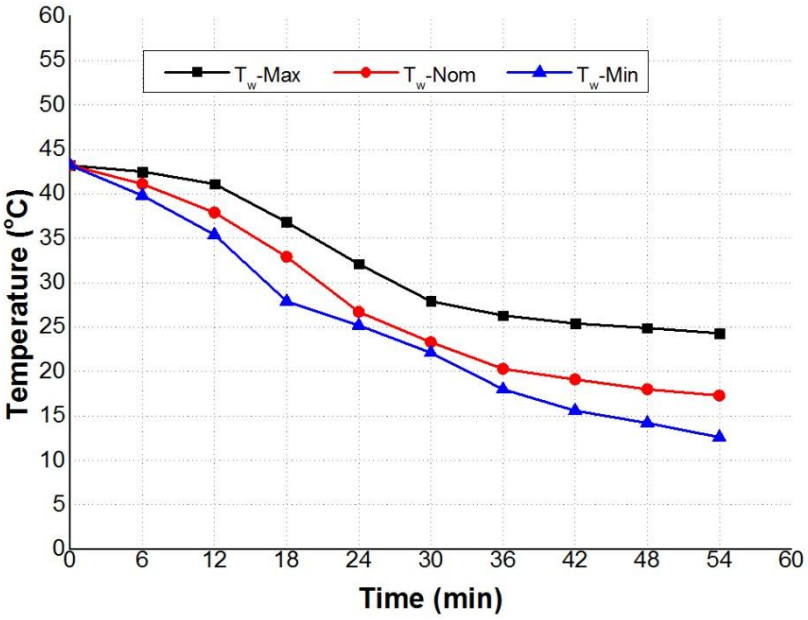

Figure 5. 22 Water temperature change with simulating operation

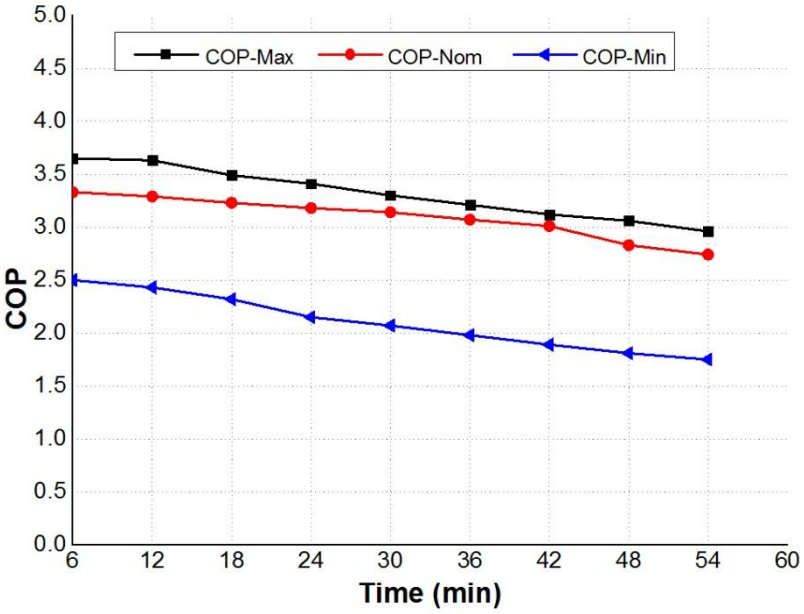

Figure 5. 23 COP change with simulating operation

5.4.2.2.2 Experimental Results

The testing on the influence of temperature and pressure as a function of time for decreasing water temperature of the hybrid heat pump system was carried out in the lab. Figure 5.24, Figure 5.25 and Figure 5.26 show the influence of evaporating and condensing pressure as a

function of time for decreasing water temperature during operates at nominal, minimum and maximum load conditions, respectively. Figure 5.27, Figure 5.28 and Figure 5.29 show the influence of suction and discharge temperature as a function of time for decreasing water temperature during operates at nominal, minimum and maximum load conditions, respectively.

Based on the figures, we can see the period for water temperature dropping to 15^{o}C takes more and more time with the room temperature increasing when novel system uses hot water in solar collector for space heating. That is because the heating load decreases with room temperature increasing, the same amount of water can maintained longer. With water temperature at 20^{o}C, the water temperature decreases slowly due to the heat transfer area being a certain value. Before water temperature reaches 20^{o}C, the heat transfer area is relatively large, the water temperature decreases rapidly. The heat transfer area is relatively reduced with the water temperature decreasing, resulting in the heat transfer rate declining and the water temperature decreasing slowly.

When operating at the maximum load conditions, with the water temperature decreasing, the pressures of condensing and evaporating and temperatures of suction and discharge are particular increase because the difference between water temperature and ambient temperature is relatively large. When the system is stable, the decreasing trend gradually increases. When water temperature is at 20^{o}C, because of lower water temperature, the pressures of condenser and evaporating and the temperatures of suction and discharge are declined faster.

When operating at the minimum load conditions, with the water temperature decreasing, the pressures of condensing and evaporating and the temperatures of suction and discharge decreases slowly because the water temperature decreases are small and the heat transfer rate is relatively low.

Furthermore, it follows that the water decreasing temperature should avoid low temperature, preferably no less than 15^{o}C. If the water temperature is lower than 15^{o}C, the evaporating temperature is so low that most of the refrigerant liquid cannot extract heat, which results in a reduction of heating capacity, even cracking the glass tubes of solar collector.

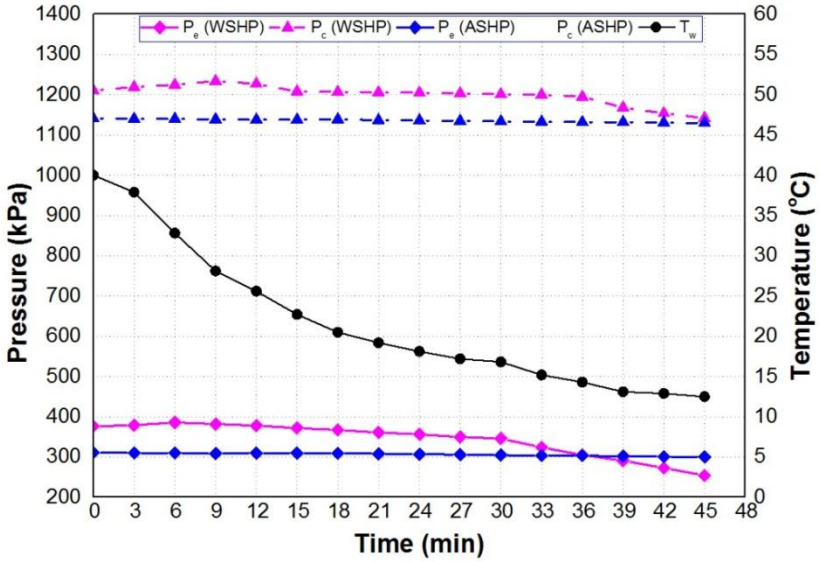

Figure 5. 24 Evaporating and condensing pressure as a function of time for decreasing water temperatures during experimental operation at nominal load condition (ambient 7^{o}C/room 20^{o}C)

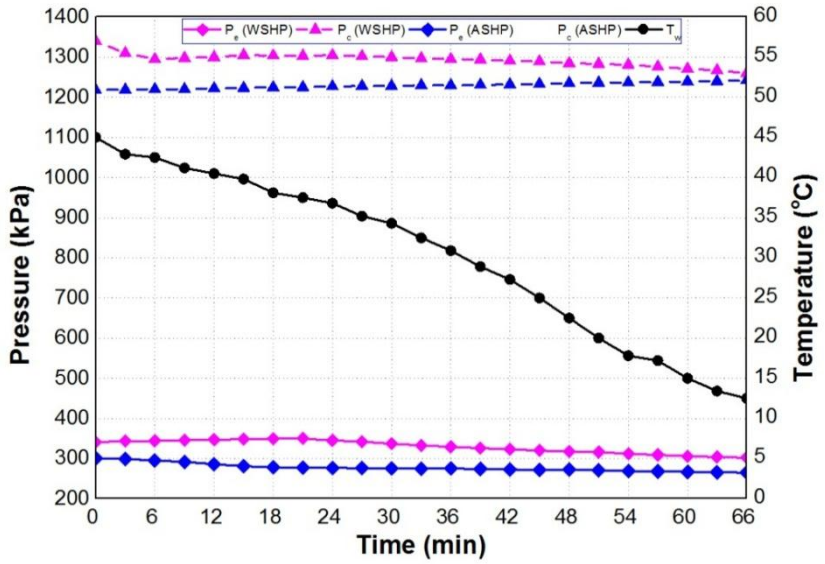

Figure 5. 25 Evaporating and condensing pressure as a function of time for decreasing water temperatures during experimental operation at minimum load condition (ambient 24^{o}C/room 27^{o}C)

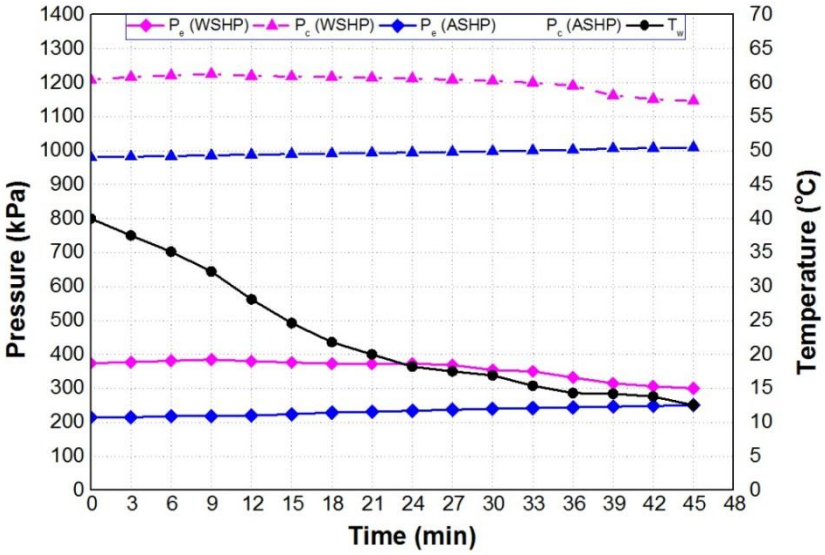

Figure 5. 26 Evaporating and condensing pressure as a function of time for decreasing water temperatures during experimental operation at maximum load condition (ambient 2^{o}C/room 20^{o}C)

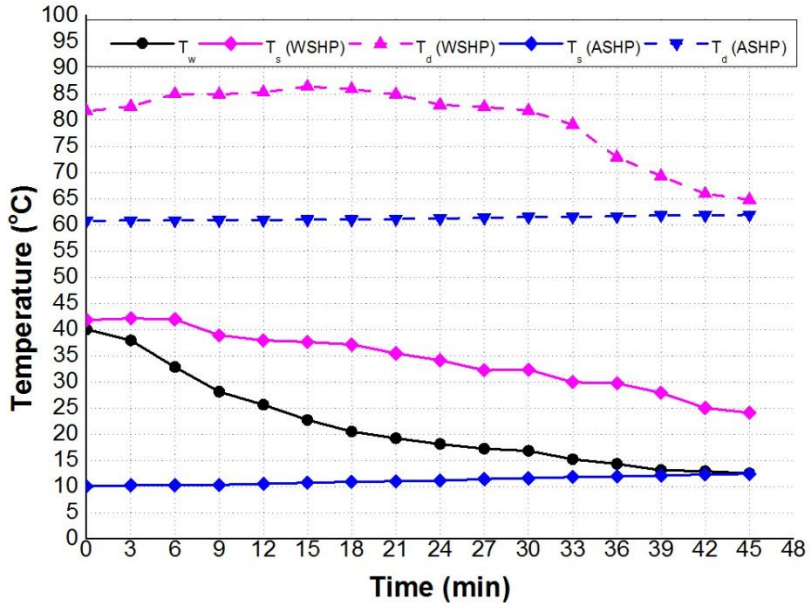

Figure 5. 27 Variation of suction and discharge temperature at increasing water temperature during experimental operation at nominal load condition (ambient 7°C/room 20°C)

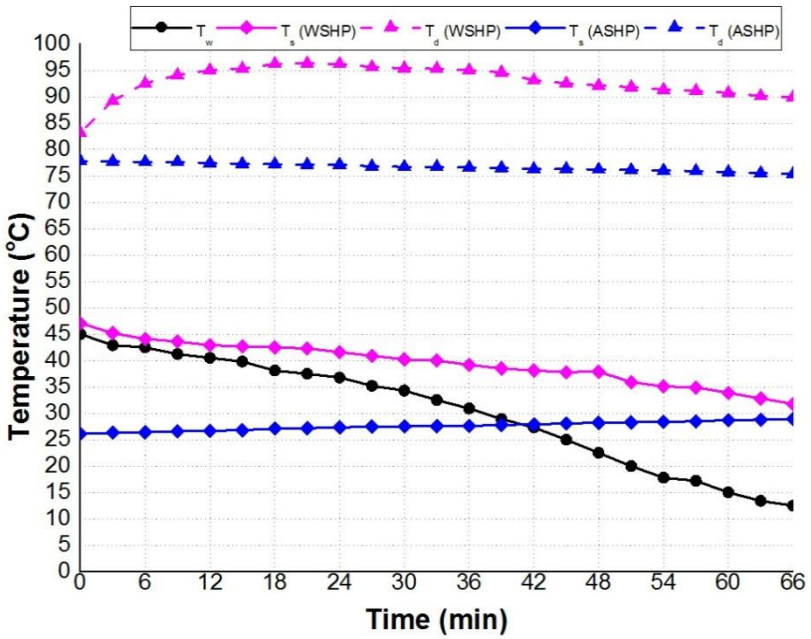

Figure 5. 28 Variation of suction and discharge temperature at increasing water temperature during experimental operation at minimum load condition (ambient 24°C/room 27°C)

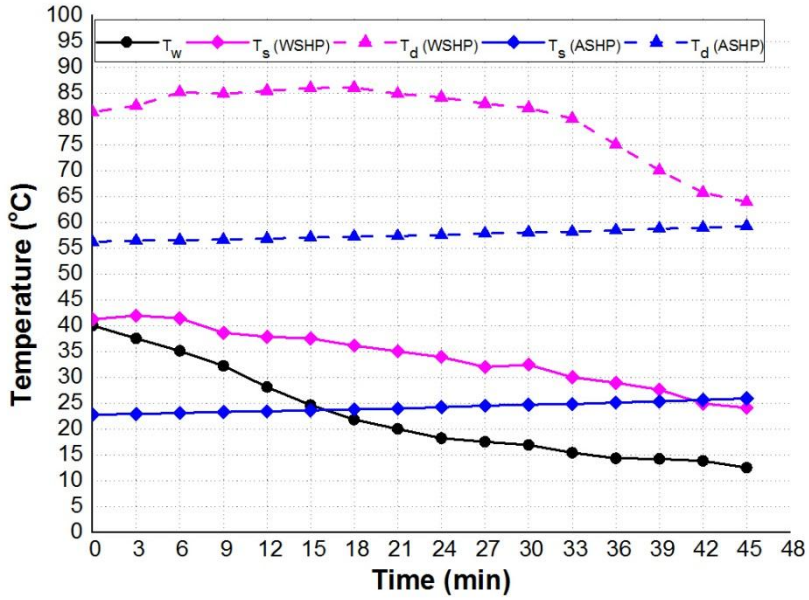

Figure 5. 29 Variation of suction and discharge temperature at increasing water temperature during experimental operation at maximum load condition (ambient 2^{o}C/room 20^{o}C)

5.4.2.2.3 Comparison of Simulation and Experimental Results

For the purpose of analysis of the COP as the function of time for decreasing water temperature, Figure 5.30, Figure 5.31 and Figure 5.32 show the variation of COP at decreasing water temperature during nominal, minimum, and maximum load conditions. From these Figures, we can see that COP declines with the decreasing water temperature. Before water temperature reaches at 20^{o}C, the COP declines relatively slowly.

When operates at nominal and maximum load conditions, the temperature differences between ambient temperature and hot water temperature and the heat load are relatively large. The operating time is relatively longer than operates at minimum load conditions when using hot water for space heating.

As the ambient temperature increases, the heating load is increased. Compared with traditional ASHP, COP varies from2.7 to 3.71, 2.65 to

3.58, and 2.32 to 2.86 when the ambient temperature at 2^{o}C, 7^{o}C, and 24^{o}C, respectively.

When operating at nominal load conditions, the COP is still higher than the COP of ASHP during an entire process even when the water temperature decreases at 15^{o}C. It reflects a great energy saving of novel SAHP than traditional ASHP for space heating in summer.

When operates at the minimum load conditions, the COP is only a little higher than the COP of ASHP. Before water temperature reaches 20^{o}C, the COP decreases rapidly. It can be seen that the COP of solar water for space heating is not as high as expected when ambient and room temperature is high.

When operating at the maximum load conditions, the COP of ASHP is very low due to the ambient temperature being particularly low at 2^{o}C. Using solar water for space heating, extracting heat from hot water, the COP is much higher than traditional the COP of ASHP. When operates at daytime with great solar radiation, the water temperature could maintain a high temperature, the COP will be further improved. Furthermore, when the system is operating at the extremely low ambient temperatures, it uses solar water for defrosting and later converts to ASHP. It reflects an efficient energy saving of novel SAHP over traditional ASHP for space heating in extremely low ambient temperatures in winter.

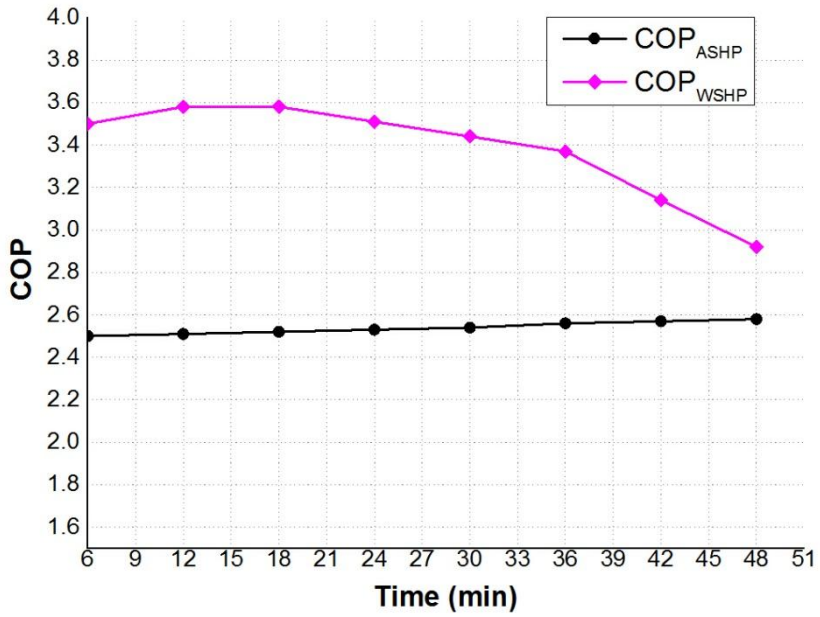

Figure 5. 30 Variation of COP during experimental operation at nominal load condition (ambient 7^{o}C / room 20^{o}C)

Figure 5.33, Figure 5.34 and Figure 5.35 show the comparison of evaporating and condensing pressure, suction and discharge temperature, and the COP on nominal load conditions, respectively. Therefore, the errors of parameter are within the allowable range, except the Solar-Water heat pump domestic hot water supply cycle is not steady when compared with the ASHP for heating only. It means using the dynamic model to simulate could result in large errors. This is due to the operating cycle changes with the indoor and ambient temperature and humidity, hot water temperature as well as other parameters change, therefore there is no stable condition. Furthermore, the COP is not as high as expected due to the U-type heat exchanger, indoor and outdoor heat exchangers are all designed for the heating mode.

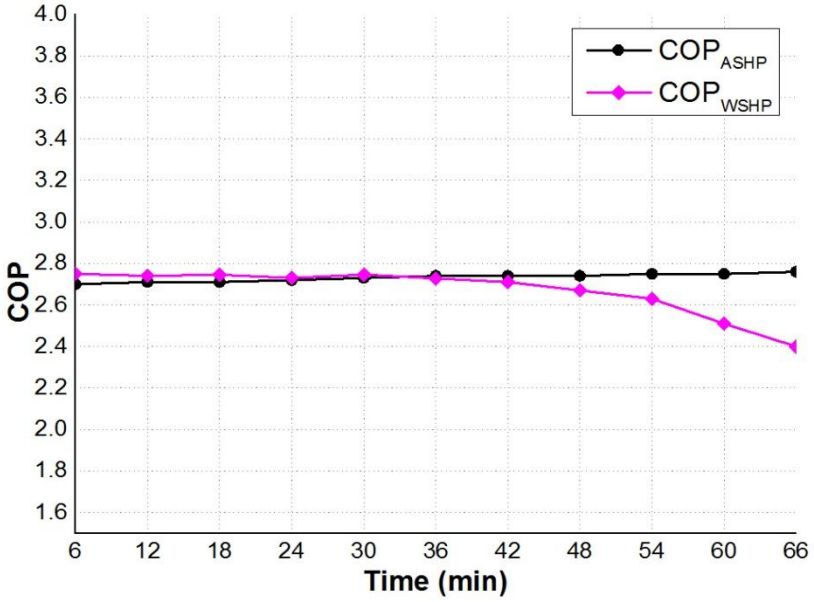

Figure 5. 31 Variation of COP during experimental operation at minimum load condition (ambient 24^{o}C / room 27^{o}C)

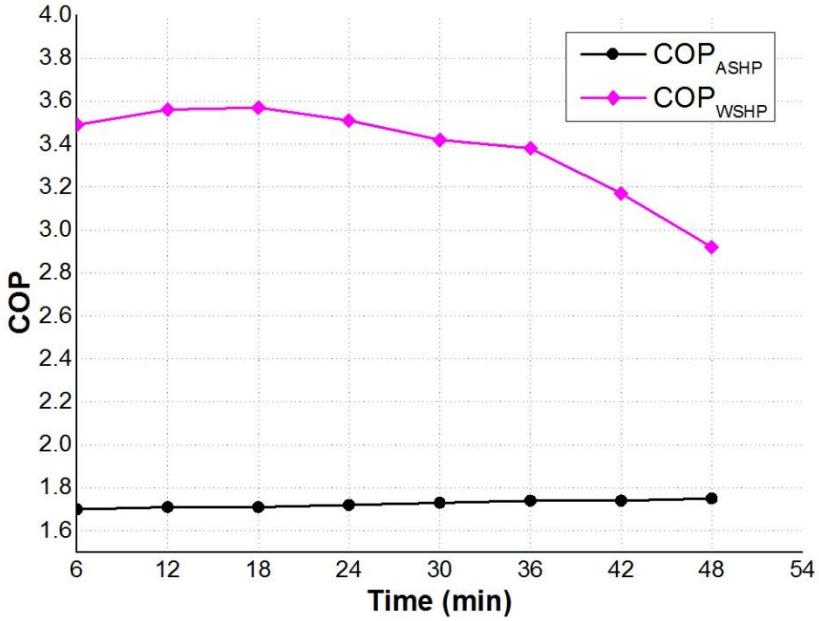

Figure 5. 32 Variation of COP during experimental operation at maximum load condition (ambient 2^{o}C / room 20^{o}C)

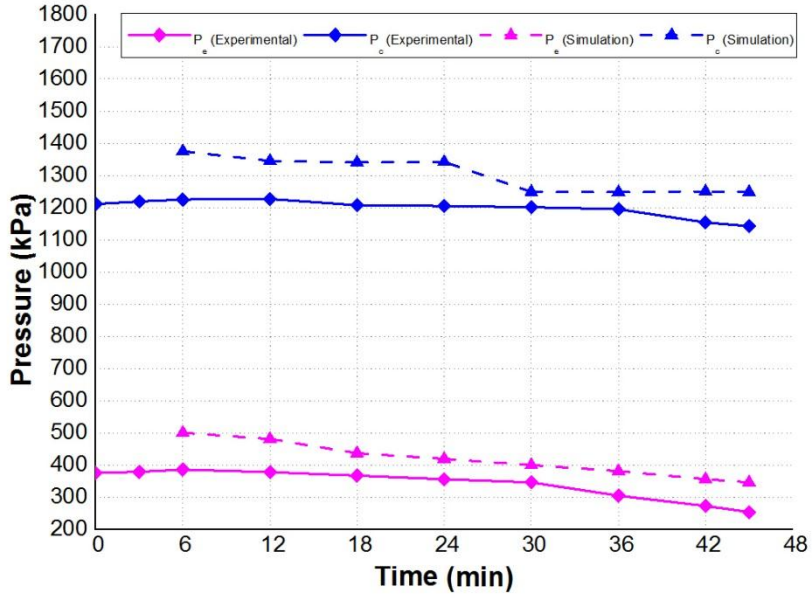

Figure 5. 33 Comparison of evaporating and condensing pressure at increasing water temperature on nominal load condition

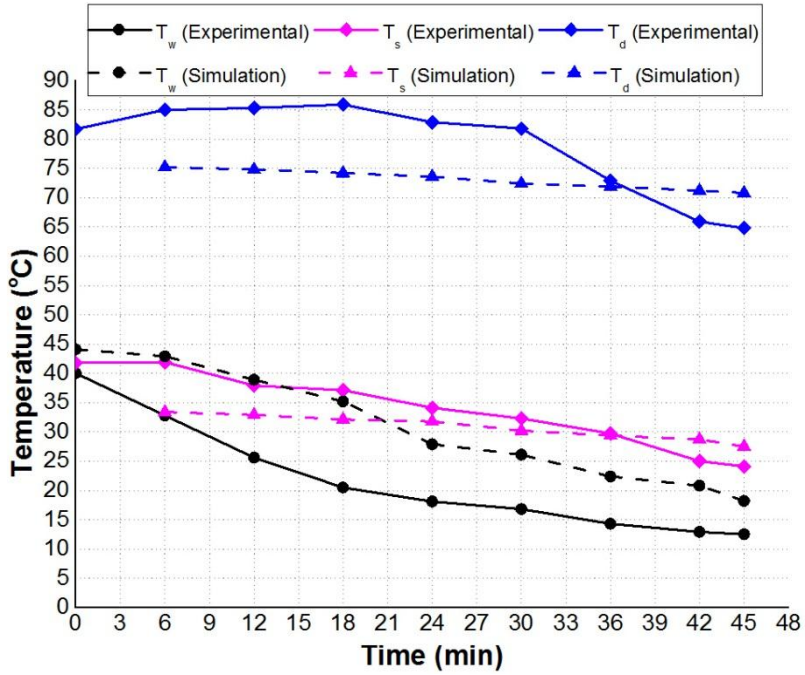

Figure 5. 34 Variation of suction and discharge temperature at increasing water temperature on nominal load condition

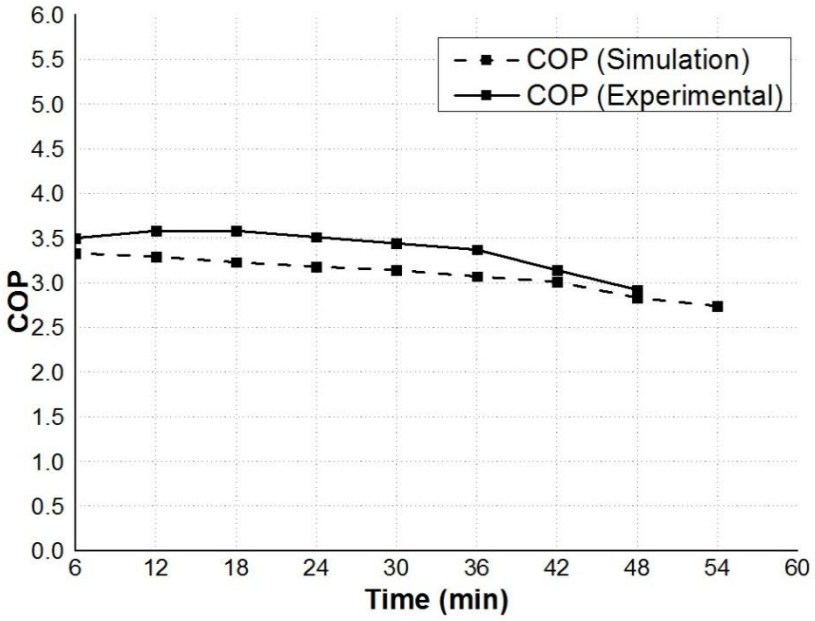

Figure 5. 35 Comparison of COP (simulation results and experimental results) for space heating and domestic hot water supply on nominal load condition

5.4.3 Performance of SAHP under Extreme Cold Condition

In order to analysis the heating performance of system, the working conditions in extreme cold conditions are shown in Table 5.11.

Table 5. 11 Working conditions in extremely cold seasons

Condition	Ambient temperature	Room temperature	Hot water temperature
Guarantee hot water usage	-25^{o}C	20^{o}C	40^{o}C
Do not guarantee hot water usage	-25^{o}C	20^{o}C	40^{o}C

The suction and discharge temperature as a function of time for hot water usage at extremely cold conditions are shown in Figure 5.36. Using the U-type heat exchanger as the evaporator, it has no relation with the indoor temperature. The hot water needs to reach 40^{o}C, and the

required heat load is not high enough, therefore, the system needs 6 minutes of preheating itself for stable operation.

The suction and discharge temperature as the function of time for space heating usage at the extremely cold conditions are shown in Figure 5.37. Using the U-type heat exchanger as the condenser, it has nothing to do with the outdoor temperature. The heat load is large because the heat load is large when the room temperature is 20^{o}C. It needs 13 minutes when working steady.

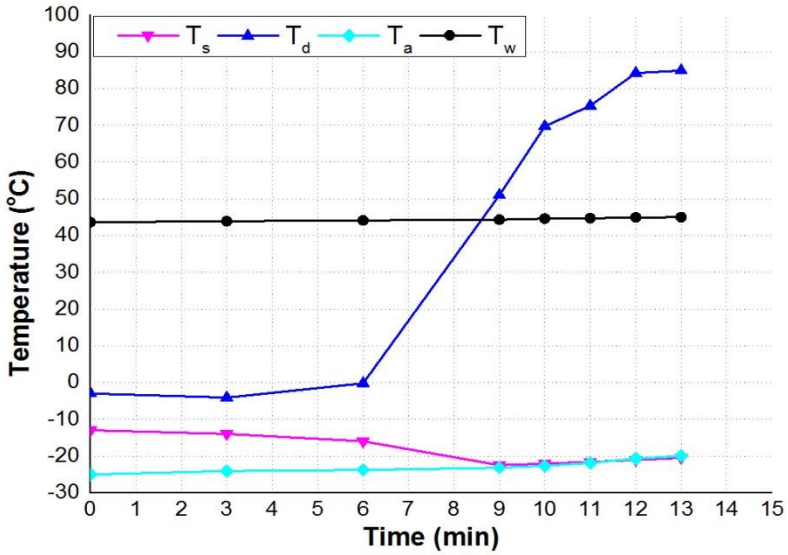

Figure 5. 36 Parameters of guaranteed hot water usage

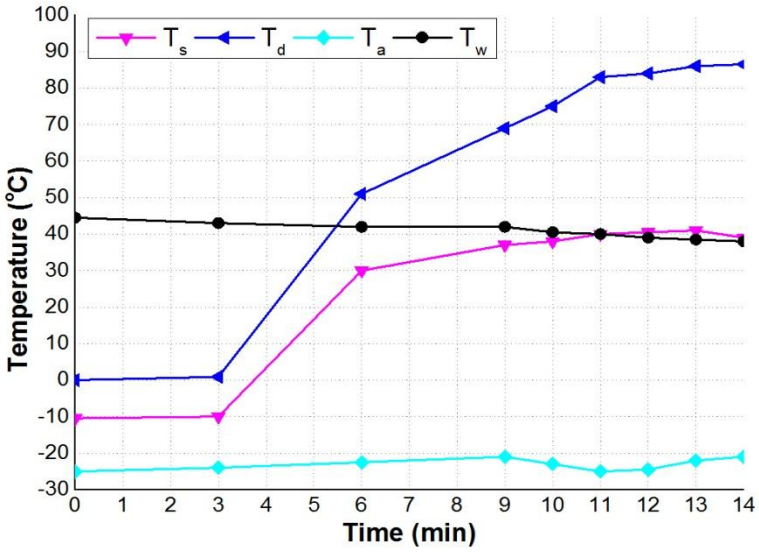

Figure 5. 37 Parameters of do not guarantee hot water usage

5.4.4 Performance of SAHP under Transitional Season

In order to analysis the performance of system, the working conditions in transitional seasons are shown in Table 5.12.

Table 5. 12 Working conditions in transition seasons

Condition	Ambient temperature	Hot water temperature
Nominal condition	20^{o}C	15^{o}C ~ 40^{o}C
Maximum condition	7^{o}C	15^{o}C ~ 40^{o}C

The testing on the influence of temperature and pressure as a function of time for increasing water temperature of the hybrid heat pump system is carried out. Figure 5.38 and Figure 5.39 show the influence of evaporating and condensing pressure as a function of time for decreasing water temperature during operation at nominal and maximum load conditions, respectively. Figure 5.40 and Figure 5.41 demonstrate the influence of suction and discharge temperature as a function of time for decreasing water temperature during operates at nominal and maximum load conditions, respectively.

Based on the data mention above, it follows that the time of water reaching 40^{o}C gets shorter and shorter with the increasing ambient temperature. When the ambient temperature is increased, the temperature difference between refrigerant temperature in outdoor heat exchanger and ambient temperature increases. Therefore, the heat transfer increases. However, the rate of temperature rises slowly with water temperature at 35^{o}C. This is because the area of heat exchange in the solar thermal collector system is designed with a certain value according the nominal conditions. The heat transfer area is relatively large before the water temperature reaches 35^{o}C. It means large heat transfer rate causes the temperature to rise sharply before water

temperature reaches 35^{o}C. Unfortunately, with the water temperature is increasing to 35^{o}C, the reducing heat transfer area leads to the decline of heat transfer, which makes the rate of water temperature rise slightly.

The condensing pressure and discharge temperature increases significantly with the increasing water temperature. Before water temperature reaches 35^{o}C, the condensing pressure and discharge temperature rises faster because water temperatures rise rapidly.

In addition, evaporating pressure and suction temperature slightly increase with the increasing water temperature in the whole process. Due to the water temperature is not too high, the refrigerant in U-type heat exchanger works well from vapour to liquid, then throttles into outdoor heat exchanger by capillary. The capillary has no adjustment function, the evaporating pressure and suction temperature are determined mainly by sub-cooling of refrigerant before entered in capillary. Sub-cooling is small and leads to the slight rise of evaporating pressure and suction temperature.

The evaporating pressure increases with the increasing ambient temperature. When the ambient temperature is increasing, the temperature difference between refrigerant temperature in outdoor heat exchanger and ambient temperature increases. Meanwhile, the heating load increases. However, the ambient temperature increases more than the temperature difference, so the evaporating pressure is increased effectively.

Furthermore, it is evident that the water heating temperature should be avoided high temperature, preferably no more than 45^{o}C. If the water temperature exceeds 45^{o}C, the condensing temperature should be higher than the water temperature. In heat transfer process, it is difficult

to release latent heat of refrigerant, only sensible heat is released. There is not a complete condensation of refrigerant vapour, which results in a reduction of cooling capacity. In addition, there is an increase in condensing pressure and discharge temperature, which increases the power consumption of compressor, even shuts down to protect the compressor.

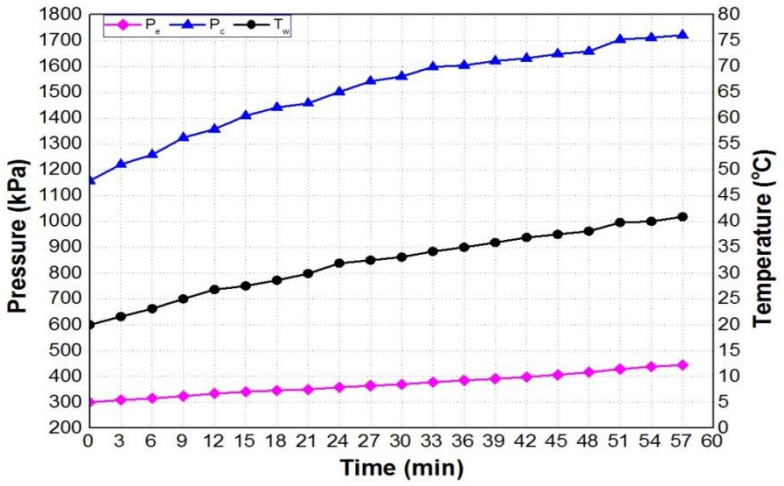

Figure 5. 38 Evaporating and condensing pressure and water temperature change during experimental operation at nominal load condition (ambient 20^{o}C)

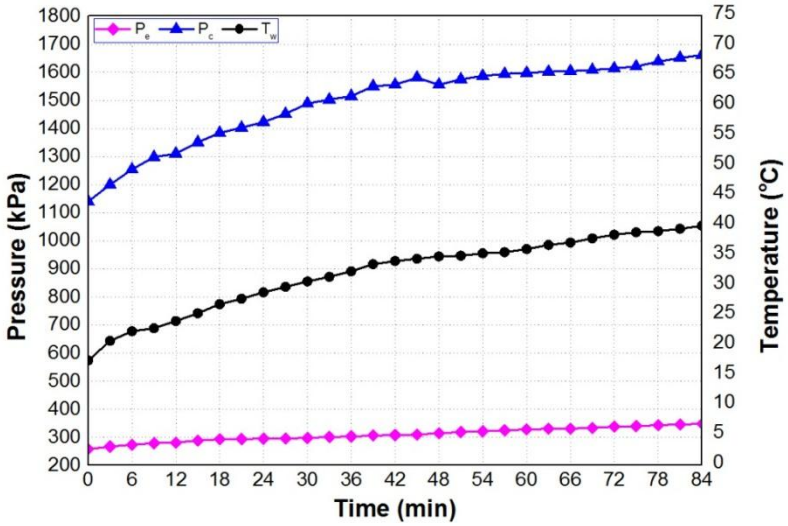

Figure 5. 39 Evaporating and condensing pressure and water temperature change during experimental operation at minimum load condition (ambient 7^{o}C)

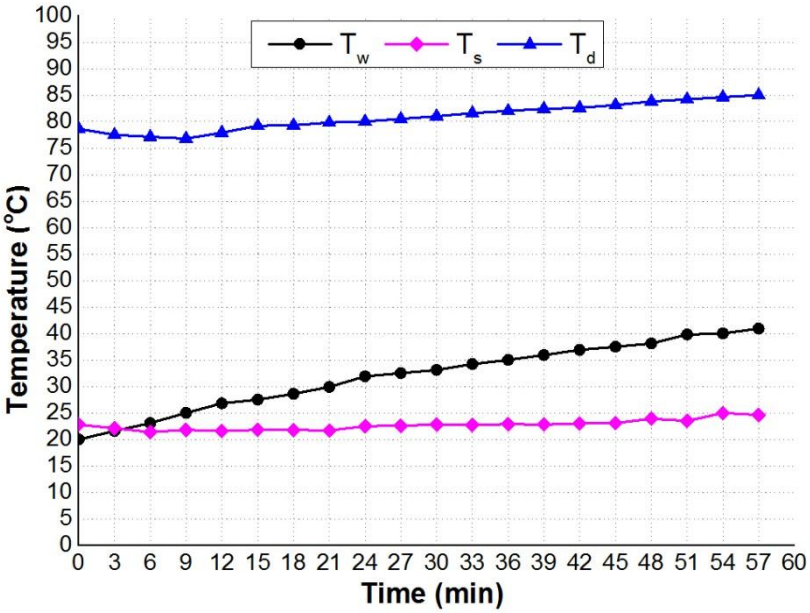

Figure 5. 40 Variation of suction and discharge temperature at increasing water temperature during experimental operation at nominal load condition (ambient 20^{o}C)

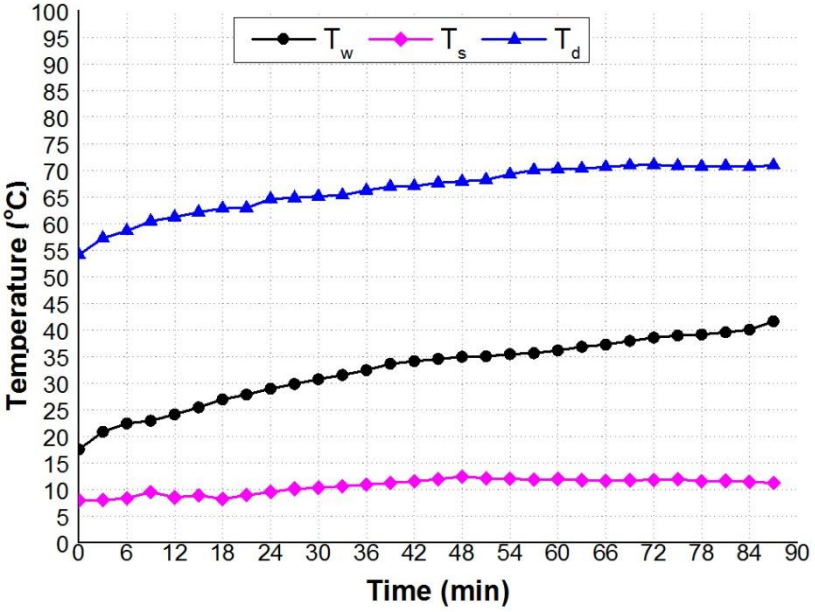

Figure 5. 41 Variation of suction and discharge temperature at increasing water temperature during experimental operation at minimum load condition (ambient 7^{o}C)

Figure 5.42 and Figure 5.43 show the variation of COP at increasing water temperature during nominal and maximum load conditions. From these Figures, we can see that the system needs about 13 minutes and

20 minutes to operate steady with ambient temperature at 20^{o}C and 7^{o}C, respectively. In addition, the COP of ASHP for hot water supply is declined with the water temperature increasing. In addition, the COP of water temperature from 20^{o}C to 30^{o}C decreases smaller than the COP of that from 30^{o}C to 35^{o}C. This is because the temperature difference between condensing temperature and water temperature is relatively reduced and the power consumption is increased. When water temperature increases from 35^{o}C to 40^{o}C, it is difficult to release condensation heat from refrigerant to water. In order to increase the water temperature, it mainly depends on the power consumption of compressor. In this period, the COP is the lowest. It concludes that the refrigerant R22 is not suitable for hot water supplement.

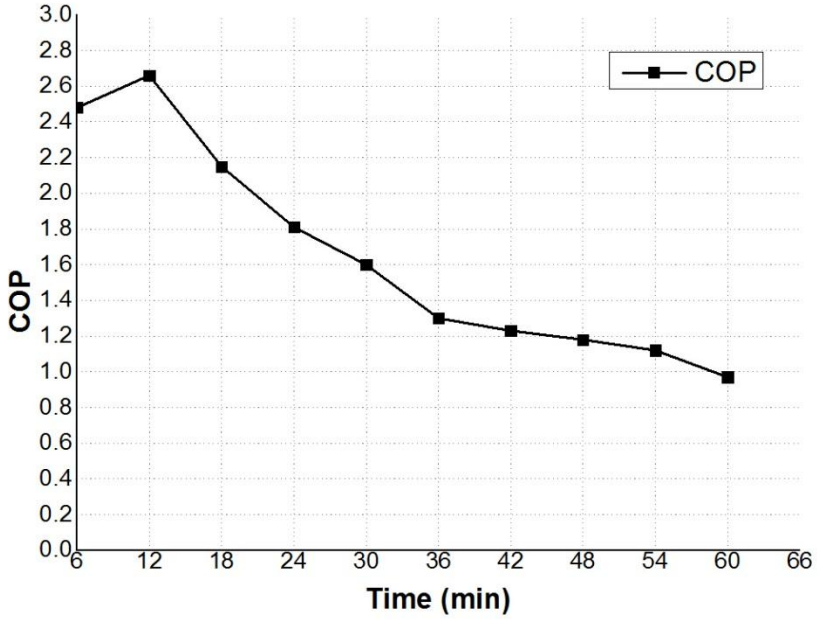

Figure 5. 42 Variation of COP during experimental operation at nominal load condition (ambient 20^{o}C)

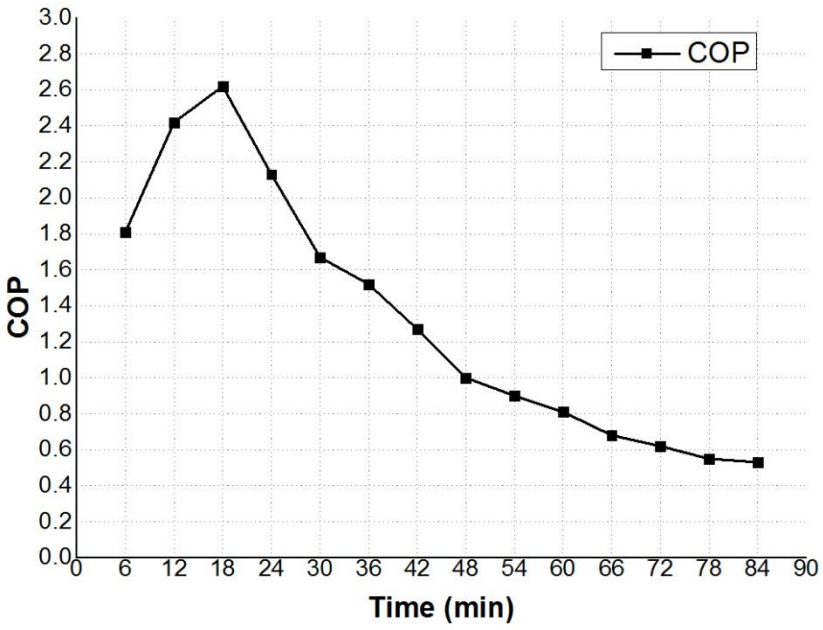

Figure 5. 43 Variation of COP during experimental operation at minimum load condition (ambient 7^{o}C)

5.5 Conclusion

Concerning the dynamic simulation and experimental results above, it can be concluded that:

- When operating in summer conditions, the COP_{total} is much higher than COP_{ASHP}, which reflects a great energy saving of novel SAHP than traditional ASHP for space cooling and domestic hot water supply in nominal load conditions (ambient 35^{o}C/ room 27^{o}C) and maximum load conditions (ambient 43^{o}C/ room 32^{o}C). In addition, when the hot water is constantly used and the cold water is continuously injected into the glass tubes, the COP_{total} will be further improved. However, COP_{total} is lower than COP_{ASHP} when the water temperature reaches 35^{o}C in minimum load conditions (ambient 21^{o}C/ room 21^{o}C). Furthermore, the water temperature should not be exceeded 45^{o}C.

- When operating in winter conditions, the COP is much higher than COP_{ASHP} during nominal load conditions (ambient 7^{o}C/ room 20^{o}C) and maximum load conditions (ambient 2^{o}C/ room 20^{o}C) even when the water temperature over 15^{o}C. When water temperature is below 15^{o}C, the COP is lower than COP_{ASHP} due to decreases rapidly. However, the COP is a little higher than COP_{ASHP} with water temperature at 20^{o}C during minimum load conditions (ambient 24^{o}C/ room 27^{o}C). Afterwards, the COP decreases rapidly.

- When operating in extremely cold conditions (ambient -25^{o}C/ room 20^{o}C/ hot water temperature 40^{o}C), the system needs 6 minutes and 13 minutes to operate steadily when guaranteeing hot water supply and guaranteeing space heating, respectively. In this situation, it has nothing to do with the indoor temperature.

- When operating in transitional seasons, the COP decreases smaller when the water temperature from 20^{o}C to 30^{o}C than the COP of that from 30^{o}C to 35^{o}C. When water temperature increases from 35^{o}C to 40^{o}C, it is difficult to release condensation heat from refrigerant to water. In order to increase water temperature, it mainly depends on the power consumption of compressor. In this period, the COP is the lowest. It concludes that the refrigerant R22 is not suitable for hot water supplement.

Chapter 6 Conclusion and Further Work

6.1 Conclusion

In this thesis, in order to achieve the aims of aesthetic, efficiency and multi-functional, four aspects of investigations are independently investigated. It is considered that solar energy to charge the heat pump system could provide a solution and additionally provide a sustainable and constant COP for long term.

Two investigations (Chapter 3) are focused on the possibilities to improve the electrical efficiency by reducing the PV temperature and to integrate architecturally with high-rise residential building sectors without water tanks. The two systems are investigated under the conditions to provide water heating. A series of indoor tests are performed at the laboratory of the school of the Built Environment, University of Nottingham. Experimental results are compared with the theoretical model predictions and the results provide satisfactory results. Regarding to novel PV/T collector panel, it can be seen that the electrical efficiency improvement made by refrigerant cooling increases with the increasing radiation. The electrical efficiency of PV/T panel is improved by up to 1.9% compared with that without cooling. Regarding to novel solar collector panel, it can be seen that the highest average daily efficiency ranging from 0.75 to 0.96 with an average of 0.83, which is higher than the traditional collectors.

The investigation of PV/T-HP (Chapter 4) focuses on the concept that the PV/T collector-evaporator is coupled with a heat pump system to provide a stable capacity for space heating and domestic hot water as well as electricity for compressor and pump usages. A series of indoor

tests are performed at the laboratory of the school of the Built Environment, University of Nottingham. Experimental results are compared with the theoretical model predictions and the results provide satisfactory results. The results can be concluded that the COP of the heat pump system increases with the increasing radiation and decreases with the condenser water supplement temperature and condenser water flow rate. The COP varied from 2.9 to 4.6, responding to the radiation from 200 W/m^2 to 800 W/m^2, at the constant condenser water supply rate of 2 L/min and water supply temperature of 35^{o}C. The COP drops from 5.2 to 3.2, responding to the condenser supply temperature from 25^{o}C to 45^{o}C, at the radiation of 600 W/m^2 and condenser water flow rate of 2 L/min. The COP drops from 6.7 to 2.8, responding to the condenser water flow rate from 1 L/min to 5 L/min, at the radiation of 600 W/m^2 and condenser water supply temperature of 35^{o}C. In addition, the condenser water supplement temperature and condenser water flow rate are little effect on the PV power output and electrical efficiency. The COP is not as high as expected due to the low capacity compressor. The compressor is selected to match the small size and low capacity of PV/T panel limited indoors. The COP of the heat pump system decreases with the increasing condenser water supply temperature.

The investigation of novel SAHP (Chapter 5) focuses on the concept that solar collector is coupled with ASHP to increase the evaporator temperature and to supply domestic hot water for an entire year, space heating in winter and cooling in the summer. Experimental results are compared with the theoretical model predictions, the reasons for error formation are analysed. When the system operates in summer and

winter conditions, the COP is much higher than the COP of ASHP in nominal load conditions and maximum load conditions.

When the system operates in minimum load conditions, the COP is lower than the COP of ASHP when the water reaches 35^{o}C in summer condition and when the water reaches 20^{o}C in winter conditions. When operating in extremely cold conditions, the system needs 6 minutes and 13 minutes to operate steadily when guaranteeing hot water supplement and guaranteeing space heating, respectively. In addition, it can be concluded that the refrigerant R 22 is not suitable for hot water supplement.

6.2 Further Works

In this research, the PV/T-HP and SAHP are investigated and presented great results. In the course of the investigation, there are still some problems that deserve further study and improvement. Although substantial work is carried out during this research, there are still some opportunities to achieve architecture integration, efficiency improvement by increasing evaporation temperature and decreasing temperature of PV modules, as well as multi-function of the system.

- Some cycles' operation is not stable, which include Cycle 1—Air source heat pump for space cooling and domestic hot water supply; Cycle 7—Air source heat pump for defrost; and Cycle 7—Solar-water source heat pump for space heating.
- According to the simulation results, because the system operates in a dynamic mode, the operating cycle changes with the indoor and ambient temperature and humidity, hot water temperature as well as other parameters change, therefore there are no stable conditions.
- Capillary is not well suited for this novel system. The capillary has no

adjustment functions. It cannot regulate the refrigerant flow with the change in working conditions. Further improvement of the novel SAHP system, thermal expansion valve should be used.

- Refrigerant R22 is not suitable for hot water supplement in this novel system. When water temperature increases from 35^{o}C to 40^{o}C, it is difficult to release condensation heat from refrigerant to water. In order to increase the water temperature, it is mainly depends on the power consumption of compressor. Further improvement of the novel SAHP system, other refrigerant such as R134a should be used.

Reference

ABHAT, A. (1982). Low temperature latent heat thermal energy storage: Heat storage materials, Solar Energy 30 (4), 313-332.

AFFOLTER, P., EISENMANN, W., FECHNER, H., ROMMEL, M., SCHAAP, A., SERENSEN, H. (2007). PVT roadmap: a European guide for the development and market introduction of PV–thermal technology. In: ECN, editor.

AFFOLTER, P., EISENMANN, W., FECHNER, H., ROMMEL, M., SCHAAP, A., SORENSEN, H. (2006). PVT roadmap. Edition of ECN 2006, Netherlands, http://www.pvtforum.org/.

AGRAWAL, N., BHATTACHARYYA, S. (2007). Studies on a two-stage transcritical carbon dioxide heat pump cycle with flash intercooling. Applied Thermal Engineering 27, 299-305.

ALEXANDER, G. (1998).Renewable energy, Overview: the context of renewable energy technologies, Oxford: Oxford University Press, 1998.

AMAR, M. (2003). A review on energy conservation in building applications with thermal storage by latent heat using phase change materials, Energy Conversion and Management 45 (2), 263-275.

ANDERSON, T.N., MORRISON, G.L. (2007). Effect of load pattern on solar-boosted heat pump water heater performance. Solar Energy 81, 1386–95.

ANDERSON, T.N., MORRISON, G.L., BEHNIA, M. (2002). Experimental analysis of a solar- boosted heat pump water heater with integral condenser. In: Proceedings of solar. Australian New Zealand Solar Energy Society.

ASHRAE, Handbook: Fundamentals. (1993). ASHRAE.

ATIPOANG, N., CHOOSAK, C., TANONGKIAT, K. (2009). Performance analysis of solar water heater combined with heat pump using refrigerant mixture. Appl Energy 86(5), 748–56.

AYNUR, T.N., HWANG, Y., RADERMACHER, R. (2008). Field performance measurements of a heat pump desiccant unit in dehumidification mode. Energy Buildings 40(12), 2141–7.

AYNUR, T.N., HWANG, Y., RADERMACHER, R. (2010). Integration of variable refrigerant flow and heat pump desiccant systems for the heating season. Energy Buildings 42(4), 468–76.

AZIZ, W., CHATURVEDI, S.K., KHEIREDDINE, A. (1999). Thermodynamic analysis of two- component, two-phase flow in solar collectors with application to a direct- expansion solar-assisted heat pump. Energy 24, 247–59.

BAALI, A.A. (1986) Improving the power of a solar panel by cooling and light concentrating. Solar and Wind Technology 3, 241-245.

BACCOLI, R., CARLINI, U., MARIOTTI, S., INNAMORATI, R., SOLINAS, E., MURA, P. (2010). Graybox and adaptative dynamic neural network identification models to infer the steady state efficiency of solar thermal collectors starting from the transient condition. Solar Energy 84, 1027-1046.

BADESCU, V. (2003). Model of a thermal energy storage device integrated into a solar assisted heat pump system for space heating. Energy Conversion and Management 44, 1589-1604.

BAKKER, M., ZONDAG, H.A., ELSWIIK, M.J., STROOTMAN, K.J., JONG, M.J.M. (2005). Performance and costs of a roof-sized PV/thermal array combined with a ground coupled heat pump. Sol Energy 78, 331–9.

BAKKER, M., ZONDAG, H.A., VAN HELDEN, W.G.J. (2002). Design of a dual flow photovoltaic/thermal panel. In: Proceedings of PV in Europe, 349–59.

BATTISTI R, C. A. (2005). Evaluation of technical improvements of photovoltaic systems through life cycle assessment methodology. Energy 30, 952-967.

BAZILIAN, M., LEEDERS, F., PRASAD, D. (2001). Photovoltaic cogeneration in the built environment. Solar Energy 71, 57-69.

BEEKLEY, D.C., MATHER, G.R. (1975). Analysis and experimental tests of solar collector arrays based on evacuated tubular solar collectors. In: Proceedings of 1975 ISES Congress, Los Angeles, CA of USA, P. 20.

BEHNIA, M., MORRISON, G.L. (1991). An experimental investigation of inclined open thermsyons. Solar Energy 67, 79–91.

BEIJER, DE. (1998). Product development in solar water heating. Renew Energy 15, 201–4.

BENEMANN, J., CHEHAB, O., SCHAAR-GABRIEL, E. (2001). Building-integrated PV modules. Solar Energy Materials and Solar Cells 67, 345-354.

BENZ, N., BEIKIRCHER, T. (1999). High efficiency evacuated flat-plate solar collector process steam production. Solar Energy 65 (2), 111–118.

BERGENE, T., LOWIK, O.M. (1995). Model calculations on a flat plate solar heat collector with integrated solar cells. Solar Energy 55, 453-462.

BERGMANN, I. (2002). Façade integration of solar thermal collectors- a new opportunity for planners and architects. Renewable Energy World 5, 89-97.

BERTSH, S.S., GROLL, E.A. (2008). Two-stage air-source heat pump for residential heating and cooling applications in northern U.S. climates. International Journal of Refrigeration 31, 1281-1292.

BHARGAVA AK, G.H.P., AGARWAL, R.K. (1991). Study of a hybrid solar system-solar air heater combined with solar cell. Energy Conversion and Management 31, 471-479.

BIAOU, A.L., BERNIER, M.A. (2008). Achieving total domestic hot water production with renewable energy. Building and Environment 43, 651-60.

BOSANAC, M., SORENSEN, B., IVAN, K., SORENSEN, H., BRUNO, N., JAMAL, B. (2003). Photovoltaic/thermal solar collectors and their potential in Denmark. Final report, EFP Project, 1713/00-0014.

BRINKWORTH, B.J. (2000). Estimation of flow and heat transfer for the design of PV cooling ducts. Solar Energy 69, 320-413.

BRINKWORTH, B.J., CROSS, B.M., MARSHALL, R.H., HONGXING, Y. (1997). Thermal regulation of photovoltaic cladding. Solar Energy 61, 169-178.

BRINKWORTH, B.J., MARSHALL, R.H., IBARAHIM, Z.A. (2000). A validated model of naturally ventilated PV cladding. Solar Energy 69, 67-81.

BRINKWORTH, B.J., SANDBERG, M. (2006). Design procedure for cooling ducts to minimize efficiency loss due to temperature rise in PV arrays. Solar Energy 80, 89-103.

BROGREN, M., KARLSSON, B. (2001). Low-concentrating water-cooled PV–thermal hybrid systems for high latitudes, 17th EUPVSEC.

BROGREN, M., KARLSSON, B., WERNER, A., ROOS, A. (2002). Design and evaluation of low concentrating, stationary, parabolic reflectors for wall-integration of watercooled photovoltaic-thermal hybrid modules. In: Proceedings of international conference PV in Europe 551–5.

BROGREN, M., NOSTELL, P., KARLSSON, B. (2000). Optical efficiency of a PV thermal hybrid CPC module for high latitudes. Solar Energy 69, 173–85.

BROGREN, M., NOSTELL, P., KARLSSON, B. (2000). Optical efficiency of a PV thermal hybrid CPC module for high latitudes. Solar Energy 69, 173-185.

BUDIHARDJO, I., MORRISON, G.L., (2009) Performance of water-in-glass evacuated tube solar water heaters. Solar Energy 83, 49–56.

BUTERA, F., ASTE, N., ADHIKARI, R.S., BRACCO, R. (2005). Ecomen a project at CRF: performance of solar facade. In: Proceedings 600 Congresso Nazionale ATI.

CADAFALCH, J. (2009). A detailed numerical model for flat plate solar thermal devices. Solar Energy 83 (12), 2157–2164.

CANALETTI, L.J., NOTTON, G., CRISTOFARI, C. (2008). New concept of solar air heater integrated in the building. ISJAEE 5, 39–44.

CARBONELL, D., CADAFALCH, J., CONSUL, R. (2013). Dynamic modelling of flat solar collectors. Analysis and validation under thermosyphon conditions. Solar Energy 89, 100-112.

CARL, L.Y. (1999). Chemical properties handbook. McGraw-Hill Book Co, New York.

CARTMELL, B.P., SHANKLAND, N.J., FIALA D, H.V. (2004). A multi-operational ventilated photovoltaic and solar air collector: application, simulation and initial monitoring feedback. Solar Energy 76, 45-53.

CERVANTES, J.G., TORRES-REYES. E. (2002). Experiments on a solar-assisted heat pump and an exergy analysis of the system. Applied Thermal Engineering 22, 1289-1297.

CHARALAMBOUS, P.G., MAIDMENT, G.G., KALOGIROU, S.A., YIAKOUMETTI, K. (2007). Photovoltaic thermal (PV/T) collectors: a review. Applied Thermal Engineering 27, 275-286.

CHARRON, R., ATHIENITIS, A.K. (2006). Optimization of the performance of double-facades with integrated photovoltaic panels and motorized blinds. Solar Energy 80, 482-491.

CHARTER, W.W.S., TAYLOR, L.E. (1976). Some performance characteristics of a solar boosted heat pump. Proceedings of the I. I. R. Conference, Melbourne, Australia 641–8.

CHATURVEDI, S.K., ABAZERI, M. (1987). Transient simulation of a capacity-modulated, direct-expansion, solar-assisted heat pump. Solar Energy 39, 421-428.

CHATURVEDI, S.K., ABDEL-SALAM, T.M., SREEDHARAN, S.S., GOROZABEL, F.B. (2009). Two-stage direct expansion solar assisted heat

pump for high temperature applications. Applied Thermal Engineering 29, 2093-9.

CHATURVEDI, S.K., CHEN, D.T., KHEIREDDINE, A. (1998). Thermal performance of a variable capacity direct expansion solar-assisted heat pump. Energy Conversion Manage 39, 181-191.

CHEN, H. (2009). A study on thermal performance of water-in-glass evacuated tube solar water heaters. Thesis for Master program, Yunnan Normal University, Kunming, China.

CHEN, J., YU, J. (2008). Performance of a new refrigeration cycle using refrigerant mixture R32/R134a for residential air-conditioner applications. Energy Buildings 40(11), 2022–7.

CHEN, L., LI, J., SUN, F., WU, C. (2008). Performance optimization for a two-stage thermoelectric heat-pump with internal and external irreversibilities. Applied Energy 85, 641-649.

CHEN, W. (2008). A comparative study on the performance and environmental characteristics of R410A and R22 residential air conditioners. Appl Therm Eng 28(1), 1–7.

CHIOU, J.P. (1982). The effect of non-uniform fluid flow distribution on the thermal performance of solar collector. Solar Energy 29 (6), 487–502.

CHOI, E. (1994). Forced convection heat transfer with phase-change-material slurries: turbulent flow in a circular tube. International Journal of Heat and Mass Transfer 37 (2), 207-215.

CHOUDHURY C, GARG H.P. (1993). Performance of air-heating collector with packed airflow passage. Solar Energy 50, 205-221.

CHOW, T.T. (2003). Performance analysis of photovoltaic-thermal collector by explicit dynamic model. Solar Energy 75, 143-152.

CHOW, T.T. (2010). A review on photovoltaic/thermal hybrid solar technologies. Appl Energy 87(2), 365–79.

CHOW, T.T., CHAN, A.L.S., FONG, K.F., LIN, Z., HE, W., JI, J. (2009). Energy and exergy analysis of photovoltaic-thermal collector with and without glass cover. Applied Energy 86, 310-316.

CHOW, T.T., HAND, J.W., STRACHAN, P.A. (2003). Building-integrated photovoltaic and thermal applications in a subtropical hotel building. Applied Thermal Engineering 23, 2035-2049.

CHOW, T.T., HE, W., JI, J. (2006). Hybrid photovoltaic-thermosyphon water heating system for residential application. Solar Energy 80, 298-306.

CHOW, T.T., PEI, G., FONG, K.F., LIN, Z., CHAN, A. L.S., HE, M. (2010). Modelling and application of direct-expansion solar-assisted heat pump for water heating in subtropical Hong Kong. Appl Energy 87(2), 643–9.

CHUA, K.J., CHOU, S.K. (2005). A modular approach to study the performance of a two-stage heat pump system for drying. Applied Thermal Engineering 25, 1363-1379.

CHURCHILL, S.W. (1983). Heat Exchanger Design Hand Book. VDI-Verlarg GmbH, Hemisphere, 2.5.8.

CHYNG, J.P., LEE, C.P., HUANG, B.J. (2003). Performance analysis of a solar-assisted heat pump water heater. Solar Energy 74, 33-44.

CLEARY, C. (1990). Hydraulic characteristics of ice slurry and chilled water flows, IEA District Heating: Advanced Energy Transmission Fluid-Final Report of Research. Novem BV, Sittard, Netherlands.

CLELAND, A.C. (1986). Computer subroutines for rapid evaluation of refrigerant thermodynamic properties. International Journal of Refrigeration 9, 346-351.

COLLINS, R.E. (1961). Flow of Fluids through Porous Materials. Reinhold Publishing Co., New York, 10.

COMAKLI, K., SIMSEK, F., COMAKLI, O., SAHIN, B. (2009). Determination of optimum working conditions R22 and R404A refrigerant mixtures in heat-pumps using Taguchi method. Appl Energy 86(11), 2451–8.

COMMUNITIES AND LOCAL GOVERNMENT. (2008). Report: ‘Code for Sustainable Homes: A Step-change in sustainable home building practice’. London.

COOPER, P.I. (1981). The Effect of Inclination on the heat loss from flat plate solar collectors. Solar Energy 27 (5), 413–420.

COVENTRY, J.S. (2005). Performance of a concentrating photovoltaic/thermal solar collector. Solar Energy 78, 211-222.

COVENTRY, J.S., LOVEGROVE, K. (2003). Development of an approach to compare the ‘value’ of electrical and thermal output from a domestic PV/thermal system. Solar Energy 75, 63-72.

COX CH, RAGHURAMAN P. (1985). Design considerations for flat-plate photovoltaic/thermal collectors. Solar Energy 35, 227-241.

CRISTOFARI, C., NOTTON, G., CANALETTI, J.L. (2009). Thermal behavior of a copolymer PV/T solar system in low flow rate conditions. Sol Energy 83(8), 1123–38.

CRUMMOND, J.E., TAHIR, M.I. (1984). Laminar viscous flow through regular arrays of parallel sold cylinders. International Journal of Multiphase Flow 10 (5), 515–540.

DANNY, H.W.L., LIU, Y. and JOSEPH, C.L. (2013) Zero energy buildings and sustainable development implications－A review. Energy, 54, 1-10

DAY, A.R., KARAYIANNIS, T.G. (1994). Review Paper: Solar assisted heat pump research and development. Building Services Engineering Research and Technology 15, 71-80.

DING, G.L. (2007). Recent developments in simulation techniques for vapour compression refrigeration systems. International Journal of Refrigeration 30, 1119-1133.

DONGSOO, J., HAK-JUN, K., OOKJOONG, K. (2003). A study on the performance of multi-stage heat pumps using mixtures. International Journal of Refrigeration 22, 402-413.

DUBEY, S., SANDHU, G.S., TIWARI. G.N. (2009). Analytical expression for electrical efficiency of PV/T hybrid air collector. Applied Energy 86, 697-705.

DUBEY, S., TIWARI, G.N. (2008) Thermal modelling of a combined system of photovoltaic thermal (PV/T) solar water heater. Solar Energy 82, 602-612.

DUBEY, S., TIWARI, G.N. (2009). Analysis of PV/T flat plate water collectors connected in series. Solar Energy 83, 1485-1498.

DUFFIE, J.A., BECKMAN, W. A. (2006). Solar engineering of thermal processes. J. Wiley & Sons

DUFFIE, J.A., BECKMAN, W.A. (1991). Solar engineering of thermal processes. New York, Wiley.

DUFFIE, J.A., BECKMAN, W.A. (2006). Solar engineering of thermal processes, 3rd ed., John Wiley & Sons, Inc, 747–75.

EICKER, U. (2003). Solar technologies of buildings. New York: John Wiley & Sons.

EICKER, U., FUX, V., INFIELD, D., LI, M. (2000). Heating and cooling of combined PV-solar air collectors facades. In: Proceedings of international conference of 16th European PV solar energy, 1836–9.

ELAZARI, A. (1998). Multi solar system-solar multi-module for electrical and hot water supply for residentially building. In: Proceedings of 2nd world conference on photovoltaic solar energy conversion, 2430–3.

Energy Saving Trust. (2010, June 7). Home Improvements and Draught proofing. Retrieved March 23, 2011. From The Energy Saving Trust Website: http://www.energysavingtrust.org.uk/Home-improvements-and-products/Home-insulation-glazing/Draught-proofing.

Energy White Paper Our Energy Future-Creating a Low Carbon Economy. (Cmnd. 5761, 2003)

ERDILE, I.M., EGELIOGLU, F. (2008). An experimental study on energy generation with a photovoltaic (PV)-solar thermal hybrid system. Energy 33, 1241-1245.

FABRICE, M., GILLES, N., CHRISTIAN, C., JEAN, L.C. (2013). Design and modelling of a new patented thermal solar collector with high building integration. Applied Energy 102, 631-639.

FARZAD, M., O'NEAL, D. (1994). The effect of void fraction model on estimation of air conditioner system performance variables under a range of refrigerant charging conditions. International Journal of Refrigerant 17, 85-93.

FLORSCHUETZ, L.W. (1979). Extension of the Hottel-Whillier model to the analysis of combined photovoltaic/thermal flat plate collectors. Solar Energy 22, 361-366.

FRANCIA, G. (1961). A new collector of solar radiant energy. In: Proceedings of the United Nations conference on new sources of energy, paper F6. Rome, Italy, 572.

FREEMAN, T.L., MITCHELL, J.W., AUDIT, T.E. (1979). Performance of combined solar-heat pump systems. Solar Energy 22, 125-135.

FUJISAWA, T., TANI, T. (1997). Annual exergy evaluation on photovoltaic thermal hybrid collector. Solar Energy Materials and Solar Cells 47, 135-148.

GANG, H.P., JIE, J., WEI, H., KELIANG, L., HANFENG, H. (2007). Performance of photovoltaic solar assisted heat pump system in typical climate zone. Journal of Energy & Environment 6.

GARG, H.P., ADHIKARI, R.S. (1998). Hybrid photovoltaic/thermal utilization systems. Final report submitted to All India Council of Technical Education, New Delhi,

GARG, H.P., ADHIKARI, R.S. (1998). Transient simulation of conversional hybrid photovoltaic/thermal (PV/T) air heating collectors. International Journal of Energy Research 22, 547-562.

GARG, H.P., ADHIKARI, R.S. (1999). Performance analysis of a hybrid photovoltaic/thermal (PV/T) collector with integrated CPC troughs. International Journal of Energy Research 23, 1295-1304.

GARG, H.P., AGARWAL, R.K. (1995). Some aspects of a PV/T collector/forced circulation flat plate solar water heater with solar cells. Energy Conversion and Management 36, 87-99.

GARG, H.P., AGARWAL, R.K. (1997). Conventional hybrid photovoltaic/thermal (PV/T) air heating collector: steady-state simulation. Renewable Energy 11, 363-385.

GARG, H.P., AGARWAL, R.K., BHARGAVA, A.K. (1991). The effect of plane booster reflectors on the performance of a solar air heater with solar cells suitable for a solar dryer. Energy Conversion and Management 35, 543-554.

GARG, H.P., AGARWAL, R.K., JOSHI, J.C. (1994). Experimental study on a hybrid photovoltaic thermal solar water heater and its performance prediction. Energy Conversion and Management 35, 621-633.

GAUR, M.K., TIWARI, G.N. (2010). Optimization of number of collectors for integrated PV/T hybrid active solar still. Appl Energy 87(5), 1763–72.

GOROZABEL CHATA, F.B., CHATURVEDI, S.K., ALMOGBEL, A. (2005). Analysis of a direct expansion solar-assisted heat pump using different refrigerants. Energy Conversion Management 46, 2614–24.

GUIAVARCH, A., PEUPORTIER, B. (2006). Photovoltaic collector efficiency according to their integration in buildings. Solar Energy 80, 65-77.

GUOYING, X., XIAOSONG, Z., SHIMING, D. (2006). A simulation study on the operating performance of a solar air source heat pump water heater. Applied Thermal Engineering 26,1257–65.

GUPTA, V.P., JOSEPH, D.D. (1973). Bounds for heat transport in a porous layer. Journal of Fluid Mechanics 57 (3), 491–514.

HAN, D.H., LEE, K.J., KIM, Y.H. (2003). Experiments on the characteristics of evapouration of R410A in brazed plate heat exchangers with different geometric configurations. Appl Therm Eng 23(10),1209–25.

HAN, Z., ZHENG, M., KONG, F., WANG, F., LI, Z., BAI, J. T. (2008). Numerical simulation of solar assisted ground-source heat pump heating system with

latent heat energy storage in severely cold area. Applied Thermal Engineering 28, 1427-1436.

HASHISH, M.A., EI-REFAIR, M.F. (1983). Reduced order dynamic model of the flat-plate solar collector. Appl. Math. Model. 7, 2-10.

HASSAN, M.M., BELIVEAU, Y. (2007). Design, construction and performance prediction of integrated solar roof collectors using finite element analysis. Constr Build Mater 21, 1069–78.

HASTINGS, S.R., MORKO, O. (2000). Solar air systems, a design handbook. London, James &James.

HAWLADER, M.N.A., CHOU, S.K., ULAH, M.Z. (2001). The performance of a solar-assisted heat pump water heating system. Applied Thermal Engineering 21, 1049–65.

HAWLADER, M.N.A., DEY, P.K., DIAB, S., CHUNG, C.Y. (2004). Solar assisted heat pump desalination system. Desalination 168, 49-54.

HAWLADER, M.N.A., RAHMAN, S.M.A., JAHANGEER, K.A. (2008). Performance of evaporator collector and air collector in solar assisted heat pump dryer. Energy Convers Manage 49(6), 1612–9.

HAWLANDER, M.N.A., CHOU, S.K., ULLAH. M.Z. (2001). The performance of a solar-assisted heat pump water heating system. Applied Thermal Engineering 21, 1049-1065.

HE, W., CHOW, T.T., LU, J., PEI, G., CHAN, L. (2006). Hybrid photovoltaic and thermal solar collector designed for natural circulation of water. Applied Energy 83, 199–210.

HEAT PUMPS: HEAT PUMP, STIRLING ENGINE, GEOTHERMAL HEAT PUMP, REFRIGERATOR. APPLICATIONS OF THE STIRLING ENGINE. (2011) Books LLC Press.

HEGAZY, A.A. (2000). Comparative study of the performance of four photovoltaic/ thermal solar air collectors. Energy Conversion and Management 41,861-881.

HELDEN, W.G.J., ZOLINGEN, R.J.C., ZONDAG, H.A. (2004). PV thermal systems: PV panels supplying renewable electricity and heat. Progress in Photovoltaic Research and Application 12, 415–26.

HELLSTROM. B., ADSTEN, M., NOSTELL, P., KARLSSON, B., WACKELGARD, E. (2003). The impact of optical and thermal properties on the performance of flat plate solar collectors. Renew Energy 28, 331–44.

HENDRIE, S.D. (1979). Evaluation of combined photovoltaic/thermal collectors. In: ISES international congress and silver jubilee, vol. 3, 1865–9.

HEPBAS, L.I., KALINCI, Y., (2009). A review of heat pump water heating systems. Renew Sust Energy Rev13(6–7), 1211–29.

HERZOG, T. (1999). Solar Design. Birkhauser.

HILMER, F., VAJEN, K., RATKA, A., ACKERMANN, H., FUHS, W. (1999). Numerical solution and validation of a dynamic model of solar collectors working with varying fluid flow rate. Solar Energy 65 (5), 305–321.

HIRASAWA, S., KAWANAMI, T. (2010). Study on collector efficiency of flat plate type evacuated solar collector to get hot water near 100 ^{o}C, Proceedings of 14th International Heat Transfer Conference, IHTC14-22242.

HIRASAWA, S., KAWANAMI, T., OKAWA, Y., SHIRAI, A. (2011). Effect of operation-control methods on collector thermal performance of flat plate type evacuated solar collector system to get hot water near 100 ^{o} C, Proceedings of 22th International Symposium on Transport Phenomena, Paper-No.11.

HIRASAWA, S., TANIGUCHI, M., NAKAUCHI, S., TANAKA, T. (2007). Experiment on boiling heat transfer performance in tube for a vacuum solar collector, Proceedings 2007 ASME-JSME Thermal Engineering Summer Heat Transfer Conference, HT2007-32149.

HODGE, E., GIBBONS, C. (2004). Convective cooling of photovoltaic. In: ISES Euro sun.

HOLLANDS, K.G.T., BRUNGER, A.P., CHARALAMBOUS, P.G. (1989). Optimization of absorber plate material content in the flat-plate solar collector, in: Proceedings of Solar Energy Society of Canada Inc. (SESCI) Annual Conference, Pentincton, British Columbia, Canada, 240–244.

HOLLANDS, K.G.T., IYNKARAN, K. (1993). Analytical model for the thermal conductance of compound honeycomb transparent insulation, with experimental validation. Solar Energy 51 (3), 223–227.

HOLLANDS, K.G.T., WRIGHT, J.L. (1983). Heat loss coefficients and effective products for flat-plate collectors with diathermanous covers. Solar Energy 30 (3), 211–216.

HOTTEL, H.C., WILLIER, A. (1958). Evaluation of flat-plate solar collector performance. In: Transactions of the conference on the use of solar energy, vol. 2. Tucson, Arizona: University of Arizona Press.

HOUGHTON, J.T., DING, Y., GRIGGS, D.J., NOGUER, M., VAN DER LINDEN, P.J., DAI, X., MASKELL, K., JOHNSON, S.A. (2001). Climate Change 2001: The Scientific Basis. Cambridge: Cambridge University Press.

http://dx.doi.org/10.1080/15435070903501274

http://www.solarenergy.ch/

HUANG BJ, LIN TH, HUANG WC, SUN FS. (2001). Performance evaluation of solar photovoltaic/thermal systems. Solar Energy 70,443-448.

HUANG, B.J., CHYNG, J.P. (2001). Performance characteristics of integral type solar-assisted heat pump. Solar Energy 71(6), 403–14.

HUANG, B.J., LIN, Y.H., TON, W.Z., HOU, T.F., CHUANG, Y.H. (2011). Building-integrated Solar Collector (BISC). In: Proceeding of world renewable energy congress, 3718–25.

HUANG, B.J., SUMATHY, K., WANG, R.Z. (2005). Heat pipe enhanced solar assisted heat pump water heating system. International Journal of Energy Research 27, 531-81.

HUANG, B.J., WANG, S.B. (1994). Identification of solar collector dynamics using physical model-based approach. Journal of Dynamics Systems, Measurement, and Control 116 (4), 755–763.

HULIN, H., XINSHI, G., YUEHONG, S. (1999) Theoretical thermal performance analysis of two solar-assisted heat pump systems. International Journal of Energy Research 23, 1-6.

IEA Heat Pump Center. (2004). How heat pumps achieve energy savings and CO2 emissions reduction-an introduction. Retrieved March 1, 2004, from IEA Heat Pump Center Web Site: http://www.heatpumpcentre.org/.

IEA solar heating and cooling programme; 2007.

IMRE, L. (1984). Solar agricultural crop dryer. Research Report (1981/1984). Technical University Budapest.

INFIELD, D., LI, M., EICKER, U. (2004). Thermal performance estimation for ventilated PV facades. Solar Energy 76, 93-98.

ISAKSON, P. (1995). Solar collector model for testing and simulation. Final report for BFR project Nr. 900280-1, Building Services Engineering, Royal Institute of Technology, Stockholm.

ITO, S. (1992). Heat pumps with direct expansion solar collectors. Transactions Japanese Association of Refrigeration (in Japanese), 9:101–15.

ITO, S., MIURA, N. (1991). A comparison of heat pump systems using different types of direct expansion solar collectors. In: Proceedings of biennial congress of the International Solar Energy Society. Denver, USA, 1655–9.

ITO, S., MIURA, N. (2000). Studies of heat pump using water and air heat sources in parallel. Heat Transfer Asian Research 29, 473-90.

ITO, S., MIURA, N. (2003). Usage of a DC fan together with photovoltaic modules in a solar air heating system. In: Proceedings of (CD-ROM) ISES world congress.

ITO, S., MIURA, N., TAKANO, Y. (2005). Studies of heat pumps using direct expansion type solar collectors. ASME Transactions 127, 60–4.

ITO, S., MIURA, N., WANG, K. (1999). Performance of a heat pump using direct expansion solar collectors. Solar Energy, 65:189–96.

JI, J., LIU, K.L., CHOW, T.T., PEI, G., HE, W., HE, H.F. (2008). Performance analysis of a photovoltaic heat pump. Applied Energy 85, 680-693.

JI, J., LIU, K.L., CHOW, T.T., PEI, G., HE, W., HE, H.F. (2008). Experimental study of photovoltaic solar assisted heat pump system. Solar Energy 82(1), 43–52.

JI, J., LIU, K.L., CHOW, T.T., PEI, G., HE, W., HE, H.F. (2009). Distributed dynamic modelling and experimental study of PV evaporator in a PV/T solar-assisted heat pump. Int J Heat Mass Transfer 52(5–6), 1365–73.

JOHN, C., GAVIN, H. (2011). Heat pumps for the home. The Crowood Press Ltd.

JONES, A.D., UNDERWOOD, C.P. (2001). A thermal model for photovoltaic systems. Solar Energy 70, 349-359.

JONES, G.F., LIOR, N.L. (1994). Flow distribution in mani-folded solar collectors with negligible buoyancy effects. Solar Energy 52 (3), 289–300.

JOSHI, A.S., TIWARI, A. (2007). Energy and exergy efficiencies of a hybrid photovoltaic thermal (PV/T) air collector. Renewable Energy 32, 2223-2241.

JOSHI, A.S., TIWARI, A., TIWARI, G.N., DINCER, I., REDDY, B.V. (2009). Performance evaluation of a hybrid photovoltaic thermal (PV/T) (glass-to-glass) system. International Journal of Thermal Sciences 48, 154-164.

JOSHI, A.S.， DINCER, I.， REDDY, B. V. (2009). Thermodynamic assessment of photovoltaic systems. Solar Energy 83, 1139-1149

JUNG, D., PARK, C., PARK, B. (1999). Capillary-tube selection for HCFC22 alternatives. Int. J Refrigeration 22, 604-14.

K SOPIAN, H.T., LIU, S., KAKAC, T.N., VEZIROGL, U. (1996). Performance analysis of photovoltaic/thermal air heaters. Energy Conversion and Management 37, 1657-1670.

K SOPIAN, H.T., LIU, S., KAKAC, T.N., VEZIROGL, U. (2000). Performance of a double pass photovoltaic thermal solar collector suitable for solar drying systems. Energy Conversion and Management 41, 353-365.

KALOGIROU, A.A., PANTELIOU, S., DENTSORAS, A. (1999). Modelling of solar domestic water heating system using artificial neural networks. Sol. Energy 65 (6), 335-342.

KALOGIROU, S.A. (2001). Use of TRYNSYS for modelling and simulation of a hybrid PV thermal solar system for Cyprus. Renewable Energy 23, 247-260.

KALOGIROU, S.A. (2004). Solar thermal collectors and applications. Progress in Energy and Combustion Science 30, 231-295.

KALOGIROU, S.A., PANTELIOU, S. (2000). Thermosyphon solar domestic water heating system: long-term performance prediction using artificial neural networks. Sol. Energy 69 (2), 163-174.

KALOGIROU, S.A., TRIPANAGNOSTOPOULOS. Y. (2006). Hybrid PV/T solar systems for domestic hot water and electricity production. Energy Conversion and Management 47, 3368-3382.

KARA, O., ULGEN, K., HEPBASLI, A. (2008). Exergetic assessment of direct-expansion solar-assisted heat pump systems: Review and modelling. Renewable and Sustainable Energy Reviews 12, 1383-1401.

KARLSSON, B., BROGREN, M., LARSSON, S., SVENSSON, L., HELLSTROM, B, SARIF, Y. (2001). A large bifacial photovoltaic-thermal low-concentrating module. In: Proceedings of 17th PV solar energy conference, 808–11.

KAYGUSUZ.K, COMAKLI.O, AYHAN, T. (1991). Solar-assisted heat pump systems and energy storage. Solar Energy 47, 383-391.

KEITH, E.H., REINHARD, R., SANFORD.A.K. (1996) Absorption chillers and heat pumps. CRC Press Inc.

KERN, E.C., RUSSELL, M.C. (2006). Combined photovoltaic and thermal hybrid collector.

KHOUKHI, M., MARUYAMA, S. (2005). Theoretical approach of a flat plate solar collector with clear and low-iron glass covers taking into account the spectral absorption and emission within glass covers layer. Renew Energy 30, 1177–94.

KONG, X.Q., ZHANG, D., LI, Y., YANG, Q.M. (2011). Thermal performance analysis of a direct-expansion solar-assisted heat pump water heater. Energy 36, 6830–8.

KOTAS, T.J. (1985). The exergy method of thermal plant analysis. Essex, UK: Anchor Brendon Ltd.

KRAKOW, K. I., LIN, S.A. (1983). Multiple source heat pump for cold climates. ASHRAE Transactions 89(2A), 574–89.

KRAKOW, K.I., LIN, S.A. (1983). Computer model for the simulation of multiple source heat pump. ASHRAE Transactions 89(2A), 590–616.

KRAUTER, S., ARAUJA, R.G., SCHROER, S., HANITSH, R., SALHI, M.J., TRIEBEL, C. (1999). Combined photovoltaic and solar thermal systems for facade integration and building insulation. Solar Energy 67, 239-248.

KUANG, Y.H., SUMATHY, K., Wang, R.Z. (2003). Study on a direct-expansion solar-assisted heat pump water heating system. International Journal of Energy Research 27, 531-548.

KUANG, Y.H., WANG, R.Z. (2006). Performance of a multi-functional direct-expansion solar-assisted heat pump system. Solar Energy 80, 795–803.

KUMAR, R., POSEN, M.A. (2011). A critical review of photovoltaic-thermal solar collectors for air heating. Applied Energy 88, 3603-3614.

LALOT, S., LECOEUCHE, S. (200)1. Identification of solar collectors during service using artificial neural networks. In: Proceedings of the ISES 2001 Solar World Congress, p. 128.

LALOVIC, B. (1986). A hybrid amorphous silicon photovoltaic and thermal solar collector. Solar Cells 19, 131-138.

LASNIER, F., ANG, T.G. (1990). Photovoltaic Engineering Handbook. Princeton.

LAZZARINA, R.M., CASTELLOTTI, F. (2007). A new heat pump desiccant dehumidifier for supermarket application. Energy Buildings 39(1), 59–65.

LEE, W.M., INFIELD, D.G., GOTTSCHALG, R. (2001). Thermal modelling of building integrated PV systems. In: Proceedings of 17th PV solar energy conference, 2754–7.

LI, H., YANG, H. (2010). Study on performance of solar assisted air source heat pump systems for hot water production in Hong Kong. Appl Energy 87(9), 2818–25.

LI, W., TAO, W.Q., KANG, H.J., LI, H.Z., XIN, R.C. (1997). Experimental study on heat transfer and pressure drop characteristics for fin and tube heat exchangers. Journal of Mechanical Engineering 33, 81-86.

LI, Y.W., WANG, R.Z., WU, J.Y., XU, Y.X. (2006). Experimental performance analysis and optimization of a direct expansion solar-assisted heat pump water heater. Energy 32, 1361-1374.

LI, Y.W., WANG, R.Z., WU, J.Y., XU, Y.X. (2007). Experimental performance analysis and optimization of a direct expansion solar-assisted heat pump water heater. Energy 3 21361–74.

LIU, K., JI, J., CHOW, T.T., PEI, G., HE, H., JIANG, A. (2009). Performance study of a photovoltaic solar assisted heat pump with variable-frequency compressor – a case study in Tibet. Renew Energy 34(12), 2680–7.

LIU, L., ZHANG, H. (2011). Energy-exergy analysis of a direct expansion solar assisted heat pump floor heating system. In: International conference on materials for renewable energy & environment (ICMREE), 20–22May2011, p213–21.

LIU, N., LIN, S., HAN, L., ZHU, M. (2005). Moderately high temperature water source heat pumps using a near-azeotropic refrigerant mixture. Appl Energy 80(4), 435–47.

LIU, Z., LI, X., WANG, H., PENG, W. (2008). Performance comparison of air source heat pump with R407C and R22 under frosting and defrosting. Energy Convers Manage 49(2), 232–9.

LONG, J.Y., ZHU, D.S. (2008). Numerical and experimental study on heat pump water heater with PCM for thermal storage. Energy Buildings 40(4), 666–72.

MA, G., LI, X. (2007). Exergetic optimization of a key design parameter in heat pump systems with economizer coupled with scroll compressor. Energy Convers Manage 48(4), 1150–9.

MA, G.Y., ZHAO, H.X. (2008). Experimental study of a heat pump system with flash-tank coupled with scroll compressor. Energy Buildings 40(5), 697–701.

MACARTHUR, J.W. (1984). Theoretical analysis of the dynamic interactions of vapour compression heat pumps. Energy Conversion and Management 24, 49-66

MAHJOURI, F. (1998). Vacuum tube liquid vapour (heat pipe) collectors. Thermo Technologies.

MARIA, C.M.P., CHRISTIAN, R. (2007). Towards an improved architectural quality of building integrated solar thermal systems (BIST). Solar Energy 81, 1104-1116.

MAURER, C., PFLUG, T., LAURO, P.D. (2012). Solar heating and cooling with transparent façade collectors in a demonstration building. Energy Pricedia 30, 1035-1041.

MILIBAND, E. (2008). United Kingdom Climate Change ACT 2008. UK: Change Committee on Climate.

MOHANRAJ, M., JAYARAJ, S., MURALEEDFARAN, C. (2010). Exergy assessment of a direct expansion solar-assisted heat pump working with R22 and R407c/LPG mixture. International Journal of Green Energy 7(1), 65–83.

MOHANRAJ, M., JAYARAJ, S., MURALEEDHARAN, C. (2009). A comparison of the performance of a direct expansion solar assisted heat pump working with R22 and a mixture of R407C–liquefied petroleum gas. Proceedings of the Institution of Mechanical Engineers, Part A: Journal of Power and Energy 223, 821.

MOHANRAJ, M., JAYARAJ, S., MURALEEDHARAN, C. (2009). Exergy analysis of direct expansion solar-assisted heat pumps using artificial neural networks. International Journal of Energy Research 33, 1005–20.

MOHANRAJ, M., JAYARAJ, S., MURALEEDHARAN, C. (2009). Performance prediction of a direct expansion solar assisted heat pump using artificial neural networks. Appl Energy 86(9), 1442–9.

MORITA, Y., FUJISAWA, T., TANI, T. (2000). Moment performance of photovoltaic/thermal hybrid panel (numerical analysis and exergetic evaluation). Electrical Engineering in Japan 133, 43-51.

MORRISON, G.L. (1994). Simulation of packed solar heat pump water heaters. Solar Energy 53(3), 249–57.

MORRISON, G.L., BUDIHARDJO, I., BEHNIA, M. (2004). Water-in-glass evacuated tube solar water heaters. Solar Energy 76, 135–140.

MOSHFEGH B, SANDBERG M. (1998). Flow and heat transfer in the air gap behind photovoltaic panels. Renewable and Sustainable Energy Reviews 2, 287-301.

MOSHFEGH, B., SANDBERG, M., BLOEM, J.J., OSSENBRINK, H. (1995). Analysis of fluid flow and heat transfer within the photovoltaic facade on the ELSA building. In: Proceedings of JRC ISPRA 13th European PV solar energy conference nice.

MUNARI, M.C., ROECKER, C. (2007). Towards an improved architectural quality of building integrated solar thermal systems (BIST). Sol Energy 81, 1104–16.

MUSHCHAWECK, J., SPIRKL, W. (1993). Dynamic solar collector performance testing. Solar Energy Materials and Solar Cells 30, 95–105.

NAHAR, N.M., GARG, H.P. (1980). Free convection and shading due to gap spacing between absorber plate and cover glazing in solar energy flat plate collectors. Applied Energy 7, 129-45.

NAPHON, P. (2005). On the performance and entropy generation of the double-pass solar air heater with longitudinal fins. Renewable Energy 30, 1345-1357.

NARENDRA, S.S.C., KAUSHIK, R.D.M. (2000). Exergetic analysis of a solar thermal power system. Renewable Energy 19,135-143.

NKWETTA, D.N., SMYTH, M. (2012). Performance analysis and comparison of concentrated evacuated tube heat pipes solar collectors. Appl Energy 98, 22–32.

NOBUYYKI, H. (2006). Renewable energy: RD & D priorities: insights from IEA technology program.

O'DELL, M.P., MITCHELL, J.W., BECKMAN, W.A. (1984). Design method and performance of heat pumps with refrigerant filled solar collectors. Journal of Solar Energy Engineering—Transactions oftheASME106,159–64.

OMOJARO, P., BREITKOPF, C. (2013). Direct expansion solar assisted heat pumps: A review of applications and recent research. Renewable and Sustainable Energy Reviews 22, 33-45.

OREL, Z.C., GUNDE, M.K., HUTCHINS, M.G. (2002). Spectrally selective solar absorbers in different non-black colors. In: Proceedings of WREC VII (CD–ROM), Cologne, Germany.

OSSENBRINK, H.A., RIGOLINI, C.O., VEBBE, O. (1994). Building integration of an amorphous silicon photovoltaic facade. In: Proceedings of IEEE 1st world conference on PV energy conversion, 770–3.

OTHMAN, M.Y.H., YATIM, B., SOPIAN, K., BAKAR, M.N.A. (2005). Performance analysis of a double-pass photovoltaic/thermal (PV/T) solar collector with CPC and fins. Renewable Energy 30, 2005-2017.

OZER, K., ULGENA, K., HEPBASLI, A. (2008). Exergetic assessment of direct-expansion solar-assisted heat pump systems: review and modelling. Renewable and Sustainable Energy Reviews 12, 1383–401.

OZGENER, O., HEPBASLI, A. (2005). Experimental performance analysis of a solar-assisted ground-source heat pump greenhouse heating system. Energy and Buildings 37,101-110.

OZTURK, H.H. (2004). Experimental determination of energy and exergy efficiency of the solar parabolic-cooker. Solar Energy 77, 67-71.

PAN, G., LI, Z. (2006). Investigation on incomplete condensation of non-azeotropic working fluids in high temperature heat pumps. Energy Convers Manage 47(13–14), 1884–93.

PARIDA, B., INIYAN, S., GOIC, R. (2011). A review of solar photovoltaic technologies. Renewable and Sustainable Energy Review 15, 1625-1636.

PARK, K.J., JUNG, D. (2009). Performance of heat pumps charged with R170/R290 mixture. Appl Energy 86(12), 2598–603.

PARK, K.J., SHIM, Y.B., JUNG, D. (2008). Performance of R433A for replacing HCFC22 used in residential air-conditioners and heat pumps. Appl Energy 85(9), 896–900.

PARSONS, R.A. (1995). ASHRAE Handbook: heating, ventilating, and air-conditioning applications. In: Chapter 30. Atlanta: ASHRAE.

PEDERSEN, P.H. (2003). Evaluation of The Possibilities of Substituting Potent Greenhouse Gases (HFCs, PFCs and SF6)-Environmental Project No.771.

PEI, G., JI, J., HAN, C., FAN, W. (2007). Performance of solar assisted heat pump using PV evaporator under different compressor frequency. In: Proceedings of ISES world congress, vols. I–V, 935–9.

PERERS, B. (1993). Dynamic method for solar collector array testing and evaluation with standard database and simulation programs. Solar Energy 50 (6), 517–526.

PETELA, R. (2003). Exergy of undiluted thermal radiation. Solar Energy 74, 469-488.

PIERSON, P., PADET, J. (1990). Time constant of solar collectors. Sol. Energy 44 (2), 109-114.

POSNANSKY, M., GNOS, S., COONEN, S. (1994). The importance of hybrid PV building integration. In: Proceedings of first world conference on photovoltaic energy conversion, 998–1003.

POTTLER, K., SIPPEL, C.M., BECK, A., FRICKE, J. (1999). Optimized finned absorber geometries for solar air heating collectors. Solar Energy 67, 35-52.

PRAKASH, J. (1994). Transient analysis of a photovoltaic thermal solar collector for cogeneration of electricity and hot air water. Energy Conversion and Management 35, 967-72.

PRAPAS, D.E., NORTON, B., MILONIDIS, E., PROBERT, S.D. (1988). Response function for solar-energy collectors. Sol. Energy 40, 371-383.

RAGHURAMAN, P. (1981). Analytical prediction of liquid and air photovoltaic/thermal flat-plate collector performance. Transactions of the ASME Journal of Solar Energy Engineering 103, 291-298.

RAISUL, I.M., SUMATHY, K., GONG, J., KHAN, S.U. (2012). Performance study on solar assisted heat pump water heater using CO2 in a transcritical cycle. In: International conference on renewable energies and power quality.

RAJAPAKSHA, L. (2007). Influence of special attributes of zeotropic refrigerant mixtures on design and operation of vapour compression refrigeration and heat pump systems. Energy Convers Manage 48(2), 539–45.

ROBLES, O.B., RUIZ, V.E., CANSECO, S.H., ORNEJO, M.R.C., TRAPAGA, M. (2007). Photovoltaic/thermal solar hybrid system with bifacial PV module and transparent plane collector. Solar Energy Materials and Solar Cells 91(20), 1966–71.

ROSELL, J., VALLVERDU, X., LECHON, M.I.M. (2005). Design and simulation of a low concentrating photovoltaic/thermal system. Energy Conversion and Management 46, 3034-3036.

SANDBERG, M., MOSHFEGH, B. (2002). Buoyancy-induced air flow in photovoltaic facades: effect of geometry of the air gap and location of solar cell modules. Building and Environment 37, 211-218.

SANDNES, B., REKSTAD, J. (2002). A photovoltaic/thermal (PV/T) collector with a polymer absorber plate. Experimental study and analytical model. Solar Energy 72, 63-73.

SCARPA, F., TAGLIAFICO, L.A., TAGLIAFICO, G. (2011). Integrated solar-assisted heat pumps for water heating coupled to gas burners; control criteria for dynamic operation. Applied Thermal Engineering 31, 59–68.

SCHNIEDEERS, J. (1997). Comparison of the energy yield predictions of stationary and dynamic solar collector models and the models accuracy in the description of a vacuum tube collector. Solar Energy 61 (3), 179–190.

SCHOTT, T. (1985). Operational temperatures of PV modules. In: 6th PV solar energy conference, 392–6.

SHAH, L.J., FURBO, S. (2004). Vertical evacuated tubular-collectors utilizing solar radiation from all directions. Applied Energy 78, 371–395.

SHAH, L.J., FURBO, S. (2007). Theoretical flow investigations of an all glass evacuated tubular collector. Solar Energy 81, 822–828.

SHAH, M.M. (1979). A general correlation for heat transfer during film condensation inside pipes. International Journal of Heat Mass Transfer 22, 547-556.

SHARAN, S.N., MATHUR, S.S., KANDPAL, T.C. (1985). Economic evaluation of concentrator photovoltaic systems. Solar and Wind Technology 2, 195-200.

SHEN, P.I. (1992). The effect of friction on flow distribution in dividing and combining flow manifolds. ASME J. Fluids Eng. 114, 121–123.

SHIGEKI, H., RYOHEI, T., TSUYOSHI, K., KATSUAKI, S. (2013). Reduction of heat loss from solar thermal collector by diminishing natural convection with high porosity porous medium. Solar Energy 97, 305-313.

SLOANE, B.D., KRISE, R.C., KENT, D.D. (1979). Demonstration of a heat pump water heater. A subcontracted report.

SOLANKI, S.C., DUBEY, S., TIWARI, A. (2009). Indoor simulation and testing of photovoltaic thermal (PV/T) air collectors. Applied Energy 86, 2421-2428.

SOLDO, V., CURKO, T., BALEN, I. (2004). Thermal performance of a direct expansion solar assisted heat pump. In: International refrigeration and air conditioning conference 724. http://docs.lib.purdue.edu/iracc/724s

SOPIAN K, Y., KS, L.H.T., KAKAC, S., VEZIROGLU, T.N. (1996). Performance analysis of photovoltaic thermal air heaters. Energy Conversion and Management 37, 1657-1670.

SOTERIS, K. (2003). The potential of solar industrial process heat applications. Applied Energy 76, 337-361.

SOZEN, A., MENLYK, T., UNVAR, S. (2008). Determination of efficiency of flat plate solar collector using neural network. Expert Systems with Applications 35, 1533-1539.

SUDHAKAR, S.V., SHARON, M. (1994). Fabrication and performance evaluation of a photovoltaic/thermal hybrid system. Journal of the Solar Energy Society of India 4(1), 1–7.

SUSHIL, K., CHATURVEDI, J., Y, SHEN. (1984). Thermal performance of a direct expansion solar-assisted heat pump. Solar Energy 33, 155-162.

SWARDT, C.A.D., MEYER, J.P. (2001). A performance comparison between an air source and a ground source reversible heat pump. International Journal of Energy Research 25, 899-910.

TANAKA, N., KOTOH, S. (2007). The current status of and future trends in heat pump technologies with natural refrigerants. Mitsubishi Electr Adv 25, 1-4.

TANG, R., YANG, Y., GAO, W. (2011). Comparative studies on thermal performance of water-in-glass evacuated tube solar water heaters with different collector tilt angles. Solar Energy 85, 1381-1389.

TANG, R.S., GAO, W.F., YU, Y.M., CHEN, H. (2009). Optimal tilt-angle of all-glass evacuated tube solar collectors. Energy 34 (9), 1387–1395.

THE, Y.L., OOI, K.T. (2009). Experimental study of the revolving vane (RV) compressor. Appl Therm Eng 29(14–15), 3235–45.

THE, Y.L., OOI, K.T. (2009). Theoretical study of a novel refrigeration compressor – Part I: Design of the revolving vane (RV) compressor and its frictional losses. Int J Refrig 32(5), 1092–102.

THE, Y.L., OOI, K.T. (2009). Theoretical study of a novel refrigeration compressor – Part II: Performance of a rotating discharge valve in the revolving vane (RV) compressor. Int J Refrig 32(5), 1103–11.

THE, Y.L., OOI, K.T. (2009). Theoretical study of a novel refrigeration compressor – Part III: Leakage loss of the revolving vane (RV) compressor and a comparison with that of the rolling piston type. Int J Refrig 32(5), 945–52.

TIAGO, M., OLIVEIRA, A.C. (2009). Energy and economic analysis of an integrated solar absorption cooling and heating system in different building types and climates. Appl Energy 86, 949–57.

TIGGELBECK, S.T., MITRA, N.K., FIEBIG, M. (1993). Experimental investigations of heat transfer enhancement and flow losses in a channel with double rows of longitudinal vortex generators. International Journal of Heat and Mass Transfer 26(9), 2327–37.

TIWARI, A., SODHA, M.S. (2006). Performance evaluation of hybrid PV/thermal water/air heating system: a parametric study. Renewable Energy 31, 2460-2474.

TIWARI, A., SODHA, M.S. (2006). Performance evaluation of solar PV/T system: an experimental validation. Solar Energy 80, 751-759.

TIWARI, A., SODHA, M.S. (2007). Parametric study of various configurations of hybrid PV/thermal air collector: experimental validation of theoretical model. Solar Energy Materials and Solar Cells 91, 17-28.

TIWARI, A., SODHA, M.S., CHANDRA, A., JOSHI, J.C. (2006). Performance evaluation of photovoltaic thermal solar air collector for composite climate of India. Solar Energy Materials and Solar Cells 90, 175-189.

TONUI, J.K., TRIPANAGNOSTOPOULOS, Y. (2007). Air cooled PV/T solar collectors with low cost performance improvements. Solar Energy 81, 498-511.

TONUI, J.K., TRIPANAGNOSTOPOULOS, Y. (2007). Improved PV/T solar collectors with heat extraction by forced or natural air circulation. Renewable Energy 32, 623-637.

TONUI, J.K., TRIPANAGNOSTOPOULOS, Y. (2008). Performance improvement of PV/T solar collectors with natural air flow operation. Solar Energy 82, 1-12.

TORRES, R.E., CERVANTES, G.J. (2001). Optimal performance of an irreversible solar-assisted heat pump. Exergy 1, 107–11.

TORRES, R.W., PICON, N.M., CERVANTES, G.J. (1998). Energy analysis and optimization of a solar-assisted heat pump. Energy 23, 337–44.

TORRES-REYES, E., PICON NUNE, Z.M., CERVANTESDE GORTARI, J. (1998). Exergy analysis and optimization of a solar-assisted heat pump. Energy 23, 337–44.

TRIPANAGNOSTOPOLOUS, Y., SOULIOTIS, M., BATTISTI, R., CORRADO, A. (2006). Performance, cost and life-cycle assessment study of hybrid PVT/AIR solar systems. Progress in Photovoltaic Research and Applications 14, 65-76.

TRIPANAGNOSTOPOLOUS, Y., SOULIOTIS, M., NOUSIA, T. (2000). Solar collectors with colored absorbers. Sol Energy 68, 343–56.

TRIPANAGNOSTOPOULOS, Y. (2007). Aspects and improvements of hybrid photovoltaic/thermal solar energy systems. Solar Energy 81,117-231.

TRIPANAGNOSTOPOULOS, Y. (2012). Photovoltaic/thermal solar collectors. Comprehensive Renewable Energy 3.

TRIPANAGNOSTOPOULOS, Y., NOUSIA, T H., SOULIOTIS, M., YIANOULIS. P. (2002). Hybrid photovoltaic/thermal solar systems. Solar Energy 72, 217-234.

TRIPANAGNOSTOPOULOS, Y., NOUSIA, T.H., SOULIOTIS, M. (2000). Low cost improvements to building integrated air cooled hybrid PV-thermal systems. In: Proceedings of 16th European PV solar energy conference, vol. 2, 1874-99.

TRIPANAGNOSTOPOULOS, Y., NOUSIA, T.H., SOULIOTIS, M. (2001). Test results of air cooled modified PV modules. In: Proceedings 17th PV solar energy conference, 2519–22.

TRIPANAGNOSTOPOULOS, Y., SIABEKOU, C.H. (2007). The Fresnel lens concept for solar control of buildings. Solar Energy 81, 661-675.

TRIPANAGNOSTOPOULOS, Y., TZAVELLAS, D., ZOULIA, I., CHORTATOU, M. (2001). Hybrid PV/T systems with dual heat extraction operation. In: Proceedings of the 17th PV solar energy conference, 2515–8.

US STANDARD CATEGORIZATION. (2009). DIN8900 Part 1 Heat Pumps. UK: Electricity Council Research Center.

VAN HELDEN, W. G. J., VAN ZOLINGEN, R. J. C., ZONDAG, H. A. (2004). PV thermal systems: PV panels supplying renewable electricity and heat. Pes Appl 12, 415-26.

VATS, K., TIWARI, G.N. (2012). Energy and exergy analysis of a building integrated semi-transparent photovoltaic thermal (BISPVT) system. Appl Energy 96, 409–16.

WANG, W., MA, Z., JIANG, Y., XU, S., YANG, Z. (2005). Field test investigation of a double-stage coupled heat pump heating system for cold region. International Journal of Refrigerant 28, 672-679.

WANG, X., HWANG, Y., RADERMACHER, R. (2008). Investigation of potential benefits of compressor cooling. Appl Therm Eng 28(14–15), 1791–7.

WANG, X., HWANG, Y., RADERMACHER, R. (2009). Two-stage heat pump system with vapour-injected scroll compressor using R410A as a refrigerant. International Journal of Refrigeration 32, 1442-1451.

WANG, X.A., WU, L.G. (1990). Analysis and performance of flat-plate solar collector arrays. Solar Energy 45 (2), 71–78.

WAZWAZ, J., SALMI, H., HALLAK, R. (2002). Solar thermal performance of a nickel pigmented aluminium oxide selective absorber. Renew Energy 27, 277–92.

WEITBRECHT, V., LEHMANN, D., RICHTER, A. (2002). Flow distribution in solar collectors with laminar flow conditions. Solar Energy 73 (6), 433–441.

WINANDY, E.L., LEBRUN, J. (2002). Scroll compressors using gas and liquid injection: experimental analysis and modelling. Int J Refrig 25, 1143–56.

WINSTON, R. (1974). Principles of solar concentrators of a novel design. Solar Energy 16, 89-95.

www.solenergi.dk/rapporter/pvtpotentialindenmark.pdf.

YANG, H.X., MARSHALL, G.H., BRINKWORTH, B.J. (1994). An experimental study of the thermal regulation of a PV-clad building roof. In: Proceedings of 12th European photovoltaic solar energy conference, 1115–8.

YANG, W., SHI, M., LIU, G., CHEN, Z. (2009). A two-region simulation model of vertical U0-tube ground heat exchanger and its experimental verification. Applied Energy 86. 2005-2012.

YANG, Y., WANG, Q., XIU, D., ZHAO, Z., SUN, Q. (2012). A building integrated solar collector: All ceramic solar collector. Energy and Buildings.

ZIVI, S.M. (1964). Estimation of steady-state voild fraction by means of the principle of minimum energy production. ASME Journal of Heat Transfer 86, 247-252.

ZOGOU, O., STAPOUNTZIS, H. (2011). Energy analysis of an improved concept of integrated PV panels in an office building in central Greece. Appl Energy 88(3), 853–66.

ZONDAG, H., BAKKER, M., HELDEN, W.G.J., AFFOLTER, P., EISENMANN, W., FECHNER, H. (2005). PVT roadmap: a European guide for the development and market introduction of PVT technology. In: Proceedings of (CD) 20th European photovoltaic solar energy conference.

ZONDAG, H.A., DE VRIES, D.W., VAN HELDEN, W.G.J., VAN ZOLENGEN, R.J.C., STEENHOVEN, A.A. (2002). The thermal and electrical yield of a PV thermal collector. Solar Energy 72, 113-128.

ZONDAG, H.A., DE VRIES, D.W., VAN HELDEN, W.G.J., VAN ZOLENGEN, R.J.C., STEENHOVEN, A.A. (2003). The yield of different combined PV-thermal collector designs. Solar Energy 74, 253-269.

ZONDAG, H.A., VRIES, D.W., STEENHOVEN, V. (1999). Thermal and electrical yield of a combi-panel. In: Proceedings of ISES Bi-annual Conference on CD-ROM, Jerusalem.

Appendix

Appendix I: Mathematical Model and Simulation of ASHP

A mathematical model for the novel SAHP system has been developed and used subsequently for evaluating the performance. It was assumed that the system was operated at a quasi-state condition within every time step in numerical simulation.

Compressor Model

The mathematical model used in this simulation was the same utilized in the Chapter 5 and details in Section 5.3.1.

Capillary and Liquid Tube Mode

Capillary tubes are commonly used as expansion valves in small scale heat pump systems. In addition, a liquid tube connects capillary and evaporator which contains a low quasi two phase mixture. The diameter of the liquid tube is small so the pressure drop needs to be considered. In this part, the empirical model is used for capillary and liquid tube flow. The empirical models are more popularly used than the distributed parameter models.

Jung et al. (1999) suggested the following refrigerant flow model based on a multiple variable regression analysis of both numerical and experimental results.

$$m = C_1 d^{C_2} L^{C_3} T_K^{C_4} 10^{C_5 \cdot DSC} \quad \text{(Equation 1)}$$

Where d is the inner diameter, L is the length of the capillary tube, and DSC is the degree of sub-cooling.

According to Jung et al. (1999), $C_1 = 0.249029,\ C_2 = 2.543633,\ C_3 = -0.42753,\ C_4 = 0.746108$ and $C_5 = 0.013922$ for R22.

Condenser Model

There are three zones when the refrigerant inside the condenser tube, sub-cooled liquid zone, two phase zone, and superheated vapour zone, showed in Figure 1. For each zone, the equation is same.

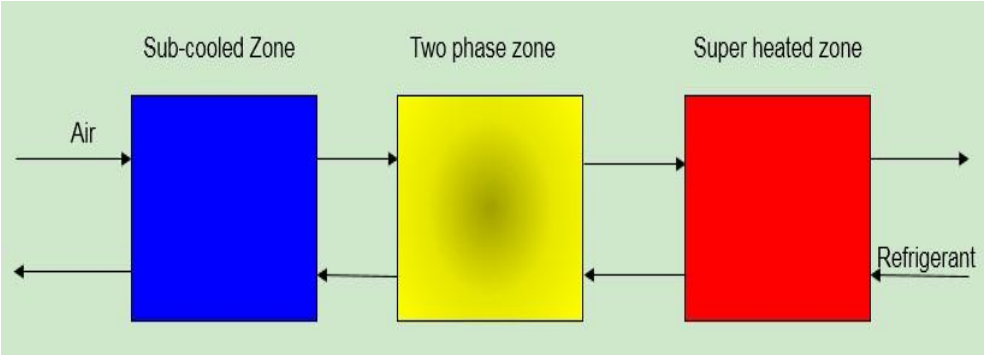

Figure 1. Three zones of the condenser tube

In this part, the zone lumped model are used to investigate (Ding, 2007). The numerical model was developed based on the following assumptions:

- The transparent fluid in the condenser is in cross flow and one dimensional steady flow.
- The pressure drop inside the condenser is affect by the small tube inner diameter, so the acceleration and friction pressure drops are both important.
- Neglecting the thermal resistance in the tube wall, only convective heat transfer resistance is considered.
- Neglecting the effect of gravity of the tube flow.

Base Model

The heat transfer on the air side can be expressed as:

$Q_a = m_a(h_{a2} - h_{a1})$ (Equation 2)

The heat transfer on the refrigerant side can be expressed as:

$Q_r = m_r(h_{r1} - h_{r2})$ (Equation 3)

The heat transfer equation between inner and outer of the tube can be expressed as:

$Q_a = \zeta Q_r$ (Equation 4)

The overall heat thermal equation of each zone can be expressed as:

$Q_r = \mathrm{U}A_i(T_{rm} - T_{am})$ (Equation 5)

The mean temperature of refrigerant side can be expressed as:

$T_{rm} = \frac{T_{r1}+T_{r2}}{2}$ (Equation 6)

The mean temperature of air side can be expressed as:

$T_{am} = \frac{T_{a1}+T_{a2}}{2}$ (Equation 7)

The tube length in each zone can be expressed as:

$\mathrm{L} = \frac{A_i}{\pi d_i}$ (Equation 8)

Where Q, h, T and m is heat transfer, enthalpy, thermodynamic temperature and mass flow, respectively. A is the area of each zone, α and r mean air side and refrigerant side. m is the mean temperature, and i is inner tube. Leakage coefficient ξ is assumed to equal 0.9.

The overall heat transfer coefficient based on the nominal inside area, can be expressed as:

$\mathrm{U} = (\frac{1}{\alpha_i} + \frac{A_i}{\alpha_o A_o})^{-1}$ (Equation 9)

Where α_i and α_o are the heat transfer coefficient of refrigerant and air interface, and $\frac{A_i}{A_o}$ is the effective heat transfer area ratio of condenser.

Therefore, the tube length in each zone is given by:

$$\mathrm{L} = \frac{(\frac{1}{\alpha_i}+\frac{A_i}{A_0\alpha_o})m_r(h_{r1}-h_{r2})}{(T_{rm}-T_{am})\pi d_i} \quad \text{(Equation 10)}$$

Convective Heat Transfer Coefficient on Refrigerant Side

The refrigerant flows in the sub-cooled and superheated zone are both single phase flow, so the convective heat transfer coefficient can be calculated with the Dittus-Boelter Equation (1979):

$$Nu_i = 0.023Re^{0.8}Pr^{0.3} \quad \text{(Equation 11)}$$

$$Nu_i = \frac{a_i d_i}{\lambda} \quad \text{(Equation 12)}$$

$$\mathrm{Re} = \frac{G_i d_i}{\mu} \quad \text{(Equation 13)}$$

The refrigerant flow in the two phase zone is two phase flow, so the convective heat transfer coefficient can be calculated with the Shah Equation (1979):

$$\alpha_{TP} = \alpha_1[(1-x)^{0.8} + \frac{3.8x^{0.78}(1-x)^{0.04}}{R^{0.38}}] \quad \text{(Equation 14)}$$

$$\mathrm{R} = {}^{p}/_{P_c} \quad \text{(Equation 15)}$$

Where α_{TP} is the heat transfer coefficient assuming the mass flow are liquid and air together, α_1 is the heat transfer coefficient assuming all the mass flow is liquid and is calculated with the Dittus-Boelter equation, and p is the reduced pressure.

Convective Heat Transfer Coefficient on Air Side

For plain fins, the air side heat transfer coefficient is calculated with the Li et al. (1997):

$$\mathrm{Nu} = 0.982Re^{0.424}(\frac{S_f}{d_3})^{-0.0887}(\frac{NS_2}{d_3})^{-0.1590} \quad \text{(Equation 16)}$$

$d_3 = d_o + 2\delta$ (Equation 17)

$u_{max} = {}^{u_y}/_{\varepsilon}$ (Equation 18)

$\varepsilon = \frac{(S_1 - d_o)(S_f - \delta)}{S_1 S_f}$ (Equation 19)

$u_y = \frac{q_a \times 1000}{A_y}$ (Equation 20)

$\mathrm{Nu} = \frac{a_i d_3}{\lambda}$ (Equation 21)

$\mathrm{Re} = \frac{\mu_{max} d_3}{\nu}$ (Equation 22)

Where S_f is the fin space, S_1 is the tube spacing perpendicular to the air flow, S_2 is the tube spacing in the air flow, d_3 is the tube outside diameter including the fin thickness, d_o is the external diameter of the tube, δ is the fin thickness, N is the number of tube rows in air flow direction, q_a is the mass flow of air, and A_y is the air side effective heat transfer area.

Convective Heat Transfer on Water Side of Novel Solar Thermal Collector System

The water side heat exchanger of novel solar thermal collector system is used as condenser.

The overall heat thermal equation of each zone can be expressed as:

$Q_w = m_w C_{pw}(T_{w2} - T_{w1})$ (Equation 23)

The overall heat transfer coefficient based on the nominal inside area can be expressed as:

$\mathrm{U} = (\frac{1}{\alpha_i} + \frac{A_i}{\alpha_w A_o})^{-1}$ (Equation 24)

The heat transfer equation between inner and outer of the tube can be expressed as:

$Q_w = \xi Q_r$ (Equation 25)

The tube length in each zone is given by:

$$L = \frac{(\frac{1}{\alpha_i} + \frac{A_i}{A_0 \alpha_o}) m_r (h_{r1} - h_{r2})}{(T_{rm} - T_{am}) \pi d_i} \quad \text{(Equation 26)}$$

Numerical Procedure

Based on the above detailed analysis of condenser, the flow chart of the simulation program is shown in Figure 2.

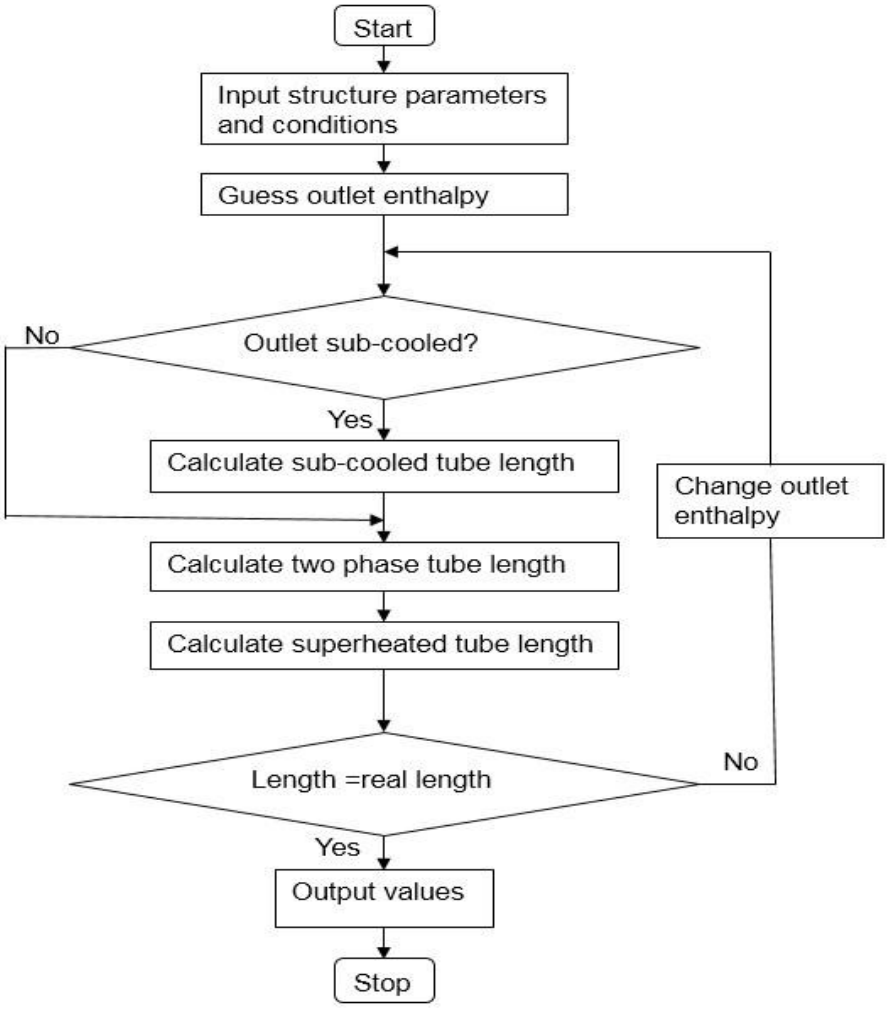

Figure 2. Flow chart of the simulation program of condenser

Evaporator Model

There are two zones when the refrigerant inside the evaporator, two phase zone, and superheated vapour zone. For each zone, the equation is same. In this part, the zone lumped model are used also used to investigate the

evaporator (Ding, 2007). The numerical model was developed based on the following assumptions:

- The transparent fluid in the condenser is in cross flow and one dimensional steady flow.
- Neglecting the thermal resistance in the tube wall, only convective heat transfer resistance is considered.
- Neglecting the effect of gravity of the tube flow.

Base Model

The heat transfer on the refrigerant side can be expressed as:

$Q_r = m_r(h_{r1} - h_{r2}) = \alpha_i A_i (T_w - T_{rm})$ (Equation 27)

$T_{rm} = \frac{T_{r1}+T_{r2}}{2}$ (Equation 28)

Where α_i is the refrigerant heat transfer coefficient, A_i is the surface area of the tube, T_w is the tube outside diameter, T_{rm} is the mean temperature of refrigerant.

The heat transfer on the air side can be expressed as:

$Q_a = m_a(h_{a1} - h_{a2}) = \xi \alpha_{os} A_o (T_{am} - T_w)$ (Equation 29)

$T_{am} = \frac{T_{a1}+T_{a2}}{2}$ (Equation 30)

$\xi = \frac{h_1 - h_2}{C_p(t_1 - t_2)}$ (Equation 31)

Where α_{os} is the air heat transfer coefficient, T_{am} is the mean temperature of air.

The heat transfer equation between inner and outer of the tube can be expressed as:

$Q_a = \gamma Q_r$ (Equation 32)

Where γ is the leakage coefficient and is assumed equal as 0.9.

The tube length in each zone can be expressed as:

$$\mathrm{L} = \frac{Q_r}{(T_w - T_{rm})\pi\alpha_i d_i} = \frac{\gamma Q_r}{(T_{am} - T_w)\varepsilon\pi\alpha_o d_i} \quad \text{(Equation 33)}$$

Convective Heat Transfer Coefficient on Refrigerant Side

The refrigerant flow in the superheated zone is single phase flow, so the convective heat transfer coefficient can be calculated with the Dittus-Boelter Equation (1979):

$$\mathrm{Nu} = 0.023 Re^{0.8} Pr^{0.3} \quad \text{(Equation 34)}$$

$$Nu_i = \frac{\alpha_i d_i}{\lambda} \quad \text{(Equation 35)}$$

$$\mathrm{Re} = \frac{G_i d_i}{\mu} \quad \text{(Equation 36)}$$

The refrigerant flow in the two phase zone is two phase flow, the heat transfer coefficient can be expressed by:

$$\frac{\alpha_{TP}}{\alpha_1} = C_1 (C_0)^{C_2} (25Fr)^{C_3} + C_3 (B_o)^{C_4} F_{f1} \quad \text{(Equation 37)}$$

$$\alpha_1 = 0.0023 Re_{ix}^{0.8} \frac{\lambda_1 Pr_1^{0.4}}{d_i} \quad \text{(Equation 38)}$$

$$\mathrm{Re} = \frac{G_i(1-x)d_i}{\mu_i} \quad \text{(Equation 39)}$$

$$C_o = \left(\frac{1-x}{x}\right)^{0.8} \left(\frac{\rho_g}{\rho_1}\right)^{0.5} \quad \text{(Equation 40)}$$

$$B_o = \frac{q}{G_r^r} \quad \text{(Equation 41)}$$

$$Fr_i = \frac{G_r^2}{9.8\rho_1^2 d_i} \quad \text{(Equation 42)}$$

$$\alpha_{TP} = \alpha_1 \left[(1-x)^{0.8} + \frac{3.8 x^{0.78} (1-x)^{0.04}}{R^{0.38}}\right] \quad \text{(Equation 43)}$$

$$\mathrm{R} = {}^{p}/_{P_c} \quad \text{(Equation 44)}$$

Convective Heat Transfer Coefficient on Air Side

For plain fins, the air side heat transfer coefficient is calculated with the Li et al. (1997):

$$\mathrm{Nu} = 0.982Re^{0.424}(\frac{S_f}{d_3})^{-0.0887}(\frac{NS_2}{d_3})^{-0.1590}$$ (Equation 45)

$$d_3 = d_o + 2\delta$$ (Equation 46)

$$u_{max} = {u_y}/{\varepsilon}$$ (Equation 47)

$$\varepsilon = \frac{(S_1 - d_o)(S_f - \delta)}{S_1 S_f}$$ (Equation 48)

$$u_y = \frac{q_a \times 1000}{A_y}$$ (Equation 49)

$$\mathrm{Nu} = \frac{a_i d_3}{\lambda}$$ (Equation 50)

$$\mathrm{Re} = \frac{\mu_{max} d_3}{\nu}$$ (Equation 51)

Where S_f is the fin space, S_1 is the tube spacing perpendicular to the air flow, S_2 is the tube spacing in the air flow, d_3 is the tube outside diameter including the fin thickness, d_o is the external diameter of the tube, δ is the fin thickness, N is the number of tube rows in air flow direction, q_a is the mass flow of air, and A_y is the air side effective heat transfer area.

Convective Heat Transfer on Water Side of Novel Solar Thermal Collector System

The water side heat exchanger of novel solar thermal collector system is used as evaporator. The overall heat thermal equation of each zone can be expressed as:

$$Q_w = m_{wc_{pw}}(T_{w2} - T_{w1}) = \alpha_w A_o (T_{wm} - T_w)$$ (Equation 52)

The heat transfer equation between inner and outer of the tube can be expressed as:

$$Q_w = \gamma Q_r$$ (Equation 53)

The tube length in each zone is given by:

$$L = \frac{Q_r}{(T_w - T_{rm})\pi\alpha_i d_i} = \frac{\gamma Q_r}{(T_{watm} - T_w)\varepsilon\pi\alpha_o d_i}$$ (Equation 54)

Numerical Procedure

Based on the above detailed analysis of condenser, the flow chart of the simulation program is shown in Figure 3.

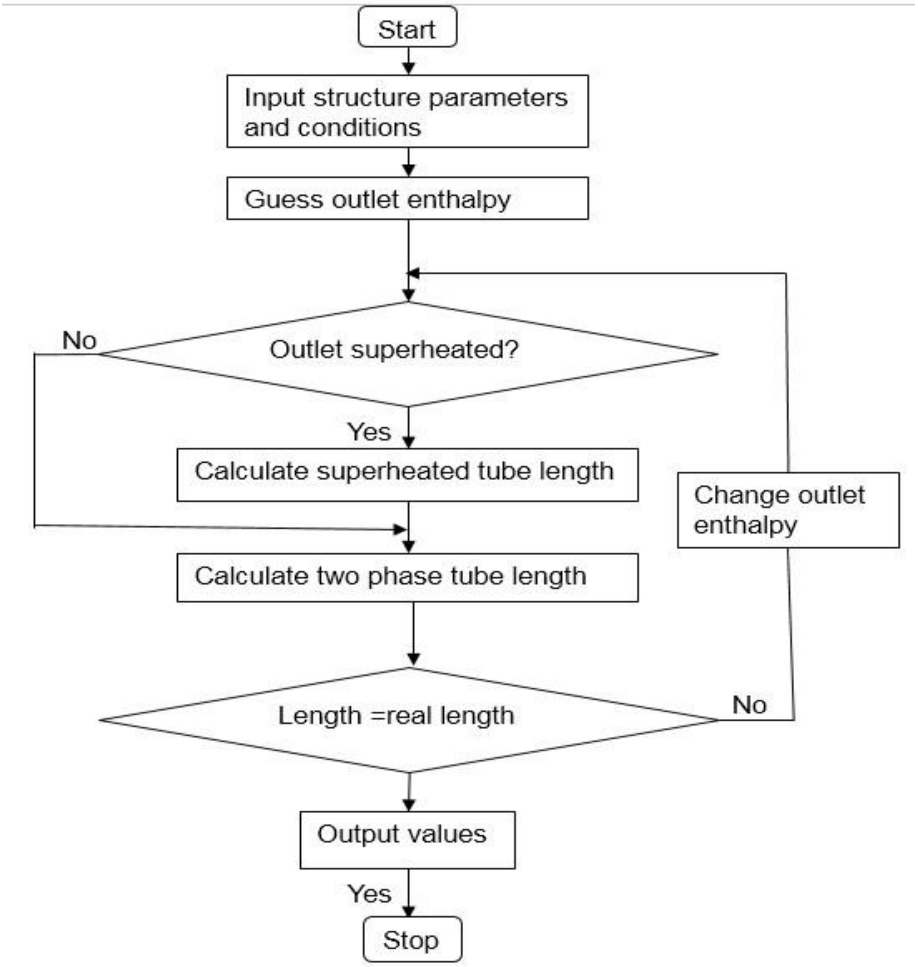

Figure 3. Flow chart of the simulation program of condenser

Refrigerant Charge

The amounts of refrigerant charge are close related to the operation of the refrigerant cycle and the performance of the system. Excessive or small refrigerant will cause the system performance degradation. In order to achieve the high performance, a moderate amount of refrigerant should be necessary.

Therefore, after make sure the other parameters of system, the amount of refrigerant are needed in the system should to calculated accuracy.

When the SAHP system operates, most of the refrigerant works in the evaporator and condenser, only a small percent of refrigerant in the compressor and the connecting pipes. The refrigerant charge is calculated according to the component configurations and the refrigerant states in each component.

Compressor

$m_{com} = \bar{\rho} V_{com}$ (Equation 55)

Where $\bar{\rho}$ is the average density of refrigerant, based on the inlet and outlet of average vapour temperature.

Condenser

The void fraction can be calculated with the Zivi equation (1964):

$\alpha_i = \frac{1}{1+\left(\frac{1}{x}-1\right)\cdot S\cdot\frac{\rho_g}{\rho_f}}$ (Equation 56)

$\mathrm{S} = (\frac{\rho_f}{\rho_g})^{\frac{1}{3}}$ (Equation 57)

For the two phase zone in the condenser:

$m_1 = \left[\alpha_i \rho_g + (1-\alpha_i)\rho_f\right] \mathrm{A} L_{TP}$ (Equation 58)

For the superheated zone and sub-cooled zone in the condenser:

$m_2 = \rho \mathrm{A} L_{SP}$ (Equation 59)

The refrigerant charge for the condenser is:

$m_{com} = m_1 + m_2$ (Equation 60)

Where m_1 and m_2 are the refrigerant charge for the two phase zone and single phase zone, respectively, χ is the quality of the two phase zone, L_{TP} and L_{SP} are the tube length of the two phase zone and single phase zone, respectively, and A is the area of the tube.

Capillary

The void fraction can be calculated with the Zivi Equation (1964):

$$\alpha_i = \frac{1}{1+\left(\frac{1}{x}-1\right)\cdot S\cdot\frac{\rho_g}{\rho_f}} \quad \text{(Equation 61)}$$

$$S = \left(\frac{\rho_f}{\rho_g}\right)^{\frac{1}{3}} \quad \text{(Equation 62)}$$

For the two phase zone in the capillary:

$$m_1 = \left[\alpha_i\rho_g + (1-\alpha_i)\rho_f\right]AL_{TP} \quad \text{(Equation 63)}$$

For the superheated zone and sub-cooled zone in the capillary:

$$m_2 = \rho A L_{SP} \quad \text{(Equation 64)}$$

The refrigerant charge in the capillary is:

$$m_{com} = m_1 + m_2 \quad \text{(Equation 65)}$$

Where m_1 and m_2 are the refrigerant charge for the two phase zone and single phase zone, respectively, χ is the quality of the two phase zone, L_{TP} and L_{SP} are the tube length of the two phase zone and single phase zone, respectively, and A is the area of the tube.

Evaporator

The void fraction can be calculated with the Hughmark model (1994)

$$\chi = \frac{\chi_1+\chi_2}{2} \quad \text{(Equation 66)}$$

For the two phase zone in the evaporator:

$$m_1 = \left[\chi\rho_g + (1-\chi)\rho_f\right]AL_{TP} \quad \text{(Equation 67)}$$

For the single phase zone in the evaporator:

$$m_2 = \rho A L_{SP} \quad \text{(Equation 68)}$$

The refrigerant charge in the evaporator is:

$$m_e = m_1 + m_2 \quad \text{(Equation 69)}$$

Where m_1 and m_2 are the refrigerant charge for the two phase zone and single phase zone, respectively, χ is the quality of the two phase zone, L_{TP} and L_{SP} are the tube length of the two phase zone and single phase zone, respectively, and A is the area of the tube.

Whole System

The refrigerant charge for the whole system is:

$$m_{sys} = m_e + m_{com} + m_{con} + m_{cap} \quad \text{(Equation 70)}$$

Appendix II: Thermodynamic Properties

The Thermodynamic Properties of R22

The refrigerant thermodynamic properties are evaluated using the Cleland correlation (1986).

Saturation Pressure and Saturation Temperature

$$P_{sat} = \exp(a_1 + \frac{a_2}{t_{sat}+a_3}) \quad \text{(Equation 71)}$$

$$t_{sat} = \frac{a_2}{lnP_{sat}-a_1} - a_3 \quad \text{(Equation 72)}$$

Where $a_1 = 21.25384$, $a_2 = -2025.4518$, and $a_3 = 247.94$.

Enthalpy of Liquid

$$h_1 = a_4 + a_5 t_l + a_6 t_l^2 + a_7 t_l^3 \quad \text{(Equation 73)}$$

Where $a_4 = 200000$, $a_5 = 1170.36$, $a_6 = 1.68674$, $a_7 = 5.2703\text{E}-3$, and t_l is the liquid temperature (^{o} C).

Enthalpy of Saturated Gas

$$h_g = h_{i1} + a_{12} \text{ (Equation 74)}$$

$$h_{i1} = a_8 + a_9 t_{sat} + a_{10} t_{sat}^2 + a_{11} t_{sat}^3 \text{ (Equation 75)}$$

Where $a_8 = 250027$, $a_9 = 367.265$, $a_{10} = -1.84142$, $a_{11} = -11.4556\text{E}-3$, and $a_{12} = 155482$.

Enthalpy of Superheated Gas

$$h_v = h_{i2} + a_{12} \quad \text{(Equation 76)}$$

$$\frac{h_{i2}}{h_{i1}} = 1 + a_{13\Delta} t_{SH} + a_{14} \Delta t_{SH}^2 + a_{15} \Delta t_{SH} t_{sat} + a_{16\Delta} t_{SH}^2 t_{sat} + a_{17} \Delta t_{SH} t_{sat}^2 + a_{18} \Delta t_{SH}^2 t_{sat}^2 \quad \text{(Equation 77)}$$

Where $a_{13} = 2.85446\text{E}-3$, $a_{14} = 4.0129\text{E}-7$, $a_{15} = 13.3612\text{E}-6$, $a_{16} = -7.11617\text{E}-8$, $a_{17} = 14.1194\text{E}-8$, $a_{18} = -9.53229\text{E}-10$, and Δt_{SH} is the superheated gas temperature.

Specific Volume of Saturated Gas

$$\nu_g = \exp(a_{19} + a_{20}/(t_{sat} + 273))(a_{21} + a_{22}t_{sat} + a_{23}t_{sat}^2 + a_{24}t_{sat}^3)$$
(Equation 78)

Where $a_{19} = -11.82344$, $a_{20} = 2390.321$, $a_{21} = 1.01859$, $a_{22} = 5.09433\text{E} - 4$, $a_{23} = -14.8664\text{E} - 6$, and $a_{24} = -2.49547\text{E} - 7$.

Specific Volume of Superheated Gas

$$\nu_s = \upsilon(1 + a_{25\Delta}t_{SH} + a_{26}\Delta t_{SH}^2 + a_{27}\Delta t_{SH}t_{sat} + a_{28\Delta}t_{SH}^2 t_{sat} + a_{29}\Delta t_{SH}t_{sat}^2 + a_{30}\Delta t_{SH}^2 t_{sat}^2)$$ (Equation 79)

Where $a_{25} = 5.23275\text{E} - 3, a_{26} = -5.59394\text{E} - 6, a_{27} = 3.45555\text{E} - 5, a_{28} = -2.31649\text{E} - 7, a_{29} = 5.80303\text{E} - 7$, and $a_{30} = -3.20189\text{E} - 9$.

Viscosity of Saturated Liquid

$$\mu_f = a_{31} + a_{32}(t_l + 5) + a_{33}(t_l + 5)^2 + a_{34}(t_l + 5)^3 + a_{35}(t_l + 5)^4$$
(Equation 80)

Where $a_{31} = 2.749248\text{E} - 4$, $a_{32} = 1.619606\text{E} - 6$, $a_{33} = 1.082842\text{E} - 8$, $a_{34} = -7.666408\text{E} - 11$, and $a_{35} = 4.625583\text{E} - 13$.

Viscosity of Saturated Gas

$$\mu_g = a_{36} + a_{37}t_{sat} + a_{38}t_{sat}^2 + a_{39}t_{sat}^3$$ (Equation 81)

Where $a_{36} = 1.199478\text{E} - 5$, $a_{37} = 3.284776\text{E} - 8$, $a_{38} = -9.775641\text{E} - 11$, and $a_{39} = 4.326923\text{E} - 13$.

Specific Volume and Entropy of Saturated Liquid

$$\nu_f = (a_{40} + a_{41}t_l + a_{42}t_l^2)/1000$$ (Equation 82)

$$S_f = (a_{43} + a_{44}t_l) \cdot 1000$$ (Equation 83)

Where $a_{40} = 0.7839803$, $a_{41} = 1.549103\text{E} - 3$, $a_{42} = 2.378806\text{E} - 5$, $a_{43} = 1.0013$, and $a_{44} = 4.1\text{E} - 3$.

Entropy of Saturated Gas

$$S_g = (a_{45} + a_{46}t_{sat} + a_{47}t_{sat}^2) \cdot 1000$$ (Equation 84)

Where $a_{45} = 1.749564$, $a_{46} = -1.246137\text{E} - 3$, and $a_{47} = -1.788576\text{E} - 7$

Prandtl Number of Saturated Liquid

$Pr_f = a_{48} + a_{49}(t_{sat} + 5) + a_{50}\,(t_{sat} + 5)^2 + a_{51}(t_{sat} + 5)^3 + a_{52}(t_{sat} + 5)^4 + a_{53}(t_{sat} + 5)^5 + a_{54}(t_{sat} + 5)^6$ (Equation 85)

Where $a_{48} = 3.174701$, $a_{49} = 3.832566\text{E} - 3$, $a_{50} = 1.889572\text{E} - 4$, $a_{51} = -4.51374\text{E} - 7$, $a_{52} = -1.60986\text{E} - 8$, $a_{53} = 3.054299\text{E} - 10$, and $a_{54} = 7.625272\text{E} - 12$.

Prandtl Number of Saturated Gas

$Pr_g = a_{55} + a_{56}(t_{sat} + 5) + a_{57}\,(t_{sat} + 5)^2 + a_{58}(t_{sat} + 5)^3 + a_{59}(t_{sat} + 5)^4 + a_{60}(t_{sat} + 5)^5$ (Equation 86)

Where $a_{55} = 0.5769468$, $a_{56} = 1.458742\text{E} - 2$, $a_{57} = -1.719931\text{E} - 4$, $a_{58} = -9.664936\text{E} - 6$, $a_{59} = 3.338471\text{E} - 7$, and $a_{60} = -2.670963\text{E} - 9$.

Thermal Conductivity of Saturated Liquid

$\lambda_f = a_{61} + a_{62}t_l + a_{63}t_l^2 + a_{64}t_l^3 + a_{65}t_l^4$ (Equation 87)

Where $a_{61} = 9.764182\text{E} - 2$, $a_{62} = -4.934572\text{E} - 3$, $a_{63} = 2.034819\text{E} - 7$, $a_{64} = -1.129152\text{E} - 8$, and $a_{65} = 1.45079\text{E} - 10$.

Thermal Conductivity of Saturated Gas

$\lambda_s = a_{66} + a_{67}(t_{sat} - 10) + a_{68}\,(t_{sat} - 10)^2 + a_{69}(t_{sat} - 10)^3 + a_{70}(t_{sat} - 10)^4 + a_{71}(t_{sat} - 10)^5$ (Equation 88)

Where $a_{66} = 1.109942\text{E} - 2$, $a_{67} = 3.095758\text{E} - 5$, $a_{68} = -2.890469\text{E} - 7$, $a_{69} = -2.236787\text{E} - 9$, $a_{70} = 3.397571\text{E} - 11$, and $a_{71} = 3.28133\text{E} - 13$.

The Thermodynamic Properties of Moist Air

Atmospheric air (moist air) contains many gaseous components as well as water vapour and miscellaneous contaminants. As a two component mixture of dry air and water vapour, the amount of water vapour in moist air varies from zero to a maximum that depends on temperature and pressure. However, pressure refers to saturation, a state of neutral equilibrium between moist air

and the condensed water phase. In there, the thermodynamic equations and sub-routine based on heat exchanger models are given.

Vapour Pressure of Water (Hyland and Wexler, 1983)

Temperature range: -100 ^{o} C ~ 0 ^{o} C

$$\ln P_{q,b} = C_1/T + C_2 + C_3 T + C_4 T^2 + C_5 T^3 + C_6 T^4 + C_7 lnT \quad \text{(Equation 89)}$$

Temperature range: 0 ^{o} C ~ 200 ^{o} C

$$\ln P_{q,b} = C_8/T + C_9 + C_{10} T + C_{11} T^2 + C_{12} T^3 + C_{13} lnT \quad \text{(Equation 90)}$$

Where $C_1 = -5674.5359$, $C_2 = 6.392547$, $C_3 = -9.677843\mathrm{E}-3$, $C_4 = 6.2215701\mathrm{E}-7$, $C_5 = 2.0747825\mathrm{E}-9$, $C_6 = -9.4840240\mathrm{E}-13$, $C_7 = 4.1635019$, $C_8 = -5800.2206$, $C_9 = 1.3914993$, and $C_{10} = -4.8640239\mathrm{E}-2$, $C_{11} = 4.1764768\mathrm{E}-5$, $C_{12} = -1.4452093\mathrm{E}-8$, and $C_{13} = 6.5459673$.

Density of Moist Air

$$\rho_a = 0.00349\frac{B}{T} - 0.00134\frac{\varphi P_{q,b}}{T} \quad \text{(Equation 91)}$$

Where φ is relative density of moist air and B is barometric pressure.

Humidity Ration

$$\mathrm{d} = \frac{0.622\varphi P_{q,b}}{B - \varphi P_{q,b}} \quad \text{(Equation 92)}$$

Specific Enthalpy

$$h_a = 1.005 t_a + d(2500 + 1.84 t_a) \quad \text{(Equation 93)}$$

Specific Heat

$$C_{p,a} = \frac{1.005 + 1.84d}{1+d} \quad \text{(Equation 94)}$$

Viscosity and Thermal Conductivity

$$\mu_a = 17.268 \times 10^{-6} \left(\frac{T}{273.15}\right)^{0.7} \quad \text{(Equation 95)}$$

$$\lambda_a = 2.4066 \times 10^{-2} \left(\frac{T}{273.15}\right)^{0.9} \quad \text{(Equation 96)}$$

Dew Point Temperature

$P_s = \frac{d}{0.622+d} \times B$ (Equation 97)

When $0^oC \leq t \leq 70^oC$,

$t_d = -35.957 - 1.8762\ln P_s - 1.1689 ln^2 P_s$;

When $-60^oC \leq t \leq 0^oC$,

$t_d = -60.45 + 7.0322\ln P_s + 0.3700 ln^2 P_s$;

The Thermodynamic Properties of Water

Calculated the heat transfer of novel solar thermal collector system, thermodynamic properties of water should be used. In there, the thermodynamic equations and sub-routine based on heat exchanger models are given.

Viscosity of Water

$\mu = \frac{\mu_o}{b_1+b_2 t+b_3 t^2}$ (Equation 98)

Where μ_o is the dynamic viscosity at 0 °C, $\mu_o = 1793.636 \times 10^{-6} Pa \cdot s$, $b_1 = 1.0000000$, $b_2 = 3.3700000\mathrm{E}-2$, and $b_3 = 2.2100000\mathrm{E}-4$.

Thermal Conductivity of Water

$\lambda_w = b_4 + b_5 t + b_6 t^2$ (Equation 99)

Where $b_4 = 5.5602098\mathrm{E}-1$, $b_5 = 2.3376923\mathrm{E}-3$, and $b_6 = -1.0804196\mathrm{E}-5$.

Density of Water

$\rho_w = b_7 + b_8 t + b_9 t^2$ (Equation 100)

Where $b_7 = 1.0005776\mathrm{E}+3$, $b_8 = -7.0629371\mathrm{E}-2$, and $b_9 = -3.5664336\mathrm{E}-3$.

Specific Heat Capacity of Water at Constant Pressure

$C_{pw} = b_{10} + b_{11}t + b_{12}t^2$ (Equation 101)

Where $b_{10} = 4.2152727, b_{11} = -1.6342424\mathrm{E}-3$, and $b_{12} = 1.6515152\mathrm{E}-5$.

Prandtl Number of Water

$Pr_w = \frac{C_p \mu}{\lambda}$ (Equation 102)

Numerical Procedure

The simulation of the whole system was carried out using Visual Basic and then presented the results, showed in Figure 4.

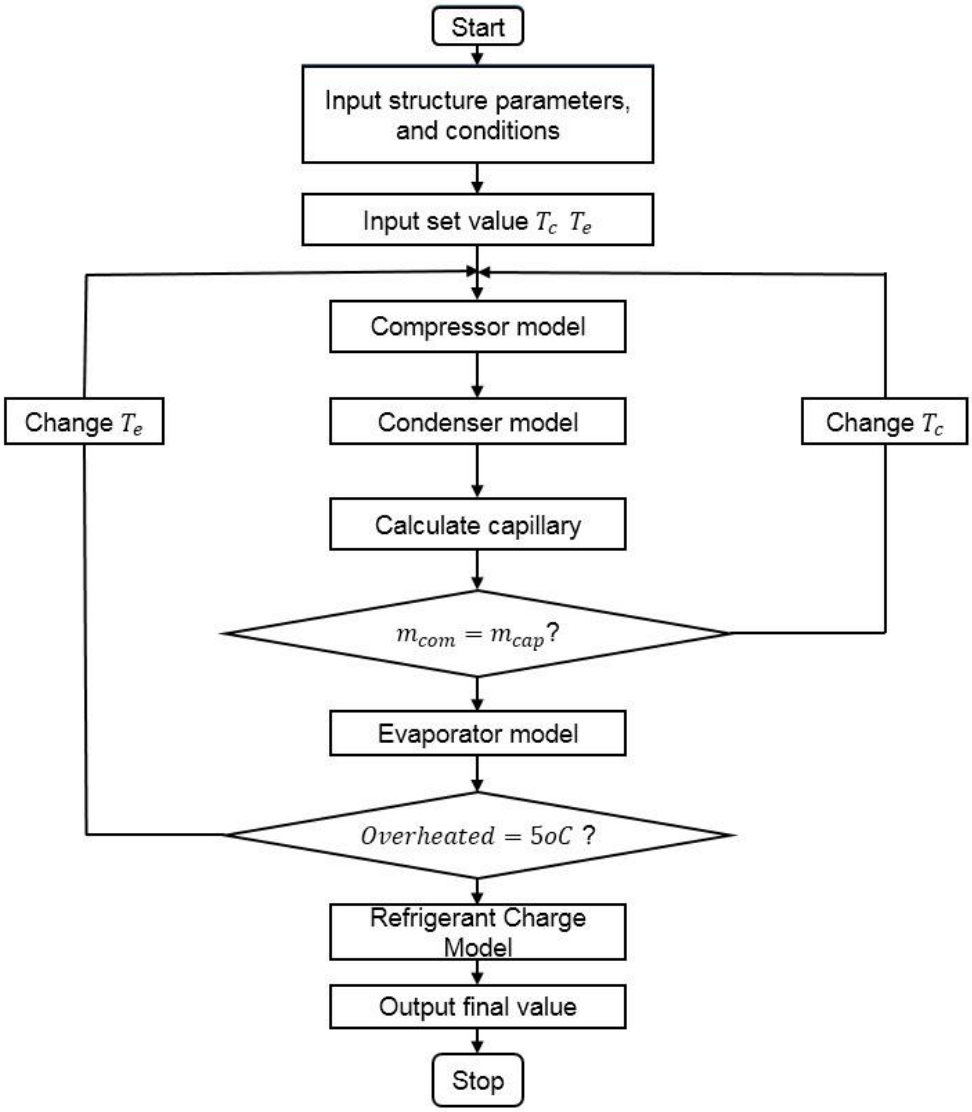

Figure 4. Flow chart of the simulation program of novel SAHP

Appendix III: Heat source (21 Tungsten Halogen (500W) lamps)

In order to simulate the sun, a variable movable lights simulator made up of 21, 500W halogen lamps was used in the lab (Figure 4.21). This adjustable light simulated the solar radiations, and was placed tilted at 15 degrees in order to have horizontal radiations on the solar collector. Also, a light regulator switch also shown in Figure 5, which allowed the variation of radiations to obtain the sun radiations range from 200 W/m^2 to 1000 W/m^2.

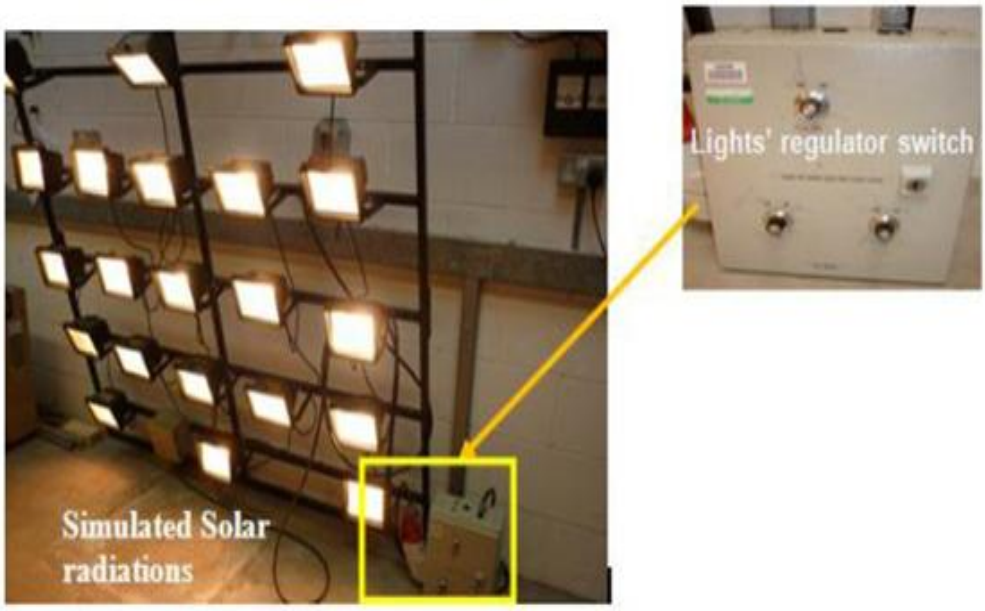

Figure 5 Twenty-one 500W halogen lamps simulator and the regulator switch.

Appendix IV: Measurement Equipment

The specifications of all the measurement equipment are shown in the Table 1. In order to evaluate the preliminary thermal performance of the novel heat pump system, a series of experiments was conducted at the laboratory. The procedures followed to conduct the measurement equipment are described below.

Table 1. Specification of the measurement equipment

Item	Device	Quantity	Location
1	Pyranometer (Kipp & Zonen CMP11, Netherlands)	1	Solar collector panel
2	Plug-in power & energy monitor (Energy Monitor World, UK)	1	Compressor input (AC)
3	Pressure transducer (RS 461-341, UK)	4	Inlet and outlet of compressor, capillary, solar collector and outdoor heat exchanger
4	Adhesive thermocouple type K (RS 621-2287, UK)	6	Solar collector plate
5	PT100 temperature sensor (RS 611-8264, UK)	13	Inlet and outlet of outdoor heat exchanger, solar collector panel, and indoor heat exchanger
6	Data logger (DT500, UK)	1	
7	Calibrated flow indicator (RS 186-0049)	1	Water pipe after pump
8	Hot bulb anemometer	2	Indoor heat exchanger and outdoor heat exchanger
9	Digital thermometer (Digitron T208)	1	Room temperature

Measuring the Temperature

The temperatures were measured in the testing rig using K-type thermocouples, T-type thermocouples and platinum resistance thermometers (RTDs). The room temperatures were measured using the high performance humidity and temperature meter and a digital thermometer. The characteristics and illustrations are showed in Table 2 and Figure 6.

Table 2. The characteristics of temperature measurement equipment (Technology Pico, 2001)

Types	Description
T-type thermocouple probe	Operating range: -418^{o}C to 700^{o}C, low accuracy
RTD (PT100)	Operating range: -250^{o}C to 850^{o}C, very high accuracy
K-type thermocouple	Operating range: -20^{o}C to 250^{o}C, high accuracy
Digital thermometer	Range from -199^{o}C to +199.9^{o}C Accuracy: 0.01%rdg. $\pm$ 0.2^{o}C Resolution: 0.1^{o}C
Digital temperature and humidity meter	Range: humidity: 0-100%RH, temperature: -20^{o}C – 60^{o}C Accuracy: humidity: $\pm$ 3.5%RH, temperature: $\pm$ 2^{o}C Resolution: 0.1%RH, 0. ^{o}C Operation temperature: 0^{o}C –40^{o}C (<80%RH)

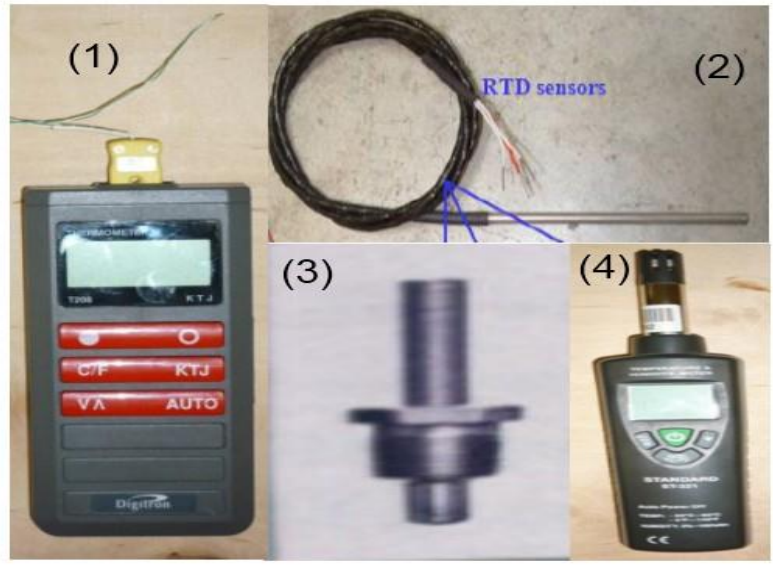

(1)Digital thermometer (2)K-type thermocouple
(3)T-type thermocouple (4) Digital temperature and humidity meter

Figure 6. Illustration of the temperature sensors of the testing rig

Measured the Pressures

Pressure are measured with GP pressure transmitter, which is a multipurpose, high performance stainless steel 0-100Mv output transducer transmitting at 4 ~ 20mA output range (Table 3). The pressure range is 0-10bar. It is a temperature compensated strain gauge technology with a $\pm$0.25% accuracy full scale. Figure 7 shows both the GP pressure transducer and the mode of installation on the test rig with the extension output cable to the data logger.

Figure 7. GP pressure transducer

Table 3. Specification of the pressure transducer

Category	Pressure sensors
Proof pressure	2×Range (×5 Burst Pressure)
Analogue output	4 to 20 mA
Supply voltage	12 to 36 Vdc 0-5V output (Transducers) -40 to +100/125^{o}C transmitter/transducer range 2×rated overpressure up to 250mb

Measuring water mass flow rate

Mass flow rate of the water was measured using flow meter, shown in Figure 8.

Figure 8. Water flow meter

Measuring the compressor power consumption

A digital power meter was used to measure the power consumption of the compressor every five minutes, shown in Figure 9.

Measuring the simulated solar radiation

A solar pyrometer CM11 (shown in Figure 10) was placed at the middle of the solar collector panel and used to measure the instantaneous solar radiation. The specification of the CM11 pyrometer is shown in Table 4.

Figure 9. The single phase watt hour meter

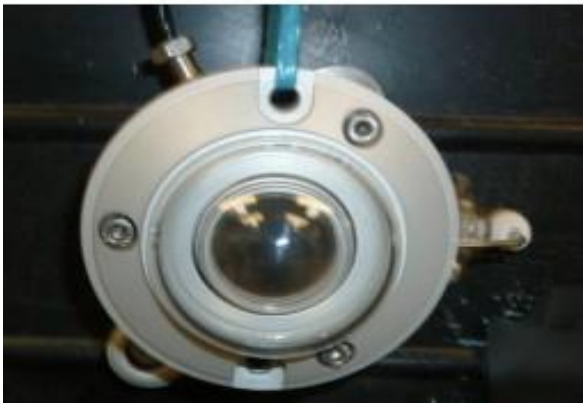

Figure 10. Kipp & Zonen, CM11 pyranometer

Table 4. Specifications of the CM11 pyrometer

Spectral range	305-2800nm (50% points)
Sensitivity	4.56×10^{-6} V/W m^2
Accuracy	Humidity: ± 3.5%RH Temperature: ± 2°C
Response time (95%)	15 sec
Temperature dependence of sensitivity	< ± 1 W/m^2%(beam 1000Wm^2)
Directional error	< ± 1% (-10 to +40°C)
Impedance (nominal)	700-1500Ω
Operation temperature	-40°C to +80°C

Data Collect-Data Taker DT500

All data was measured, monitored and controlled by a personal computer via data logger software. In order to record experimental data (solar radiation, compressor temperatures, condenser and evaporator temperatures), the Data-Taker DT500 is connected to the computer (shown in Figure 11), and using appropriate software, one stores data in the computer for future reference and then transfer to spreadsheet for examination.

Figure 11. Data Taker DT500